Molecular Characterisation and Preclinical Evaluation of a Small Molecule Protease-Activated Receptor 2 (PAR2) Antagonist in a Prostate Inflammation Model

Yosra A. F. Lozon

B. Pharm., M.Sc.

A thesis submitted in fulfilment of the requirements for the degree of

Doctor of Philosophy

Strathclyde Institute of Pharmacy and Biomedical Sciences (SIPBS)

The University of Strathclyde

Glasgow, UK

June 2025

Declaration

This thesis is the result of the author's original research. It has been composed by the author and has not been previously submitted for examination, which has led to the award of a degree. The copyright of this thesis belongs to the author under the terms of the United Kingdom Copyright Act as qualified by University of Strathclyde Regulation 3.50. Due acknowledgment must always be made to the use of any material contained in, or derived from, this thesis.

Name: Yosra A. F. Lozon

Signature: 

Date: 03/06/2025

Acknowledgment

First and foremost, I extend my deepest gratitude to Allah (God) for granting me the strength, patience, and resilience to believe in myself and pursue my dreams. It is through His endless mercy and guidance that I found that courage to overcome challenges that once seemed impossible and preserve until the end. I could never have reached this point without my faith in Him. For this I am profoundly thankful and say "*Alhamdu lellah*" "الحمد لله", thank you Allah.

In Glasgow, I would like to begin by expressing my heartful and sincere gratitude to my supervisor, Professor Robin Plevin, for granting me the opportunity to be part of his lab and work on this project. Thank you, Robin, for your patience, dedication, and generous time you devoted to guiding me. I have been truly inspired by your passion for science, dedication and encouragement to trust the process, regardless of the outcomes. Your kind words during some of the most challenging moments, when everything felt "impossible", significantly enhance my strength to keep going, without running statistical analysis. I am also deeply grateful Dr. Kathryn McIntosh, my second supervisor, for her patience, kindness, and consistent support. Your meticulous organization and thoughtful guidance in lab work have taught me so much that it made a lasting impact on my scientific journey. My sincere thanks also go to my lab mates and fellow PhD colleagues, including Rachel Craig, Ashley Mcculloch, Mohammad Farhan, Kirsty Tinto, Haidar AlMoosawi, Natalia and Panicha, your support and presence meant a lot to me.

In Dubai, I would like to extend my gratitude to my local co-supervisor, Prof. Rajan Radhakrishnan, for his encouragement and facilitating access to laboratory facilities at

Mohammad Bin Rashid University (MBRU), as well as welcoming me in his research team. I am especially grateful to my friend and MBRU colleague, Dr. Asha Cyril, for her generosity, constant support and immense patience during every phase of my studies in Dubai. I also thank all lab members at MBRU, especially Mr. Kumar, Surendra, Anaga, Najma and Haneen, for their assistance and kindness. I would like to acknowledge my home institution, Dubai Pharmacy College, now College of Pharmacy under Dubai Medical University (DMU), for facilitating my collaboration with MBRU team. To all, much of the work presented in this thesis would not have been possible without collective support.

To my fellow "PhD journey" companions, Zahra Khalifa and Eiman Ali, thank you for your continued support and for making this experience more bearable and joyful with your wonderful company. A special thanks goes to Dr. Ibrahim Khadra and Prof. Amina Mandy, whose early efforts were instrumental in initiating this project alongside my supervisor Robin.

Super special thanks to my parents, my sisters and brothers and the full dearest family, especially my lovely nephews, for being the greatest source of love and strength. To my extended family in my homeland, Gaza, your love has reached me across every border and hardship. Despite the hard days you have endured, you never failed to support me and follow my progress in this long journey. Words cannot express my gratitude for having you in my life, without your sacrifices, continuous encouragement and support I won't be able to achieve this point. Finally, Big thanks to my dearest friends and mentors; Dr. Rabah, Dr. Hiba Faiz, Dr. Iman Abdeen for their ongoing support, love and belief in me. Your presence has been the most precious gift in my

life. There are many more dear people whose names may not be mentioned here, but each has made invaluable contributions to this journey. Without you, I would not be here.

Thank you all very much.

Yosra Lozon

Poster presentation:

1. Lozon, Y., McIntosh, K., Plevin, R. (2024). Protease activated receptor 2: a novel therapeutic drug target. Poster presented at 2nd AUU Health and biomedical postgraduate Symposium, Abu-Dhabi, UAE.

Abstract

Aim: Protease-activated receptor 2 (PAR2), a G protein-coupled receptor (GPCR) activated by endogenous proteases, plays a key role in inflammation and pain. AZ8838, a potent small-molecule PAR2 antagonist, has shown strong inhibition of PAR2-triggered intracellular signalling, although its comprehensive inhibitory profile remains unclear. Chronic prostatitis/chronic pelvic pain syndrome (CP/CPPS) is a common, yet poorly understood condition characterised by persistent pelvic pain and prostate inflammation, with limited insight into the underlying molecular mechanisms. This study aimed to characterize the PAR2 inhibitory effects of AZ8838 using *in vitro* cellular assays and investigate the involvement of PAR2 in prostate inflammation and pain using an *in vivo* carrageenan-induced prostatitis (CIP) model.

Methods: AZ8838 was characterised *in vitro* in NCTC2544-hPAR2/NF-κB-L, DU145 and HEK293 cells. Assays included NF-κB luciferase reporter activity, p65 nuclear translocation (immunofluorescence), ERK phosphorylation (Western blotting), intracellular Ca^{2+} assay and IL-8 release (ELISA). Receptor internalisation was assessed in DU145 cells transfected with PAR2-YFP. In the *in vivo* study, localised prostate inflammation and pelvic pain were induced in male Wistar rats by intraprostatic injection of 3% λ-carrageenan. Histological and molecular analyses of prostate and dorsal root ganglia (DRG) tissues were performed using haematoxylin and eosin (H&E) staining, immunofluorescence, qRT-PCR, and Western blotting to evaluate PAR2 expression and localisation. Pain behaviour was assessed using von Frey filaments (mechanical allodynia) and the Hargreaves test (thermal hyperalgesia).

Results: In this project, AZ8838 showed significant inhibition of trypsin- and 2fLIG-induced PAR2 cellular responses, including NF-κB reporter activity (IC_{50} = 0.06 μM;

95% CI 0.002 – 0.136 for trypsin, and IC_{50} = 0.38 μM; 95% CI 0.26 – 0.52 for 2fLIG), p65 nuclear translocation, ERK phosphorylation activity (IC_{50} = 15.54 μM; 95% CI 9.8 – 29.74 for trypsin, and IC_{50} = 9.83 μM; 95% CI 6.82 – 14.6 for 2fLIG), receptor internalisation, intracellular calcium mobilisation activity (IC_{50} = 0.78 μM; 95% CI 0.38 – 1.32 for 2fLIG), in a concentration-dependent manner in most experiments. In NCTC2544-hPAR2/NF-κB-L, AZ8838 significantly inhibited 2fLIG-induced IL-8 release (IC_{50} = 0.63 μM; 95% CI 0.15 – 1.0), whereas neither trypsin nor 2fLIG stimulated IL-8 release in DU145 prostate cells. In case of TNF-α induced NF-κB reporter activity, AZ8838 did not show the same inhibitory effect. For *in vivo* studies, PAR2 was significantly upregulated at the protein level in prostate tissue of CIP rats, whereas its mRNA expression was paradoxically downregulated, suggesting potential post-transcriptional regulation. Interestingly, no significant changes in PAR2 expression were observed in dorsal root ganglia (DRG), despite the pronounced pain behaviours. AZ8838 pretreatment significantly attenuated mechanical allodynia and thermal hyperalgesia. Histological analyses showed a weak reduction in prostate inflammation and leukocyte infiltration.

Conclusion: Overall, both the *in vitro* and *in vivo* studies results presented in this thesis provide a detailed PAR2 inhibition profile of AZ8838 and evidence for the involvement of PAR2 in prostate inflammation and pain, suggesting the therapeutic potential of PAR2 antagonism as a drug target in inflammatory pain conditions. Future studies are warranted to explore the broader mechanistic implications of PAR2 antagonism and the interaction of PAR2 with other key inflammatory and pain mediators relevant to CP/CPPS.

Table of Contents

Declaration ii
Acknowledgment iii
Poster presentation: v
Abstract vi
Table of Contents viii
List of abbreviations xii
List of Figures xiii
List of Tables xvi
Chapter 1 **Introduction** 1
1.1 Introduction 2
1.2 Pain as a biological alarm system 3
1.3 Mechanism of pain perception and pain pathways: 4
1.4 Inflammatory pain 7
1.4.1 Overview of inflammatory pain 7
1.4.2 Mechanisms of inflammatory pain: peripheral and central sensitisation 8
1.4.3 Neurogenic Inflammation 10
1.5 Prostate gland and Prostatic inflammation (prostatitis) 11
1.6 An overview of G-protein Coupled Receptors (GPCRs) 15
1.6.1 General structure and classification of GPCRs 16
1.6.2 Activation mechanism of GPCRs 18
1.6.3 G proteins: subtype-specific signalling 21
1.6.4 Inactivation and desensitisation of GPCR 25
1.7 Discovery of the unique activation mechanism of PARs 27
1.7.1 Mechanism of activation of PARs 29
1.7.2 Termination of PARs activity 32
1.8 An overview of PARs biological roles 34
1.9 PARs in inflammation 38
1.10 Protease activated receptor 2 (PAR2) 43
1.10.1 Structural features: 44
1.10.2 PAR2 activation and signalling: 45
1.10.3 Modulation of PAR2 signalling: 49
1.10.4 Agonists and antagonists for PAR2: 54
1.10.5 PAR2 role in inflammation: 65
1.10.6 PAR2 in prostate inflammation: 67
1.10.7 PAR2 and pain 68
1.11 Hypothesis and Aim: 73

Chapter 2 **Materials and Methods** 75
2.1 Materials and reagents 76
2.1.1 General reagents 76
2.1.2 Reagents for cell culture 80
2.1.3 Compound preparation 80
2.1.4 Equipment 81
2.1.5 Antibodies 82
2.2 Cell culture 82
2.2.1 NCTC2544-hPAR2/NF-κB-L cells 83
2.2.2 DU145 cells 84
2.2.3 Human embryonic kidney (HEK 293) cells 84
2.2.4 Cell cryopreservation and thawing (cell recovery) 85
2.3 Animals 85
2.3.1 Ethics and animal care 85
2.3.2 Drugs and reagents 86
2.3.3 Induction of inflammation 86
2.3.4 Perfusion fixation and sample collection 88
2.4 NF-κB-Luciferase reporter gene activity assay 90
2.5 Western Blotting 90
2.5.1 Preparation of whole cell lysates or tissue homogenates 90
2.5.2 Sodium Dodecyl Sulphate Polyacrylamide Gel Electrophoresis (SDS-PAGE) 91
2.5.3 Electrophoretic transfer of proteins samples 92
2.5.4 Membrane blocking and immunological detection of proteins 93
2.5.5 Membrane stripping and re-probing 94
2.5.6 Densitometric analysis of Western blots 95
2.6 FLUO-4 intracellular Calcium mobilization assay 95
2.7 PAR2-YFP transfection and internalization assay 96
2.8 ELISA for human IL-8 99
2.9 Immunofluorescence studies on cells and tissues 100
2.9.1 Immunofluorescence on cells 100
2.9.2 Quantitative nuclear colocalization analysis 101
2.9.3 Immunofluorescence on tissue sections 102
2.9.4 Fluorescence quantitative analysis 103
2.10 Histologic examination 103
2.11 RNA isolation and quantitative real time polymerase chain reaction (qRT-PCR). 104
2.12 Behavioral studies: 105
2.12.1 Mechanical allodynia assessment (Von frey filaments) 106
2.12.2 Thermal hyperalgesia assessment (Hangreaves' test) 107

2.12.3 Behavioral quantification 107
2.13 Data Analysis 108
Chapter 3 **Characterization of the PAR2 antagonist, AZ8838** 109
3.1 Introduction 110
3.1.1 Identification of AZ8838 small molecule PAR2 antagonist 110
3.1.2 Overview of AZ8838 PAR2 functional investigations 111
3.2 The effect of AZ8838 on PAR2 mediated NF-κB reporter activation 112
3.2.1 The effect of 2fLIG and trypsin on basal NF-κB reporter activity 112
3.2.2 AZ8838 effects on trypsin- and 2fLIG -induced NF-κB reporter activity. 116
3.2.3 The effect of AZ8838 on TNFα- induced NF-κB reporter activity 119
3.3 Effect of AZ8838 on PAR2-mediated p65 translocation in NCTC2544-hPAR2/NF-κB-L cells 123
3.3.1 The effect of 2fLIG on nuclear translocation of p65 in NCTC2544-hPAR2/NF-κB-L cells. 124
3.3.2 Effect of AZ8838 on PAR2-induced p65 nuclear translocation in NCTC2544-hPAR2/NF-κB-L cells. 129
3.4 The effect of AZ8838 on PAR2-induced phosphorylation of ERK1/2. 133
3.4.1 Effects of 2fLIG and trypsin on ERK phosphorylation in NCTC2544-hPAR2/NF-κB-L cells. 133
3.4.2 Effect of AZ8838 on PAR2-induced ERK phosphorylation in NCTC2544-hPAR2/NF-κB-L cells. 141
3.4.3 Effects of trypsin and 2fLIG on ERK phosphorylation in DU145 cells. 144
3.4.4 Effect of AZ8838 trypsin- and 2fLIG-induced ERK phosphorylation in DU145 cells. 151
3.5 Effect of AZ8838 on PAR2-induced intracellular calcium mobilization. 155
3.5.1 Effects of 2fLIG and trypsin on intracellular calcium mobilization. 155
3.5.2 Effect of AZ8838 on 2fLIG-induced intracellular Ca^{2+} mobilization. 159
3.6 Effect of AZ8838 on PAR2 internalization in DU145 cells. 162
3.6.1 Time and concentration effect on 2fLIG-mediated PAR2 internalization. 162
3.6.2 Effect of AZ8838 on 2fLIG-stimulated PAR2 internalization in PAR2-YFP-transfected DU145 cells. 168
3.7 Effects of AZ8838 on PAR2-mediated release of IL-8 in NCTC2544-hPAR2/NF-κB-L cells. 170
3.7.1 PAR2 activators' effect on IL-8 release in NCTC2544-hPAR2/NF-κB-L and DU145 cells. 170
3.7.2 Effect of AZ8838 on PAR2-stimulated release of IL-8 NCTC2544-hPAR2/NF-κB-L cells. 175
3.8 Discussion 177
3.8.1 Modulation of PAR2-induced NF-κB pathway activation and Ca^{2+} mobilization. 177

3.8.2 Modulation of MAP Kinase cascade (ERK1/2 phosphorylation) & PAR2 internalization. 180

3.8.3 Modulation of IL-8 levels. 184

3.9 Conclusion 185

Chapter 4 **Investigation of AZ8838 *in vivo* effects in prostate inflammation model** 186

4.1 Introduction 187

4.2 Carrageenan-induced prostatitis (CIP) causes significant weight loss, prostate enlargement, and histological changes. 188

4.3 Expression levels of PAR2 in prostate and lumbar/sacral DRGs: 195

4.3.1 Immunofluorescence reveals PAR2 upregulation in prostate but not DRG of CIP rats. 195

4.3.2 Significant changes in the expression of PAR2 in prostate, not DRG, of CAR-treated rats using qRT-PCR and Western blotting. 203

4.4 Behavioral assessment of PAR2 antagonist, AZ8838. 205

4.4.1 Mechanical allodynia assessment using von Frey filaments. 206

4.4.2 Thermal hyperalgesia assessment using Hargreave's (Plantar) test. 209

4.5 Discussion. 212

4.5.1 Carrageenan-induced prostatitis (CIP): inflammatory and pain components 212

4.5.2 AZ8838 ameliorates carrageenan-induced pain, with insignificant anti-inflammatory effects 219

4.5.3 Implications, study limitations and future directions 222

4.6 Conclusion 224

Chapter 5 **General Discussion** 225

5.1 Introduction 226

5.2 Mechanistic insights from *in vitro* and *in vivo* findings 228

5.3 AZ8838 as a PAR2 antagonist: mechanism of action in pain and inflammation 230

5.4 Study limitations, challenges and future directions 232

5.4.1 Study limitations and challenges in targeting PAR2 as a therapeutic strategy 232

5.4.2 Implications for CP/CPPS and future directions 234

5.5 General conclusion 235

Chapter 6 **References** 237

List of abbreviations

2fLIG	2-furoyl-LIGRLO-NH2
ANOVA	Analysis Of Variance
CHO-hPAR2	Chinese hamster ovary cells stably expressing human PAR2
CP/CPPS	Chronic prostatitis/ chronic pelvic pain syndrome
DMSO	Dimethyl sulfoxide
DNA	Deoxyribonucleic acid
DRG	Dorsal root ganglia
DU145	Epithelial cell isolated from the brain of a male with prostate cancer
EAP	Experimental autoimmune prostatitis model
EC_{50}	half-maximal effective concentration
ECL2	Extracellular loop 2
ELISA	Enzyme-Linked Immunosorbent Assay
ERK1/2	Extracellular signal-regulated kinase 1/2
GIT	Gastro-intestinal tract
GM-CSF	Granulocyte-macrophage colony-stimulating factor
HDM	Human dust mites
HEK293	Human embryonic kidney cells
hPBEC	Human primary bronchial epithelial cells
HT-29	Human colon adenocarcinoma cells
HUVEC	Human umbilical vein endothelial cells
IC_{50}	Half-maximal inhibitory concentrations
IL-1α	Interleukin 1α
IL-6	Interleukin 6
IL-8	Interleukin 8
IP3	Inositol triphosphate
LPS	Bacterial lipopolysaccharide
MAPK	Mitogen activated protein kinases
MC	Mander's coefficient
MCP-1	Monocyte chemoattractant protein-1
MCP-1/CCL2	Monocyte chemoattractant protein-1
mRNA	messenger RNA
NCTC2544-hPAR2/NF-κB-L	Human skin epithelial-like cell line stably co-expressing human PAR2 (hPAR2) and NF-κB-Luciferase
NF-κB	Nuclear factor-kappa B
PAR2	Protease-activated receptor 2
PAR2-AP	PAR2-activating peptides
PC	Pearson's coefficient
PLC	Phospholipase C
RFU	Relative fluorescence units
RNA	Ribonucleic acid
TM	Trans-membrane
TNFα	Tumour necrosis factor
YFP	Yellow fluorescent protein

List of Figures

FIGURE 1.1: SCHEMATIC ILLUSTRATION OF PAIN PERCEPTION AND PATHWAYS. 6
FIGURE 1.2: SCHEMATIC ILLUSTRATION OF THE ANATOMICAL LOCALISATION AND HISTOLOGY OF HUMAN PROSTATE 12
FIGURE 1.3: STRUCTURE OF A GPCR AND ITS HETEROTRIMERIC G PROTEIN COMPLEX 17
FIGURE 1.4: GPCR ACTIVATION MECHANISM. 19
FIGURE 1.5: GPCR DISTINCT GA-MEDIATED SIGNAL TRANSDUCTION MECHANISMS. 25
FIGURE 1.6: MECHANISMS OF GPCR DESENSITISATION. 26
FIGURE 1.7: MECHANISMS OF PROTEASE-ACTIVATED RECEPTOR (PAR) ACTIVATION 30
FIGURE 1.8: AN OVERVIEW OF THE MAIN BIOLOGICAL ROLES OF PARS IN DIFFERENT CELL TYPES 37
FIGURE 1.9: PARS ACTIVATION-MEDIATED INFLAMMATORY OR PROTECTIVE EFFECTS. 42
FIGURE 1.10: STRUCTURAL REPRESENTATION OF PAR2 WITH KEY INTERACTION SITES. 45
FIGURE 1.11: OVERVIEW OF PAR2 ACTIVATION AND SIGNAL TRANSDUCTION. 48
FIGURE 2.1: SCHEMATIC REPRESENTATION OF THE SURGICAL CUT LOCATION FOR THE MURINE PROSTATE INFLAMMATION INDUCTION MODEL 87
FIGURE 2.2: STEPS OF TRANSCARDIAL PERFUSION FIXATION IN A RAT. 89
FIGURE 2.3: ILLUSTRATIVE PAR2-YFP PLASMID MAP. 97
FIGURE 2.4: POLYEHTYLENEIMINE (PEI) TRANSFECTION. 98
FIGURE 2.5: TIMELINE OF BEHAVIOURAL STUDIES. 105
FIGURE 2.6: APPLICATION SITE FOR MECHANICAL AND THERMAL STIMULI 106
FIGURE 3.1: AZ8838 STRUCTURE AND BINDING TO PAR2 111
FIGURE 3.2: TIME-DEPENDENT ACTIVATION OF NF-KB REPORTER ACTIVITY INDUCED BY 2FLIG AND TRYPSIN IN NCTC2544-HPAR2/NF-KB-L CELLS. 113
FIGURE 3.3: CONCENTRATION-DEPENDENT INCREASE IN NF-KB REPORTER ACTIVITY INDUCED BY 2FLIG AND TRYPSIN IN NCTC2544-HPAR2/NF-KB-L CELLS. 115
FIGURE 3.4: CONCENTRATION RESPONSE CURVES OF NF-KB REPORTER ACTIVATION BY 2FLIG AND TRYPSIN IN NCTC2544-HPAR2/NF-KB-L CELLS. 116
FIGURE 3.5: INHIBITION OF PAR2-MEDIATED NF-KB REPORTER ACTIVITY BY AZ8838 IN NCTC2544-HPAR2/NF-KB-L CELLS. 118
FIGURE 3.6: AZ8838 CONCENTRATION-DEPENDENT INHIBITION OF PAR2-INDUCED NF-KB REPORTER ACTIVITY. 119
FIGURE 3.7: TIME- AND CONCENTRATION-DEPENDENT ACTIVATION OF NF-KB REPORTER ACTIVITY BY TNFA IN NCTC2544-HPAR2/NF-KB-L CELLS. 121
FIGURE 3.8: CONCENTRATION-RESPONSE CURVE OF TNFA INDUCED NF-KB REPORTER ACTIVITY IN NCTC2544-HPAR2/NF-KB-L CELLS. 122
FIGURE 3.9: AZ8838 HAS NO EFFECT ON TNFA-INDUCED NF-KB ACTIVATION IN NCTC2544-HPAR2/NF-KB-L CELLS 123
FIGURE 3.10: CONTROL FOR IMMUNOFLUORESCENCE LABELLING OF P65 IN NCTC2544-HPAR2/NF-KB-L CELLS 125
FIGURE 3.11: TIME-COURSE ANALYSIS OF P65 NUCLEAR TRANSLOCATION IN NCTC2544-HPAR2/NF-KB-L CELLS FOLLOWING STIMULATION WITH 2FLIG. 127
FIGURE 3.12: QUANTITATIVE COLOCALIZATION ANALYSIS OF NUCLEAR LOCALIZATION OF P65 IN 2FLIG STIMULATED NCTC2544-HPAR2/NF-KB-L CELLS. 129
FIGURE 3.13: AZ8838 INHIBITS 2FLIG-INDUCED P65 NUCLEAR TRANSLOCATION IN NCTC2544-HPAR2/NF-KB-L CELLS. 131
FIGURE 3.14: QUANTITATIVE COLOCALIZATION ANALYSIS OF NUCLEAR LOCALIZATION OF P65 IN NCTC2544-HPAR2/NF-KB-L CELLS IN RESPONSE TO 2FLIG ALONE AND AZ8838 CO-TREATMENT. 133
FIGURE 3.15: TIME COURSE OF 2FLIG-INDUCED ERK1/2 PHOSPHORYLATION IN NCTC2544-HPAR2/NF-KB-L CELLS 135

FIGURE 3.16: TIME COURSE OF ERK1/2 OF TRYPSIN-INDUCED PHOSPHORYLATION IN NCTC2544-HPAR2/NF-KB-L CELLS. 136
FIGURE 3.17: KINETIC ANALYSIS OF PAR2-MEDIATED ERK1/2 PHOSPHORYLATION IN NCTC2544-HPAR2/NF-KB-L CELLS. 137
FIGURE 3.18: CONCENTRATION-DEPENDENT PHOSPHORYLATION OF ERK1/2 BY 2FLIG IN NCTC2544-HPAR2/NF-KB-L CELLS. 138
FIGURE 3.19: CONCENTRATION DEPENDENT PHOSPHORYLATION OF ERK1/2 BY TRYPSIN IN NCTC2544-HPAR2/NF-KB-L CELLS. 139
FIGURE 3.20: CONCENTRATION-RESPONSE CURVES FOR PAR2-INDUCED ERK1/2 PHOSPHORYLATION IN NCTC2544-HPAR2/NFKB-L CELLS. 140
FIGURE 3.21: AZ8838 INHIBITS 2FLIG-INDUCED ERK1/2 PHOSPHORYLATION IN NCTC2544-HPAR2/NF-KB-L CELLS 142
FIGURE 3.22: AZ8838 WEAKLY INHIBITS TRYPSIN-INDUCED ERK1/2 PHOSPHORYLATION IN NCTC2544-HPAR2/NF-KB-L CELLS. 143
FIGURE 3.23: CONCENTRATION-RESPONSE CURVES OF AZ8838 AGAINST 2FLIG- AND TRYPSIN-INDUCED ERK1/2 PHOSPHORYLATION IN NCTC2544-HPAR2/NF-KB-L CELLS 144
FIGURE 3.24: TIME COURSE OF 2FLIG-STIMULATED ERK1/2 PHOSPHORYLATION IN DU145 CELLS 146
FIGURE 3.25: TIME COURSE OF TRYPSIN-STIMULATED ERK1/2 PHOSPHORYLATION IN DU145 CELLS 147
FIGURE 3.26: KINETICS OF 2FLIG- AND TRYPSIN-STIMULATED ERK1/2 PHOSPHORYLATION IN DU145 CELLS 148
FIGURE 3.27: CONCENTRATION-DEPENDENT 2FLIG-STIMULATED ERK1/2 PHOSPHORYLATION IN DU145 CELLS. 149
FIGURE 3.28: CONCENTRATION-DEPENDENT TRYPSIN-STIMULATED ERK1/2 PHOSPHORYLATION IN DU145 CELLS. 150
FIGURE 3.29: COMPARATIVE CONCENTRATION-RESPONSE CURVES FOR ERK1/2 PHOSPHORYLATION BY PAR2 AGONISTS IN DU145 CELLS. 151
FIGURE 3.30: AZ8838 INHIBITS 2FLIG-INDUCED ERK1/2 PHOSPHORYLATION IN DU145 CELLS 152
FIGURE 3.31: AZ8838 DOES NOT ALTER TRYPSIN-INDUCED ERK1/2 PHOSPHORYLATION IN DU145 CELLS. 153
FIGURE 3.32: AZ8838 SELECTIVELY INHIBITS 2FLIG-INDUCED ERK1/2 PHOSPHORYLATION IN DU145 CELLS. 154
FIGURE 3.33: CONCENTRATION-DEPENDENT 2FLIG-STIMULATED INTRACELLULAR Ca^{2+} MOBILISATION IN HEK293 CELLS. 157
FIGURE 3.34: CONCENTRATION-DEPENDENT TRYPSIN-STIMULATED INTRACELLULAR Ca^{2+} MOBILISATION IN HEK293 CELLS. 158
FIGURE 3.35: COMPARATIVE CONCENTRATION-RESPONSE CURVES FOR 2FLIG- AND TRYPSIN-STIMULATED INTRACELLULAR Ca^{2+} MOBILISATION IN HEK293. 159
FIGURE 3.36: INHIBITION OF 2FLIG-STIMULATED INTRACELLULAR Ca^{2+} MOBILISATION BY AZ8838 IN HEK293 CELLS. 161
FIGURE 3.37: AZ8838 INHIBITS OF 2FLIG-INDUCED INTRACELLULAR Ca^{2+} MOBILISATION IN HEK293 CELLS. 161
FIGURE 3.38: VALIDATION OF PAR2-YFP TRANSFECTION IN PAR2-YFP-TRANSFECTED DU145 CELLS. 163
FIGURE 3.39: TIME COURSE OF PAR2 INTERNALIZATION IN PAR2-YFP-TRANSFECTED DU145 CELLS UPON 10 µM 2FLIG STIMULATION. 166
FIGURE 3.40: CONCENTRATION EFFECT ON PAR2 INTERNALISATION IN PAR2-YFP-TRANSFECTED DU145 CELLS FOLLOWING 30-MINUTE 2FLIG TREATMENT. 167
FIGURE 3.41: AZ8838 EFFECTS ON 2FLIG-INDUCED PAR2-INTERNALISATION IN PAR2-YFP-DU145 CELLS. 169
FIGURE 3.42: EFFECT OF PAR2 AGONISTS ON IL-8 LEVELS 172

FIGURE 3.43: CONCENTRATION-DEPENDENT 2FLIG-INDUCED IL-8 RELEASE IN NCTC2544-HPAR2/NF-KB-L. 174
FIGURE 3.44: AZ8838 INHIBITS 2FLIG-INDUCED IL-8 RELEASE IN NCTC2544-HPAR2/NF-KB-L CELLS. 176
FIGURE 4.1: HISTOLOGICAL EVALUATION OF PROSTATE TISSUE AT DIFFERENT TIME POINTS FOLLOWING CIP INDUCTION. 189
FIGURE 4.2: GROSS MORPHOLOGIC AND HISTOLOGIC CHANGES IN RAT PROSTATE (H&E STAIN, ×10). 191
FIGURE 4.3: HIGH-MAGNIFICATION HISTOLOGICAL IMAGES OF PROSTATE TISSUES FROM DIFFERENT TREATMENT GROUPS 192
FIGURE 4.4: HISTOLOGICAL EVALUATION OF PROSTATE INFLAMMATION REVEALS LIMITED ANTI-INFLAMMATORY EFFECT OF AZ8838 PRETREATMENT. 194
FIGURE 4.5: CONFIRMATION OF PAR2 EXPRESSION IN SENSORY NEURONS USING NEUN IN DRG SECTIONS. 196
FIGURE 4.6: LOCALISATION OF PAR2 IN THE NEURONS OF THE DORSAL ROOT GANGLIA (DRG) 198
FIGURE 4.7: CARRAGEENAN DO NOT ALTER NEURONAL PAR2 EXPRESSION COMPARED TO SHAM (SAL) GROUP. 199
FIGURE 4.8: SEMI-QUANTITATIVE ANALYSIS OF IF IMAGES SHOWING NO CHANGE IN PAR2 EXPRESSION IN DRGS BETWEEN THE CAR-TREATED GROUP AND THE SHAM (SAL) GROUP. 200
FIGURE 4.9: LOCALISATION OF PAR2 IN RAT PROSTATE TISSUE SECTIONS. 201
FIGURE 4.10: CAR-TREATMENT ENHANCED PAR2 EXPRESSION IN PROSTATE TISSUE COMPARED TO THE SHAM (SAL) GROUP. 202
FIGURE 4.11: PAR2 EXPRESSION INCREASED IN PROSTATE TISSUE OF THE CAR-TREATED GROUP COMPARED TO THE SHAM (SAL) GROUP, AS INVESTIGATED BY IMMUNOFLUORESCENCE. 203
FIGURE 4.12: CARRAGEENAN-INDUCED INFLAMMATION DECREASES PAR2 MRNA EXPRESSION, WITH NO SIGNIFICANT ALTERATIONS IN DRG 204
FIGURE 4.13: CARRAGEENAN-TREATMENT INCREASES PAR2 PROTEIN EXPRESSION IN PROSTATE, WITH NO SIGNIFICANT ALTERATIONS IN DRG 205
FIGURE 4.14: AZ8838 TREATMENT ALLEVIATES CARRAGEENAN (CAR)-INDUCED MECHANICAL ALLODYNIA IN THE PROSTATE INFLAMMATION MODEL. 209
FIGURE 4.15: AZ8838 REDUCES CARRAGEENAN (CAR)-INDUCED THERMAL HYPERALGESIA ASSESSED BY THE HARGREAVES TEST. 212

List of Tables

TABLE 1.1: NATIONAL INSTITUTES OF HEALTH (NIH) CONSENSUS DEFINITION AND CLASSIFICATION OF PROSTATITIS (KRIEGER, NYBERG AND NICKEL, 1999).....13
TABLE 1.2: THE FOUR FAMILIES OF GA-PROTEINS SUBUNIT ISOFORMS (MANNING AND BLUMENTHAL, 2023). 21
TABLE 1.3: PAR TETHERED LIGANDS AND PAR-SELECTIVE AGONIST PEPTIDES (RAMACHANDRAN ET AL., 2012) 32
TABLE 1.4: LIST OF ACTIVATING AND DISARMING PROTEASES OF PAR2.....55
TABLE 1.5: PAR2 AGONISTS AND ANTAGONISTS.....61
TABLE 2.1: LIST OF MATERIALS AND REAGENTS USED FOR IN VITRO STUDIES 76
TABLE 2.2: LIST OF PHARMACOLOGICAL AGONISTS OR ANTAGONISTS FOR *IN VITRO* STUDIES 78
TABLE 2.3: LIST OF MATERIALS AND REAGENTS USED FOR *IN VIVO* STUDIES. 78
TABLE 2.4: LIST OF PHARMACOLOGICAL AGONISTS OR ANTAGONISTS FOR *IN VIVO* STUDIES 79
TABLE 2.5: LIST OF REAGENTS USED FOR CELL CULTURE.....80
TABLE 2.6: LIST OF PREPARED SOLUTIONS 80
TABLE 2.7: LIST OF EQUIPMENT.....81
TABLE 2.8: LIST OF ANTIBODIES.....82
TABLE 2.9: CELL LINES USED WITH RESOURCES.....83
TABLE 3.1: *IN VITRO* PHARMACOLOGY OF AZ8838 177
TABLE 4.1: EFFECTS OF AZ8838 ON CARRAGEENAN-INTRAPROSTATIC INJECTION-INDUCED CHANGES ON BODY WEIGHT, PROSTATIC WET WEIGHT, AND THE PROSTATIC INDEX.....189

Chapter 1

Introduction

1.1 Introduction

Inflammation is a fundamental defence mechanism against noxious stimuli that has been well-studied since ancient times. The hallmark signs of inflammation; redness, heat, swelling, pain, and in cases of persistent inflammation, loss of function, are the well-documented physiological changes that occur regardless of the affected tissue (Actor, 2019). Among these signs, pain is estimated to be the most common reason for adults to seek medical care (Todd et al., 2007, Dahlhamer et al., 2018, Finley et al., 2018). Pain affects not only physical health and work productivity, but is also associated with adverse social, psychological and general quality of life outcomes (Kawai et al., 2017, Landmark et al., 2024). Interestingly, while pain can negatively impact psychosocial well-being, evidence also suggests that certain psychosocial factors, like sleeplessness, depression, anxiety, tiredness, and a body mass index (BMI greater than 30, can predict chronic pain incidence and spread across multiple body sites as demonstrated by a recent data-driven prognostic model (Tanguay-Sabourin et al., 2023). Advances in cell biology and microscopy in the 19th century raised a cell-based definition of inflammation that was recognized by altered cellular populations due to local vascular sources and tissue proliferation (Scott et al., 2004). The progressive cellular and molecular research revealed a complex network of signals exchanged between affected tissues and immune cells. Pain is a cardinal sign of inflammation, but a complex interplay between psychological and biological factors. One of the main triggers of inflammatory pain is the pro-inflammatory mediators such as prostaglandins, cytokines, chemokines, neuropeptides, proteases and growth factors that are liberated at sites of inflammation and capable of sensitising peripheral pain-sensing neurons (Basbaum et al., 2009, Nagaraja et al., 2023). Nociception is the

process of detection of mechanical, thermal and chemical stimuli via these specialized peripheral nerves known as nociceptors (Woolf and Ma, 2007, Basbaum et al., 2009). The cell bodies of nociceptors in the human body are located in dorsal root ganglia (DRG), while the cell bodies of face nociceptors lie in the trigeminal ganglion. During inflammation, neural response to noxious stimuli is enhanced or prolonged, a phenomenon known as hyperalgesia. Also, neurons may respond even to innocuous stimuli (allodynia) or may trigger or enable pain to spread to tissues distinct from the site of inflammation (secondary hyperalgesia). This hypersensitive state of nociceptors could be explained as a result of neural plasticity, an adaptive state to chronic exposure to nociceptive stimuli (Latremoliere and Woolf, 2009).

1.2 Pain as a biological alarm system

The International Association for the Study of Pain (IASP) defines pain as "an unpleasant sensory and emotional experience associated with, or resembling that associated with, actual or potential tissue damage" (Raja et al., 2020). While often regarded as a negative experience, pain is essential for survival, preventing further injury and promoting recovery. Acute pain serves as a biological alarm system, by prompting immediate protective actions to prevent further injury by signalling potential or actual tissue damage. Patients with congenital insensitivity to pain, who lack the ability to perceive these warning signals, are at a high risk of self-hurt and severe injuries due to their inability to detect harmful stimuli (Goodwin and McMahon, 2021). On the other hand, chronic pain persists beyond the normal healing process, lasting more than three months (Treede et al., 2019), and mostly contributes to tissue damage. Overall, pain can be categorised as nociceptive pain, neuropathic pain and nociplastic pain (Cao et al., 2024). Nociceptive pain represents the physiological

protective system and is the pain associated with non-neural tissue damage and mediated through the activation of nociceptors (IASP, 2021). Inflammatory pain is the predominant representative of this pain category and occurs in response to tissue damage and subsequent immune activation, encouraging rest and recovery by discouraging movement that could exacerbate injury. It is induced through the release of inflammatory molecules like prostaglandins, cytokines, and bradykinin, which sensitise nociceptors (Cao et al., 2024). Neuropathic pain arises from direct damage to the somatosensory nervous system, including central or peripheral fibres, often leading to chronic pain conditions like diabetic neuropathy and postherpetic neuralgia (Treede et al., 2008). Nociplastic pain is a distinct category of chronic pain, differentiated from nociceptive and neuropathic pain, as it occurs without clear organic lesions, nociceptor activation or identifiable neuropathic damage. However, it presents with clinical features indicative of altered nociceptive function (Fitzcharles et al., 2021).

1.3 Mechanism of pain perception and pain pathways:

Nociception, or perception of pain, is the neural processing of noxious stimuli. Several molecules, cells and neural tissue are involved in the process of pain perception, transmission and modulation (Figure 1.1). Peripheral nociceptive neurons serve as the primary initiators of pain sensation, detecting harmful stimuli and converting them into electrical signals. Their nerve endings are distributed across various peripheral tissues, including skin, muscles, joints, and internal organs, while their cell bodies reside in dorsal root ganglia (DRG) and the trigeminal ganglion. IASP defines these neurons as “high-threshold”, distinguishing them from other sensors to ensure that normal tactile sensations are perceived without triggering pain (IASP, 2021). At the molecular level, the nociceptive terminals express a wide range of ion channels and G-protein coupled

receptors (GPCRs) that perceive external stimuli and trigger neural excitability. Key pain-transducing ion channels and receptors include transient receptor potential (TRP) channels, purinergic receptor (P2X) channels and Acid-sensing ion channels (ASICs) all of which detect and amplify pain signals (De Logu and Geppetti, 2019). Additionally, voltage-gated sodium channels (VGSCs) and voltage-gated calcium channels (VGCCs), respond to voltage changes induced by the ion current across the membrane and propagate these signals as a series of action potentials (Park and Luo, 2010, Goodwin and McMahon, 2021). Alongside ion channels, GPCRs are essential modulators of pain-related signalling and control pain transmission through μ-, δ-, κ-opioid receptors, CB1 and CB2 cannabinoid receptors, the calcitonin gene-related peptide (CGRP) receptor complex (CLR/RAMP1: calcitonin receptor-like receptor/ receptor activity–modifying protein 1), protease-activated receptor 2 (PAR2), chemokine receptors such as CCR2/ CXCR4, and prostaglandin EP2 and EP4 (Uniyal et al., 2023). These receptors exert a global effect on pain involving neuronal excitability, inflammatory response, neurotransmitter release, and intercellular communication (Doyen et al., 2020).

The detected pain signal is transmitted to the spinal cord via primary nociceptive fibres of two main types: myelinated Aδ fibres, conducting sharp, localised pain rapidly, and unmyelinated C fibres, conducting slow, burning, diffuse pain. At the dorsal horn of the spinal cord, the primary afferent neurons relay their signals to secondary afferent neurons, which cross to the contralateral side of the spinal cord and ascend primarily via the spinothalamic tract towards the brainstem and thalamus. The thalamus serves as a relay centre, from which third-order central neurons transmit pain signals to the primary somatosensory cortex. It represents the central hub for perception of pain, its

localisation and determining pain intensity, while the central amygdala and prefrontal cortex contribute to the affective and cognitive aspects of pain perception. The spinothalamic tract conveys pain signals from limbs and visceral organs, whereas the trigeminothalamic tracts transmit pain from the head and face, making these two fundamental pathways to pain transmission (Cao et al., 2024).

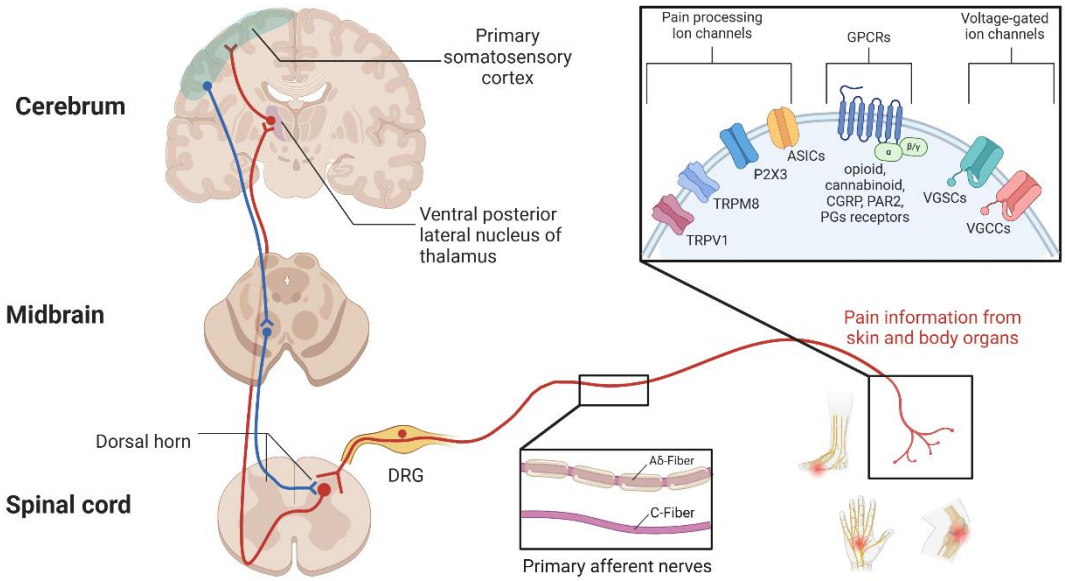

Figure 1.1: Schematic illustration of pain perception and pathways.
Pain perception in skin and other organs is mediated through nociceptive neuronal terminals (in box, right). The inset depicts represent the main ion channels and receptors involved in nociception, showing the pain-processing ion channels (e.g., TRPV1, TRPM8, ASICs, P2X3), G-protein coupled receptors (GPCRs) (e.g., opioid, cannabinoid, CGRP, PAR2, prostaglandin receptors), and voltage-gated ion channels (e.g., VGSCs, VGCCs) in pain signal processing, transduction and modulation. Primary afferent nociceptive fibres, including Aδ-fibres (fast, sharp localised pain) and C-fibres (slow, burning diffuse pain), detect noxious stimuli in peripheral tissues and relay signals to the dorsal root ganglion (DRG). The signals propagated in the dorsal horn of the spinal cord, where secondary neurons cross to the contralateral side and ascend mainly via the spinothalamic tract (STT) through the midbrain to the ventral posterior lateral nucleus of the thalamus. From the thalamus, tertiary neurons project pain signals to the primary somatosensory cortex, where pain perception, localisation, and intensity processing occur. The ascending pathway is depicted as red neurons, while the descending regulatory (inhibition or facilitation) pathways are depicted as blue neurons. *Abbreviations*: acid-sensing ion channels (ASICs), purinergic P2X3 receptors, transient receptor potential vanilloid 1 (TRPV1), and melastatin 8 (TRPM8), G-protein coupled receptors (GPCRs), calcitonin gene-related peptide (CGRP), protease-activated receptor 2 (PAR2), prostaglandin (PGs) receptors, voltage-gated sodium channels (VGSCs) and voltage-gated calcium channels (VGCCs). This figure was created using Biorender.com.

In addition to ascending transmission, several brain areas engage in pain modulation through descending inhibitory or facilitatory pathways, maintaining a balance under normal conditions (blue tract in Figure 1.1). Structures like the periaqueductal gray (PAG) and the rostral ventromedial medulla (RVM) participate in the inhibitory descending system, suppressing nociceptive information through different mechanisms, including the release of endogenous opioids like endorphins and enkephalins that suppress pain signals (Huang et al., 2019). Conversely, the anterior cingulate cortex (ACC), besides the RVM, also contributes to the facilitatory descending system, which enhances responses to noxious stimuli by reducing pain thresholds (Lockwood and Dickenson, 2020). This pain modulation mechanism provides the scientific basis for analgesic treatments such as opioids, which mimic endogenous pain inhibitors, and nonsteroidal anti-inflammatory drugs (NSAIDs), which reduce inflammation-induced pain by blocking prostaglandin production.

1.4 Inflammatory pain

1.4.1 Overview of inflammatory pain

As discussed in Section 1.2, inflammatory pain is considered a representative of nociceptive pain. While acute inflammatory pain serves as a critical physiological response to prevent further damage, chronic inflammatory pain can become maladaptive, pathological, constituting a major burden on societies (Cohen et al., 2021, Schoenfeld et al., 2024). If pain persists typically beyond three months, as outlined by the International Classification of Diseases, 11th edition (ICD-11), it is identified as chronic and pathological (Treede et al., 2019). Inflammatory pain is characterised by a general enhanced responsiveness of nociceptive neurons, presented as increased pain

intensity and duration due to noxious stimuli (hyperalgesia) and the pain perception from normally non-painful stimuli (allodynia) (IASP, 2021). This occurs as a result of direct activation or sensitisation (modulatory) of these neurons by inflammatory mediators released by immune cells (e.g., prostaglandins, bradykinin, and cytokines such as TNF-α and IL-1β) or by neuron itself (e.g., substance P and CGRP), leading to a reduced excitability threshold and enhanced sensitivity, a state known as peripheral sensitisation, which causes primary hyperalgesia. Secondary hyperalgesia, which occurs in tissue surrounding but not directly affected by the noxious stimuli (e.g., increased pain sensitivity in area of skin adjacent to a burn or around an inflamed joint), and allodynia, where normally innocuous stimuli become painful (e.g. light touch causing pain in nerve injury or post-herpetic neuralgia), arise from persistent harmful stimuli that induce long-term changes within the CNS. These changes alter the interpretation of sensory inputs, a state known as central sensitisation (Vardeh and Naranjo, 2017).

1.4.2 Mechanisms of inflammatory pain: peripheral and central sensitisation

At the core of inflammatory pain is the release of pro-inflammatory mediators from immune cells, damaged tissues, and activated neurons at the site of injury. These mediators include cytokines (e.g., TNF-α, IL-1β, IL-6), chemokines (e.g., CCL2, CXCL1, CXCL8), prostaglandins, bradykinin, proteases, neuropeptides, growth factors and ATP, all of which contribute to peripheral sensitisation. The underlying mechanism of peripheral sensitisation involves posttranslational modification, mainly phosphorylation, of ion channels at nerve terminals and long-term transcriptional changes of pain-processing ion channels, receptors, or other proteins within DRG contained cell bodies (Vardeh and Naranjo, 2017). Certain inflammatory mediators

exert their effect by stimulating GPCRs, triggering intracellular signalling cascade that leads to protein kinase A (PKA) and protein kinase C (PKC) mediated phosphorylation of key ion channels involved in pain perception and transmission. Commonly involved ion channels in this sensitisation include TRPV1, TRPV4, voltage-gated sodium (VGSCs) and calcium channels (VGSCs), that become hyperexcitable upon phosphorylation, leading to amplified pain signalling (Amadesi et al., 2006, Laedermann et al., 2015, Huang and Zamponi, 2017).

Sustained pain signals mediate a state of central sensitisation that leads to enhanced release of excitatory neurotransmitters, including glutamate and substance P, in the spinal dorsal horn. Glutamate activates postsynaptic α-amino-3-hydroxy-5-methyl-4-isoxazolepropionic acid (AMPA) and N-methyl-D-aspartate (NMDA) receptors, leading to Ca^{2+} influx and downstream activation of kinases like calcium/calmodulin-dependent protein kinase II (CaMKII), PKC, and mitogen-activated protein kinase (MAPK), leading to phosphorylation of ion channels and transcriptional changes that increase neuronal excitability. Neurokinin-1 (NK1) receptors are activated by substance P, further amplifying excitatory signalling by prolonging the depolarisation state, and contribute to long-term synaptic plasticity (Salter and Woolf, 2005). Collectively, these receptor-mediated events increase pain intensity and duration (Matsuda et al., 2019). Repetitive C-fibre signals induce progressively increased dorsal horn output, a phenomenon known as wind-up, which reflects short-term NMDA-dependent temporal plasticity that does not outlast the duration of the prolonged stimuli (Vardeh and Naranjo, 2017). Other mechanisms of central sensitisation include heterosynaptic potentiation, where subthreshold non-painful stimuli, such as light touch, activate pain pathways, causing allodynia. In addition, persistent pain signals

may induce glial cell activation or modulation in the spinal cord, particularly microglia and astrocytes, contributing to maintenance of chronic inflammatory pain (Baral et al., 2019). Activated glial cells can release pro-inflammatory cytokines (e.g., TNF-α, IL-1β) and chemokines (e.g., CCL2, CXCL1), enhancing nociceptive signalling. Prolonged peripheral inflammation also alters descending pain modulation pathways, that typically function to suppress excessive nociceptive input. This system becomes dysregulated, leading to a shift toward descending facilitation, where pain signals are amplified rather than suppressed. This contributes to the transition from acute to chronic pain, making pain persist even after the initial inflammatory insult has resolved.

1.4.3 Neurogenic Inflammation

An important subtype of inflammatory pain conditions is neurogenic inflammation, in which the activation of nociceptive sensory neurons drives the inflammatory process. Peripheral terminals of C-fibres release neuropeptides such as substance P and CGRP that act on endothelial cells, mast cells and immune cells, amplifying inflammation through multiple receptor-mediated mechanisms. Substance P activates the NK1 receptors on mast cells and endothelial cells, leading to mast cell degranulation, plasma extravasation, and leukocyte adhesion. CGRP, acting through CLR/RAMP1 receptor complex, induces potent vasodilation and recruitment of immune cells to the site of inflammation. Stimulation of TRPV1 and TRPA1 ion channels on sensory neurons further enhances neuropeptides release. Additionally, proteases liberated by mast cell degranulation activates PAR2, triggering further release of SP and CGRP and reinforcing the inflammatory loop (Marek-Jozefowicz et al., 2023). Neurogenic

inflammation is implicated in conditions such as migraine, complex regional pain syndrome (CRPS), atopic dermatitis and other chronic inflammatory diseases.

Several chronic inflammatory conditions are associated with persistent pain, including arthritis, inflammatory bowel disease and chronic pelvic pain syndromes. Among these, chronic pelvic pain syndromes constitute one of the common causes of chronic pain in males. In the next section, prostatic inflammation will be explored, including its classification, with a particular focus on chronic prostatitis/chronic pelvic pain syndrome (CP/CPPS), examining its pathophysiology, nociceptive pathways, and current therapeutic approaches.

1.5 Prostate gland and Prostatic inflammation (prostatitis)

The prostate is a walnut-sized gland in men that is part of the male reproductive system. It is located just below the bladder, surrounding the urethra (Figure 1.2). Its secretions are crucial for nourishment and transport of sperm. The gland is composed of glandular tissue, that is the secretory acini, which produces the prostatic fluid. The acini are supported with fibromuscular stroma that facilitate the expel of the fluids through the ducts to urethra (Oelke, 2020).

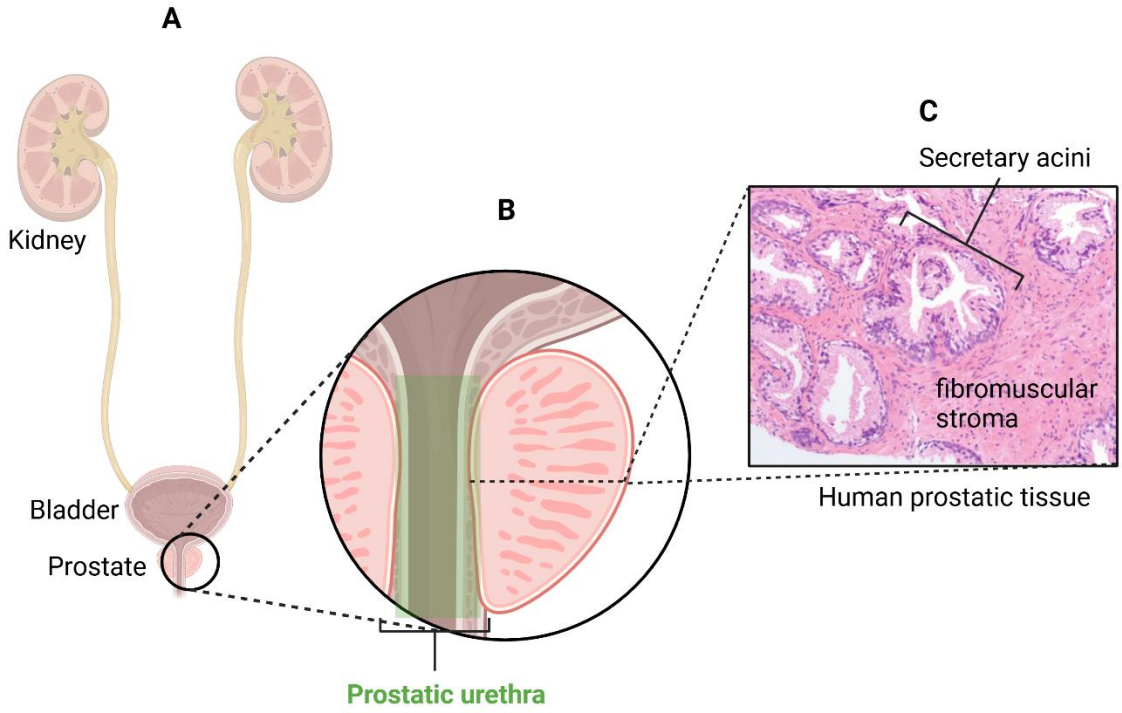

Figure 1.2: Schematic illustration of the anatomical localisation and histology of human prostate. **A:** illustrates the urinary system and the location of the prostate below the bladder. **B**: provides a close-up of the prostate with the prostatic urethra highlighted in green. **C:** shows the histological structure of the human prostate, displaying the secretory acini and fibromuscular stroma. This illustration was created using Biorender.com, and the prostate section was adopted from (Shah and Zhou, 2019).

Prostatitis describes a group of painful inflammatory conditions affecting the prostate gland, which may or may not involve bacterial infection. In some cases, inflammation may extend to areas surrounding the prostate (Krieger et al., 2008, NIDDK, 2014). Prostatic inflammatory conditions could be acute or chronic and are classified based on their aetiology. In 1994, the National Institutes of Health (NIH) established a consensus classification system to categorise different types of prostatitis based on symptoms and underlying causes, creating four distinct clinical categories (Krieger et al., 1999). Among these, acute and chronic bacterial prostatitis are the best understood, though they account for only 5-10% of all symptomatic cases (Davis NG, 2025). The majority of prostatitis cases are diagnosed as chronic prostatitis/chronic pelvic pain syndrome (CP/CPPS), category III (Table 1.1), which is a painful condition without

infectious origin (Murphy et al., 2009). According to a meta-analysis for the prevalence of chronic pain in low and middle-income countries, chronic pelvic/prostatitis pain accounts for 4% (95% CI 0-14) in the general population (Jackson et al., 2016). It is estimated that up to 25% of men will be diagnosed with prostatitis in their lifetime (Zhang et al., 2019). Several studies reported that 50% of the male population experience CP/CPPS-related symptoms at some point of their lives (Zhang et al., 2020a). A recent cross-sectional study found that the prevalence of chronic prostatitis exceeded 35% of the study sample, accounting for over 89% of all reported cases of prostatic inflammatory conditions documented over a 4-year study period (Prince Kasongo et al., 2024).

Table 1.1: National Institutes of Health (NIH) consensus definition and classification of prostatitis (Krieger, Nyberg and Nickel, 1999).

NIH classification	Definition
Category I: acute bacterial prostatitis	Acute infection of the prostate gland
Category II: chronic bacterial prostatitis	Recurrent infection of the prostate
Category IIIA: Inflammatory CPPS	White cells in semen/EPS/VB3 (VB3 or post-prostatic massage)
Category IIIB: non-inflammatory CPPS	No white cells in semen/EPS/VB3
Category IV: asymptomatic inflammatory prostatitis	Abnormal semen analysis Elevated PSA values Incidental findings in the biopsied prostate
*Abbreviations: **CPPS**: chronic pelvic pain syndrome; **EPS**: expressed prostatic secretions; **VB3**: voided bladder urine culture 3; **PSA**: prostatic-specific antigen.*	

CP/CPPS remains a complex and poorly understood condition with no clear aetiology. It is still debatable whether it stems from an inflammatory process or is primarily a neuromuscular pain disorder (Potts and Payne, 2007). Multiple factors, including inflammation, neurogenic pain, and psychosocial influences, are all considered potential contributors to the disease and research in this area remains ongoing (Ma et al., 2025). The condition is characterized by chronic pelvic pain, testicular discomfort,

painful ejaculation and voiding difficulties, often resulting in genitourinary symptoms (Marszalek et al., 2007, Pontari, 2025).

Owing to the ambiguous nature of the disease, treatment has primarily focused on symptomatic management rather than addressing an underlying cause. In response to this gap, an expert panel developed the NIH-Chronic Prostatitis Symptom Index (NIH-CPSI), a 13-item questionnaire based on scoring symptoms in three domains: pain, urinary symptoms and quality of life (Litwin et al., 1999). This tool has been validated as an outcome measure for monitoring treatment efficacy (Clemens et al., 2009, Wagenlehner et al., 2013). A multicentred cohort study demonstrated that pain frequency and severity, regardless of its location/type, have the greatest impact on quality of life for CP/CPPS patients, which brings a huge burden to the patient and society (Wagenlehner et al., 2013). Current management of CP/CPPS is multimodal and tailored to the patient phenotype (Nickel and Shoskes, 2010). In the United Kingdom (UK), clinical practice is guided primarily by the Prostate Cancer UK/ Prostatitis Expert Reference Group (PERG) consensus guideline published in 2015 (Rees et al., 2015). This guideline emphasises a multimodal approach, rather than a single standard pathway, and discourages repeated antibiotic use in the absence of documented infection. Pharmacological options include α-adrenergic receptor blockers such as tamsulosin or alfuzosin in men with voiding symptoms, together with non-steroidal anti-inflammatory drugs (NSAIDs) such as ibuprofen, naproxen or celecoxib for pain relief. Short courses of antibiotics (e.g., ciprofloxacin, ofloxacin or doxycycline) are reserved for patients with a clear clinical suspicion of bacterial infection. In patients whose pain persists, second-line strategies may be considered, including neuromodulators such as amitriptyline, gabapentin or pregabalin. In selected

men with co-existing benign prostatic hyperplasia, 5-α-reductase inhibitors (like finasteride or dutasteride) may be used. In agreement with other guidelines, multidisciplinary care is recommended, including physical and cognitive therapy (Polackwich and Shoskes, 2016, Pontari, 2025). Recent advancements in understanding CP/CPPS have directed management goals towards a comprehensive, individualised treatment approach. The UPOINT classification system—urinary, psychosocial, organ-specific, infection, neurologic/systemic, and tenderness domains—offers an all-inclusive approach for diagnosis and treatment, emphasising the need to treat all contributing factors, including psychological stress and pelvic floor dysfunction (Cai et al., 2024). This holistic approach, incorporating physical therapy, medications, and psychological support, is a promising strategy, especially in complex cases, leading to improved symptom management and quality of life.

1.6 An overview of G-protein Coupled Receptors (GPCRs)

GPCRs constitute the largest family of membrane proteins identified and serve as a major drug target. This class of membrane receptors accounts for 4% of human genes (Kooistra et al., 2021) and 13% of membrane proteins (Muratspahić et al., 2019). From over 800 identified GPCRs, at least 108 are targets of ~34% of FDA approved drugs (Hauser et al., 2018). They are macromolecules that exhibit a seven-transmembrane α-helical motif and are mainly situated in the cell-surface membrane. GPCRs are engaged in cell communication recognizing large number of paracrine and endocrine signals besides sensations including smell, taste and vision (Dalesio et al., 2018). GPCRs are highly dynamic mediating multiple biological functions of signal transduction, initiated by a wide range of extracellular stimuli, including photons, ions, lipids, neurotransmitters, hormones, peptides, and odorants (Latorraca et al., 2017).

1.6.1 General structure and classification of GPCRs

GPCRs share a conserved structural framework consisting of seven transmembrane (7TM) helices, interconnected by three intra- (ICL1-3) and three extracellular loops (ECL1-3) besides an extracellular N-terminal and an intracellular C-terminal (Figure 1.3The extracellular part is responsible for ligand binding as a means of transmitting extracellular signals, while the intracellular part is responsible for interacting with heterotrimeric G-protein, arrestins and G protein-coupled receptor kinases (GRKs) (Rosenbaum et al., 2009). G-protein (GTP-binding protein) is the principal switch connecting the receptor with second messenger-generating enzymes (Lefkowitz, 2013). It consists of three subunits (α, β, γ) anchored to the inner membrane surface by lipid modifications (Zhang et al., 2004). In its inactive (basal) state, G_α binds a guanosine diphosphate (GDP).

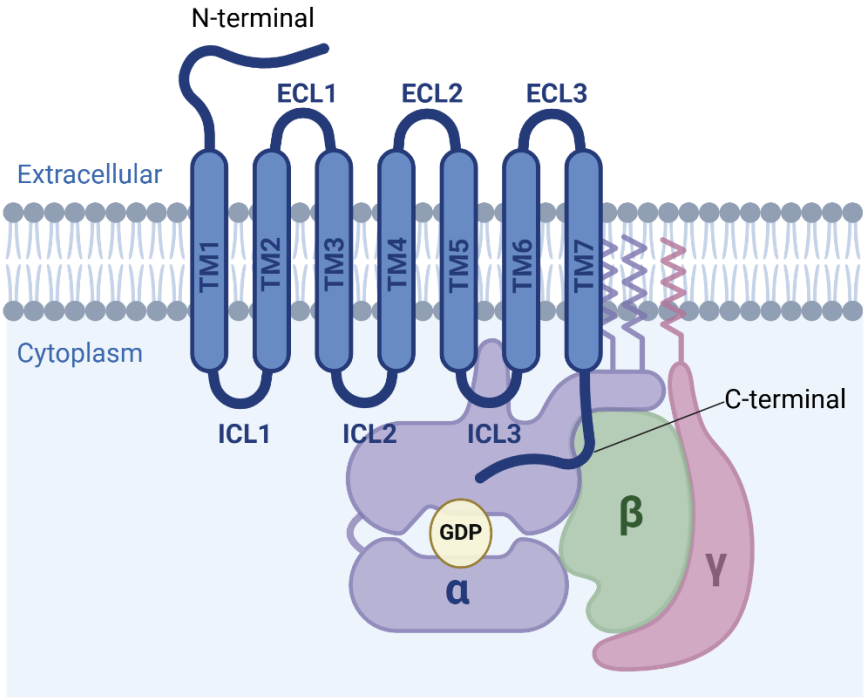

Figure 1.3: Structure of a GPCR and its heterotrimeric G protein complex.
A schematic representation showing the typical structure of a GPCR, consisting of seven-transmembrane (7TM) α-helical domains embedded within the cell membrane. The extracellular region consists of an N-terminal extracellular domain, three extracellular loops (ECL1, ECL2, and ECL3), while the intracellular domain consists of three intracellular loops (ICL1, ICL2, and ICL3), and a C-terminal. The C-terminal region interacts with the heterotrimeric G protein complex, composed of Gα, Gβ, and Gγ subunits linked to the inner membrane. In its inactive state, the Gα subunit is bound to guanosine diphosphate (GDP). Upon receptor activation, GDP is exchanged for guanosine triphosphate (GTP), leading to the dissociation of the Gα subunit from the Gβγ dimer, initiating downstream signalling cascades. (Visual created using Biorender.com).

GPCRs are divided into six families based on their sequence similarity: rhodopsin-like (family A), secretin (family B), glutamate (family C), fungal mating pheromone (family D), cyclic AMP (family E) and frizzled/smoothened (family F) receptors (Hu et al., 2017). The rhodopsin-like family is the largest family of GPCRs and is characterised by conserved sequence motifs that imply shared structural features and activation mechanisms. Overall, the seven TM domains exhibit significant homology among GPCRs, whereas the N-terminal region serves as the primary structural variable. Despite these shared characteristics, each GPCR possesses unique combinations of signal transduction activities, engaging multiple G-protein subtypes,

G-protein-independent signalling pathways and complex regulatory mechanisms. There are GPCRs that are known as “orphan” receptors, for which endogenous ligands and exact functions are yet to be recognised (Jobe and Vijayan, 2024).

1.6.2 Activation mechanism of GPCRs

GPCRs can respond to a diverse range of extracellular activating ligands, including neurotransmitters, hormones, lipids, ions, and peptides. Their activation follows a well-characterised sequence of molecular events that trigger intracellular signalling cascades (see Figure 1.4A). GPCRs initiate canonical (G protein-dependent) signalling through ligand-induced conformational rearrangements within their seven-transmembrane (7TM) helical bundle. This conformational transition allosterically reduces the affinity of the Gα subunit for GDP, resulting in its release and rapid replacement with GTP, as GPCRs are intrinsically guanine nucleotide exchange factors (GEF) (Eichel and von Zastrow, 2018). GTP binding stabilises an active conformation in the Gα subunit, leading to the dissociation of the Gα monomer and a Gβγ heterodimer. Both free molecules are now competent to interact with downstream effectors (enzymes or channels), initiating signalling cascades, responsible for various physiological and pathophysiological processes (Manning and Blumenthal, 2023).

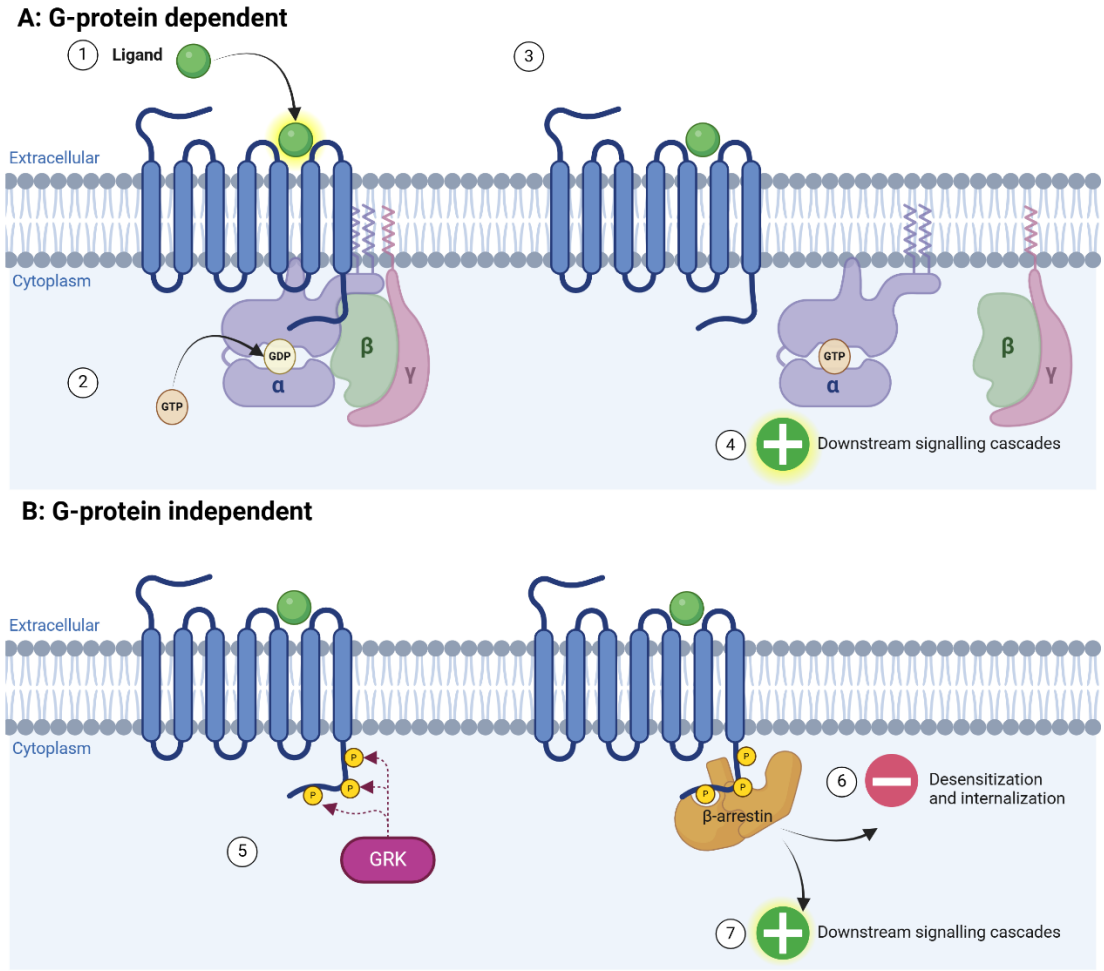

Figure 1.4: GPCR Activation Mechanism.
An illustration of the main steps of GPCR-mediated signal transduction. **A: G-protein dependent signalling:** The process is triggered by ligand (green) binding to the extracellular domain of the GPCR (Step 1), inducing a conformational change in its seven-transmembrane (7TM) helical structure. This leads to G protein activation (Step 2), facilitating the exchange of GDP for GTP in the α-subunit of the heterotrimeric G protein complex (α, β, γ), thereby activating the G protein. This induces the dissociation of the G protein (Step 3) into the Gα subunit and the Gβγ heterodimer, allowing both components to engage distinct intracellular effectors. These interactions turn on downstream signalling cascades (Step 4), leading to cellular responses. **B: G-protein independent signalling:** GPCRs can engage in G protein-independent pathways through β-arrestins. This process is initiated by phosphorylation of intracellular receptor residues (Step 5) by GPCR kinases (GRKs), facilitating β-arrestin recruitment. GPCR-β-arrestin coupling facilitates receptor desensitisation and internalisation (Step 6), for terminating GPCR signalling. β-arrestins also serve as scaffolding proteins, initiating the activation of distinct intracellular signalling cascades (Step 7). (Visual created using Biorender.com).

The specificity of GPCR signalling is imposed by the subtype of heterotrimeric G proteins recruited upon ligand-mediated activation. Based on structural homology, Gα proteins are sorted into four families, G_s, $G_{i/o}$, $G_{q/11}$, and $G_{12/13}$, modulating distinct intracellular pathways (introduced in subsection 1.6.3). The free Gβγ subunits also participate in signal transduction, directly modulating the activity of ion channels, phospholipases, and kinases (Campbell and Smrcka, 2018).

GPCR can initiate a non-canonical (G-protein independent) signalling mediated by arrestins (Gurevich and Gurevich, 2019). Arrestins are classified into four subtypes: arrestin-1 and arrestin-4, mainly expressed in the eye, besides arrestin-2 (β-arrestin 1) and arrestin-3 (β-arrestin 2), which are widely expressed across various tissues. The naming of these effectors originates from the initially recognised function in "arresting" GPCR activity, facilitating desensitisation and internalisation of the receptor. However, research findings indicate that arrestins act as scaffolding proteins that engage distinct intracellular signalling networks, independent of G proteins (Jean-Charles et al., 2017). Arrestin-GPCR coupling is triggered by the phosphorylation of specific intracellular receptor residues by GPCR kinases (GRKs), leading to arrestin recruitment and receptor internalisation (Figure 1.4B). Traditionally, this event was thought to terminate receptor activity; however, emerging evidence suggests that this internalisation can also redirect receptor signalling to intracellular effectors, thereby modulating the dynamics of GPCR activity. MAPK pathway, including extracellular signal-regulated kinases (ERKs) is one of the signalling pathways that can be activated in an arrestin-dependent fashion (Gurevich and Gurevich, 2019). Additionally, GPCR-arrestin coupling mediates receptor trafficking, relocating the receptor within the membrane (Thomsen et al., 2022). Furthermore, arrestins are involved in the biased

signalling paradigm where specific ligands can selectively mediate either G protein- or arrestin-mediated pathways, promoting functional selectivity in GPCR responses.

1.6.3 G proteins: subtype-specific signalling

GPCR function specificity and downstream target regulation are largely dependent on the identity of the Gα subunit, that are classified into four main families comprising more than 16 subunit isoforms (refer to Table 1.2). Additionally, a total of five Gβ and 12 Gγ isoforms were identified that contribute less to the specificity of the signalling cascade yet complement or modulate Gα subunit activity (Manning and Blumenthal, 2023, Conflitti et al., 2025). Despite the importance of these Gβ and Gγ subunits for physiology and fine-tuning GPCR activity, specific biochemical classification has not yet been achieved.

Table 1.2: The four families of Gα-proteins subunit isoforms (Manning and Blumenthal, 2023).

Family	Subunit isoform	Effector protein/second messenger
Gαs	$\alpha_{s\ short}$, $\alpha_{s\ long}$ α_{olf}	Adenyl cyclase/ ↑ cAMP
Gαi	α_{i1}, α_{i2}, α_{i3} α_{oA}, α_{oB} α_{t1}, α_{t2} α_{g} α_{z}	Adenyl cyclase/ ↓ cAMP
Gαq/11	α_{q} α_{11}, α_{14}, α_{15}, α_{16}	PLCβ/ DAG/IP_3
Gα12/13	α_{12}, α_{13}	RhoGEFs/RhoA
*Abbreviations: **cAMP**: cyclic adenosine monophosphate; **PLCβ**: Phospholipase Cβ; **DAG**: Diacylglycerol; **IP3**: Inositol 1,4,5-trisphosphate; **GEFs**: Guanine nucleotide exchange factors*		

1.6.3.1 $G\alpha_s$ family

The $G\alpha_s$ family includes three isoforms, $G\alpha_{s\ short}$, $G\alpha_{s\ long}$, and $G\alpha_{olf}$, that exhibit variable tissue expression but share a common function regulating cyclic adenosine monophosphate (cAMP) (Wettschureck and Offermanns, 2005). Upon ligand binding to GPCR, $G\alpha_s$ exchanges GDP with GTP, leading to its dissociation and direct activation of adenylyl cyclase (AC) (Figure 1.5A). AC in turn catalyses the conversion

of adenosine triphosphate (ATP) to cAMP, the primary second messenger responsible for initiating intracellular cascades. Several cAMP-dependent cytoplasmic effector proteins are activated, including protein kinase A (PKA) and several exchange proteins directly activated by cAMP (EPAC). Activated PKA results in the phosphorylation of diverse target proteins involved in regulating energy utilisation, transcriptional activity, and ion channel activity (Mellon et al., 1989, Zhao et al., 2015, Yang, 2018). In contrast, EPAC proteins function as guanine nucleotide exchange factors that regulate small GTPases, affecting cell adhesion, migration, and calcium signalling (Holz et al., 2006, Raymond et al., 2007). cAMP signalling is stopped by phosphodiesterases (PDEs), which hydrolyse cAMP into AMP, effectively terminating the signal. The interplay between PKA and EPAC can be synergistic, independent, or even antagonistic, depending on their cellular context. For instance, in mouse fibroblasts (preadipocytes), PKA (by suppressing Rho/ROCK kinase) and EPAC (through Ras-related protein 1 [Rap1]) cooperate synergistically to promote adipocyte differentiation (Petersen et al., 2008). Meanwhile, PKA and EPAC were reported to function independently in endothelial cells, regulating migration and barrier function via distinct signalling routes (Lorenowicz et al., 2008). In contrast, Menon et al. (2012) described antagonistic interactions in prostate cancer cells, where EPAC/Rap1 activation promoted vascular endothelial growth factor (VEGF) expression under hypoxia, while PKA activation supresses Rap1 signalling reducing VEGF output (Menon et al., 2012).

1.6.3.2 $G\alpha_i$ family

The $G\alpha_i$ family consists of multiple isoforms, including $G\alpha_{i1}$, $G\alpha_{i2}$, $G\alpha_{i3}$, $G\alpha_o$, $G\alpha_z$, and $G\alpha_t$, which exhibit overlapping but distinct physiological functions (de Oliveira et al.,

2019). Most $G\alpha_i$ family members, except $G\alpha_z$, are pertussis toxin (PTX)- sensitive, allowing pharmacological inhibition and assessment of $G\alpha_i$-specific functions. Dissociated $G\alpha_i$-GTP can inhibit most forms of AC, reducing cytoplasmic levels of cAMP, providing a functional counterbalance to $G\alpha_s$-mediated signalling (Figure 1.5B) (Manning and Blumenthal, 2023). Additionally, $G\alpha_{i/o}$ activity, along with its $G\beta\gamma$ dimer, directly modulates ion channels, including the activation of G-protein-dependent inwardly rectifying K^+ channels (GIRK) (Lüscher and Slesinger, 2010), and inhibition of several subtypes of voltage-gated Ca^{2+} channels (Thomas et al., 2025). These mechanisms enable $G\alpha_{i/o}$ proteins to fine-tune synaptic transmission and neuronal excitability. For instance, μ opioid receptors activated by analgesics like morphine couple via $G\alpha_{i/o}$ to open GIRK channels and inhibit voltage-gated Ca^{2+} channels, leading to reduced neural excitability and analgesia (Che and Roth, 2023). Similarly, the $GABA_B$ receptors, when activated by drugs like baclofen, exert presynaptic neurotransmitter release and postsynaptic hyperpolarisation through $G\alpha_i$/o-mediated suppression of Ca^{2+} channels and activation of GIRK channels (Hleihil et al., 2021). These examples illustrate how pharmacological modulation of $G\alpha_i$/o-coupled receptors can regulate neural excitability, making them potential therapeutic targets (Yudin and Rohacs, 2018).

1.6.3.3 $G\alpha_{q/11}$ family

The $G\alpha_q$ family includes $G\alpha_q$, $G\alpha_{11}$, $G\alpha_{14}$ and $G\alpha_{16}$ ($G\alpha_{15}$ is the mouse ortholog of $G\alpha_{16}$). $G\alpha_{q/11}$ monomer released upon ligand-mediated stimulation of GPCRs directly activate an enzyme, phospholipase Cβ (PLCβ), that hydrolyses phosphatidylinositol 4,5-bisphosphate (PIP2), a membrane phospholipid. This hydrolysis generates two key second messengers, diacylglycerol (DAG) and inositol 1,4,5-trisphosphate (IP3)

(Figure 1.5C). DAG can directly activate protein kinase C, which like PKA, phosphorylates several effector protein targets involved in cellular proliferation, differentiation, apoptosis and migration (Black and Black, 2012, Fogh et al., 2014, Pieles and Morsczeck, 2024). For IP3, it binds to its specific receptors (IP3R) on the sarcoplasmic and endoplasmic membranes, initiating intracellular Ca^{2+} release. The increased cytoplasmic Ca^{2+} levels regulate several cellular processes, including gene transcription, contraction and exocytosis (Domeier et al., 2008, Dewenter et al., 2017, Predescu et al., 2019).

1.6.3.4 $G\alpha_{12/13}$ family

Finally, $G\alpha_{12/13}$ directly interacts with Rho guanine nucleotide exchange factors (RhoGEFs) (Figure 1.5D). These RhoGEFs facilitate the exchange of GDP with GTP on RhoA, inducing its activation. RhoA, in turn, stimulates Rho-associated kinases (ROCK) that govern cellular contractility, proliferation, survival and migration (Coffield et al., 2004, Liu et al., 2009, Guo et al., 2022). This pathway is vital in the nervous system, regulating cortical development, neuronal migration, axonal guidance and neurotransmitter release, making it critical for neurodevelopmental processes (Molliver, 2009, Suzuki et al., 2009).

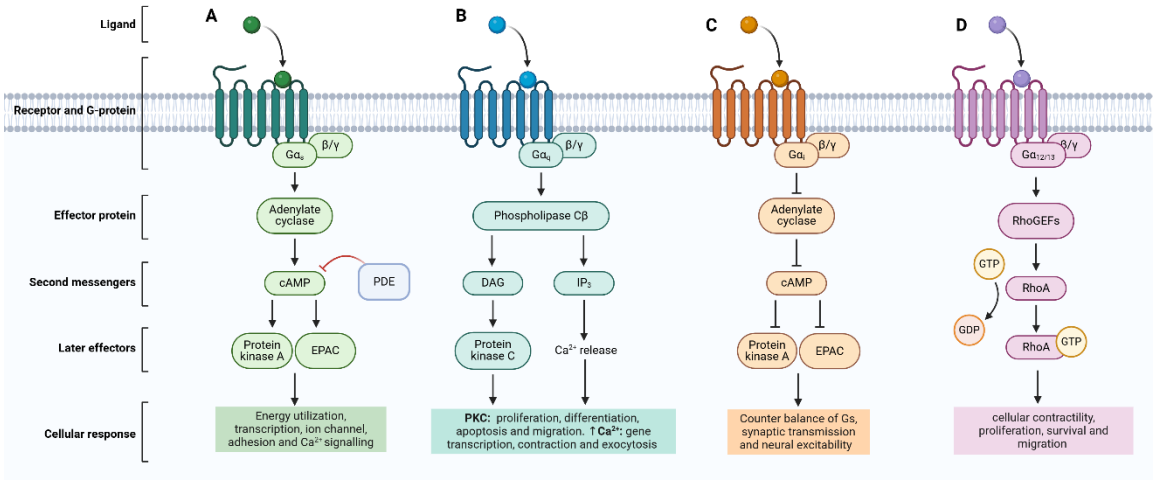

Figure 1.5: GPCR Distinct Gα-Mediated Signal Transduction Mechanisms.
An illustration of the four major GPCR signalling pathways mediated by different Gα subunits. (**A**) $G\alpha_s$-mediated signalling: Upon ligand binding, the GPCR activates $G\alpha_s$, which in turn stimulates adenylate cyclase, leading to the production of cyclic adenosine monophosphate (cAMP). cAMP activates protein kinase A (PKA) and exchange proteins directly activated by cAMP (EPAC). Phosphodiesterases (PDEs) regulate this pathway by degrading cAMP. (**B**) $G\alpha_q$-mediated signalling: GPCR activation of $G\alpha_q$ stimulates phospholipase Cβ (PLCβ), which hydrolyses phosphatidylinositol 4,5-bisphosphate (PIP2) to generate diacylglycerol (DAG) and inositol 1,4,5-trisphosphate (IP3). DAG activates protein kinase C (PKC), while IP3 induces Ca^{2+} mobilisation from intracellular stores. (**C**) $G\alpha_i$-mediated signalling: Activation of $G\alpha_i$ leads to the inhibition of adenylate cyclase, thereby reducing cAMP levels and counteracting Gαs signalling. (**D**) $G\alpha_{12/13}$-mediated signalling: The $G\alpha_{12/13}$ subunits activate Rho guanine nucleotide exchange factors (RhoGEFs), which facilitate the exchange of GDP for GTP on RhoA, leading to its activation. These signalling pathways activate distinct effectors and second messengers, which in turn regulate various cellular processes, leading to the downstream responses illustrated in the figure. Visual created by Biorender.com.

1.6.4 Inactivation and desensitisation of GPCR

Following activation, repeated agonist-mediated GPCR activation is minimised by a process known as desensitisation. The main desensitisation mechanism occurs through a group of enzymes known as GPCR kinases (GRKs), which phosphorylate specific C-terminal residues of the receptor. This initiates β-arrestin recruitment, preventing its reassociation with G-protein and triggering receptor endocytosis, degradation (receptor downregulation mainly after prolonged agonist exposure) or restored to cell membrane (Rajagopal and Shenoy, 2018). Inside the cell, Gα-mediated signalling is terminated by the intrinsic GTPase activity of the Gα subunit that hydrolyses GTP

back to GDP, facilitating the reassociation of the inactive Gαβγ heterotrimer and resetting the signalling state of the receptor (Manning and Blumenthal, 2023).

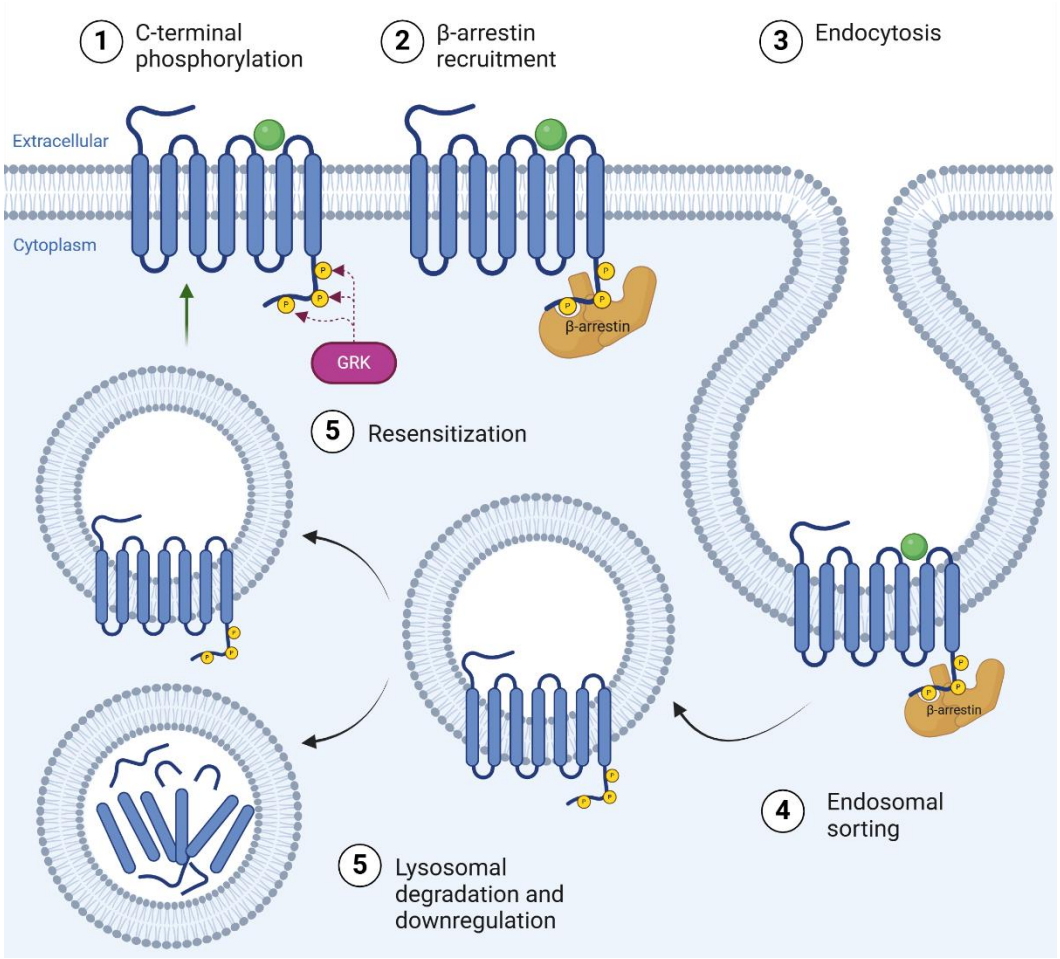

Figure 1.6: Mechanisms of GPCR desensitisation.
Schematic representation of GPCR desensitisation, internalisation, and fate following activation. (**1**) Following agonist-mediated activation, the receptor undergoes C-terminal phosphorylation by G protein-coupled receptor kinases (GRKs). (**2**) This mediates the recruitment of β-arrestins, which uncouple the receptor from G proteins. (**3**) The β-arrestin–bound receptor is then internalised via clathrin-mediated endocytosis. (**4**) In endosomes, receptors are sorted either for (**5**) lysosomal degradation and downregulation or for recycling back to the plasma membrane to allow receptor resensitisation. Visual created by Biorender.com.

Protease-activated receptors- a unique family of G protein-coupled receptors.

1.7 Discovery of the unique activation mechanism of PARs

Although the function and mitogenic actions of thrombin and trypsin were specified since the early 1970s (Burger, 1970, Kaplan and Bona, 1974, Chen and Buchanan, 1975), the receptors responsible for mediating their actions, protease-activated receptors (PAR) were initially recognised only in the 1990s. Although this group of receptors has a wide range of functions in both physiological and pathological tissue conditions, they have only recently gained appreciable consideration as potential therapeutic targets for several disease conditions. In investigating the actions of thrombin, which were independent of coagulation but still dependent upon serine protease activity, PAR1 was the first member to be cloned directly using a *Xenopus* oocyte expression system and mRNA detected in human platelets and vascular endothelial cells (Vu et al., 1991). The other members of this group, PAR2 (Nystedt et al., 1994, Nystedt et al., 1995a) (a thrombin-insensitive PAR), PAR3 (Ishihara et al., 1997) and PAR4 (Xu et al., 1998), were characterised and cloned soon thereafter.

Activation of this unique class of receptors involves the proteolytic activity of enzymes known as serine proteases. These enzymes function by hydrolysing peptides through a catalytic triad composed of aspartate (Asp), histidine (His) and serine (Ser) (Blow et al., 1969). Serine proteases are produced as inactive precursors (zymogens), which require selective enzymatic cleavage at specific sites to produce physiologically active forms. This is known as zymogen activation or “limited proteolysis” (Neurath and Walsh, 1976, Walsh and Ahmad, 2002). This precise activation mechanism prevents uncontrolled proteolysis while allowing rapid local responses when triggered. With

the cloning of the PARs and other proteins regulated by serine-directed proteolysis, these enzymes have emerged as critical signalling molecules, rather than merely degradative enzymes. Serine proteases, such as trypsin, thrombin, elastase, and kallikreins, are now recognised to act as extracellular signalling molecules that modulate receptor activation, cytokine release, and tissue remodelling. These proteases cleave and activate PARs on various cell types, triggering intracellular responses that drive inflammation, vascular permeability, immune cell recruitment and pain sensitisation (Hollenberg et al., 1997, Oikonomopoulou et al., 2006). For example, kallikreins KLK6 and KLK14 have been shown to activate PAR2 and PAR4, inducing oedema and enhancing pain responses (Oikonomopoulou et al., 2007); neutrophil elastase cleaves PAR2, initiating inflammatory signals in vascular and immune cells (Zhao et al., 2015); and trypsin stimulate cytokine release and immune cells activation via PAR2 (Miike et al., 2001).

Classically, GPCRs couple reversibly the binding of small hydrophilic agonist molecules at its extracellular domains to the activation of the heterotrimeric G proteins, that lead the modulation of downstream signalling effector proteins (Wettschureck and Offermanns, 2005, Rosenbaum et al., 2009). In this respect the PAR family displays the typical basic structural features shared in all other GPCRs, having a central core domain consisting of seven transmembrane helices connected by three extracellular and three intracellular loops (refer to 1.6). However as indicated above they exhibit proteolytic activation rather than simple agonist binding (Bockaert and Pin, 1999). Endogenous serine proteases induce localized proteolysis at the N-terminus of their receptors to unmask a ‘tethered ligand’ that represents an existing linked amino acid sequence within N-terminus of the receptor. The unmasked tethered ligand

(approximately six amino acid sequence) reacts with the specific sequence at extracellular domains, mostly ECL2 (Han and Nieman, 2020), of the receptor inducing conformational changes of the transmembrane domains and trigger receptor activity (Vu et al., 1991, Nystedt et al., 1995a).

1.7.1 Mechanism of activation of PARs

Typically, PARs are triggered upon proteolysis of their extracellular N-termini by non-specific serine proteases. N-terminal structure contributes largely to specificity of receptor selective response to specific agonists. Thrombin can efficiently activate PAR1 and PAR3, while individual PAR2 are completely unresponsive with weak responsiveness of PAR4. This has been linked to a structural motif within N-terminal, a hirudin-like thrombin binding motif, present in both PAR1 and PAR3 (Macfarlane et al., 2001), but absent in PAR2 and PAR4 (Jacques and Kuliopulos, 2003). Thrombin and trypsin are serine proteases that can cleave PARs 1, 2 (only trypsin) and 4 at localized recognition sites resulting in the unmasking of a motif that acts as 'canonical' tethered ligand binding to other extracellular loops of the receptors inducing receptor activation and coupling of the intracellular Gα-protein subtypes, including $G\alpha_{q/11}$, $G\alpha_{12/13}$, and $G\alpha_{i/o}$, initiating intracellular signalling cascades (Mackie et al., 2002, Traynelis and Trejo, 2007, Chandrabalan and Ramachandran, 2021). For PAR3, similar cleavage of its N-terminus occurs upon serine protease binding, but the receptor's ability to function on its own is not confirmed. It has been shown that PAR3 acts as a cofactor for the thrombin mediated activation of PAR4 in experiments involving mice platelets expressing both receptors (Nakanishi-Matsui et al., 2000). In these experiments, at low concentrations of thrombin, blocking mouse PAR3 (mPAR3) and knocking out the mPAR3 gene abolished thrombin signalling.

Autonomous activity of PAR3 also was demonstrated upon thrombin exposure resulting in IL-8 release in several human cell lines (Ostrowska and Reiser, 2008).

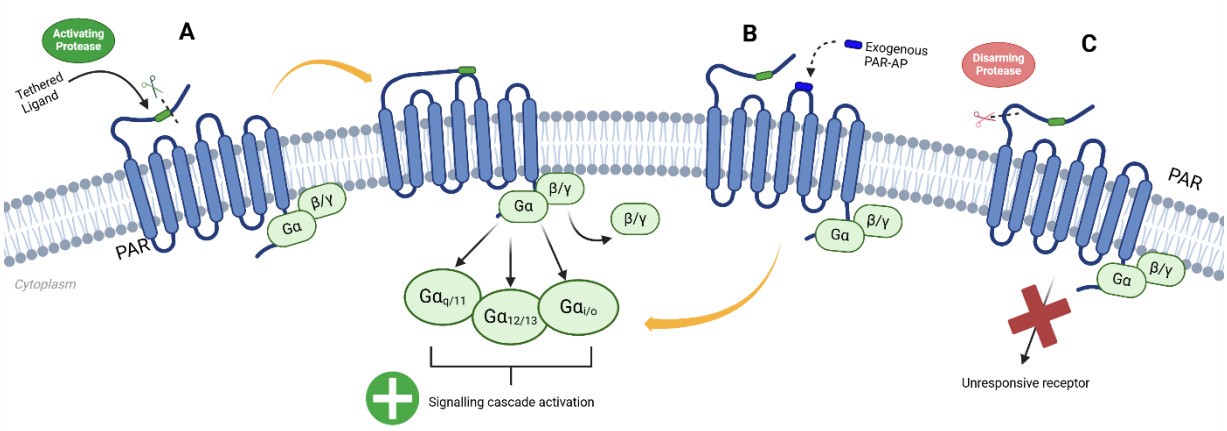

Figure 1.7: Mechanisms of Protease-Activated Receptor (PAR) Activation.
Schematic representation of activation mechanisms of protease-activated receptors (PARs). (**A**) An activating protease cleaves the receptor's extracellular N-terminal domain, unmasking a tethered ligand, which subsequently binds to the receptor's extracellular loop 2 (ECL2), triggering intracellular signalling. This activation involves the dissociation of heterotrimeric G proteins (Gα, Gβ, Gγ), the Gα monomer and Gβγ dimer. Gα: $G\alpha_{q/11}$, $G\alpha_{12/13}$, or $G\alpha_{i/o}$, initiates downstream signalling cascades that regulate cellular responses. (**B**) Exogenous PAR-activating peptides (PAR-APs) can directly stimulate PARs without requiring proteolytic cleavage. (**C**) A disarming protease cleaves the receptor at a distinct site, disrupting the tethered ligand sequence and rendering the receptor unresponsive, thereby preventing further signalling. Visual created by Biorender.com.

As an alternative, it was found later that PARs, PAR1 and PAR2, could be activated via a G-protein-independent mechanism whereby the tethered ligand exposed by proteases leads a β-arrestin-mediated signalling scaffold (DeFea, 2008). Furthermore, the receptor-silencing serine proteases that cleave the N-terminus of the receptor, distinct from the tethered ligand sequence, leading to thrombin or trypsin non-responsive PARs (known as disarming of PAR), may induce receptor activation as well. Recent data have indicated that some proteases, such as activated protein C or APC (Mosnier et al., 2012) and neutrophil elastase (Ramachandran et al., 2011) can cleave N-termini of PARs at sites downstream of the 'canonical' tethered ligand

sequence, unmasking a ‘non-canonical’ ligand that can dock with the receptor and trigger PAR activity by a mitogen-activated protein kinase (MAPK) pathway without elevation of intracellular calcium levels that is induced by the canonical tethered ligand-induced receptor activation. This ability of PARs to activate one pathway in preference to another depending on the activating ligand is known as biased agonism (Kenakin, 2011, Hollenberg et al., 2014).

The cloning of PAR1 and subsequent pharmacology demonstrated that the receptor could be activated by short synthetic peptides derived from the ‘tethered ligand’ sequence in absence of thrombin-induced proteolytic activity (Vu et al., 1991, Scarborough et al., 1992). This also applies to PAR2 and PAR4 although again, PAR3 appears to be an exception, as peptides typical to its thrombin-unmasked sequence at N-terminus did not induce PAR3 signalling, but instead induced PAR1 and PAR2 activity (Hansen et al., 2004, Kaufmann et al., 2005). Such synthetic peptides, known as PAR activating peptides (PAR-AP), are designed and employed as selective receptor agonists when studying the physiological involvement and pharmacological modulation of PARs, especially in settings where more than one subtype of PAR is expressed (see table 1). It is relevant to note that PAR-AP selectivity is not absolute, as higher concentrations of these peptides have been observed to activate other PAR subtypes or off-target receptors (Blackhart et al., 1996, Hollenberg et al., 1997, Tsujii et al., 2008).

Table 1.3: PAR tethered ligands and PAR-selective agonist peptides (Ramachandran et al., 2012)

PAR subtype	**Protease-revealed tethered ligand sequence**	**Selective agonist peptides**
PAR1	Ser-Phe-Leu-Leu-Arg-Asn (human)	Thr-Phe-Leu-Leu-Arg-NH_2
	Ser-Phe-Phe-Leu-Arg-Asn (mouse, rat)	Ser-Phe-Leu-Leu-Arg-Asn-NH_2 (activates PAR1 and PAR2)
PAR2	Ser-Leu-Ile-Gly-Lys-Val (human)	Ser-Leu-Ile-Gly-Lys-Val-NH_2
	Ser-Leu-Ile-Gly-Arg-Leu (mouse, rat)	Ser-Leu-Ile-Gly-Arg-Leu-NH_2
PAR3	Thr-Phe-Arg-Gly-Ala-Pro (human)	None; PAR3 agonist peptide activates PAR1 and PAR2
PAR4	Gly-Tyr-Pro-Gly-Gln-Val (human)	Ala-Tyr-Pro-Gly-Gln-Val-NH_2
	Gly-Tyr-Pro-Gly-Lys-Phe (mouse)	Ala-Tyr-Pro-Gly-Lys-Phe-NH_2
PAR, protease-activated receptor.		

1.7.2 Termination of PARs activity

For the majority of GPCRs, effective desensitisation and downregulation events are required to guard against acute supramaximal stimulation or chronic activation (see section 1.6.4). Multiple mechanisms govern the termination of PAR signalling. In this respect, PAR1 was extensively studied, followed by PAR2, with limited data available regarding the termination of other PARs. Initial studies demonstrated that subsequent to protease-unmasked tethered ligand activation, several GPCR kinases (GRKs) phosphorylate specific sites within the cytosolic C-terminal of the receptor (Nanevicz et al., 1996), as in the case of PAR1 (Shapiro and Coughlin, 1998, Trejo, 2003). Reports have shown that GRKs involved in PAR1 phosphorylation include GRK3 (earlier identified as β-adrenergic receptor kinase2 or BARK2 (Ishii et al., 1994) and GRK5 (Tiruppathi et al., 2000) leading to rapid desensitisation of thrombin-induced activity of PAR1. Interestingly, PAR1 mutated (substitution with alanine) at these putative phosphorylation sites within the C-terminal still demonstrated some responsiveness to thrombin (Ishii et al., 1994, Nanevicz et al., 1996), indicating alternative termination mechanisms. Evidence indicates interaction of β-arrestin with the cytosolic domains of the receptor, preventing binding of G-proteins, suggesting a

crucial role in PAR1 desensitisation that appears to be independent of phosphorylation events by GRKs (Chen et al., 2004), but not PAR1 internalisation or trafficking (Paing et al., 2002). Evidence has shown that PAR1, like many GPCRs, undergoes internalisation and possible lysosomal degradation that is a clathrin-dynamin-dependent process and involves deubiquitination of activated receptors (Wolfe et al., 2007).

On the contrary, PAR2 activity induces multiple phosphorylation events of serine and threonine residues within the cytosolic C-tail of the receptor (Ricks and Trejo, 2009a). This event was found to be crucial for β-arrestin 1 and 2 recruitment and uncoupling of G-protein, consequently, termination of receptor signalling (Bohm et al., 1996a, Ricks and Trejo, 2009a). Moreover, PAR2 internalisation and lysosomal degradation are also β-arrestin-dependent (DeFea et al., 2000b, Stalheim et al., 2005). PAR2 β-arrestin-tagged receptors are targeted for early receptor endosomal internalisation, which does not appear to be recycled (Stalheim et al., 2005), and consequent differential sorting for lysosomal degradation in a process involving deubiquination of the receptor (Déry et al., 1999, Hasdemir et al., 2009b).

The mechanisms that regulate termination of PAR3 and PAR4 signalling remain largely unclear. Nevertheless, studies demonstrated that PAR4 internalisation is β-arrestin-independent and is a slower process, in comparison to PAR1 (Shapiro et al., 2000), that is mediated by clathrin- and dynamin-dependent pathways (Smith et al., 2016). In addition, evidence showed the involvement of PAR2-heterodimerization as a key regulator of PAR4 trafficking and signalling (Cunningham et al., 2012) which may imply co-termination mechanisms.

1.8 An overview of PARs biological roles

PARs regulate a vast range of cellular responses in different tissue types. PAR1 was initially identified as a mediator of thrombin-induced cellular effects independent of the coagulation cascade (Vu et al., 1991). Later, it was confirmed that PAR family is expressed across multiple cell types in the vasculature to mediate protease functions modulating coagulation, vascular tissue inflammation and repair (Borissoff et al., 2011) (see the overview in

Figure 1.8). In general, PARs are largely involved in regulation of platelet aggregation, vascular permeability, nitric oxide (NO) liberation and leukocyte adhesion. Thrombin activates PAR1 and PAR4 on platelets, with species-specific differences, leading to platelet aggregation, granular secretions and procoagulant activity (Coughlin, 2005). Proteases can activate PARs on vascular endothelial and smooth muscle cells affecting vascular resistance, blood flow, permeability and angiogenesis (Thiyagarajan et al., 2008, Zhang et al., 2023). Typically, PAR activation causes dilation of pre-contracted blood vessels in an endothelial-released nitric oxide-mediated mechanism (Coughlin, 2001). Although, NO-independent mechanisms were identified that mediate PAR-induced vasodilation (Hamilton and Cocks, 2000, Hamilton et al., 2001), under specific conditions, proteases were also reported to induce PAR-mediated vascular constriction (Tay-Uyboco et al., 1995, Roy et al., 1998, Habibi et al., 2025).

In the CNS, PARs are expressed in neuronal cells and astrocytes. Since PARs can increase $[Ca^{2+}]_i$, they play a role in controlling excitability, neurotransmitter release and cell survival. Moreover, thrombin and PAR activators affect the morphology of neurons and astrocytes (Beecher et al., 1994, Sweeney et al., 2017) and show inhibitory

effects on neuronal outgrowth formation (Kim et al., 2021). Thrombin effects on neuron and astrocyte survival were concentration- and exposure time-dependent. In general, low levels of thrombin or PAR1 activator are protective (Striggow et al., 2000, Rajput et al., 2020) while prolonged exposure to a high concentration induces neurodegeneration and apoptosis (Striggow et al., 2000, Citron et al., 2016). PAR1 and PAR2 are involved in synaptic plasticity and neurotransmitter release (Price et al., 2021). PAR2 is expressed in microglia, astrocytes and neurons, mainly mediating neuroinflammatory responses and pro-inflammatory cytokines release (Steinhoff et al., 2000b, Noorbakhsh et al., 2006, Eftekhari et al., 2024). PAR4 has been shown to contribute to neuroinflammatory processes, and its selective inhibitors demonstrated neuroprotective effects in a traumatic brain injury model (Luo et al., 2021, Zhuo et al., 2022, Fleischer et al., 2024).

In the gastrointestinal (GI) tract, PARs, particularly PAR1 and PAR2, are distributed throughout the tract, contributing to various GI functions (Ossovskaya and Bunnett, 2004, Ceuleers et al., 2016, Pontarollo et al., 2020). GI tissue is highly exposed to proteases that are secreted into the lumen as digestive enzymes or extrinsically liberated from pathogens or inflammatory cells. Under physiological conditions, PAR1, PAR2 and PAR4 are capable of modulating GI motility, exocrine secretions, cellular signalling and local neurotransmission (Kawabata, 2003, Sung et al., 2018, Mirakhur and Diener, 2022). Under stress or inflammation, PARs, especially PAR1 and PAR2, appear to significantly contribute to mucosal and pancreatic injury, inflammation and pain (Kawabata et al., 2008, Mirakhur and Diener, 2022).

In the respiratory system, PARs (PAR1-PAR4) are expressed in several cell types, including airway epithelial cells (bronchial and alveolar), airway smooth muscle cells,

fibroblasts, and resident immune cells, such as mast cells and macrophages (Lan et al., 2002). These receptors are activated by endogenous cleaving proteases, such as airway trypsin (Kawano et al., 1997, Danahay et al., 2001) and mast cell tryptase (Louis et al., 2000), or exogenous proteases, like inhaled dust mite allergens (Li et al., 2019). Under normal conditions, PAR1, PAR2 and PAR4 are capable of modulating airway smooth muscle tone and pulmonary resistance (Lan et al., 2000, Hagras and Kamel, 2020). Moreover, stimulation of airway PARs induces tissue repair, regeneration and remodelling (Panettieri Jr et al., 1995, Akers et al., 2000, Chambers et al., 2001). PARs showed increased expression in inflammatory airway conditions, besides elevated levels of proteases, suggesting a key role in airway inflammatory responses. Specifically, PAR2 has been implicated in allergic airway inflammation, mediating eosinophil infiltration and airway hyperreactivity (Lin et al., 2015, Asaduzzaman et al., 2018). Additionally, PAR1 contributes to pulmonary fibrosis, suggesting that different PAR subtypes may induce distinct inflammatory responses in the airways (Reed and Kita, 2004, Shea et al., 2017). Based on these observations, PARs play a modulatory role in airway homeostasis and participate in the pathophysiology of airway inflammatory conditions like asthma, chronic obstructive pulmonary disease (COPD) and other respiratory diseases, reviewed in (Reed and Kita, 2004, Sokolova and Reiser, 2007, Menou et al., 2017, Zhuo et al., 2022).

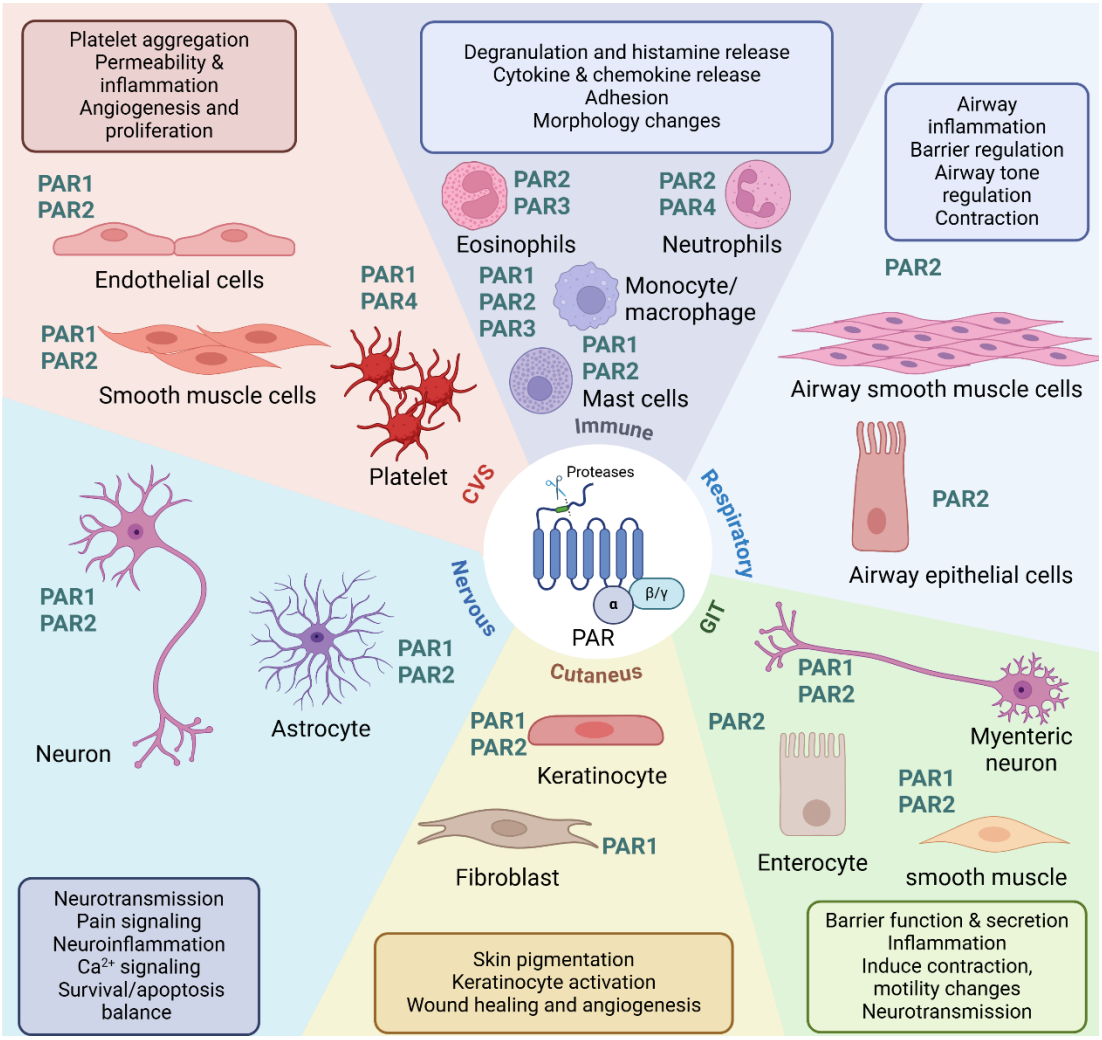

Figure 1.8: An overview of the main biological roles of PARs in different cell types.
This figure provides a comprehensive overview of the biological roles of PARs across various organ systems and cell types. For each system, the relevant cell types mainly expressing specific PAR subtypes (indicated next to each cell illustration in dark green) are shown, along with a summary of the main PAR-mediated functions of that system described in labelled boxes. Abbreviations: PAR: protease-activated receptor, CVS: cardiovascular system, GIT: gastrointestinal tract. Figure prepared using Biorender.com, inspired from (Peach et al., 2023).

Cutaneous biology and pathophysiology are another area where proteases display a crucial role (Guenther and Melzig, 2015, Xu et al., 2024). PARs, especially PAR1 and PAR2, are expressed in several cutaneous cell types like keratinocytes, several layers in epidermis, inner root sheath or hair follicle and myoepithelial cells of sweat glands (Santulli et al., 1995, Steinhoff et al., 1999). There is considerable interest in the role of PAR2 in skin pigmentation (Hashimoto et al., 2023). Although melanocytes do not

express PAR2, the activation of PAR2-expressing keratinocytes by trypsin has been shown to induce skin darkening through a mechanism that involves interaction with neighbouring melanocytes (Seiberg et al., 2000, Moreiras et al., 2022). PAR2 was found to be overexpressed in keratinocytes upon exposure to ultraviolet irradiation, leading to skin pigmentation (Scott et al., 2001, Enomoto et al., 2011). In contrast, the topical application of serine protease inhibitor was found to cause skin lightening (Paine et al., 2001). As PAR1 activation stimulates the proliferation of fibroblasts, keratinocytes, and induces angiogenesis, several investigations have demonstrated the essential contribution of PAR1 in cutaneous wound healing (Xue et al., 2005, Kiseleva et al., 2015, Turner et al., 2019).

1.9 PARs in inflammation

Inflammation serves as the body's primary defence mechanism, involving a series of events including vascular dilation, oedema formation and inflammatory cell infiltration. A growing body of evidence suggests the significant role of PARs in multiple inflammatory diseases, as discussed in several reviews (Bunnett, 2006, Vergnolle, 2009, Ma and Dorling, 2012, Heuberger and Schuepbach, 2019, Zhuo et al., 2022). Following PAR1 and PAR2 activation *in vivo* using their respective activating peptides, key features of inflammation were found to be evident, including redness, oedema, inflammatory cell recruitment, heat and pain (Vergnolle et al., 1999, Chen et al., 2008, Sevigny et al., 2011). However, numerous studies have demonstrated anti-inflammatory effects of PARs activation or even dual effects in specific conditions (Bae et al., 2009, Zhuo et al., 2022). Specific examples of these anti-inflammatory and dual effects will be discussed at the end of this section.

The activation and desensitisation of PARs suggest that these receptors function as emergency sensors activated once and then rapidly degraded or recycled. The discovery of PARs provided a molecular explanation of the proinflammatory effects of thrombin and other proteases (Cirino et al., 1996). Early evidence of thrombin's inflammatory role came from the studies showing that pretreatment with hirulog, a thrombin inhibitor, reduced carrageenan-induced rat paw oedema (Cirino et al., 1996). Beyond its well-established role in platelet aggregation and coagulation, thrombin exerts several pro-inflammatory effects, including vasodilation, increased vascular permeability and chemotaxis, primarily mediated through PAR1 (Cirino et al., 2000). PAR1 activation has been linked to the release of key inflammatory mediators such as histamine and cytokines (Déry et al., 1998). Moreover, thrombin-mediated PAR1 signalling was essential for inflammatory tissue chemokine gradients and leukocyte recruitment (Chen et al., 2008).

For PAR2, its activation has been linked to increased vascular permeability (Kawabata et al., 1998, Vergnolle et al., 1999), bronchoconstriction (Ricciardolo et al., 2000), leukocyte migration and infiltration (Vergnolle, 1999, Vergnolle et al., 1999) and other pro-inflammatory events. PAR2 is highly expressed in inflammatory cells such as mast cells, macrophages, monocytes, fibroblasts and neutrophils, demonstrating key roles in activation and degranulation of these cells (Howells et al., 1997, Shpacovitch et al., 2004). Notably, PAR2-mediated oedema is driven by a neurogenic mechanism, involving the release of substance P (SP) and CGRP by local sensory neurons, stimulating corresponding receptors on endothelial cells (Steinhoff et al., 2000a). However, PAR2 inhibitor, GB83 4μM, partially attenuated neutrophil elastase (NE)-induced human endothelial permeability, indicating direct involvement of endothelial

PAR2 in oedema (Liu et al., 2019). Furthermore, it was found that PAR2 signalling involves transcription factors, for example, CUX1, a homeodomain protein which is a downstream effector of PAR2, and induces the expression of inflammatory mediators including interleukin-1alpha (IL-1α), cyclo-oxygenase-2 (COX-2) and matrix metalloprotease-10 (MMP-10) in fibroblasts and endothelial cells (Wilson et al., 2009). Also, PAR2 contributes to cell proliferation and tissue remodelling during inflammation. For example, in rheumatoid arthritis, fibroblast proliferation has been shown to be driven by PAR2 rather than PAR1 (Xue et al., 2012). Notably, environmental factors such as smoking can amplify PAR2 activity. A study demonstrated that pre-exposure to cigarette smoke extract upregulates PAR2 in normal human bronchial epithelial cells, thereby enhancing inflammatory response to neutrophil elastase (Lee et al., 2018).

Several studies have also demonstrated the role of PAR4 in inflammatory events. Activation of PAR4 by its specific activating peptides induced local inflammatory reactions, including swelling and granulocyte recruitment (Vergnolle et al., 2002) that were inhibited upon pretreatment with a PAR4 antagonist, pepducin P4pal-10 (0.5 mg/Kg, i.p.) in local carrageenan-induced rodent paw oedema (Houle et al., 2005). In this study, further investigations into the mechanisms underlying PAR4-induced oedema demonstrated the involvement of neutrophils and key components of the kallikrein-kinin system. A series of *in vivo* studies assessing the role of PAR4 in joint pain and inflammation showed its pro-inflammatory effects, suggesting PAR4 blockage as a potential therapeutic strategy for joint inflammatory diseases (McDougall et al., 2009, Russell et al., 2010, Russell et al., 2011). Likewise, studies using pleural inflammation models have reinforced the role of PAR4 in driving

inflammatory responses. Activation of PAR4 has been shown to promote neutrophil recruitment, resulting in increased vascular permeability and local tissue inflammation. These effects were significantly reduced by PAR4 antagonist, trans-cinnamoyl-YPGKF-NH2 or tcY-NH2 (Braga et al., 2010, Gomides et al., 2012, Gomides et al., 2014).

PARs also modulate immune responses, exerting protective effects in various tissues. In the cardiovascular system, PAR2 activation has been shown to mitigate myocardial reperfusion injury. Infusion of PAR2-AP caused significantly improved myocardial function, reduced oxidative stress, reduced the ischemic risk zone, and upregulated PAR2 expression (Napoli et al., 2000). In the respiratory system, activation of PAR1 and PAR2 in murine and human airway preparations induced bronchodilatation through prostaglandin E2 (PGE2) release (Cocks et al., 1999). Similarly, *in vivo* PAR2 activation led to prolonged inhibition of bronchoconstriction. Given the widespread expression of PARs in epithelial and endothelial cells, similar protective functions have been proposed in other organs such as the GI tract and kidneys. In line with this, low thrombin concentrations and activated protein C were found to enhance endothelial cell integrity via PAR1 signalling (Feistritzer et al., 2005). Moreover, a recent study demonstrated that PAR2 contributed to reno-protection in glomerular endothelial injury induced by vascular endothelial growth factor (VEGF) inhibition, which is commonly used as an adjuvant in cancer chemotherapy (Oe et al., 2019).

Beyond its roles in vascular and epithelial protection, PAR2 has also been implicated in neuroprotection and immune modulation. For example, an *in vitro* study using cortical neural cultures demonstrated PAR2-dependent neuroprotective effects of trypsin against glutamate excitotoxicity (Nikolakopoulou et al., 2016). Similarly,

cotreatment of primary murine macrophages with lipopolysaccharide (LPS) and increasing concentrations of PAR2-AP resulted in a reduction of proinflammatory mediators, including TNF-α and IL-6, while enhancing the release of anti-inflammatory cytokines IL-10 (Nhu et al., 2012).

These findings underscore the complex role of PARs, which not only contribute to inflammation but also exhibit protective and anti-inflammatory effects in various physiological and pathological contexts (

Figure 1.9).

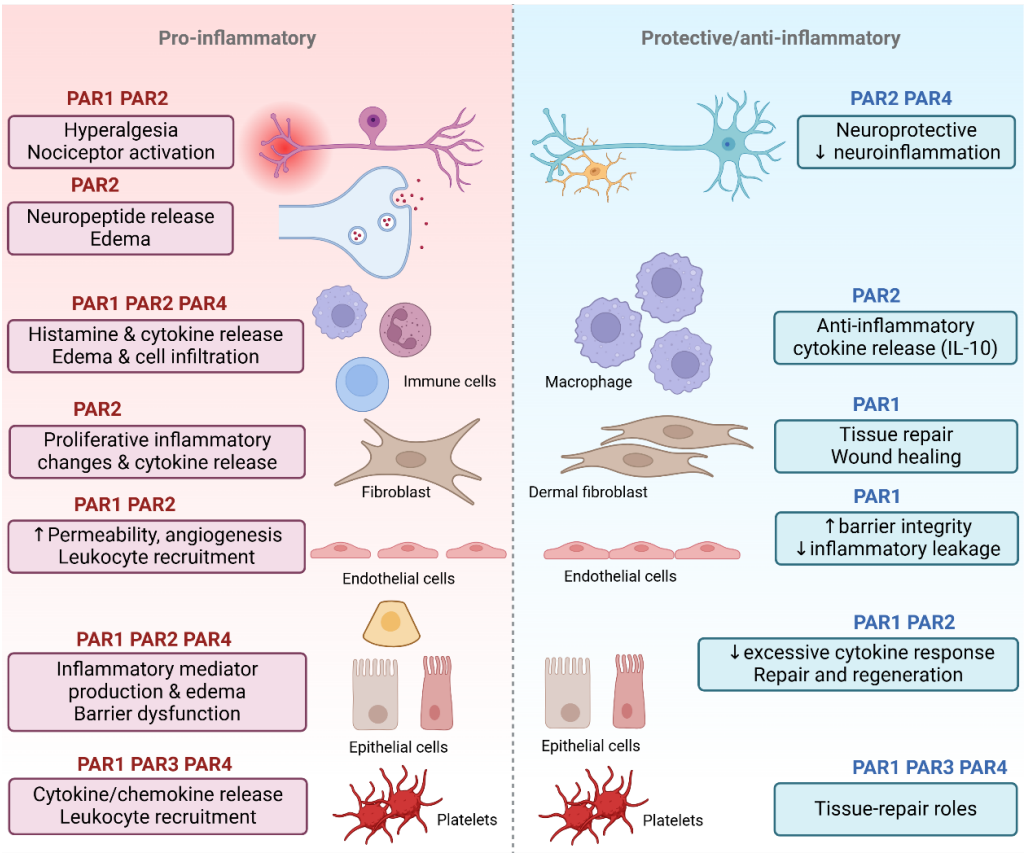

Figure 1.9: PARs activation-mediated inflammatory or protective effects.
The left panel summarises pro-inflammatory actions of PAR1, PAR2, PAR3, and PAR4 across various cell types, including immune, neural, endothelial, epithelial, fibroblast, and platelet populations. The right panel highlights protective and anti-inflammatory effects of the PAR subtypes, emphasising roles in neuroprotection, cytokine regulation, tissue repair, and barrier maintenance. Labelled boxes include PAR functions, and specific PARs involved in each function are indicated above. Figure prepared using Biorender.com, referring to (Vergnolle et al., 2001b, Zhuo et al., 2022).

1.10 Protease-activated receptor 2 (PAR2)

Due to its central role in inflammation, whether driving pro-inflammatory or anti-inflammatory responses, PAR2 has been a major focus of research in various inflammatory conditions compared to other PAR family members. Unlike PAR1 and PAR4, PAR2 is uniquely activated by trypsin (Nystedt et al., 1994) and a range of trypsin-like proteases such as mast cell tryptase, acrosin, cathepsin G, and tissue factor VIIa/factor Xa complex (Vesey et al., 2007). Notably, even at high concentrations, thrombin does not activate PAR2 (Ossovskaya and Bunnett, 2004). PAR2 was first cloned in 1995 and found to be widely expressed in human tissues, including the pancreas, kidneys, colon, small intestine, liver, prostate, lung, heart, trachea, central and peripheral neurons and astrocytes (Nystedt et al., 1995a, Bohm et al., 1996b, Peach et al., 2023). In general, PAR2 is widely expressed in epithelial cells, including vascular endothelial cells, airway epithelial cells, keratinocytes, T cells, neutrophils, synoviocytes and chondrocytes (Macfarlane et al., 2001, Peach et al., 2023). In normal prostate tissue, PAR2 is expressed strictly on epithelial cells, while in pathological tissue as cancer or benign prostate hyperplasia, PAR2 is located mainly in stromal prostate cells (Mannowetz et al., 2010). Several studies have shown upregulation of PAR2 under inflammatory conditions like arthritis, GI inflammatory conditions and prostatitis; these findings, in addition to the fact that many PAR2-activating proteases are actually produced during inflammation, support a key role for this receptor in inflammation (Cenac et al., 2002, Cederqvist et al., 2005, Kelso et al., 2007, Liu et al., 2014a, Roman et al., 2014, Kim et al., 2016).

1.10.1 Structural features:

Screening of the murine genomic library led to the identification of a PAR2 clone encoding a 397-residue protein with typical GPCR characteristics. This murine PAR2 shares 36% sequence identity with human PAR1 (Cheng et al., 2017) and is encoded by the human gene *F2RL1,* which is located within a gene cluster on human chromosome 5q13 (Nystedt et al., 1995b, Schmidt et al., 1997). Cleavage-activation site resides in the extracellular N-terminal domain, which consists of 46 residues (Ossovskaya and Bunnett, 2004). The trypsin cleavage site has been identified in human PAR2 as $SKGR^{36} \downarrow S^{37}LIGKV$ (see Figure 1.10). Structurally, PAR2 follows the classical GPCRs architecture (refer to the subsection 1.6.1), comprising seven transmembrane (TM) helices, three intracellular loops (ICL1-3), three extracellular loops (ECL1-3), an intracellular C-terminal domain (50 residues in length) and an extracellular N-terminal domain including a signal peptide and a propeptide region (Cheng et al., 2017). Among these structural features, ECL2 connects TM4 and TM5, and forms a GPCR-conserved disulfide bond between Cys148 in ECL2 and Cys226 in TM3, essential for proper receptor folding and confers structural stability to the receptor (Hamm, 2001, Cheng et al., 2017). Additionally, PAR2 undergoes post-translational modifications that regulate receptor desensitisation, with specific residues involved in these modifications illustrated in Figure 1.10.

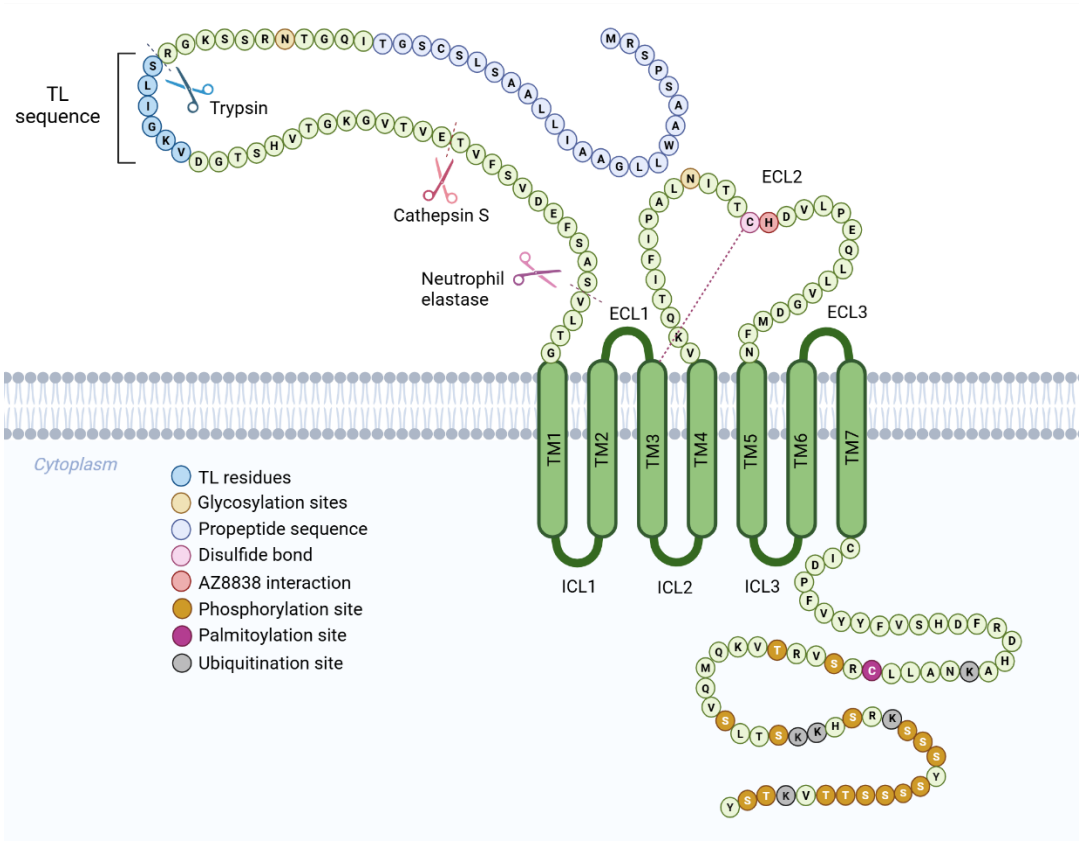

Figure 1.10: Structural representation of PAR2 with key interaction sites.

Schematic illustration of the structure of PAR2, showing the basic structural domains of GPCRs including the transmembrane domains (TM1–TM7), extracellular loops (ECL1-3) and intracellular loops (ICL1-3), with detailed amino acid sequence of N-terminal, ECL2 and C-terminal. The canonical tethered ligand (TL) sequence, shown in blue, is cleaved by specific proteases such as trypsin, while cathepsin S and neutrophil elastase act as non-canonical activating proteases, cleaving the N-terminal at distinct sites. Key post-translational modifications are highlighted, including N-glycosylation sites (yellow), palmitoylation sites (purple), phosphorylation sites (orange), and ubiquitination sites (grey). Disulfide bonds (pink dashed lines) between ECL2 and TM3 and the AZ8838 interaction site (red circle) are shown. AZ8838 is the tested PAR2 antagonist in this thesis, see section 3.1 for details on AZ8838 pharmacology. Figure prepared using Biorender.com with reference to (Adams et al., 2011, Chandrabalan and Ramachandran, 2021).

1.10.2 PAR2 activation and signalling:

As a GPCR, PAR2 mediates intracellular signalling primarily through the activation of the heterotrimeric G-proteins. Upon activation by proteolytic cleavage, unmasking its tethered ligand or activation by other agonists, PAR2 predominantly couples to $G\alpha_q$,

$G\alpha_i$ and $G\alpha_{12/13}$ (Soh et al., 2010), activating the downstream signalling cascades (Oldham and Hamm, 2007, Oldham and Hamm, 2008). Afterwards, the type of signalling pathway engaged is largely dependent on cell type and the activating protease or agonist. Studies reported that PAR2, similar to PAR1, can activate $G\alpha_q$, stimulating phospholipase Cβ (PLCβ), promoting the production of IP3 and DAG, which trigger Ca2+ mobilisation and, consequently, activation of PKC (Steinhoff et al., 2005). This pathway has been confirmed in multiple cell types, including human kidney, intestinal epithelial cells (Bohm et al., 1996a, Bohm et al., 1996b), rat hippocampal neurons and astrocytes (Bushell et al., 2006), as well as myocytes and fibroblasts (Ossovskaya and Bunnett, 2004). Other than Ca^{2+} response, PAR2 activation has been linked to the production of prostaglandins and interleukins, suggesting activation of phospholipase A_2 (Kong et al., 1997, Shpacovitch et al., 2004, Lee et al., 2010). Downstream effectors that respond to PAR2 activation include MAP kinases, ERK1/2 in particular, besides RhoA (Ras homology A), nuclear factor kappa-B (NF-κB) and activator protein-1 (AP-1) (Steinhoff et al., 2005). PAR2 has also been shown to interact with toll-like receptor-4 (TLR4) in immune responses. Co-immunoprecipitation studies demonstrated that PAR2 physically associates with TLR4 upon exposure to a PAR2-AP, resulting in NF-κB activation (Nhu et al., 2010). Functional synergism between PAR2 and TLR4 was confirmed using macrophages deficient in either PAR2 or TLR4. In $PAR2^{-/-}$ or $TLR4^{-/-}$ macrophages, IL1β expression was significantly diminished upon exposure to PAR2-AP or LPS, respectively (Rallabhandi et al., 2008). Similar cooperativity between PAR2 and TLR2 and TLR3 was evident in mucosal epithelial cells (Nhu et al., 2010). Additionally, in specific cell types, PAR2 activation trans-activates epidermal growth

factor (EGF) receptors, linking it to cellular proliferation (Darmoul et al., 2004, Li et al., 2022). In respiratory and umbilical endothelial cells (Klarenbach et al., 2003, Yagi et al., 2006), as well as prostate cancer cells (Greenberg et al., 2003), PAR2-AP leads to Rho activation and induction of focal adhesion kinase (FAK) phosphorylation, promoting actin cytoskeleton remodelling, cell adhesion and migration. This demonstrates the crucial role of PAR2 in cellular dynamics, including endothelial barrier regulation, wound healing and cancer progression (Rahman et al., 2018, Jiang et al., 2021, Bandara and MacNaughton, 2022). Notably, studies demonstrated that PAR2 activation using PAR2-AP reduced transepithelial resistance, increased paracellular permeability, and disrupted E-cadherin-mediated adhesion in primary human airway epithelial cells, indicating a direct role in epithelial barrier dysfunction in airway inflammation (Winter et al., 2006).

Interestingly, PAR2 is capable of eliciting G-protein-independent signalling through β-arrestin-mediated ERK1/2 activation (Wang and DeFea, 2006, Zoudilova et al., 2007). Upon PAR2 activation, PKC isoforms (Bohm et al., 1996a) mediate PAR2 cytosolic C-terminal phosphorylation (Ricks and Trejo, 2009b) and consequent β-arrestin binding. This interaction assembles a MAP kinase large signalling complex composed of PAR2, β-arrestin, Raf-1, and activated ERK1/2, which is retained at the plasma membrane or the early endosome. This sustained ERK1/2 activation regulates cytosolic targets, distinguishing it from classical GPCR-mediated ERK1/2 signalling, which is transient (DeFea et al., 2000a). The effect on the time course of PAR2-induced ERK1/2 activation was evident in studies employing C-terminal mutant PAR2 (preventing β-arrestin binding), resulting in detectable but short-lived PAR2-mediated

ERK1/2 signalling compared to the prolonged response in wild-type PAR2 (DeFea et al., 2000a, Stalheim et al., 2005).

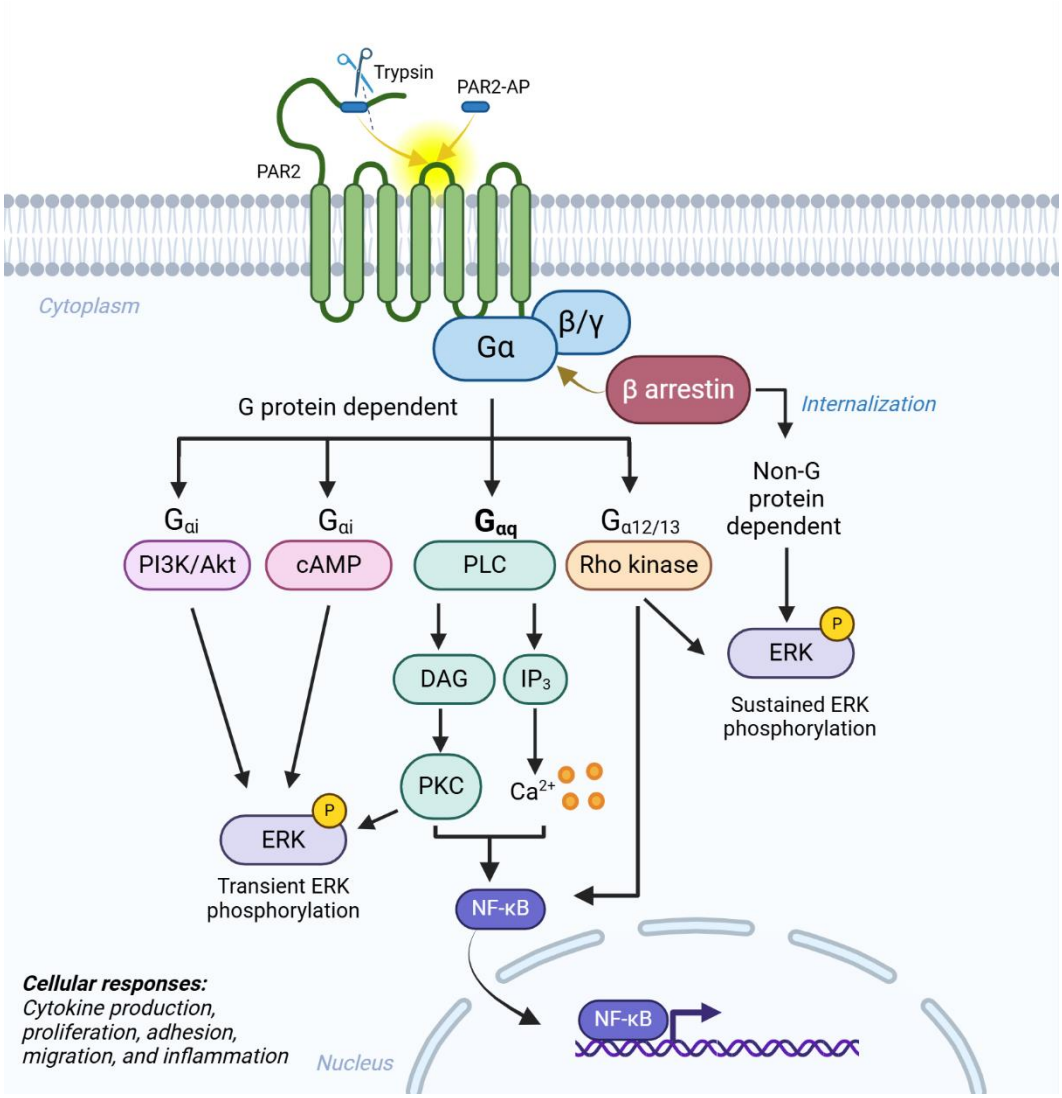

Figure 1.11: Overview of PAR2 activation and signal transduction.
Schematic representation of PAR2 activation and downstream signalling. Upon proteolytic cleavage or synthetic agonist stimulation, PAR2 couples to $G\alpha_q$, $G\alpha_i$, or $G\alpha_{12/13}$, activating intracellular pathways depending on the Gα subtype, including PLCβ-IP3/DAG-Ca^{2+}-PKC, cAMP or PI3K/Akt/MAPKs, or Rho kinase, respectively. These intracellular signals activate transcription factors NF-κB pathway. In parallel, PKC-mediated phosphorylation of PAR2 facilitates β-arrestin recruitment, promoting G-protein-independent sustained ERK1/2 activation. Visual created by Biorender.com.

In addition to mediating GPCR-independent signalling, β-arrestin uncouples PAR2 from GPCR signalling, mediating receptor desensitisation and internalisation machinery via a dynamin- and clathrin-dependent mechanism (Déry et al., 1999, Ricks and Trejo, 2009b) (Figure 1.6). Since PAR2 activation is irreversible due to proteolytic cleavage, β-arrestins promote the lysosomal degradation of used receptors rather than their recycling. Unlike other GPCRs, which display abundant cell surface expression and low intracellular levels, PAR2s are highly detectable in many cells, predominantly intracellularly compared to the cell surface, requiring intracellular receptor pools for trafficking or de novo synthesis for resensitisation (Déry et al., 1999). β-arrestins thus play a dual role in PAR2 regulation; as a molecular scaffold permitting sustained ERK1/2 activation, and as a key regulator of PAR2 desensitisation and degradation. An additional deactivation mechanism involves the ubiquitination of activated PAR2, which prevents cell surface recycling through a ubiquitin-protein ligase, c-Cbl (Jacob et al., 2005). Also, trafficking of internalised PAR2 from endosomes to lysosomes for degradation is another termination machinery that is reliant on deubiquination of endosomal PAR2 (Hasdemir et al., 2007, Hasdemir et al., 2009a). Ultimately, the equilibrium between desensitisation and resensitisation is crucial for effective PAR2 signalling across both physiological and pathological conditions.

1.10.3 Modulation of PAR2 signalling:

Various complex mechanisms regulate PAR2 signalling, influencing both G protein-dependent and independent pathways and ultimately shaping the downstream effects of PAR2. These regulatory mechanisms are discussed in the following sections.

1.10.3.1 Post-transitional receptor modifications:

Post-transitional modifications of PAR2 receptors play a critical role in regulating PAR2 signalling, influencing activation, desensitisation, trafficking and downstream signalling outcomes. As discussed in the previous section (section 1.10.2), phosphorylation and ubiquitination primarily function to drive receptor deactivation and trafficking. In addition, N-glycosylation and palmitoylation are modulatory mechanisms that fine-tune PAR2 activity. N-glycosylation at the N-terminal site (N^{30}) negatively affects PAR2 activity in response to cleavage by mast cell tryptase (refer to Figure 1.10). Studies using mutant rat PAR2 receptor devoid of this N-glycosylation site, while retaining another PAR2 N-glycosylation site within ECL2 (N^{222}), showed that PAR2 responded to tryptase with more selectivity and potency (> 30 folds) compared to wild type (Compton et al., 2001). However, the effect of N-glycosylation differs depending on the activating protease. When activated by trypsin or synthetic peptide SLIGRL-NH_2, mutation of PAR2 at N-glycosylation sites resulted in loss of sensitivity to these activators. Further investigations revealed this loss of activity was due to a significant reduction of cell surface expression rather than direct functional modulation (Compton et al., 2002). Using glycosylation inhibitor, tunicamycin, significantly reduces PAR2-induced tissue factor (TF) synthesis and secretion in human kidney tubular epithelial cells, indicating that glycosylation is essential for optimal PAR2-mediated procoagulant activity in these cells (Humphries et al., 2021).

Unlike N-glycosylation, palmitoylation enhances receptor expression and modulates its signalling. Palmitoylation is a thioesterification process that typically occurs at cysteine residues located 10–14 amino acids downstream of the last transmembrane domain (TM7). Autoradiographic assays confirmed that PAR2 undergoes

palmitoylation at cysteine residue (C^{361}) within the intracellular C-tail (Botham et al., 2011). Interestingly, a mutant human PAR2 with replacement of alanine at C^{361} exhibited greater cell surface expression compared to wild type. However, this mutation led to decreased sensitivity and efficacy towards both trypsin and SLIGKV with differential effect of internalization kinetics and decreased both $G\alpha_{q/11}$ coupling and β-arrestin-1/2 recruitment to PAR2 (Thibeault and Ramachandran, 2020). This demonstrated the relevance of palmitoylation's modulatory role on the PAR2 receptor, regulating its availability, signal sensitivity, and desensitisation dynamics.

1.10.3.2 Heterodimerisation:

Like other GPCRs, PARs undergo heterodimerisation, forming physical pairs of receptor units that expand their signalling capabilities and functionality. There is strong evidence that PAR1 can transactivate PAR2 *in vivo,* as demonstrated in a sepsis mouse model (Kaneider et al., 2007). In this study, PAR1 switched from an endothelial barrier-disruptive to a protective role via a PAR2-dependent mechanism involving the $G\alpha_i$-Rac signalling pathway. The protective effects of PAR1 were lost upon silencing PAR2 receptors using small interfering RNA (Kaneider et al., 2007), underscoring the functional interplay between these receptors.

Similarly, PAR1-PAR2 interactions have been implicated in vascular remodelling. In a study using arterial injury-induced hyperplasia, the administration of a PAR1 agonist, pepducin, led to a hyperplastic response in vascular smooth muscle cells (Sevigny et al., 2011). However, a histological analysis revealed that hyperplasia was completely absent in $PAR2^{-/-}$ mice, like the effect in the $PAR1^{-/-}$ group, suggesting that PAR1-driven hyperplasia requires functional PAR2 signalling. In addition to the

vasculature, PAR1-PAR2 dimerisation has been observed in carcinogenesis (Shi et al., 2004). Thrombin-activated PAR1 was found to induce the formation of PAR1-PAR2 heterodimer, which exhibited distinct regulation compared to the individual receptor. Moreover, these heterodimers triggered a β-arrestin-mediated activation of ERK1/2 in the cytoplasm (Lin and Trejo, 2013). Similarly, PAR2-PAR4 heterodimerization has been shown to play a role in the membrane trafficking of PAR4. This interaction disrupted PAR4 binding to the endoplasmic reticulum protein, COP1 β-subunit (β-COP1), instead facilitating its interaction with the chaperone protein 14-3-3ζ, which affects receptor stability and function. FRET imaging and co-immunoprecipitation confirmed the physical association of PAR2-PAR4 dimers (Cunningham et al., 2012). Collectively, these studies provide evidence that PARs undergo dimerisation, which modulates signalling, trafficking, and function.

1.10.3.3 Biased signalling:

Also referred to as 'agonist-directed trafficking', functional selectivity' or 'agonist-selective signalling', biased signalling is the ability of a single receptor to elicit distinct signalling responses depending on the activating ligand. This occurs because different ligands stabilise unique receptor conformations, leading to selective engagement of specific intracellular pathways, a phenomenon well-established with GPCRs signalling (Urban et al., 2007, Zheng et al., 2010). This phenomenon allows different agonists to fine-tune receptor signalling, potentially influencing physiological or pathological responses. Studies have demonstrated that different PAR2-AP can selectively engage distinct signalling pathways. In KNRK cells stably expressing PAR2, SLIGRL-NH_2 peptide, which matches the rat PAR2 tethered ligand sequence, induced both calcium and MAPK pathways, while the synthetic SLAAAA-NH_2

peptide triggered MAPK but not calcium signalling (Ramachandran et al., 2009). Additionally, mutations in the initial two amino acids of the tethered ligand sequence of the rPAR2 uncoupled the receptor from $G\alpha_q$-mediated calcium signalling, while still activating the MAPK pathway in a β-arrestin-independent and Rho-kinase-dependent manner (Ramachandran et al., 2009).

Beyond synthetic ligands, endogenous proteases can induce PAR2-biased signalling. Human neutrophil elastase (NE) unmasked a 'non-canonical' PAR2 tethered ligand, selectively activating $G_{12/13}$-MAPK pathway while bypassing calcium signalling and β-arrestin recruitment (see Figure 1.10). However, a synthetic peptide mimicking this 'non-canonical' TL sequence (VLTGKLTTVFL-NH_2) failed to activate PAR2 via either calcium signalling or the MAPK pathway (Ramachandran et al., 2011).

PAR2 antagonists can selectively inhibit specific PAR2 signalling pathways, while allowing others to remain active. GB88 is a PAR2 antagonist that blocks agonist-stimulated calcium signalling yet paradoxically activates the MAPK pathway and promoting PAR2- β-arrestin interactions at levels parallel to that induced by trypsin or PAR2-AP (Lohman et al., 2012, Suen et al., 2012). Thus, GB88 functions as a 'biased partial agonist-antagonist' simultaneously activating MAPK signalling and blocking trypsin-induced PAR2 calcium signalling. Recently, matrix metalloproteases (MMPs) were found to cleave PAR2 at a novel N-terminal site in SW1353 chondrocytes overexpressing PAR2. A synthetic peptide corresponding to this neo-tethered ligand sequence failed to induce calcium mobilisation and other canonical activation responses, yet conserved MAPK phosphorylation further supports biased signalling mechanisms in PAR2 activation (Falconer et al., 2019).

1.10.4 Agonists and antagonists for PAR2:

1.10.4.1 Activating and disarming proteases:

As with all PARs, proteolytic cleavage at the extracellular N-domain of PAR2 leads to irreversible removal of the terminal propeptide sequence (Figure 1.10) and exposure of the tethered ligand sequence, -S^{37}LIGKV- for most of the activating proteases for PAR2 (Nystedt et al., 1995a), which interacts with the ECL2 leading to conformational changes and trigger intracellular signalling. Beyond trypsin, human PAR2 can be proteolytically activated by several endogenous or exogenous proteases (listed in Table 1.4). However, proteolytic cleavage at sites distinct from the activation site within the N-terminus can inactivate PAR2, effectively disarming the receptor and inhibiting downstream signalling. This is either due to cleavage at a site distinct from the activation site within the N-terminal of the receptor, leading to the removal of the tethered ligand, or cleavage at other domains, disrupting the receptor integrity and signalling (Ramachandran et al., 2012). A list of PAR2-disarming proteases is provided in Table 1.4. It is important to note that activating proteases are not true ligands of PAR2. Many of these proteases have broad substrate specificity and can activate multiple receptors, including other members of the PAR family. This lack of specificity has created a critical need for the development of specific agonists to enable precise investigations of PAR2-specific activity and function. For example, trypsin, the primary activating protease of PAR2, can also activate PAR4 (Xu et al., 1998)

Table 1.4: List of activating and disarming proteases of PAR2.

Activating proteases	**Disarming proteases**
Trypsin **(Nystedt et al., 1994)**	Plasmin (Loew et al., 2000)
Mast cell tryptase **(Molino et al., 1997)**	Protease 3 (Loew et al., 2000)
TF:Factor Xa: Factor VIIa **(Camerer et al., 2000)**	Calpain (Loew et al., 2000)
Acrosin **(Smith et al., 2000)**	Cathepsin G (Dulon et al., 2003)
Matriptase/MT-SP1 **(Takeuchi et al., 2000)**	Elastase (Dulon et al., 2005)
human airway trypsin-like protease (HAT) **(Miki et al., 2003)**	
Trypsin IV (Cottrell et al., 2004a)	
Granzyme A **(Hansen et al., 2005)**	
TMPRSS2 **(Wilson et al., 2005)**	
Chitinase **(Hong et al., 2008)**	
KLK2, 4, 5, 6, 14 **(Oikonomopoulou et al., 2006, Mize et al., 2008)**	
Bacterial gingipains **(Uehara et al., 2005)**	
House dust mite cysteine protease Der P1 **(Adam et al., 2006)**, mite serine proteases Der P2, Der P3 (Sun et al., 2001)	
Mold allergen serine protease (Pen C 13) **(Chiu et al., 2007)**	

1.10.4.2 PAR2 activating peptides (PAR2-AP):

In its inactive state, the PAR2 tethered ligand remains masked, requiring proteolytic cleavage for its activation. However, synthetic peptides that mimic the tethered ligand sequence can activate PAR2 without undergoing proteolysis. Many PAR2-AP have been designed to match or resemble the original sequence of the human PAR2 tethered ligand (SLIGKV) (Macfarlane et al., 2001). Structure-activity relationship studies comparing synthetic activating peptides have led to key structural determinants of potency and selectivity. A minimum of five amino acid peptides is required to achieve micromolar agonist potency via PAR2 (Hollenberg et al., 1996). Substitution of serine at the N-terminal with acidic, basic or large hydrophobic residues significantly reduces agonist activity. The terminal amino group is critical for activity, as its acetylation reduces agonist activity by more than 25-fold compared to the parent peptide, whereas removal of the amino group reduces activity only by fourfold. Glycine at position 4

can be replaced by alanine or Cha (beta-cyclohexyl-L-alanine), despite that Cha-substituted peptides also activated PAR1. Moreover, the Addition of a 2-furoyl moiety in substitution for serine at the N-terminal enhances potency by approximately 10-fold (Kawabata et al., 2004). Extending the peptide to seven residues may or may not improve potency, depending on the N-terminal residue (Barry et al., 2006). While these peptides serve as direct and specific activators of PAR2 (McGuire et al., 2004), they are prone to degradation, particularly in *in vivo* studies, and have limited potency, requiring the use of relatively high concentrations to induce PAR2 activity that could affect selectivity and may lead to cross-reactivity (Gardell et al., 2008).

1.10.4.3 Non-peptidic agonists:

Despite the availability of potent PAR2-APs, their poor bioavailability remains a significant limitation for in vivo PAR2 investigations. This challenge has driven the development of non-peptidic PAR2 agonists, which offer improved stability and pharmacokinetics. Notable examples include AC-55541 (full agonist), AC-98170 (partial agonist) and AC-264613 (full potent agonist) (Gardell et al., 2008, Seitzberg et al., 2008). Comparative studies evaluating the potency and efficacy of these agonists against classical PAR2-APs revealed that AC-264613 and 2-furoyl-LIGRLO-NH_2 were the most potent, with a similar EC50 value of 0.1 μM for Ca^{2+} mobilisation in KNRK cells transiently transfected with human PAR2 receptors. AC-55541 showed slightly lower potency at 0.25 μM yet remained ~40 times more potent than SLIGRL-NH_2 (EC_{50} 10 μM) (Gardell et al., 2008). Further research led to the development of the new non-peptidic PAR2 agonist molecule, GB110, which was developed from a basic hexapeptide with additional non-peptidic moieties. GB110 selectively triggers PAR2-mediated intracellular Ca^{2+} release in human colorectal carcinoma cells,

exhibiting an EC_{50} of 0.28 μM, a potency comparable to synthetic PAR2-APs. Additionally, GB110 demonstrates superior serum stability, making it a valuable research tool in human-based studies (Barry et al., 2010).

1.10.4.4 Peptide-based antagonists:

Given its critical role in regulating many cellular responses under both physiological and pathological conditions, the development of selective PAR2 antagonists holds significant potential for research and therapeutic applications. However, progress in identifying potent, specific PAR2 antagonists has been slower compared to that of PAR1-specific antagonists. Early studies identified peptide-based inhibitors, like FSLLRY-NH_2 and LSIGRL-NH_2, which blocked trypsin-induced PAR2 activation seemingly indirectly, but were ineffective against PAR2-AP-mediated activation (Al-Ani et al., 2002). Later, K-12940 and K-14585 were reported as competitive antagonists capable of inhibiting both protease- and PAR2-AP-mediated cellular and biological responses *in vitro* and *in vivo* (Kanke et al., 2009), with the latter showing dual effect on PAR2 signalling (Goh et al., 2009). Further research has led to the identification of C391, a low-molecular-weight, dose-dependent antagonist of trypsin- and peptidomimetic agonist-induced PAR2 activation. C391 was derived from the modification of 2-furoyl-LIGRLO-NH_2, resulting in a structurally distinct molecule with potent inhibitory properties. This compound blocked PAR2-mediated intracellular Ca^{2+} mobilisation (IC_{50} = 1.3 μM) and MAPK signalling (IC_{50} = 14.3 μM) (Boitano et al., 2015). Further research identified C781, a β-arrestin-biased PAR2 antagonist that selectively inhibits β-arrestin/MAPK signalling, while Gαq/Ca^{2+} signalling remained unaffected. Moreover, C781 significantly reduced NE- and PAR2-AP-induced pain responses, reducing mechanical hypersensitivity (Schiff et al., 2023).

C781 attenuated hypersensitivity in mast cell-mediated pain models using compound 48/80, but showed no effect on λ-carrageenan-induced hyperalgesia, suggesting a specific role in protease-driven signalling (Kume et al., 2023b).

1.10.4.5 Pepducins: intracellular allosteric PAR2 Antagonists:

A distinct class of PAR2 antagonists is the pepducins, which are short peptides derived from the ICLs of the GPCR and are linked to hydrophobic moieties, such as palmitate (Kuliopulos and Covic, 2003). This lipopeptide structure enables reversible incorporation of the molecule into the lipid bilayer and interaction with the GPCR-G protein interface in an intracellular allosteric modulatory mode (O'Callaghan et al., 2012, Zhang et al., 2015). Using rodent inflammatory models, P2pal-18S and PZ235 showed inhibitory effects on cellular and biological responses of PAR2 activation by several specific and non-specific agonists (Shearer et al., 2016). PZ-235 significantly inhibited PAR2-mediated activation of NF-κB and TNF-α in human keratinocytes and reduced IL-4 and IL-13 levels in mast cells. In the animal dermatitis model, PZ-235 significantly reduced skin thickening, leukocyte infiltration, and itching behaviours (Barr et al., 2019). Recently, P2pal-18S was found to attenuate neuroinflammation in the experimental autoimmune encephalomyelitis (EAE) model of multiple sclerosis (MS), reducing T-cell and macrophage infiltration into the CNS as well as demyelination (Eftekhari et al., 2024). Although the study did not measure blood-brain barrier (BBB) permeability, the effects of P2pal-18S suggest its ability to reach the CNS *in vivo*.

1.10.4.6 Non-peptidic small molecule antagonists:

The first non-peptidic reversible PAR2 antagonist, GB83, inhibited PAR2 activation by multiple agonists at micromolar concentrations (Barry et al., 2010). Although recently, GB83 was shown to function as a "bona fide" PAR2 agonist in HT-29 cells, inducing intracellular calcium signalling, ERK1/2 phosphorylation, and receptor internalisation in a delayed and sustained manner compared to trypsin and PAR2-AP (Heo et al., 2022). A more potent derivative, GB88, was later developed from the agonist GB110, which was capable of blocking PAR2-induced Ca^{2+} mobilisation by endogenous proteases, synthetic peptides, and non-peptidic agonists at an IC_{50} of approximately 2 μM. Interestingly, GB88 selectively inhibited PAR2-mediated pathways, leaving ERK phosphorylation unaffected. Furthermore, it was found to be orally bioactive; therefore, it has been employed for PAR2 *in vivo* investigations using a range of animal models of human inflammatory and proliferative diseases (Suen et al., 2012), like PAR2-induced paw oedema (Lieu et al., 2016), chronic collagen-induced model of arthritis (Lohman et al., 2012), nephrotoxic serum nephritis (Han et al., 2019), and periodontal disease (Francis et al., 2023). Additional antagonists and their effects are shown in Table 1.5. Meanwhile, Astra-Zeneca and Heptares reported an imidazole-based competitive antagonist (AZ8838, IC50 2.3 μM vs SLIGRL) and a benzimidazole-based negative allosteric modulator (AZ3451, IC50 5.4 nM vs SLIGRL) that bind to PAR2, leading to inhibition of PAR2-activation induced cellular responses (Cheng et al., 2017). It was defined that AZ8838 binds to PAR2 in an occluded pocket formed by TM 1-3, 7, and ECL2, enabling competitive inhibition of tethered ligand binding. For AZ3451, it binds to PAR2, which binds to a site facing the lipid bilayer within TM2, TM3, and TM4, stabilising a receptor conformation that

inhibits PAR2-AP binding (Kennedy et al., 2020). Later, a research group identified an imidazopyridazine compound (I-191) as a non-competitive PAR2 antagonist, capable of inhibiting multiple PAR2 agonists in a concentration-dependent manner in human cancer cell lines. Additionally, I-191 acts as a negative allosteric modulator of the agonist 2f-LIGRL-NH2 (Jiang et al., 2018). More recently, I-287, a negative allosteric modulator (NAM) of PAR2, demonstrated functional selectivity by inhibition of $G\alpha_q$- and $G\alpha_{12/13}$-mediated signalling while sparing $G\alpha_{i/o}$ and β-arrestin recruitment. I-287 significantly reduced IL-8 secretion in human epithelial and endothelial cells and demonstrated *in vivo* anti-inflammatory effects in a mouse model of Complete Freund's Adjuvant (CFA)-induced inflammation (Avet et al., 2020). The continuous research for novel PAR2 antagonists remains a potential interest for the pharmaceutical industry as well as the academic field.

Table 1.5: PAR2 agonists and antagonists

Class	Agonist/ Antagonist	Name	Receptor/Cell/Tissue type	Cellular response
Peptide	Agonist	SLIGRL/−NH2	Rat: vascular and gastric smooth muscle	Induces calcium release (Al-Ani et al., 1995)
		SLIGKV/−NH2	Human: Human PAR2 expressed in *Xenopus* oocytes	Induces calcium release (Blackhart et al., 1996)
		2f-LIGRLO/−NH2	Human: KNRK cells expressing PAR2, HEK293 cells; Rat: KNRK cells expressing rat PAR2	Induces calcium release (McGuire et al., 2004)
	Antagonist	FSLLRY-NH2	Rat	Inhibits neuropathic pain (Wei et al., 2016)
		LSIGRL-NH2	Human: KNRK cells	Blocks trypsin, not SLIGRL-induced calcium release (Al-Ani et al., 2002)
Peptide-based	Antagonist	K14585, K12940	Human: NCTC2544 cells expressing PAR2	Reduces SLIGKV-induced calcium release (Goh et al., 2009)
			Human: NCTC2544 cells expressing PAR2	Inhibits SLIGRL-induced NF-κB activation (Kanke et al., 2009)
		C391	Human: 16HBE14o- cells Mouse	Blocks calcium release and MAPK activation, and reduces compound 48/80-induced thermal hyperalgesia. (Boitano et al., 2015)
	β-arrestin-biased antagonist	C781	Human: 16HBE14o- cells Mouse	Inhibits β-arrestin/MAPK signalling without significant effect on Gq/Ca^{2+} signalling (Schiff et al., 2023) Attenuates airway hyperresponsiveness and inflammation in an acute *Alternaria alternata*-challenged model (Schiff et al., 2023) Prevented and reversed mechanical and spontaneous nociceptive behaviours induced by PAR2-AP, mast cell activators, and NE, but had no effect on carrageenan-induced pain (Kume et al., 2023b).

Non-peptide small molecule	Agonist	GB110	Human: six cell types: A549, Panc-1, MKN1, MKN45, MDA-MB231, HUVEC ; Rat	Induces calcium release and paw oedema in rats (Suen et al., 2012)
		GB83	Human: HT-29	Induces calcium mobilisation, ERK and p38 MAPK phosphorylation, and PAR2 internalisation in a delayed kinetics compared to trypsin and SLIGRL (Heo et al., 2022)
		AC-5541, AC-264613	Human: HEK293T, KNRK cells, NIH3T3 cells Rat	Induces PI hydrolysis, calcium release, cellular proliferation, besides intrapaw or systemic administration, produced hyperalgesia and inflammation (Gardell et al., 2008)
			Human: HEK293T, KNRK cells, NIH3T3 cells Rat Mouse	Induces PI hydrolysis, calcium release, cellular proliferation, beside intrapaw or systemic administration produced hyperalgesia and inflammation (Gardell et al., 2008) Reduced locomotor activity and sucrose preference, increased serum IL-6 and altered cytokine mRNA expression in the brain (Moudio et al., 2022)
		AZ2429	Human: 1321N1-hPAR2, U2OS-hPAR2	Stimulated calcium release, inositol phosphate (IP1) production, phosphorylation of ERK1/2, and β-arrestin-2 recruitment (Kennedy et al., 2020)
	Antagonist	ENMD-1068	Human: primary cultures of rheumatoid arthritis (RA) synovial tissue	Inhibit PAR2-mediated release of INFα and IL1β in RA synovium (Kelso et al., 2007)
			Mouse Mouse HSC	Reduces joint inflammation (Kelso et al., 2006) Blocks calcium release and reduces liver fibrosis (Sun et al., 2017)
		GB83	Human: HT29	Inhibits trypsin and PAR2-AP calcium release (Barry et al., 2010)
		GB88	Human: six cell types: A549, Panc-1, MKN1, MKN45, MDA-MB231, HUVEC	Blocks PAR2-induced calcium release (Suen et al., 2012)
			Rat	Reduces acute paw oedema, inhibits PAR2-AP induced inflammation (Suen et al., 2012)

		AZ8838 AZ3451	Human: 1321N1-hPAR2, U2OS-hPAR2 Rat	Blocks PAR2-AP-induced calcium release and β-arrestin recruitment (Cheng et al., 2017) inhibited calcium release, inositol phosphate (IP1) production, phosphorylation of ERK1/2, and β-arrestin-2 recruitment; reduced paw swelling, mast cell degranulation and neutrophil activation (Kennedy et al., 2018)
		I-191	Human: HT29 and MDA-MB-231 cells	Inhibit multiple cellular and pro-inflammatory responses of PAR2 in cancer cell lines (Jiang et al., 2018)
		I-287	Human: HEK293, HCT 116, and CMT-93 cells Primary epithelial and endothelial cells Mouse	Negative allosteric regulator on $G\alpha_q$ and $G\alpha_{12/13}$, while sparing $G_{i/o}$ and β-arrestin2 recruitment (Avet et al., 2020) Blocks PAR2-mediated IL-8 secretion (Avet et al., 2020) Reduce paw oedema and inflammation in Freund's adjuvant (CFA)-induced model (Avet et al., 2020).
Pepducin	Antagonist	P2pal-18S	Mouse: in vivo and isolated mouse pancreatic acini	Inhibits PAR2-induced calcium transients in acinar cells and decreases the severity of biliary pancreatitis (Michael et al., 2013)
		PZ-235	Mouse	Suppress fibrosis, hepatocellular necrosis, reactive oxygen species production, steatosis, and inflammation (Shearer et al., 2016)
			Human: LX-2 human hepatic stellate cell	Inhibits PAR2 Ca^{2+} signalling (Shearer et al., 2016)
Antibiotic	Antagonist	Tetracyclines (Tetracycline, Doxycycline, Minocycline)	Human: NHEK cells	Inhibits SLIGRL-induced IL-8 release (Ishikawa et al., 2009)
			Mouse	Topical application of tetracycline decreases PAR2-induced skin inflammation (Liu et al., 2016)
			Rat	Subantimicrobial doses of doxycycline inhibit PAR2-induced inflammation (Castro et al., 2016)
Antibody	Antagonist	SAM11	Mouse	Attenuated carrageenan/kaolin-induced inflammation (Kelso et al., 2006) Reduced joint damage in the collagen-induced arthritis model (Crilly et al., 2012) inhibited OVA- and CE-induced airway hyperresponsiveness and inflammation (Asaduzzaman et al., 2015, Asaduzzaman et al., 2018)
		MAB3949	Human: A549 human epithelial cells	Blocks PAR2- induced calcium mobilisation (Cheng et al., 2017)

			Human	
		MEDI0618	Human: 1321N1-hPAR2, Primary human dural fibroblasts and microvascular endothelial cells Mouse: brain endothelial cells	Blocks matriptase-induced calcium signalling (Kopruszinski et al., 2025). inhibited PAR2-induced calcium influx and prevented periorbital and hindpaw allodynia in all migraine-like models (Kopruszinski et al., 2025)

1.10.5 PAR2 role in inflammation:

Since early studies focusing on PAR2, it was reported that stimulation of cultured human umbilical vein endothelial cells (HUVEC) with inflammatory cytokines, including tumour necrosis factor α (TNF-α), interleukin 1α (IL-1α) and bacterial lipopolysaccharide (LPS), elevated the expression of PAR2 messenger RNA (mRNA) dose-dependently (Nystedt et al., 1996, Ritchie et al., 2007). Most studies have confirmed that the activation of PAR2 contributes to the increased production of cytokines in an inflammatory context. Nevertheless, different experimental conditions showed variable outcomes upon PAR2 stimulation, whether induced by a PAR2-activating peptide (PAR2-AP), agonists or activating proteases, resulting in either a significant elevation or no noticeable impact on the baseline levels of inflammatory mediators. PAR2 stimulation with PAR2-AP in vitro was found to increase levels of TNFα (Vesey et al., 2013, Nishimoto et al., 2023), IL-6 (Jairaman et al., 2015, Daines et al., 2020), IL-8 (Yoshida et al., 2007, Jairaman et al., 2015, Heuberger et al., 2019), IL-4 (García-González et al., 2019), and granulocyte-macrophage colony-stimulating factor (GM-CSF) (Jairaman et al., 2015) compared to baseline in multiple cell types. A study has reported that stimulation of PAR2 (PAR2-AP: SLIGRL-NH2, 30 μM) enhanced the release of inflammatory cytokines, including IL-1β, IL-6, and monocyte chemoattractant protein-1 (MCP-1/CCL2), in cultured macrophages when pre-incubated with LPS. However, this activation did not exert any change from the baseline levels of these cytokines in the absence of LPS pretreatment (Barra et al., 2022). A similar earlier study has shown a concentration-dependent reduction in TNFα, IL-6, IL-12 p40 release in murine cultured macrophage and an opposite effect

upon the anti-inflammatory IL-10 with increasing doses of PAR2-AP, SLIGKV-NH2 (Nhu et al., 2012), suggesting a protective anti-inflammatory role of PAR2 activity in a specific context. Genetic deletion of the receptor *in vivo* has demonstrated a similar protective "anti-inflammatory" profile of PAR2. In the gastrointestinal tract (GIT), levels of mRNA encoding pro-inflammatory cytokines, including IL-8, IL-1β and IL-6, as well as their protein levels in colonic lysates of a murine colitis model, were significantly increased in PAR2-KO mice compared to the wild type littermates (Her et al., 2021). Although an earlier study applying the same collitits model demonstrated an opposite finding with regard to the inflammatory cytokines, despite pathohistological damage being more evident in PAR2KO mice (He et al., 2018). In line with these findings, PAR2 antagonist peptide (FSLLRY-NH2) induced a significant increase of mRNA levels of TNFα and monocyte chemoattractant protein-1 (MCP-1) in kidney tissue in a systemic lupus erythematosus murine model (Itto et al., 2019). These studies suggest that PAR2 activity could ameliorate or exacerbate inflammation depending on the experimental settings in some inflammatory conditions. Aside from changes in the levels of inflammatory mediators, it has been revealed that PAR2 is a major player in other forms of inflammatory tissue pathologies. Examining bone and cartilage inflammatory changes, genetic deletion of PAR2 in mice greatly reduced osteoarthritic-related pathological damage and changes (Huesa et al., 2016), joint swelling and synovial infiltration (Ferrell et al., 2003) when compared to wild-type animals. In the respiratory system, PAR2 antagonist pretreatment significantly ameliorated neutrophil infiltration, adhesion, and other lung inflammatory indicators (Silva et al., 2023). Numerous studies have emphasised the critical function of PAR2 in inflammatory disease-related pain nociception. Generally,

multiple studies have reported enhanced mechanical allodynia (Zhao et al., 2015) and thermal hyperalgesia (Lieu et al., 2016) upon peripheral PAR2-activating proteases or PAR2-AP administration in rodents. Moreover, a recent study has confirmed enhanced thermal hyperalgesia when central PAR2 (intrathecal injection of PAR2-AP) was stimulated in a peripheral cutaneous inflammation model (Mrozkova et al., 2021). These studies provided evidence in support of PAR2's immunological role in inflammatory disease, pinpointing an increase in key inflammatory-associated cytokines and linking a role for PAR2 to the induction of hyperalgesic responses. In the upcoming subsection, the data from the literature investigating the role of PAR2 in prostate inflammation, which is the subject of this study, will be discussed.

1.10.6 PAR2 in prostate inflammation:

Despite being widely studied in a variety of specific tissue inflammatory conditions, few researchers have investigated the involvement of PAR2 in prostate inflammation. It is confirmed that PAR2 is expressed in human prostate epithelial cells and is responsive to PAR2-AP and trypsin in terms of increased intracellular Ca^{2+} levels (Cottrell et al., 2004b). Implicating a murine experimental autoimmune prostatitis (EAP) model, Roman et al have provided evidence of PAR2 involvement in several features of this form of prostate inflammation (Roman et al., 2014). Increased expression of PAR2 was evident in EAP mice, suggesting a potential role of PAR2 in inflammatory processes within prostate tissue. Immunofluorescence staining revealed a noticeable increase in PAR2 expression in the prostate of mice subjected to EAP compared to naïve mice, which was confirmed by immunoblotting of prostate tissue lysate for PAR2 protein. Notably, real-time PCR analysis of microdissected prostate specimens, aimed at separating epithelial and stromal cells, demonstrated a greater

than threefold increase in PAR2 mRNA levels in the prostate epithelium and a nearly 4.5-fold increase in the prostate stroma of the EAP group compared to the naïve group. Histopathology assessment of prostate sections did not show a significant effect of PAR2 genetic deletion in terms of inflammation score and mast cell infiltration. Nevertheless, PAR2 knock-out (PAR2-KO) mice lost the enhanced intracellular Ca^{2+} levels induced by 1 nM capsaicin delivered to dorsal root ganglia (DRG) isolated from EAP mice and compared to naive cohorts, indicating the possibility that PAR2 is more linked to a hyperalgesia state (chronic pelvic pain) rather than prostate inflammation per se. In line with these results, behavioural assessment of mice at day 20 post-EAP showed that the inhibition of PAR2 using neutralising antibody (SAM11) significantly reduced pelvic pain compared to an isotope control group at days 7 and 10 after treatment, supporting the involvement of PAR2 in visceral nociception from prostate inflammation. Apart from pain, the same research group demonstrated that the absence of PAR2 and inhibition of the receptor using its specific SAM11 antibodies consistently retained normal bladder function (voiding pressure, void rate, bladder capacity and bladder compliance) using the murine EAP model (Roman et al., 2016). This could provide therapeutic relevance for PAR2 functional inhibition for the management of chronic prostatitis/ chronic pelvic pain syndrome (CP/CPPS) patients, as pelvic pain is one of the most common complaints in this condition besides lower urinary dysfunction (Marszalek et al., 2007).

1.10.7 PAR2 and pain

Several studies indicated a significant role of PAR2 in inflammatory, neuropathic, and cancer-evoked pain. The receptor, identified on primary sensory afferent nerves and dorsal root ganglia (DRG), has been associated with prolonged thermal and

mechanical hyperalgesia in both peripheral and visceral organs (Steinhoff et al., 2000b, Kawabata et al., 2001, Vergnolle et al., 2001a, Coelho et al., 2002, Kirkup et al., 2003, Nguyen et al., 2003). Interestingly, the selective activation of PAR2 induced hyperalgesic priming, a form of neuronal plasticity that transforms a nociceptor's response to pain into a long-lasting, intensified response. This phenomenon was confirmed through behavioural assessments in mice, where a single intraplantar injection of PAR2-AP induced prolonged mechanical hyperalgesia. After ensuring complete resolution (after 14 days post-PAR2-AP injection), a subthreshold dose of PGE2 (100 ng) elicited an enhanced pain response lasting for 24 hours (Tillu et al., 2015). This may indicate a direct contribution of PAR2 activation to chronic pain conditions. In 2007, Kayssi *et at* were the first to describe the sensitisation of visceral nociceptive neurons by PAR2 agonists, showing PAR2 activation induced sustained hyperalgesia. This finding was supported by immunohistochemical and electrophysiological assessments in murine colonic tissue (Kayssi et al., 2007). Consistent results were obtained in human colonic biopsies from irritable bowel disease (IBS) patients, confirming the release of proteases in IBS patients and the PAR2-dependent hypersensitisation of visceral neurons, leading to persistent hyperalgesia and allodynia (Cenac et al., 2007). Later, several studies continued to highlight the significant involvement of PAR2 in persistent pain associated with IBS and possible therapeutic relevance (Bueno, 2008, Wang et al., 2015, Jimenez-Vargas et al., 2018).

Investigations of PAR2-mediated hyperalgesia and neural regulation provided early evidence that PAR2 sensitises the transient receptor potential vanilloid 1 (TRPV1), activated by capsaicin, protons or heat, at molecular, functional, as well as behavioural

levels (Amadesi et al., 2004, Dai et al., 2004). This PAR2-mediated potentiation of TRPV1 was found to be dependent on protein kinase Cε (PKCε) and PKA in both cell culture and *in vivo* models (Amadesi et al., 2006). Consistent with these findings, PAR2-mediated TRPV1 sensitisation has been implicated in joint pain (Helyes et al., 2010) and oesophageal hypersensitivity (Wu et al., 2015). TRPV1 inhibition or deletion significantly reduced intraarticular SLIGRL-NH_2-induced mechanical allodynia (Helyes et al., 2010). Likewise, a TRPV1 antagonist partially reduced PAR2-induced oesophageal hypersensitivity in human oesophageal epithelial cells (Wu et al., 2017). Additionally, PAR2 activation sensitised the altered tonicity-gated cation channel TRPV4, a mediator of mechanical hyperalgesia, demonstrated by increased Ca^{2+} signalling and current intensity in cell cultures, besides murine mechanical hyperalgesia. This effect was found to be dependent on PLCβ, PKA, PKD and selected PKC isozymes (Grant et al., 2007). Further studies showed that PAR2 activation stimulated a transient increase in $[Ca^{2+}]_i$, which was significantly sustained in cells co-expressing TRPV4 and blocked by treatment with a TRPV4 antagonist (Poole et al., 2013). Moreover, PAR2 functionally interacts with P2X3 receptor, an ATP-gated ionotropic receptor expressed by sensory neurons, potentiating P2X3 responses by functional membrane translocation rather than phosphorylation (Wang et al., 2012).

Evidence shows that PAR2 contributes to nerve injury-induced hyperexcitability. In models of chronic compression (CCD) or dissociation of DRG in rats, PAR2 inhibition or knockdown via siRNA significantly suppressed hyperexcitability and hyperalgesia, providing evidence of PAR2 involvement in neuropathic pain (Huang et al., 2012). Chemotherapy-induced neuropathic pain was found to be PAR2-dependent as well, and it was linked to sensitisation of TRPV1, TRPV4 and TRPA1 (ankyrin) in a

paclitaxel-induced neuropathic pain in mice (Chen et al., 2011). Recently, PAR2 knockout mice showed a significant reduction of paclitaxel (PTX)-induced mechanical allodynia, spontaneous pain, satellite glial cell activation, and intra-epidermal fibre loss compared to wild-type. In addition, treatment with the peptidomimetic PAR2 antagonist, C781, significantly reduced mechanical allodynia (Kume et al., 2023a).

Pain is one of the main symptoms of specific types of cancer, and PAR2 activation has been identified as a major mechanism of cancer-related pain. Lam and Schmidt first demonstrated that PAR2 activation induces cancer-dependent allodynia via proteolytic activity in the tumour microenvironment (Lam and Schmidt, 2010). Injecting supernatant from human head and neck, but not from normal keratinocytes, induced prolonged mechanical allodynia in the hind paw of mice. This enhanced nociceptive effect was completely absent when supernatants were incubated with serine protease inhibitor before injection and in PAR2-KO mice, indicating the direct involvement of PAR2 in mediating cancer pain. Follow-up studies have led to the confirmation of the direct role of PAR2 in acute and chronic cancer pain, possibly by PAR2 upregulation using novel murine cancer pain models (Lam et al., 2012). Additional studies showed the significant involvement of PAR2 in nociceptive signalling in rat models of bone cancer pain (Bao et al., 2014, Liu et al., 2014b, Bao et al., 2015c). Furthermore, using the same bone cancer-evoked pain in rats, PAR2 antagonist peptide (FSLLRY-NH_2) potentiated antinociceptive effects of systemic morphine by sensitisation of μ-opioid receptors (Bao et al., 2015a, Bao et al., 2015b). Similarly, in pancreatic cancer pain, human pancreatic cancer biopsies showed significantly higher trypsin and protease activities compared to healthy tissue samples, and administration of the PAR2 antagonist peptide (FSLLRY-NH2) also induced a significant reduction of pain

behaviour in mice injected with human pancreatic cancer cell supernatants (Zhu et al., 2017). These observations suggest PAR2-mediated signalling contributes to hypersensitisation of nociceptors, leading to cancer-evoked pain triggered by trypsin-like serine proteases secreted by cancer cells. Collectively, these studies strongly suggest that targeting PAR2 could offer therapeutic value for the management of pain associated with chronic inflammation, neuropathy or cancer.

1.11 Hypothesis and Aim:

Project overview:

Prostate inflammation is one of the main causes of chronic pelvic pain conditions, including chronic prostatitis/chronic pelvic pain syndrome (CP/CPPS). PAR2, a GPCR uniquely activated by N-terminal proteolytic cleavage, has been widely shown to be involved in inflammatory and pain signalling pathways. AZ8838 is a small molecule PAR2 antagonist that has been shown for its inhibition potential of intracellular PAR2-induced responses. Although its mechanism and inhibitory effects have been studied, its comprehensive PAR2 inhibition profile has not been fully explored, particularly in the context of prostate inflammation.

Hypothesis:

The central hypothesis is that AZ8838 effectively inhibits PAR2-induced pro-inflammatory signalling pathways and cellular responses. Utilising *in vitro* characterisation of AZ8838, it is hypothesised that examining the antagonist *in vivo* may demonstrate its potential therapeutic relevance in carrageenan-induced prostatitis (CIP), attenuating inflammatory responses and pain sensitisation.

Research questions:

This research project is guided by the following overarching questions:

1. How does AZ8838 modulate key intracellular pathways downstream of PAR2 activation?

   This will be addressed through *in vitro* assays measuring the effects on NF-κB and MAPK signalling, PAR2 internalisation, calcium mobilisation, and the

release of the pro-inflammatory chemokine IL-8 in PAR2-expressing cell systems.

2. Does pharmacological inhibition of PAR2 attenuate inflammation and pain *in vivo*?

   This will be evaluated using the CIP model, assessing localised inflammatory responses, PAR2 expression in prostate and sensory neurons, and pain-related behaviours (mechanical allodynia and thermal hyperalgesia).

3. Can the *in vitro* mechanisms of PAR2 inhibition be correlated with *in vivo* outcomes to explain pain modulation and local inflammatory responses in the prostate?

   Findings from *in vitro* analyses of AZ8838-mediated PAR2 inhibition will be compared with *in vivo* observations from the CIP model, focusing on changes in pain-related behaviours and histological evidence of inflammation in the prostate.

Chapter 2

Materials and Methods

2.1 Materials and reagents

2.1.1 General reagents

All materials and reagents used were of the highest commercial grade available and purchased from Sigma-Aldrich Chemical Company Ltd. (Pool, Dorset, U.K.) or other companies as stated below. The list of used materials and reagents is sorted according to the company in Table 2.1.

Table 2.1: List of materials and reagents used for in vitro studies

Experiment	Name	Company	Cat no.
Luciferase reporter	Steady-Glo® Luciferase Assay Substrate	Promega Corporation (Madison, USA)	E2520
	Dithiothreitol (DTT)	Fisher BioReagents™, Fisher Scientific Inc	BP172-5
	Adenosine-5'-triphosphate (ATP) disodium salt hydrate	Thermo Scientific Chemicals,	J61125.06
Western blotting	Pre-stained SDS-PAGE molecular weight marker, Precision Plus Protein™ Dual Colour Standards	Bio-Rad Laboratories (Hertfordshire, UK)	1610374
	Methanol	VWR International Ltd. (Leicestershire, UK)	BDH1135
	ROTIPHORESE® Gel 30 (37.5:1)	Carl Roth GmbH + CO. KG (Karlsruhe, Germany)	3029.1
	Sodium dodecyl sulphate (SDS)	Sigma-Aldrich	L5750
	Tris-base, Trizma® base	Sigma-Aldrich	T1503
	Ammonium persulfate	Sigma-Aldrich	A3678
	Glycine	Sigma-Aldrich	G7126
	N, N, N', N'-tetramethylethylenediamine (TEMED)	Carl Roth GmbH + CO. KG (Karlsruhe, Germany)	2372
	Western Blotting Membranes, Nitrocellulose	Amersham™ Protran® by cytiva	1060001

	Gel blotting sheets 3MM	GB005, Whatman™ by VWR International Ltd. (Leicestershire, UK)	732-4094
	Bovine Serum Albumin (BSA)	Fisher BioReagents™ Thermo Fisher Scientific UK Ltd (Leicestershire, UK)	BP9706100
	Ultra Cruz® Autoradiography film blue	Santa Cruz Biotechnology Inc.	201696
	β-Mercaptoethanol	Sigma-Aldrich	M3148
	Tween 20	Sigma-Aldrich	P6585
Calcium assay	FLUO-4 AM	Invitrogen™ by Fisher Scientific Ltd (Leicestershire, UK)	F14201
	Hank's Balanced Salt Solution (HBSS) 1X (no Ca^{2+} and no Mg^{2+})	Gibco ™, life technologies Ltd. (Leicestershire, UK)	14175-095
	Calcium Chloride, 1M solution	Sigma-Aldrich, life Science	21115
	Magnesium Chloride, 1M solution	Sigma-Aldrich, life Science	63069
	Pluronic® F-127	Sigma-Aldrich, life Science	P2443
Immunofluorescence	4',6-diamidino-2-phenylindole (DAPI)	Fisher Scientific Ltd (Leicestershire, UK)	PIEN62248
	MOWIOL® 4-88 Reagent	Merck-Calbiochem (Nottingham, UK)	475904
ELISA	96-well ELISA plate	Corning™ Costar™	9018
	Human IL-8 Uncoated ELISA kit	Invitrogen	88-8086

Table 2.2: List of pharmacological agonists or antagonists for *in vitro* studies

Name	Company	Cat no.
2-furoyl-LIGRL-Orn-NH2 (2fLIG)	Peptide Synthetics, Peptide Protein Research, PPR Ltd., (Fareham, UK).	64604
Trypsin	Sigma-Aldrich Chemical Company Ltd. (Dorset, U.K.)	T4799
Human Tumour Necrosis Factor-α (TNF-α)	Insight Biotechnology Ltd. (Wembley, UK)	TP723983
(R)-AZ8838	Apex Molecular Limited, formerly YProTech (Cheshire, UK)	-
Dimethyl sulfoxide DMSO (vehicle)	Sigma-Aldrich	D8418

Table 2.3: List of materials and reagents used for *in vivo* studies.

Experiment	Name	Company	Cat no.
Inflammation induction	λ Carrageenan	Sigma Aldrich	22049
	Ketamine: Ketamil (100 mg/mL ketamine)	Ilium	-
	Xylazine: Xylazil-20: 20 mg/mL Xylazine	Ilium	-
	Antibiotic ointment: Fusidin ointment (2% sodium fusidate)	Leo pharma	-
	Betadine Antiseptic Solution: Povidone-Iodine 10% w/v	Atlantis Consumer Healthcare	-
	Lidocaine cream: Emla 5 % Cream: 5% lidocaine and prilocaine	Aspen healthcare	-
Perfusion fixation	Sevoflurane	Baxter	-
	Paraformaldehyde	Sigma Aldrich	158127
	Stereo microscope	Leica Microsystems	EZ4
Tissue sections Immunofluorescence	Superfrost® Plus Microscope Charged Slides	Thermoscientific	6776214
	Tissue embedding medium: Optimal cutting temperature compound (OCT)	Leica biosystems	14020108926
	Mounting Medium with DAPI - Aqueous, Fluoroshield	Abcam	ab104139
Western blotting	RIPA Lysis and Extraction Buffer	Thermo Scientific™	89900
	PMSF (Phenylmethylsulfonyl fluoride)	Sigma-Aldrich	P7626

	Halt™ Protease Inhibitor Cocktail (100X)	Thermo Scientific™	87786
	Phosphatase Inhibitor Cocktail II	Thermo Scientific™	J61022.AA
	Thermo Scientific™ Pierce™ BCA Protein Assay Kits	Thermo Scientific™	23227
	30% Acrylamide/Bis Solution, 29:1	Bio-Rad Laboratories, Inc	1610156
	TEMED	Bio-Rad Laboratories, Inc	1610800
	Immun-Blot PVDF Membrane, Roll, 26 cm x 3.3 m	Bio-Rad Laboratories, Inc	1620177
	IRIS11 Prestained Protein Ladder	BIO-HELIX	PMI11-0500
	Thermo Scientific™ Pierce™ ECL Western Blotting Substrate	Thermo Scientific™	32106
qRT-PCR	RNeasy PowerLyser Kit	Qiagen, Hilden, Germany	15055-50
	QuantiTect Reverse Transcription kit	Qiagen, Hilden, Germany	205311
	TaqMan™ Fast Advanced Master Mix for qPCR	Applied Biosystems™, Foster City, USA	4444557
	pre-designed Taqman Gene Expression Assays with FAM dye labelled PAR2 gene probe (ID: Rn00588089_m1, gene: F2rl1)	Applied Biosystems™, Foster City, USA	4331182

Table 2.4: List of pharmacological agonists or antagonists for *in vivo* studies

Name	**Company**	**Cat no.**
(R) AZ8838	AOBIOUS, Massachusetts, USA	AOB; 37172
Celecoxib	Celebrex® capsules, Pfizer	-
Dimethyl sulfoxide DMSO (vehicle)	Sigma-Aldrich	D8418

2.1.2 Reagents for cell culture

Table 2.5: List of reagents used for cell culture

Name	Company	Cat no.
All Cell Culture plasticware, including flasks, Falcon tubes, and graduated pipettes. Thermo Fisher Scientific UK Ltd (Leicestershire, UK)	Corning B.V (Buckinghamshire, UK)	
96-well Black with Clear Flat Bottom, and 12-well plates	Corning®, Costar	3603
Serological pipettes 5, 10, 25 ml	Sarstedt AG & Co LTD (Leicester, UK)	_
Minimum Essential Medium (1X)	Gibco (Life Technologies, Paisley, UK)	_
L-glutamine	Gibco (Life Technologies, Paisley, UK)	_
Penicillin-Streptomycin	Gibco (Life Technologies, Paisley, UK)	_
Geneticin (G148)	Gibco (Life Technologies, Paisley, UK)	_
Blasticidin	Gibco (Life Technologies, Paisley, UK)	_
Foetal Bovine Serum (FBS)	Gibco ™, Fisher Scientific Ltd (Leicestershire, UK)	A5256701
Medium 199	Sigma-Aldrich Life Science	M4530
RPMI Medium 1640	Gibco™, Fisher Scientific Ltd	11534446
Modified Eagle's Medium (MEM) 1x	Sigma-Aldrich Life Science	2091291

2.1.3 Compound preparation

Table 2.6: List of prepared solutions

Solution	Recipe
***In vivo* experiments solutions**	
Phosphate-buffered saline (PBS)	154 mM sodium chloride, 5.36 mM potassium chloride, 1.46 mM potassium hydrogen orthophosphate, 8 mM di-sodium hydrogen orthophosphate anhydrous, pH 7.4
0.1M PB (for perfusion fixation)	Potassium phosphate monobasic anhydrous (KH_2PO_4, Mol wt 136.09) 2.7 gm, sodium phosphate dibasic anhydrous (Na_2HPO_4, Mol wt. 141.96) 11.4 gm in 1 L distilled water. pH 7.4 and filtered
4% paraformaldehyde (for perfusion fixation)	Paraformaldehyde powder 40 g in 1L 0.1 PB, NaOH added until dissolved with continuous stirring, then filtered.
Tris buffer (8.8 pH)	Tris base 1.5M; 181.7 g in about 800 mL distilled water, adjust pH to 8.8, then complete volume to 1L.

Tris buffer (6.8 pH)	Tris base 0.5M; 60.5 g in about 800 mL distilled water, adjust pH to 6.8, then complete volume to 1L.
Tawbin's 10x transfer buffer	30 g Tris base, 144 g glycine, 10 g SDS, dissolve in 1 L of distilled water. Before use: 20% methanol in 1× buffer
PBST 0.1% wash buffer	For 1L PBS, dissolve 1 mL of Tween 20
***In vitro* experiments solutions**	
Versene	(0.2% EDTA/PBS) (0.53 mM) EDTA in phosphate-buffered saline
Freeze mix	0.08% DMSO (v/v) in FBS
Lysis buffer	25 mM Tris Base (pH 7.8), 8 mM $MgCl_2$, 1% Triton X 100, 15% (v/v) Glycerol
Laemmli SDS sample buffer	63 mM Tris-HCl (pH 6.8), 2 mM $Na_4P_2O_7$, 5 mM EDTA, 50 mM DTT, 10% v/v Glycerol, 2% w/v SDS, 0.007% bromophenol blue
Buffer 1	1.5 M Tris-base, 0.4% SDS, pH 8.4
Buffer 2	0.5 M Tris base, 0.4% SDS, pH 6.8
Running buffer	25 mM Tris base, 192 mM glycine, 0.1% SDS
Transfer buffer	25 mM Tris base, 192 mM glycine, 20% (v/v) methanol
Stripping Buffer	31 mM Tris-HCl, 2% SDS, pH 6.7
NATT (wash buffer)	150 mM NaCl, 20 mM Tris base, 0.03 % (v/v) Tween 20, pH 7.4
Enhanced Chemiluminescence-1 (ECL-1)	2.5 mM luminol (diluted from a stock of 250 mM in DMSO), 1.15mM p-coumaric acid (diluted from a stock of 250 mM in DMSO), 100 mM Tris base (pH 8.5), stored at 4˚C
Enhanced Chemiluminescence-2 (ECL-2)	0.00064% H_2O_2, 100 mM tris base (pH 8.5), stored at 4˚C
ELISA wash buffer	1X PBS, 0.05% Tween 20
ELISA stop solution	2 N H_2SO_4 in distilled water

2.1.4 Equipment

Table 2.7: List of Equipment

Experiment	**Equipment**	**Company**
Tissue sectioning	Cryostat microtome	Leica, CM1860
Mini-PROTEAN® Tetra Cell, Mini Trans-Blot® Module, and PowerPac™ HC Power Supply	Bio-Rad Laboratories, Inc	1658035
Trans-Blot Turbo Transfer System	Bio-Rad Laboratories, Inc	1704150
Azure Imaging Systems	Azure biosystems	Azure 600
Calcium mobilisation assay	FlexStation III Multi-Mode Microplate Reader	Molecular Devices
ELISA	POLARstar® Omega microplate reader	BMG Labtech
Immunofluorescence	Epifluorescent Upright Microscope, Nikon Eclipse E600	Nikon Instruments Inc.

	BX63, Automated Fluorescence Microscope	Olympus
qRT-PCR	QuantStudio 5 Applied Biosystems 7500 Fast Real-Time PCR System	Thermofisher Scientific
Behavioural studies	Aesthesio®, Precise Tactile Sensory Evaluator 20-piece Kit	Danmic Global, USA
	Mesh Stands	IITC Life Science Inc.
	Plantar Test (Hargreaves Method)	IITC Life Science Inc.

2.1.5 Antibodies

The following antibodies were used at the denoted dilution.

Table 2.8: List of antibodies

Antibody	Company	Ref/Cat. number	Species	Dilution	Experiment
p-ERK (E-4) 200 µg/ml	Santa Cruz Biotechnology	Sc-7383	Mouse	1:3000	WB
ERK 1 (K-23) 200 µg/ml	Santa Cruz Biotechnology	Sc-94	Rabbit	1:4000	WB
Anti-Mouse IgG (whole molecule)–FITC antibody	Millipore Sigma	F0257	Goat	1:7500	WB
Anti-Rabbit IgG (whole molecule)-FITC antibody	Millipore Sigma	F0382	Goat	1:7500	WB
NF-κB p65 (F-6) 200 µg/ml	Santa Cruz Biotechnology	Sc-8008	Mouse	1:100	IF
FITC-conjugated anti-Mouse IgG	Millipore Sigma	F0257	Goat	1:100	IF
Recombinant Monoclonal Anti-PAR2	Abcam	ab180953	Rabbit	1:200	IF
Donkey Anti-Rabbit IgG H&L (Alexa Fluor® 647)	Abcam	ab150075	Donkey	1:800	IF
Anti-NeuN antibody [1B7] - Neuronal Marker	Abcam	ab104224	Mouse	1:800	IF

2.2 Cell culture

All cell culture work was performed using Class II biological safety cabinets, which are specifically designed for cell culturing, under aseptic conditions. The three cell lines used in this thesis include: NCTC2544-hPAR2/NF-κB-L, DU145 and Human

Embryonic Kidney cells (HEK293). Details of maintenance conditions and passaging of each cell line are described in the following subsections.

Table 2.9: Cell lines used with resources

Cell line	Resource
NCTC2544-hPAR2/NF-κB-L	Human skin epithelial cells (NCTC2544) cells clone locally developed in the laboratory stably expressing human PAR2 (clone G) and NF-κB-Luciferase promoter construct as described earlier (Kanke et al., 2001). The primary keratinocytes were cultured from neonatal foreskins obtained from the Royal Hospital for Sick Children (Edinburgh, UK)
DU145	Human prostate carcinoma epithelial cell line (HTB-81 ™) derived from a brain metastasis of prostate adenocarcinoma. This cell line is androgen receptor-negative (source: ATCC: American Type Culture Collection, USA).
HEK293	Human embryonic kidney cells (CRL-1573 ™) derived from embryonic kidney tissue and display epithelial-like morphology. These cells are highly transfectable and widely used in biomedical research (source: ATCC, USA).

2.2.1 NCTC2544-hPAR2/NF-κB-L cells

Human keratinocytes stably expressing human PAR2 and NF-κB-Luciferase promoter construct (NCTC2544-hPAR2/NF-κB-L) were cultured in Medium 199 supplemented with 10% foetal bovine serum (FBS), 1% L-glutamine, and 1% penicillin/streptomycin. Cells were incubated at 37˚C in a humidified environment with 5 % CO_2 in a T75 culture flask. Upon reaching 80-90% confluency, cells were passaged using Versene (0.2% in EDTA/PBS) to avoid PAR2 activation by trypsin. The medium was aspirated, and the cells were washed with 1.5 mL Versene before incubation with fresh 2 mL Versene for 2-3 minutes at 37˚C. Once cells began detaching, as observed under an inverted microscope, the flask was tapped to facilitate complete detachment. Versene was neutralised by adding 8 mL of Medium 199 and mixed by pipetting. The cell suspension was diluted as needed in Medium 199 and seeded into new sterile T75 cell culture flasks to maintain the cell or experimental

plates assays. The medium for the cultured cells was refreshed every 2-3 days, after being warmed to 37˚C for about 20 minutes before use. For experimental purposes, cells were quiesced in serum-free media for 18 hours prior to stimulation.

2.2.2 DU145 cells

Human epithelial prostate cancer cells (DU145) that was originally isolated from the brain of a 69-year-old, white, male with prostate cancer. DU145 were cultured in Roswell Park Memorial Institute (RPMI) Medium 1640, supplemented with 10% FBS, 1% L-glutamine, and 1% penicillin/streptomycin. Cells were maintained at 37˚C in a humidified incubator with 5 % CO_2 in a T75 culture flask. When the cells reached 80-90% confluency, they were passaged using Versene, following the procedure outlined earlier in the subsection 0. The cell suspension was diluted as required in RPMI 1640 medium and seeded into new sterile T75 cell culture flasks to maintain the cells or experimental plates for assays. For experimental purposes, cells were serum-starved in serum-free media for 18 hours prior to stimulation.

2.2.3 Human embryonic kidney (HEK 293) cells

HEK293 cells were maintained in Modified Eagle's Medium (MEM) supplemented with 10% FBS, 1% penicillin/streptomycin, 1% L-glutamine, 0.375% sodium bicarbonate and sodium pyruvate. Cells were then incubated at 37˚C in a humidified environment with 5% CO_2, and the medium was refreshed every 2-3 days. Cells were passaged using Versene as described earlier in the subsection 0, keeping the cells in a 37˚C incubator for detachment for about one minute only. The cell suspension was then diluted as needed in MEM medium before being seeded into 96-well clear plates for calcium assays or into a fresh T75 flask to maintain cell stocks. Before stimulation,

HEK293 cells were maintained in full MEM medium prior to stimulation without being starved.

2.2.4 Cell cryopreservation and thawing (cell recovery)

For preserving cell passages, cells were cultured until reaching 80-90% confluency. The same procedure outlined earlier (section, 0) for cell detachment was applied to each cell type, and the detached cells were resuspended in 8mL of their respective media. The cell suspension was transferred to a sterile 15-mL centrifuge tube and centrifuged at 1200 rotations per minute (rpm) for 3 minutes. After carefully aspirating the media without disturbing the cell pellet at the base of the tube, and cells were resuspended in 3 mL of freeze mix (refer to Table 2.6). About 0.7 to 1 mL of cell suspension in freeze mix was transferred to a 1 mL cryotube for storage at -80˚C or in liquid nitrogen. For recovery, the cells were thawed at room temperature and transferred to a T75 flask with 10 mL warmed media. The following day, the media was refreshed to remove any residuals of DMSO from the culture.

2.3 Animals

2.3.1 Ethics and animal care

Ethical approval was obtained from the Dubai Pharmacy College Research Ethics Committee (REC/PhD/2020/01), which is currently part of the College of Pharmacy under Dubai Medical University (DMU). All animal procedures adhered to the international guidelines for the care and use of laboratory animals (National Research and Institute for Laboratory Animal, 2011). Healthy male Wistar rats weighing between 200 and 250 grams were sourced from the Animal Facility of DMU, Dubai, UAE. The animals were housed in standard ventilated cages under controlled

conditions with a 12-hour light/dark cycle at 23˚C ± 2˚C. Animals had free access to standard rat feed and water *ad libitum*. Prior to the commencement of experiments, the animals were acclimatised for 14 days before the start of the experiment. All experiments were conducted in accordance with the guidelines for the use and care of animals, and protocols were approved by the Research Ethics Committee at DPCG, which is currently the Institutional Review Board (IRB).

2.3.2 Drugs and reagents

A sterile 3% (w/v) suspension of λ-carrageenan (type IV; Sigma Aldrich, 22049) was prepared by dissolving heat-sterilised carrageenan powder in sterile saline. For oral drug treatment, animal groups received AZ8838 (AOB; 37172; dissolved in 20% DMSO/80% olive oil) at doses of either 10 mg per kg or 5 mg per kg administered orally (p.o.) 30 minutes before inflammation induction surgery. For the positive control cohort, animals received celecoxib (100 mg/kg, a selective cyclooxygenase-2 (COX2) inhibitor with established anti-inflammatory and analgesic effects), prepared from Celebrex® capsules (Pfizer), suspended in 20% DMSO/80% olive oil, administered orally 30 minutes before surgery. The control group were given the vehicle (20% DMSO/80% olive oil) orally 30 minutes before the surgical procedure.

2.3.3 Induction of inflammation

An animal model of pelvic pain induced by prostate inflammation was employed according to Radhakrishnan & Nallu (Radhakrishnan and Nallu, 2009). To induce inflammation, rats received an injection of a sterile suspension of 3% λ-carrageenan in saline. Rats were anaesthetised using a mixture of ketamine 50mg/kg and xylazine 10 mg/kg injected intraperitoneally, keeping the animals on a heating pad (approximately

37˚C) to prevent hypothermia. Anaesthesia depth was confirmed by toe pinch or observation of shallow, regular breathing. The surgical area (lower abdomen above the penis, see Figure 2.1) and the scrotal skin were shaved, and the dermis in the surgical area was sterilised using three applications of 70 % v/v ethanol followed by 10 % povidone-iodine solution. To reduce post-surgical pain and minimise sensitisation of the areas adjacent to the surgical wound, 2% lidocaine was applied to the cleaned skin. After 10 minutes of lidocaine application, a 1-inch lower midline incision (laparotomy) was made in the skin and abdominal wall to expose visceral organs, including ventral lobes of the prostate gland (Jesik et al., 1982).

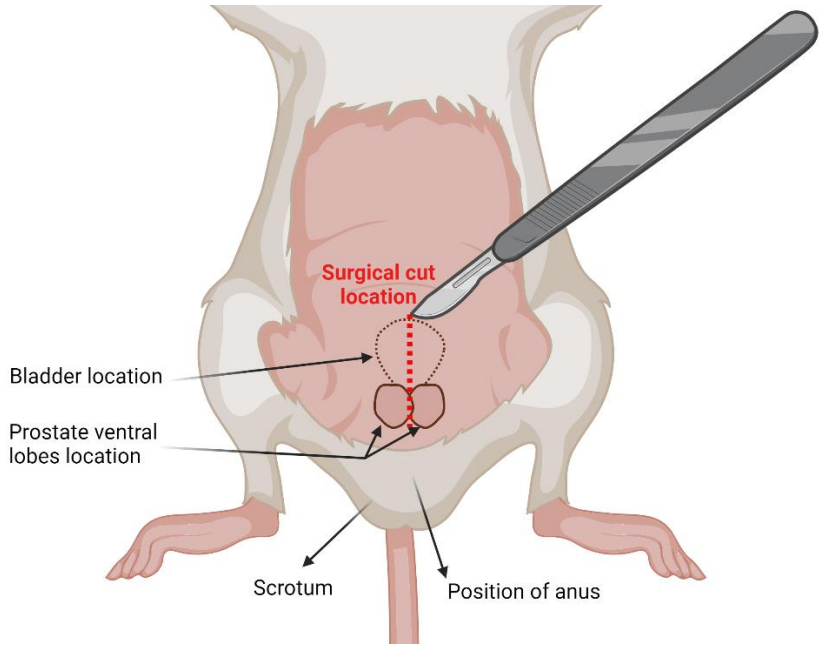

Figure 2.1: Schematic representation of the surgical cut location for the murine prostate inflammation induction model.
The illustration shows the anatomical locations used for the surgical procedure to induce prostate inflammation in male Wistar rats. A midline incision (dotted red line) is made in the lower abdomen to access the ventral lobes of the prostate (outlined in brown). The bladder is located superior to the prostate, with the scrotum and the anus inferior to it. Sterile suspension (3% λ-carrageenan or saline for the control group) is injected bilaterally into the ventral lobes of the prostate to induce inflammation. Care is taken to avoid contamination and infection, and the incision is closed using sutures and clips. This approach follows standard procedures. The illustration was created in BioRender.com

A sterile suspension of 3 % carrageenan (50 µL per lobe) was injected into both right and left ventral lobes of the prostate gland of the inflammation group (n = 6) using a 30-gauge disposable needle and a sterilised Hamilton syringe. The muscle layer wound was closed using #4.0 sterile absorbable suture material, and the skin wound was closed using sterile stainless steel wound clips with the aid of a clip applicator. The surgical procedure was carried out in a clean room, and every precaution was taken to avoid microbial infection of the prostate and the wound. Topical neomycin (an antibiotic) cream was applied to the clipped wound to promote healing. No systemic analgesics were administered before or after surgery, to avoid interference with the expected acute/chronic pain behaviours, a decision approved by the IRB. In the sham group (n = 6), the same surgical procedures were followed, with the exception that 50 µl of sterile normal saline was injected into both the right and left ventral prostate lobes instead of carrageenan. All animals were housed individually in clean cages for a 72-hour recovery period. After this period, animals were acclimatised in the laboratory for about 1 hour before perfusion. The time point adopted in this investigation (72 hours) was selected based on pilot testing across multiple post-induction time intervals and supported by previous findings by Radhakrishnan and Nallu, as it demonstrated the peak inflammatory pain response in rats (Radhakrishnan and Nallu, 2009).

2.3.4 Perfusion fixation and sample collection

Seventy-two hours after surgery, rats were deeply anesthetized using sevoflurane and transcardially perfused, by inserting a blunt needle connected to the perfusion system from left ventricle until visualized through the ascending aorta with ice-cold 0.1M phosphate buffered saline (PBS, pH 7.4) for a duration of 3 to 5 minutes, followed by

4% freshly prepared and cold paraformaldehyde (PFA) in 0.1M PBS for 15-20 minutes (see Figure 2.2). The right and left ventral prostate lobes, along with the lumbar and sacral (L5, L6 and S1) dorsal root ganglia (DRG) were carefully dissected. For immunofluorescence studies, the DRG were then post-fixed in 4% PFA for 4 hours and subsequently cryoprotected in 30% sucrose overnight at 4°C. The prostate lobes were fixed in 4% PFA directly for not less than 48 hours at room temperature. The body weight, prostatic wet weight, and prostatic index, calculated as the prostatic wet weight (mg) divided by the body weight (g), were recorded for each group.

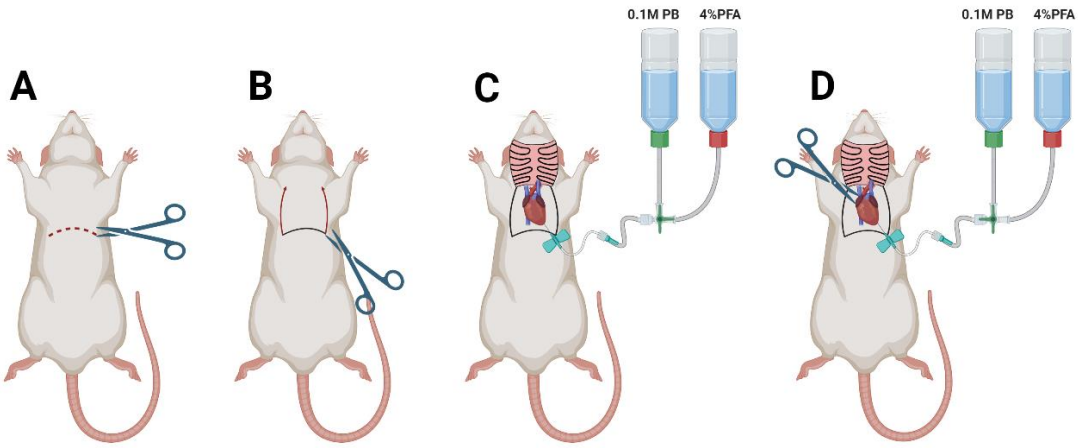

Figure 2.2: Steps of transcardial perfusion fixation in a rat.
A: the rat is anesthetized, and a 4-5 cm lateral incision is made just below the last ribs. **B**: the diaphragm is cut to expose the heart and lateral sides of ribs is cut to lift the sternum and expose the pleural cavity. **C**: an 18-gauge blunt perfusion needle is inserted through the left ventricle into the ascending aorta. The needle tip needs to be visible through the aorta without reaching the aortic arch. This needle is connected to a double perfusion system to allow initial perfusion with 0.1M Phosphate buffer (PB), pH 7.4 followed by 4% paraformaldehyde (PFA) in 0.1 PB. **D**: a small incision is made in the right atrium and perfusion started with ice-cold 0.1 M PB for 4-5 minutes followed by a 20-minutes perfusion of 4% PFA. This illustration was made using BioRender.com.

2.4 NF-κB-Luciferase reporter activity assay

NCTC2544-hPAR2/NF-κB-L cells were seeded in 96-well black plates, with 100 µL of cell suspension (prepared at the desired dilution) added per well and incubated until they reached 90-100% confluency. Cells were then rendered quiescent by incubating them in 90 µL of serum-free medium per well for 18 hours. Cells were treated with the PAR2 agonists, trypsin and 2fLIG, at varying concentrations in quadruplets for 4 hours at 37˚C. To test the effect of AZ8838, cells were pre-incubated with variable concentrations of the antagonist for 1 hour, followed by a 4-hour co-treatment with PAR2 agonists. DMSO effects and its co-treatment with the agonists were tested as vehicle controls. Near the end of the stimulation period, fresh lysis buffer was prepared, containing luciferin substrate (0.2 mM luciferin, 1 mM DTT, 1 mM ATP, and 1% BSA). To terminate the reactions, the media was aspirated, and the cells were washed quickly with 100 µL of ice-cold PBS per well. Immediately, 100 µL of lysis buffer prepared with luciferin substrate was added, and cells were incubated for 5 minutes at 37˚C. Luminescence intensity was measured using a Wallac MicroBeta TriLux 1450 luminometer (Wallac Oy, Finland), with a bottom-read measurement at 450 nm for 1 second per well.

2.5 Western Blotting

For the detection and analysis of specific intracellular protein changes, the following protocol was applied:

2.5.1 Preparation of whole cell lysates or tissue homogenates

Cells were grown to 90-100% confluency in 12-well plates and allowed to quiesce for 18 hours prior to stimulation. Following the planned stimulations, the culture plates

were placed on ice to halt the reactions, and the media were promptly aspirated. The wells were washed twice with ice-cold PBS, 500 µL per well, followed by the addition of 150 µL of hot (~85˚C) Laemmli SDS sample buffer containing DTT (see Table 2.6) to each well. Cells were scraped on ice, and the cell lysates were passed repeatedly through a 23G x 1¼" syringe to shear chromosomal DNA. Samples were transferred to Eppendorf tubes, boiled at 95˚C for 5 min to denature proteins, and stored at -20˚C until used. For tissue homogenization and protein extraction, 60 µL of lysis buffer mix (RIPA, 0.1 PMSF, 0.5 EDTA, proteinase and phosphatase inhibitor cocktail) per pooled DRG sample and 100µL per ~30mg prostate tissue specimen. Tissue samples were homogenised by sonication (3-5 cycles of 3 seconds mixing followed by 30 seconds stop at 100% amplitude). All homogenates were centrifuged at 4℃ for 15 minutes at 15,000 rpm. Protein concentrations were estimated using the BCA kit protocol, and ~60 µg of protein was used per well for electrophoresis.

2.5.2 Sodium Dodecyl Sulphate Polyacrylamide Gel Electrophoresis (SDS-PAGE)

The gel glass plates (1mm thickness) were cleaned with 70% (v/v) ethanol and assembled using a casting set. To check for leakage, distilled water was filled between the assembled plates and left for ~30 minutes before being discarded. The resolving gel was prepared with a sufficient volume to make a 10% polyacrylamide (ROTIPHORESE® Gel 30) in buffer 1 (0.375 M Tris-base, 0.1% (w/v) SDS, adjusted at pH 8.4) and 0.05% (w/v) ammonium persulphate (APS). Polymerisation was initiated by adding 0.05% N, N, N', N'-tetramethylethylenediamine (TEMED) (v/v). The gel mixture was poured between the glass plates and allowed to polymerise. Approximately 200 µL of 0.1% SDS solution was layered on top to prevent drying and

eliminate air bubbles. Once the gel was set, the SDS was discarded and the stacking gel was prepared to make 1% acrylamide and an appropriate volume of buffer 2 (0.124 M Tris-base, 0.1% SDS at pH 6.8), 0.1% (w/v) APS and 0.1% (v/v) TEMED. The stacking gel was quickly poured over the resolving gel, a Teflon comb was inserted, and the gel was allowed to polymerise for 15 minutes before the comb was carefully removed. The gels were assembled in a Bio-Rad Mini-PROTEAN II™ electrophoresis tank topped up with running buffer (Table 2.6). Aliquots of samples (25 µl) were loaded into the wells using a micro-syringe, and a pre-stained SDS-PAGE molecular weight marker was run alongside to identify the molecular weights of the target polypeptides. Protein separation was carried out using SDS-PAGE at a constant voltage of 130 V for approximately 110 minutes.

2.5.3 Electrophoretic transfer of protein samples

Separated proteins in acrylamide gels were transferred onto a nitrocellulose membrane as described earlier by Paul A *et al* (Paul et al., 1997). The gels were carefully positioned against a sheet of nitrocellulose (0.45 µm pore size) and assembled in a transfer cassette, sandwiched between two 0.92mm cellulose chromatography filter papers (Whatman® 3MM) and two sponges. The cassette was placed in a Bio-Rad mini–mini-Trans-Blot™ tank filled with transfer buffer (Table 2.6) and run at a constant current of 300mA for 110 minutes. An ice pack was used to cool the tank during the transfer process. For tissue homogenate samples, PVDF membranes were used after activation (30 seconds in methanol, followed by 2 minutes in distilled water, then for 20 minutes in freshly prepared Towbin's transfer buffer). Nitrocellulose membranes were used for protein transfer from cell lysates to ensure low background and high signal clarity, while PVDF membranes were selected for tissue homogenates

due to their higher protein-binding capacity and chemical durability, which facilitate effective transfer and detection of complex proteins. Protein transfer was performed using the semi-dry Trans-Blot Turbo Transfer System for 30 minutes at 1A and 25 V.

2.5.4 Membrane blocking and immunological detection of proteins

Following protein transfer to nitrocellulose membrane, the membranes were blocked by incubating them in a 2 % bovine serum albumin (BSA) solution in NATT wash buffer (see, Table 2.6) for ~2 hours at room temperature on an orbital shaker set at 35 rpm. After blocking, the membranes were briefly rinsed and then incubated overnight at 4˚C with the specific primary antibody for target proteins. Antibodies were prepared at the dilutions listed in Table 2.8, in 0.2% BSA in NATT buffer. The next day, membranes were washed 4 times for 20 minutes each with NATT buffer using gentle shaking. Membranes were then incubated for one hour at room temperature with the appropriate horseradish peroxidase (HRP)-conjugated polyclonal secondary antibody diluted as specified in Table 2.8 in 0.2% BSA in NATT, followed by another set of four 20-minute washes with NATT buffer. Protein bands were visualised by incubating the membranes with equal volumes of enhanced chemiluminescence (ECL) reagents 1 and 2 (refer to Table 2.6) for 2 minutes with gentle shaking. Membranes were then placed in a photographic cassette, covered with clingfilm to prevent drying, and exposed to X-ray film (Ultra Cruz® Autoradiography film blue) in the dark for the appropriate duration. The films were developed using a JPI Automatic X-ray Film Processor (Model JP-33).

For tissue homogenate samples, membranes were blocked for 45-60 minutes in 5% skimmed milk prepared in 0.1% PBST (PBS + 0.1% Tween-20). Skimmed milk was

used for tissue homogenates because it provides efficient and cost-effective blocking for proteins, and the target protein (PAR2) is not phosphorylation-dependent, a condition in which BSA would typically be preferred. After two 5-minute washes, the membranes were incubated overnight with the primary antibody at the indicated dilutions in Table 2.8 at 4 °C. The next day, the membranes were washed 4 times (each 10 minutes) at a rocking shaker with 0.1% PBST, then incubated with the secondary antibody at room temperature for one hour. Afterwards, the membranes were washed 4 times (each 10 minutes) with 0.1% PBST. Detection was carried out using an ECL Western Blotting Substrate, and membrane images were captured using the Azure Imaging System.

2.5.5 Membrane stripping and re-probing

To detect additional proteins, previously probed nitrocellulose membranes were stripped to remove bound antibodies. The same protocol was applied for PVDF membranes, with the exception that PBST 0.1% was used for all washing steps. For stripping, membranes were incubated in 15 mL of stripping buffer per membrane (see Table 2.6) after adding 0.1 M β-mercaptoethanol, for one hour at 60 ˚C on an orbital shaker set to 70 rpm. After stripping, membranes were washed three times for 5 minutes each with NATT buffer to remove the residual stripping buffer. The membranes were then re-incubated overnight at 4˚C with the specific primary antibody for the next target protein, typically, a loading control. The following day, the membranes were processed according to the same procedure of washes, secondary antibody incubation and visualisation as described in the subsection 2.5.4.

2.5.6 Densitometric analysis of Western blots

The X-ray films obtained from the Western blot analyses were scanned and saved in TIF format. Band intensities were quantified using ImageJ software (version 1.54j). Each image was first inverted using the "Invert" function, and the region of interest (ROI) was selected using the "Rectangle" tool. The mean intensity of the ROI was then measured using the "Measure" function, which calculates the average intensity of all pixels within the selected area. Background signal was measured using a rectangle of identical size placed in an adjacent blank area of the band and subtracted from the band of interest. The same procedure was conducted for the loading control protein (e.g. total ERK). Band intensities were then normalised to the corresponding control (untreated) values to calculate the fold change.

2.6 FLUO-4 intracellular Calcium mobilisation assay

HEK293 cells were seeded into clear 96-well plates and incubated at 37°C until they became confluent. Prior to the experiment, the culture media were aspirated, and cells were washed once with 50 µL per well of Hank's balanced salt solution (HBSS) containing 1 mM calcium chloride and 1 mM magnesium chloride. Cells were then loaded with 3 µM FLUO-4 AM, dissolved in 0.03% pluronic acid in HBSS (containing 1 mM CaCl2 and 1 mM MgCl2), by adding 50 µL per well and incubating for 45 minutes at 37˚C in the dark. Following incubation, cells were washed once with the same HBSS buffer without Fluo-4 AM. The plate was then placed in the FlexStation III (Molecular Devices) set at 37 ˚C, along with a "compound plate" containing the prepared agonist concentrations in HBSS. For antagonist experiments, the cell plate was incubated for an additional hour at 37 ˚C in the dark with the test antagonist

concentrations prior to measurement. Fluorescence was measured at an excitation/emission wavelength of 485/525 nm, with an auto-off wavelength set at 515 nm. The background signal was recorded for 20 s before the addition of agonists, using the instrument's built-in automated pipetting system. Kinetic changes in intracellular calcium mobilisation were measured every 3 seconds over a total period of 120 seconds. The experiment protocol and data acquisition were conducted using SoftMax® Pro 5 Software. Results, reported as relative fluorescent units (RFU), were exported to Microsoft Excel for analysis. All measurements were performed in triplicate, and mean values were calculated for each data point in an independent experiment. Baseline RFU was averaged between 10-20 second recordings, and peak RFU was determined by averaging the three highest mean RFU values. Data were normalised as peak-to baseline RFU (F_{max}/F_0) for further comparison and analysis.

2.7 PAR2-YFP transfection and internalisation assay

DU145 cells were seeded onto 13-mm coverslips in a 12-well plate and cultured until they reached 60-70% confluency. The PAR2-yellow fluorescent protein (YFP) construct used in this study was developed by Advantagen Ltd. (Dundee, UK), as described in (Cunningham, 2010) and (Cunningham et al., 2012). Briefly, the human PAR2 gene was amplified by polymerase chain reaction (PCR) from a pRSV-PAR2 plasmid (provided by Dr T. Bushell) and subcloned into the pEYFP-N1 expression vector (Clonetech). The vector was digested at defined restriction sites using *HindIII* and *BamHI* restriction enzymes. The PCR primers used for PAR2 cloning include the forward primer adg425 (5′-TCAAGCTTACCATGCGGAGCCCCAGCGC) and reverse primer adg426 (5′-CTGGATCCATAGGAGGTCTTAACAGTGGTTG). The

final construct contained an antibiotic resistance gene (Kanamycin/Neomycin) for selection in mammalian cells, as shown in Figure 2.3.

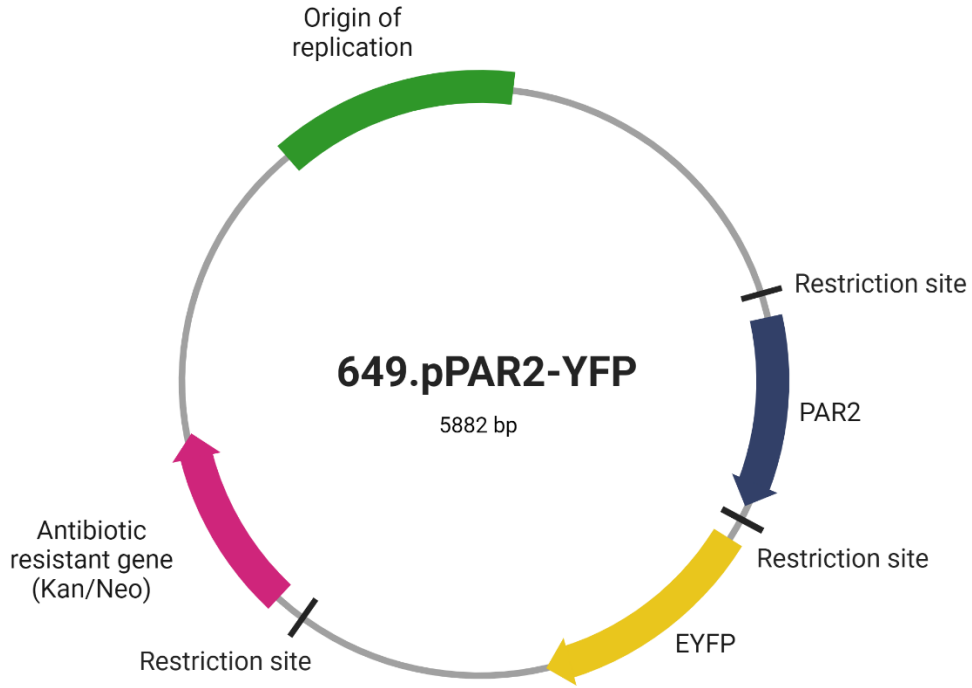

Figure 2.3: Illustrative PAR2-YFP plasmid map.
PAR2-YFP plasmid map showing the region of origin with arbitrary insertion sites of the PAR2 gene and enhanced yellow fluorescent protein (EYFP) with the kanamycin/neomycin (Kan/Neo) antibiotic resistance gene. Short black lines represent selected restriction sites within the construct. The total size of the PAR2-YFP plasmid is 5883 base pairs (bp) and 649 represent the PAR2 gene insertion location. Illustration created by BioRender.com

Cells were transfected with 1.5 µg of the pPAR2-YFP DNA vector per well (~1.5 ng/µL) using polyethylenimine (PEI), see Figure 2.4, at a PEI-to-DNA ratio of 5.7:1 (µl: µg). The plasmid DNA was diluted in full RPMI medium. For the mock control well, an equivalent volume of PEI was mixed with RPMI medium in a separate tube. Both suspensions were gently mixed by flicking the tubes and incubated on ice for 10-15 minutes. After refreshing the media in the culture plate, 100 µL of each suspension was added to the respective wells, and the plate was returned to the incubator. After approximately a 16-hour incubation period, the medium was replaced.

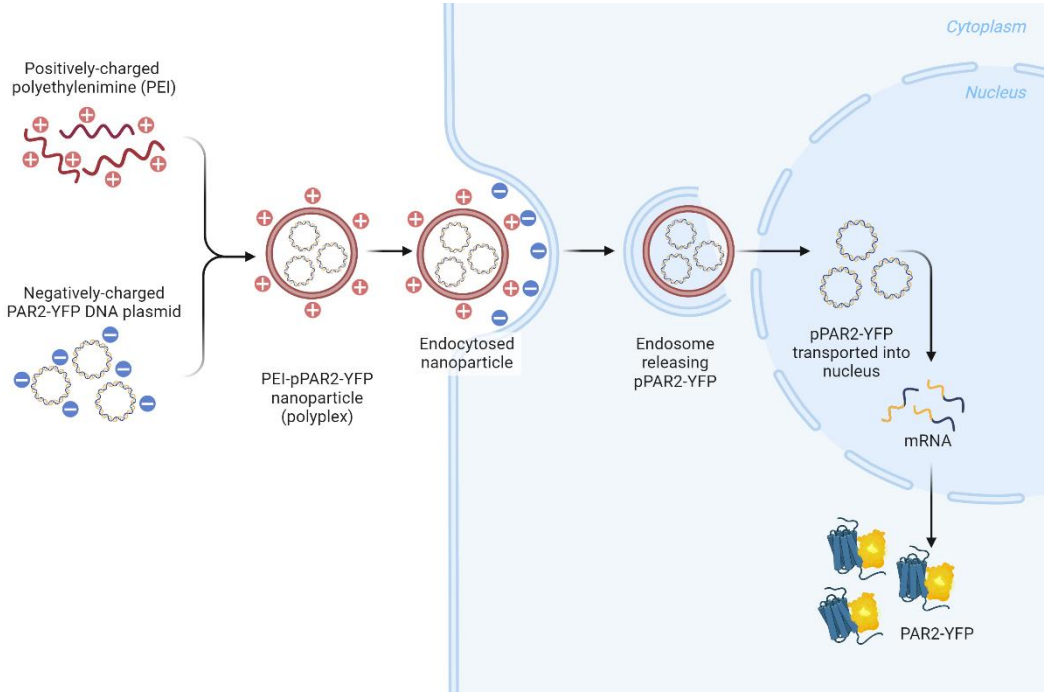

Figure 2.4: Polyehtyleneimine (PEI) transfection.
Developed based on a PEI transfection template created by Martina Maritan in Biorender.com. Lozon, Y. (2024) BioRender.com/h77k122.

Experimental stimulations with PAR2 agonists were either carried out directly or following a one-hour preincubation with the antagonist to assess the effects of AZ8838. At the end of the stimulation period, cells on coverslips were washed twice with ice-cold PBS on ice, fixed with ice-cold methanol (1 mL/well), and incubated for 10 minutes on ice. Methanol was then removed, and cells were washed twice with PBS before being incubated with 4′,6-diamidino-2-phenylindole (DAPI) diluted 1:10,000 in PBS for 30 minutes on ice. Following three additional PBS washes, the coverslips were mounted on glass slides using 20 µL Mowiol mounting medium and left to dry overnight at 4˚C. The prepared slides were stored at 4˚C until imaging. Fluorescence images were acquired using a Nikon Eclipse E600 epifluorescent upright microscope, with image capture performed using WinFluor V3.8.5 software, saved in TIFF format.

Post-processing and further image analysis were conducted using ImageJ version 1.54j and final figures were prepared using Microsoft PowerPoint.

2.8 ELISA for human IL-8

NCTC2544-hPAR2/NF-κB-L and DU145 cells were seeded in 6-well plates and incubated at 37 ˚C until reaching confluency. According to the experimental design, cells were treated either with PAR2 agonists for 24 hours or pretreated with the tested AZ8838 concentrations for one hour prior to agonist treatment. Cell-free supernatants were collected and centrifuged to determine the concentration of IL-8 using a sandwich ELISA kit (Human IL-8 Uncoated ELISA, Invitrogen, 88-8086), following the manufacturer's protocol. Briefly, ELISA 96-well plates were coated with the capture antibody specific to human IL-8 by incubating the recommended dilution overnight at 4 ˚C with gentle agitation. The next day, the plate was washed three times using the ELISA wash buffer (see Table 2.6) to remove unbound antibodies. To prevent non-specific binding, the wells were treated with the blocking buffer for one hour at room temperature, followed by a washing step. The standard dilutions of IL-8 (recombinant human IL-8 provided in the kit), along with the diluted samples (based on pilot experiments), were added to the appropriate wells in duplicate, sealed and incubated at room temperature for 2 hours. After 3-5 washes with the ELISA wash buffer, the appropriate dilution of a biotinylated detection antibody was added and incubated for one hour at room temperature. Following another wash step, HRP-conjugated avidin was added to the wells and incubated for 30 minutes. Finally, plates were washed to remove all excess reagents before the addition of HRP substrate (TMB: 3,3',5,5'-Tetramethylbenzidine). The reaction was allowed to proceed for 15 minutes in the dark, resulting in the development of a blue colour. This enzymatic reaction was

stopped by adding ELISA stop solution (see Table 2.6), which turns the colour from blue to yellow. Optical density (OD) was measured at 450 nm using the POLARstar® Omega microplate reader, and data were processed using Omega MARS 2.41 software. A four-parameter logistic fit was applied to generate a standard curve, from which IL-8 concentrations were calculated and reported in pg/mL.

2.9 Immunofluorescence studies on cells and tissues

2.9.1 Immunofluorescence on cells

NCTC2544-hPAR2/NF-κB-L cells were seeded onto 13-mm coverslips in a 12-well plate and cultured until they reached 70-80% confluency. Experimental stimulations with PAR2 agonists were either conducted directly or preceded by a one-hour preincubation with the antagonist to evaluate the effects of AZ8838. At the end of the stimulation, cells on coverslips were fixed in 3.6% (v/v) paraformaldehyde (PFA) in PBS for 15 minutes at room temperature. Residual PFA was washed with ice-cold PBS, and cells were permeabilised using 0.25% (v/v) Triton-X-100 in PBS for 10 minutes. Afterwards, the coverslips were blocked in 1% (w/v) BSA in PBS for 30-60 minutes and incubated overnight with the specific primary antibody for p65 (NF-κB p65. Cat. No. sc-8008, 1:100) in a dark, humidity chamber at room temperature. Excess antibody was washed off by two ice-cold PBS washes, and cells were subsequently incubated with mouse secondary antibody (FITC-conjugated anti-mouse, Cat. No. F0257, 1:100) for one hour in the dark in a dark humidity chamber at room temperature. Cells were washed three times with PBS to remove excess antibody, then stained with 4',6-diamidino-2-phenylindole (DAPI) at a 1:1000 dilution for 10 minutes at room temperature in the dark, followed by two PBS washes. The coverslips

were then mounted onto glass slides using 20 µL Mowiol mounting medium and allowed to dry overnight in the dark at 4˚C. The slides were stored at 4°C until they were imaged. Fluorescence images were acquired using a Nikon Eclipse E600 epifluorescence upright microscope. Image capture was performed using WinFluor V3.8.5 software, with files saved in TIFF format. Post-processing and further image analysis were conducted using ImageJ version 1.54j and Microsoft PowerPoint for figure preparation. To ensure accessibility for colour-blind readers, green was converted to magenta and blue to cyan according to Wong's guidelines (Wong, 2011).

2.9.2 Quantitative nuclear colocalization analysis

Colocalization analysis was performed as described by Bolte & Cordelières (Bolte and Cordelières, 2006) with minor modifications. ImageJ 1.54j was used, equipped with the "JACoP" plugin, used to assess colocalization between the p65 (FITC channel) and nuclear (DAPI channel) signals. The images for both FITC and DAPI channels were opened in grayscale, and from JACoP, the Pearson's coefficient (PC), M1 & M2 coefficients and Costes's automatic threshold were selected. Pearson's coefficient provides a measure of the linear correlation between pixel intensities in the two channels, with values closer to 1 indicating strong colocalization. Mander's coefficient calculates the fraction of p65 overlapping with DAPI-stained nuclei. Colocalisation was considered significant when PCC values exceeded 0.5, and further validation of the results was achieved through visual inspection of the merged images and calculation of the fraction of FITC-positive nuclei. From each slide, 4 to 7 images were analysed and mean values calculated for statistical reporting.

2.9.3 Immunofluorescence on tissue sections

Tissue specimens, including DRG and prostate, isolated from all animal treatment groups, were fixed as described earlier, refer to subsection 2.3.4, and utilised for immunofluorescence analysis. Tissue samples were sectioned at a thickness of 10 µm using a cryostat microtome, after embedding in cryo-embedding matrix (OCT), and mounted onto Superfrost ™ Plus charged slides. For immunofluorescence staining, tissue sections were air-dried at room temperature for 1 hour, then incubated in 100% acetone for 30 minutes. After acetone treatment, slides were washed with PBS (0.01M; pH 7.4) and blocked with 1% BSA in PBS containing 0.3% Tween 20 for 1 hour. Subsequently, sections were incubated overnight in a humidified dark chamber with primary PAR2 antibody (1:200, ab180953), diluted in the blocking solution. The next day, sections were washed and incubated in the dark at room temperature with the corresponding secondary antibody (1:800; ab150075) for 1 hour. After the final washes, slides were cover-slipped using Fluoroshield mounting medium with DAPI (Abcam; ab104139) and left to dry overnight. Fluorescence imaging was performed using an Olympus microscope BX63 upright microscope, and images were acquired using Olympus cellSens imaging software (Olympus Life Science, Waltham, MA, USA) and saved in TIFF format. Five randomly selected sections from each specimen, obtained at varying tissue depth, were analysed using ImageJ software (Schneider, Rasband and Eliceiri, 2012). For each section, the percentage of fluorescent cells (for DRG) and the intensity of fluorescence per unit area (for prostate sections) were quantified and compared across treatment groups.

2.9.4 Fluorescence quantitative analysis

For each DRG, 4-5 sections were imaged at varying depths to ensure representation of the sampling. Each image was assigned a unique code for blinded analysis, and two trained and independent assessors quantitatively analysed the coded images. The assessors quantified the number of PAR2-positive neurons (indicated by FITC) and the total number of neurons (marked by DAPI) in each coded image. Neurons were manually counted using ImageJ from × 10 magnification photomicrographs across tissue sections. Neuron somas were distinguished based on their morphological and size differences compared to the surrounding glial cells and confirmed through a pilot double-staining experiment using the neuronal marker NeuN. These data were used to calculate the percentage of PAR2-positive neurons for each image. The average of the two assessors' quantifications was taken for each image for further comparative analysis.

For prostate specimens, a total of five prostate sections were stained for each rat. Prostate images were analysed using ImageJ version 1.54j. Grey-scale fluorescence intensity (pixel intensities) was measured within a consistent area of interest (ROI) across the sample image. Minimum, maximum, and mean pixel intensity (Mean Fluorescence Intensity-MFI) values were calculated. For each image, three ROIs were selected, and their average fluorescence intensity was calculated as a representative value for that image and employed for further comparative analysis.

2.10 Histologic examination

The prostate lobes were fixed in 10% formaldehyde solution for a minimum of 48 hours to ensure complete fixation. Tissue samples were then processed using standard

histological methods, embedded in paraffin, sectioned at a thickness of 5 μm, and stained with haematoxylin and eosin (H&E) according to the conventional staining protocol. Prostate sections were examined with an Olympus BX63 automated fluorescence microscope under the brightfield setting, and images were captured by Olympus cellSens imaging software (Olympus Life Science, Waltham, MA, USA) and saved in TIFF format. All slides were anonymised and handed to Dr C Dagher, a consultant anatomical pathologist, for blinded assessment of inflammation and estimation of inflammatory score. The level of prostate inflammation was graded using a previously described grading system (Breser et al., 2017), with scores ranging from 0 (no inflammation) to 3 (severe inflammatory cell infiltration).

2.11 RNA isolation and quantitative real-time polymerase chain reaction (qRT-PCR).

For RT-PCR, animals were perfused only with ice-cold PBS 72 hours post-surgery. The L5, L6 & S1 dorsal root ganglia, along with prostate tissue, were collected from both sides. Total RNA was extracted using RNeasy PowerLyser Kit (Qiagen) following the manufacturer's instructions and subsequently reverse-transcribed into cDNA using QuantiTect Reverse Transcription kit (Qiagen). PAR2 expression was assessed using TaqMan Gene expression assay (Applied Biosystems). Real-time RT-PCR reactions were carried out on a QuantStudio 5 Applied Biosystems 7500 Fast Real-Time PCR System (Thermofisher Scientific) using Taqman Fast Advanced Master Mix (4444964, Life Technologies) and pre-designed Taqman Gene Expression Assays with FAM dye labelled PAR2 gene probe (ID: Rn00588089_m1, gene: *F2rl1*). Glyceraldehyde 3-phosphate dehydrogenase (GAPDH) was used as the endogenous control. Each sample was analysed in triplicate, and fold change in mRNA expression

was calculated using the threshold cycle comparison method ($2^{-\Delta\Delta CT}$) according to Livak and Schmittgen (Livak and Schmittgen, 2001).

2.12 Behavioural studies:

Pain behavioural assessments, including mechanical and thermal hyperalgesia assessments, were conducted on a cohort of male Wistar rats (n = 5 per group). Prostate inflammation was surgically induced using carrageenan, while sterile saline was used in control animals. Rats in the inflammation groups were pretreated orally (p.o.) with either vehicle (20%DMSO/80% olive oil), AZ8838 at doses of 5 mg per kg or 10 mg per kg; or celecoxib at a dose of 200 mg/kg, administered 30 minutes before inflammation induction surgery (see subsection 2.3.2). Behavioural tests were performed at several time points (baseline: 1 hour before treatment and surgical induction, and post-surgery at one, two, three, seven and 14 days, see Figure 2.5). A rest period of 15-20 minutes between mechanical and heat sensitivity testing to prevent potential overlap in response or sensitisation.

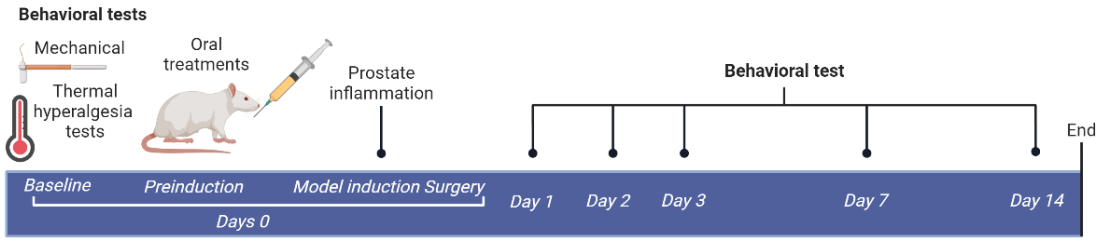

Figure 2.5: Timeline of behavioural studies.

Mechanical and thermal stimuli were applied to the scrotal skin (see Figure 2.6) according to Radhakrishnan and Nallu (Radhakrishnan and Nallu, 2009). This was confirmed in a pilot test prior to the main experiments (data not shown).

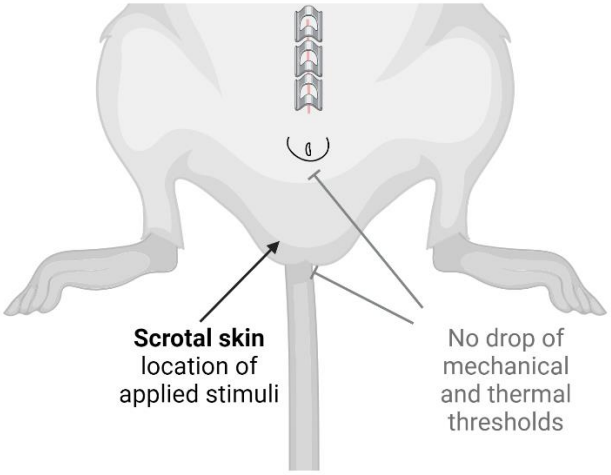

Figure 2.6: Application site for mechanical and thermal stimuli

2.12.1 Mechanical allodynia assessment (Von frey filaments)

Mechanical allodynia was assessed by measuring withdrawal thresholds to von Frey filament stimulation (Aesthesio®, Danmic Global, USA). A range of von Frey filaments (0.006 g to 10 g) was applied to the scrotal skin surface. Each filament was applied gently until a slight arching of the filament occurred. Following a 30-minute acclimatisation period in clear Plexiglas cubicles (20 cm L × 10 cm W × 15 cm H), placed on a wire mesh platform at 40.64 cm height. Mechanical stimulation began with the lowest force filament (0.002g), with each filament tested at least 4 times with approximately 30-second intervals between applications. The nociceptive threshold (in grams) was determined by the "ascending stimulus" method as described earlier (Minett et al., 2011, Deuis et al., 2017). In brief, the threshold was defined as the minimum force at which the animal exhibited a nocifensive response (i.e., withdrawal, licking, or jerking or shaking the area) in at least 60% of the repeated applications. Care was taken to distinguish nocifensive responses from casual movements. Measurements were taken once daily on designated days, including baseline (before oral treatments) and at subsequent days following surgical induction (Figure 2.5).

Mechanical testing was performed three to four times for each rat, and the average of these values was used for data analysis.

2.12.2 Thermal hyperalgesia assessment (Hangreaves' test)

To assess thermal hyperalgesia, the Hargreaves method (Hargreaves et al., 1988) was applied as detailed by Radhakrishnan and Nallu (2009), utilising the plantar test device (Model 390; series 8; IITC Life Science Instruments, Woodland Hills, CA). Rats were acclimatised for 30 minutes in Plexiglas cubicles (20 cm L × 10 cm W × 15 cm H) positioned on a glass platform elevated 25 cm above a light source. Based on preliminary tests, the light intensity was set to 35% to obtain consistent latency measurements. Radiant heat was directed at the scrotal skin, and the latency (escape latency) was recorded in seconds, defined as the time taken by the animal to respond to the heat stimulus. To ensure reliability, thermal testing was repeated three times per rat, with a 5-minute interval between each application. The mean of these readings was used for later analysis. A 20-second cut-off was employed to prevent tissue damage in non-responsive subjects. Measurements were taken once daily on designated days, both before the oral treatments (baseline) and on subsequent days following surgical induction (Figure 2.5). Careful attention was given to distinguish nocifensive behaviours from spontaneous or casual movements.

2.12.3 Behavioural quantification

Data obtained from the behavioural tests were quantified using the average of the repeated measurements. For mechanical allodynia, the mean nociceptive threshold was presented as the absolute nociceptive threshold (in grams) and as normalised to baseline threshold measurements. Further comparisons were made using the area

under the curve (AUC) value to analyse the time course of changes in nociceptive threshold. For thermal hyperalgesia, the latency to escape latency to radiant heat (in seconds) was expressed both as absolute latency and as normalized values relative to maximum cut-off latency.

2.13 Data Analysis

Data were represented as the mean ± standard error of the mean (S.E.M.) for at least three independent experiments unless stated otherwise. Statistical analyses were performed using GraphPad Prism version 10.3.1 (GraphPad Software LLC, USA). For comparison between groups of control/baseline and treatments, statistical differences between mean values were determined by one-way analysis of variance (ANOVA) followed by Dunnett's post-hoc test for multiple comparisons. For calculating the half-maximal effective concentration (EC_{50}) for agonists and the half-maximal inhibitory concentration (IC_{50}) for the AZ8838 compound, non-linear regression analysis was performed using the Hill equation to generate the concentration-response curve and estimate the EC_{50} and IC_{50}. The level of statistical significance was set as $P \leq 0.05$.

Chapter 3

Characterisation of the PAR2 antagonist, AZ8838

3.1 Introduction

Inflammatory disorders are a major global health concern, affecting millions of people and putting a significant strain on healthcare systems around the world (GBD2019IMIDCollaborators, 2023). In the middle of the molecular landscape that governs inflammation, the Protease-Activated Receptor 2 (PAR2) has emerged as a pivotal player, mediating a cascade of events that contribute to the initiation and persistence of inflammatory responses. Research has indicated that the activation of PAR2 in response to inflammation triggers a variety of signalling pathways, and attempts are currently underway to thoroughly define those associated with inflammatory reactions (Rothmeier and Ruf, 2012, Bang et al., 2021).

3.1.1 Identification of AZ8838 small molecule PAR2 antagonist

AZ8838 (Figure 3.1), an imidazole small molecule antagonist of PAR2, represents one of the potent antagonists identified through optimisation of molecules isolated by high-throughput screening led by AstraZeneca and Heptares Therapeutics (Cheng et al., 2017, Brown et al., 2018). Crystallographic studies revealed that AZ8838 was entirely buried within an allosteric pocket formed by transmembrane (TM) domains 1–3, 7, and ECL2 (Figure 3.1: AZ8838 structure and binding to PAR2.. It interacts through multiple bonds with several structural residues, rendering PAR2-specificity and stable binding kinetics. The orientation of the hydroxyl group is essential for hydrogen bonding formation, making the (R)-AZ8838 isomer a completely inactive inhibitor of PAR2 activity. Simulation studies elucidated that AZ8838's binding involves unique interactions with the ECL2 of PAR2, particularly with His227 (Figure 1.10), which plays a crucial role as a gate-keeper, through a binding-triggered rotation, in

facilitating ligand entry, prolonged residence time and later release (Cheng et al., 2017). The characterised PAR2 crystal structure with AZ8838 and AZ3451 has guided multiple efforts for further development of chemical moieties that can modulate PAR2 activity (Brown et al., 2018, Kennedy et al., 2018, Kawatkar et al., 2019, Kennedy et al., 2020, Chinellato et al., 2023).

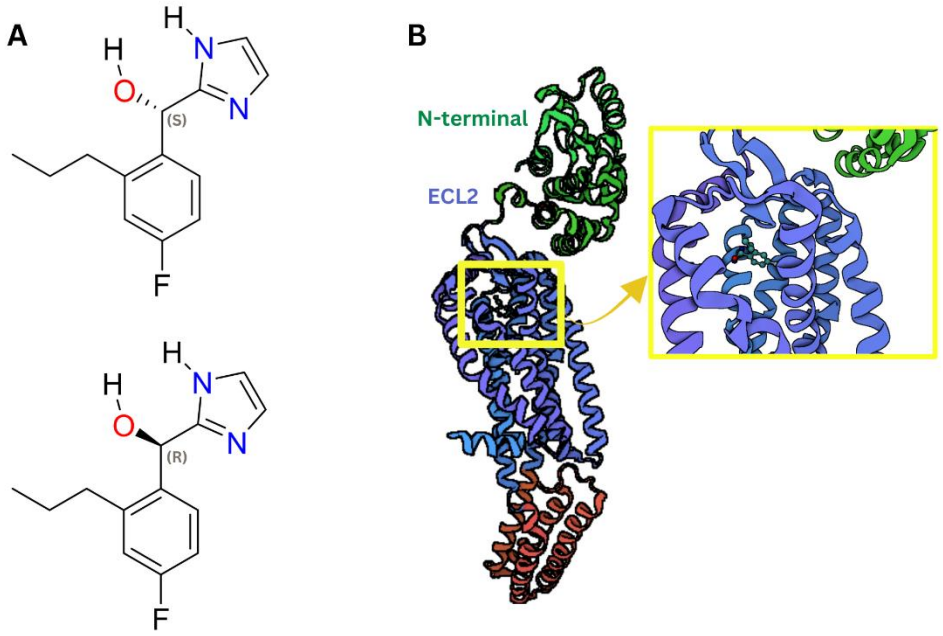

Figure 3.1: AZ8838 structure and binding to PAR2.
(A) Chemical structure of AZ8838 (4-fluoro-2-propylphenyl)(1*H*-imidazol-2-yl) methanol. Formula: C_{13} H_{15} F N_2 O. molecular weight: 234.269 (PBD, 2024) **(B)** AZ8838 orthosteric binding pocket (magnified in yellow square) in cartoon representation of PAR2. Visual created using Mol* (Sehnal et al., 2018) with PDB ID for 5NDD (Cheng et al., 2017).

3.1.2 Overview of AZ8838 PAR2 functional investigations

Besides the initial pharmacological assessment by the Cheng group, where AZ8838 was found to inhibit multiple PAR2-mediated cellular responses, including intracellular calcium flux, phosphorylation of ERK, and β-arrestin recruitment in human brain astrocytoma cell (glial) line (Cheng et al., 2017), few other studies looked into the effects of this inhibitor in other cell types. According to Kennedy *et al*,

AZ8838 was found to significantly inhibit PAR2-induced phosphorylation of ERK1/2 and β-arrestin-2 recruitment in human osteosarcoma epithelial cells stably expressing human PAR2 (U2OS-hPAR2) and inhibit calcium flux in Chinese hamster ovary cells (CHO-hPAR2) stably expressing human PAR2 and human colon adenocarcinoma cells (HT-29) endogenously expressing PAR2 (Kennedy et al., 2020). Additionally, AZ8838 was found to inhibit human dust mites (HDM)-induced Ca^{2+} signalling (Ouyang et al., 2024) and PAR2-AP (2fLIG)-induced interleukin 8 (IL-8) and interleukin 6 (IL-6) release (Bailo et al., 2020). *In vivo*, a single oral dose of AZ8838 significantly reduced paw oedema in a rodent model of acute inflammation, accompanied by reduced mast cell and neutrophil activity (Kennedy et al., 2020).

The aim of this chapter was to further characterise the pharmacological profile of AZ8838 by screening its effects on key PAR2-mediated cellular signalling events in various cell types, thereby formulating a comprehensive understanding of its effectiveness for later *in vivo* studies.

3.2 The effect of AZ8838 on PAR2 mediated NF-κB reporter activation

Nuclear factor-kappa B (NF-κB)-luciferase reporter assays were utilised to measure NF-κB-mediated gene transcription activated via PAR2 agonists (Macfarlane et al., 2005). An in-house previously generated human skin epithelial-like cell line (NCTC2544) stably co-expressing human PAR2 (hPAR2) and NF-κB-Luciferase (NCTC2544-hPAR2/NF-κB-L) was used (see Chapter 2, section 2.4).

3.2.1 The effect of 2fLIG and trypsin on basal NF-κB reporter activity

Prior to investigating the effects of AZ8838, responses to the PAR2 agonists, 2fLIG and trypsin were assessed. Initially the kinetics of activation were established in the

cells expressing PAR-2 and the NF-κB reporter gene (NCTC2544-hPAR2/NF-κB-L) as shown in Figure 3.2. Following a delay of 1-2 hours, there was a time-dependent increase in NF-κB reporter activity in response to both 2fLIG and trypsin observed over a 6-hour period, reaching a peak of 20-25-fold (20.39 ± 1.65 and 26.62 ± 1.55, $p < 0.001$) of control, respectively, at five hours of incubation time (see Figure 3.2). This surge was significantly increased compared to baseline activity, starting from three hours of incubation for both agonists (2fLIG 10.71 ± 1.65, and trypsin 10.74 ± 1.55-mean fold increase/baseline, $p < 0.0001$). At 6 hours, 2fLIG-induced activity slightly decreased, suggesting possible signalling attenuation over prolonged stimulation (Figure 3.2A). A four-hour incubation period was used for later experiments, during which sub-maximal induction of NF-κB reporter activity was observed; 2fLIG induced a 14.71 ± 1.65 fold increase, and trypsin induced a 16.29 ± 1.55 fold increase relative to control.

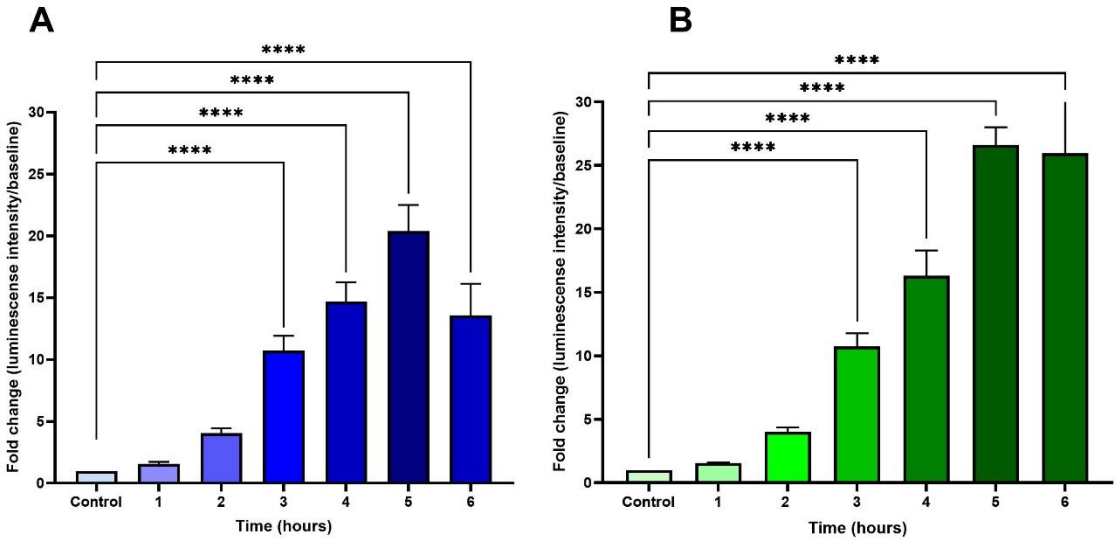

Figure 3.2: Time-dependent activation of NF-κB reporter activity induced by 2fLIG and trypsin in NCTC2544-hPAR2/NF-κB-L cells. Time course of PAR2-induced NF-κB reporter activity by **(A)** 2fLIG (1 μM) and **(B)** trypsin (0.1 μM), measured as a fold change in luminescence intensity relative to the control over 6 hours. Luciferase activity was measured as outlined in Chapter 2, section 2.4. Data are presented as mean ± SEM of 4-5 experiments. Statistical analysis was performed by one-way ANOVA. Significant differences from baseline (control) are indicated: ****$P < 0.0001$.

Having established the optimum time course for stimulation, the concentration-response for each agonist was assessed. Both 2fLIG and trypsin exhibited concentration-dependent enhanced NF-κB luciferase reporter activity compared to baseline in NCTC2544-hPAR2/NF-κB-L cells (see Figure 3.3). Incubating the cells for four hours with increasing concentrations of 2fLIG caused a statistically significant increase in NF-κB activity starting from 0.3 μM (mean of 5.11 ± 0.103 folds of baseline, $p < 0.0001$) to 10 μM (20.6 ± 0.572 mean folds of baseline), indicating a strong concentration-response relationship (Figure 3.3A). This trend shows that 2fLIG is a potent activator of PAR2, capable of inducing substantial receptor activation at micromolar concentrations. A steep rise in activation was observed between 1 μM and 10 μM, suggesting a highly responsive receptor-ligand interaction, with the potential for receptor saturation at higher ligand concentrations. Unlike 2fLIG, trypsin, as the endogenous activator of PAR2, stimulated significant activation at much lower concentrations. Notably, a 10-fold lower concentration (0.03 μM) of trypsin showed a similar significant activity enhancement (5.14 ± 0.32 mean fold of baseline, $p < 0.0001$). Similar to 2fLIG, trypsin also produced a concentration-dependent increase in luminescence intensity, indicative of PAR2-induced NF-κB reporter activity, with a maximum concentration tested at 1 μM, causing ~ 16-fold (15.96 ± 0.33) increase of NF-κB reporter activity relative to control levels (see Figure 3.3B). It is noteworthy that trypsin-induced PAR2-activity at nanomolar concentrations, compared to the micromolar range required for 2fLIG, suggesting that trypsin is a more potent activator of PAR2 in this context. However, the maximum response elicited by both agonists is almost similar at higher concentrations, indicating that both can achieve similar levels of maximal PAR2 activation in the context of eventual NF-κB reporter activity

Error! Reference source not found.

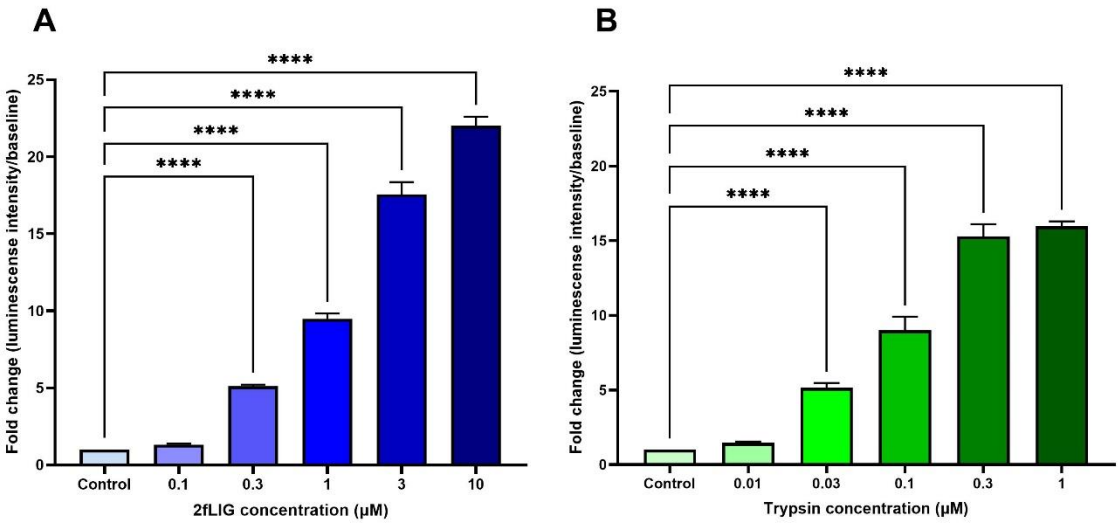

Figure 3.3: Concentration-dependent increase in NF-κB reporter activity induced by 2fLIG and trypsin in NCTC2544-hPAR2/NF-κB-L cells. Cells were stimulated with (**A**) 2fLIG or (**B**) trypsin over the indicated concentration ranges for 4 hours of exposure. Concentration dependency is shown as a fold change in luminescence intensity relative to control levels. Data are presented as mean ± SEM of 4-5 experiments. Statistical analysis was performed by one-way ANOVA. Significant differences from baseline (control) are indicated: ****P < 0.0001.

The agonist concentration-response (presented as % of maximum NF-κB activation) was fitted using the Hill equation to estimate half-maximal effective concentrations (EC_{50}) of both agonists. As depicted in Figure 3.4The trypsin (green) curve was to the left of the 2fLIG curve, demonstrating that lower concentrations of trypsin are required to achieve a similar level of NF-κB reporter activation. As seen earlier, trypsin showed about 16-fold higher potency with an EC_{50} value estimated in the nanomolar range, EC_{50} = 65.05 nM (95% CI: 40.28 to 102.6 nM), in contrast to 2fLIG, which showed an EC_{50} value estimated in the micromolar range, EC_{50} = 1.04 μM (95% CI: 0.5809 to 1.798 μM). Concentrations slightly below the EC_{80} for both agonists were used for later experiments to investigate the inhibitor effects on NF-κB reporter activity.

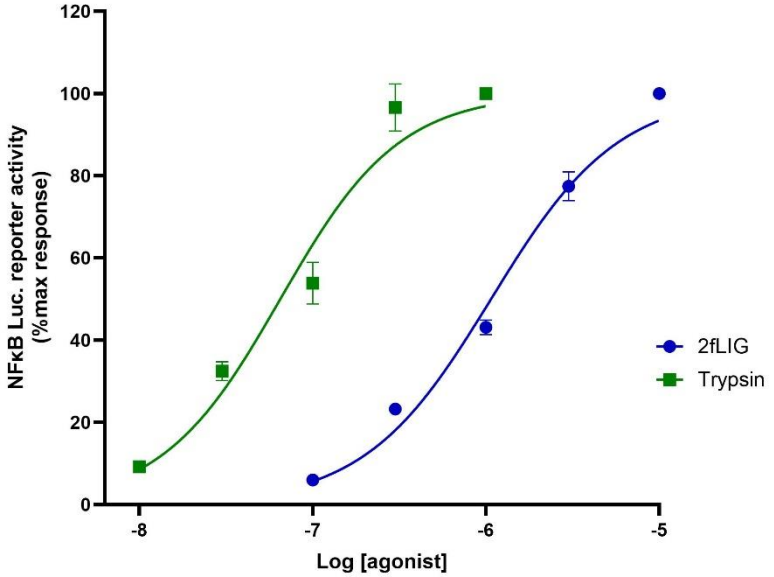

Figure 3.4: Concentration response curves of NF-κB reporter activation by 2fLIG and trypsin in NCTC2544-hPAR2/NF-κB-L cells.
Concentration-response curves depicting the percentage of maximal NF-κB reporter activity induced by 2fLIG (blue) and trypsin (green). Data were fitted using the Hill equation in GraphPad prism 10.3.1. The EC_{50} values for 2fLIG and trypsin were estimated to be 1.04 μM (95% CI: 0.5809 to 1.798 μM) and 65.05 nM (95% CI: 40.28 to 102.6 nM), respectively. The graph shows representative data of 4-5 experiments, presented as mean ± SEM.

3.2.2 AZ8838 effects on trypsin- and 2fLIG -induced NF-κB reporter activity.

To test the effect of AZ8838 on previously profiled 2fLIG and trypsin PAR2 activity, NCTC2544-hPAR2/NF-κB-L cells were pre-incubated with increasing concentrations of the inhibitor (at least triplicate for each concentration) for one hour before stimulation with PAR2 agonists for four hours. Concentrations of 1μM 2fLIG and 100 nM trypsin were used, towards the upper quartile of the concentration curve for each agonist.

As demonstrated earlier, 1μM 2fLIG induced a significant increase in NF-κB reporter activity, approximately 10 times the control values, which was not significantly altered by the presence of DMSO (2fLIG = 10.05 ± 0.897, DMSO plus 2fLIG = 11.56 ± 1.17, p = 0.5897, n=5) (see Figure 3.5A). Similarly, 100 nM trypsin stimulated a significant

increase in NF-κB reporter activity, approximately 19 times the control values, which also was not significantly affected by the presence of DMSO (trypsin = 19.9 ± 2.23, DMSO plus trypsin = 26.9 ± 3.13, p = 0.0942, n=5) (see Figure 3.5B). Pre-incubation with AZ8838 alone did not affect NF-κB reporter activity, even at the highest concentration tested.

As illustrated in Figure 3.5, there was a concentration-dependent inhibition of PAR2-mediated NF-κB activation by AZ8838 stimulated with either 2fLIG or trypsin. Against both agonists, AZ8838 showed significant reductions in luminescence intensity observed at concentrations as low as 0.1 μM (p = 0.0004). The maximal inhibition was achieved at 50 μM AZ8838, where the luminescence intensity is reduced to levels comparable to the control. The concentration-response curves for the inhibition of NF-κB activation by AZ8838 in the presence of 1 μM 2fLIG (blue) and 0.1 μM trypsin (green) are demonstrated in Figure 3.6. The IC_{50} values for AZ8838 were 0.379 μM (95% CI: 0.26 to 0.517 μM) in 2fLIG-stimulated cells and 60.03 nM (95% CI: 2.21 to 136.1 nM) in trypsin-stimulated cells.

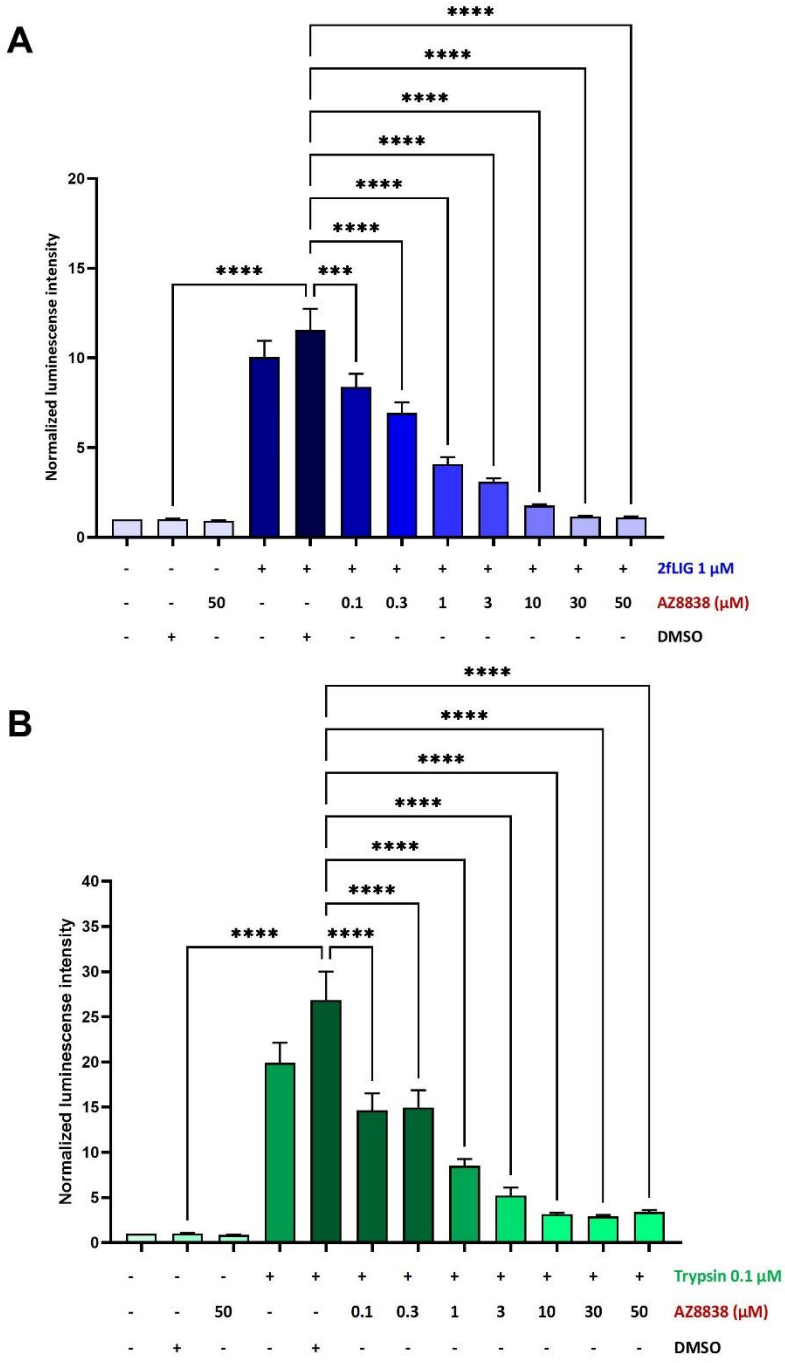

Figure 3.5: Inhibition of PAR2-mediated NF-κB reporter activity by AZ8838 in NCTC2544-hPAR2/NF-κB-L cells.

Concentration-dependent inhibition of NF-κB activation stimulated by **(A)** 1 µM 2fLIG and **(B)** 0.1 µM trypsin by variable concentrations of AZ8838**.** Graphs show representative data of 4-5 experiments, presented as mean ± SEM. Statistical analysis was performed using one-way ANOVA. Significant differences are indicated: *** P< 0.001, ****P < 0.0001.

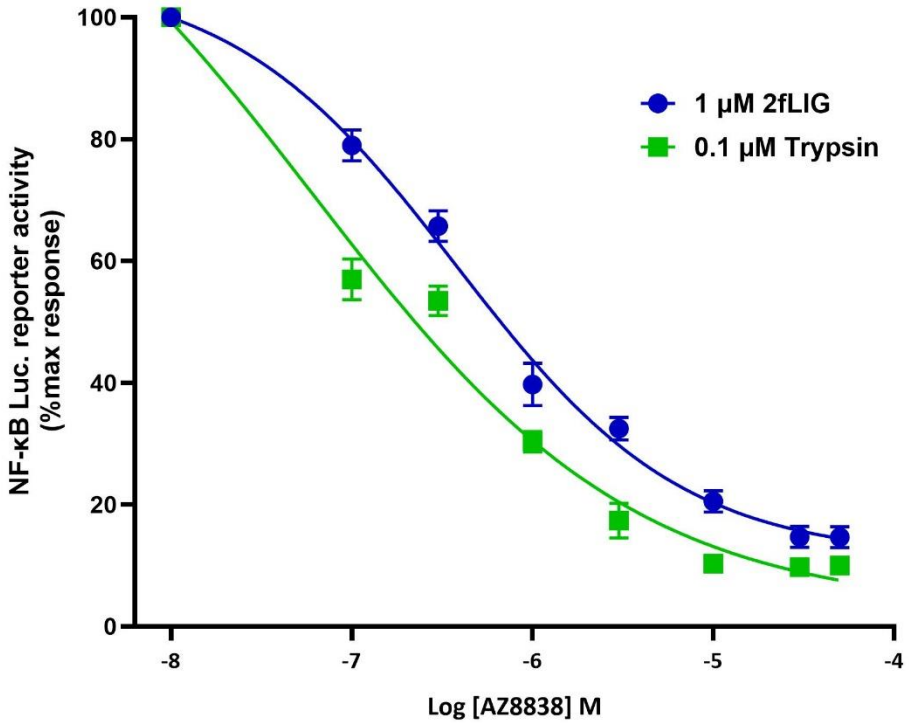

Figure 3.6: AZ8838 concentration-dependent inhibition of PAR2-induced NF-κB reporter activity.
Concentration-response curves showing the percentage of maximal NF-κB reporter activity versus varying concentrations of AZ8838 in the presence of 1 μM 2fLIG (blue) and 0.1 μM trypsin (green). Data were fitted using the Hill equation in GraphPad Prism 10.3.1. The IC_{50} value for AZ8838 was estimated to be 0.379 μM versus 2fLIG (95% CI: 0.26 to 0.517 μM) and 60.03 nM versus trypsin (95% CI: 2.21 to 136.1 nM), n=5.

3.2.3 The effect of AZ8838 on TNFα-induced NF-κB reporter activity

To confirm the selectivity of the inhibitory effect of AZ8838 on PAR2-mediated NF-κB transcriptional activity, it was tested against the TNFα response. TNFα is well-known to activate NF-κB via TNF receptor (TNFR1 and TNFR2)-mediated signalling, independent of PAR2, driving transcription of many inflammatory genes (Atretkhany et al., 2020). Moreover, elevated TNFα levels have been documented in CP/CPPS patients and experimental models (Chen et al., 2021). Cellular responses to TNFα-induced were established by examining the time-dependent effect on NF-κB reporter activity in NCTC2544-hPAR2/NF-κB-L over a period of 6 hours (see Figure 3.7A).

TNFα stimulated a strong and sustained NF-κB activation that was time-dependent, rising significantly from 2 hours to about 4-fold of control (3.9 ± 0.13, $p < 0.0001$) and progressively reaching a peak at 6 hours of 18-fold (18.6 ± 0.57, $p < 0.0001$). Four hours were used for later experiments that induced slightly submaximal activation. Like previously tested agonists, TNFα activated NF-κB reporter activity was concentration-dependent. A significant difference from control induced by TNFα started at concentrations as low as 0.3 ng/mL (mean fold increase: 3.3 ±0.21, $p = 0.001$), reaching maximum activation at 10 ng/mL (mean fold increase: 14.23 ± 0.61, $p < 0.0001$) as shown in Figure 3.7B. However, a slight reduction in NF-κB reporter activity was observed at the highest concentration of 20 ng/mL, indicating a possible saturation of activity or cellular cytotoxicity at high concentrations. The estimated EC_{50} for TNFα was 0.818 ng/mL (95% CI: 0.661 to 1) (Figure 3.8, Figure 3.7C).

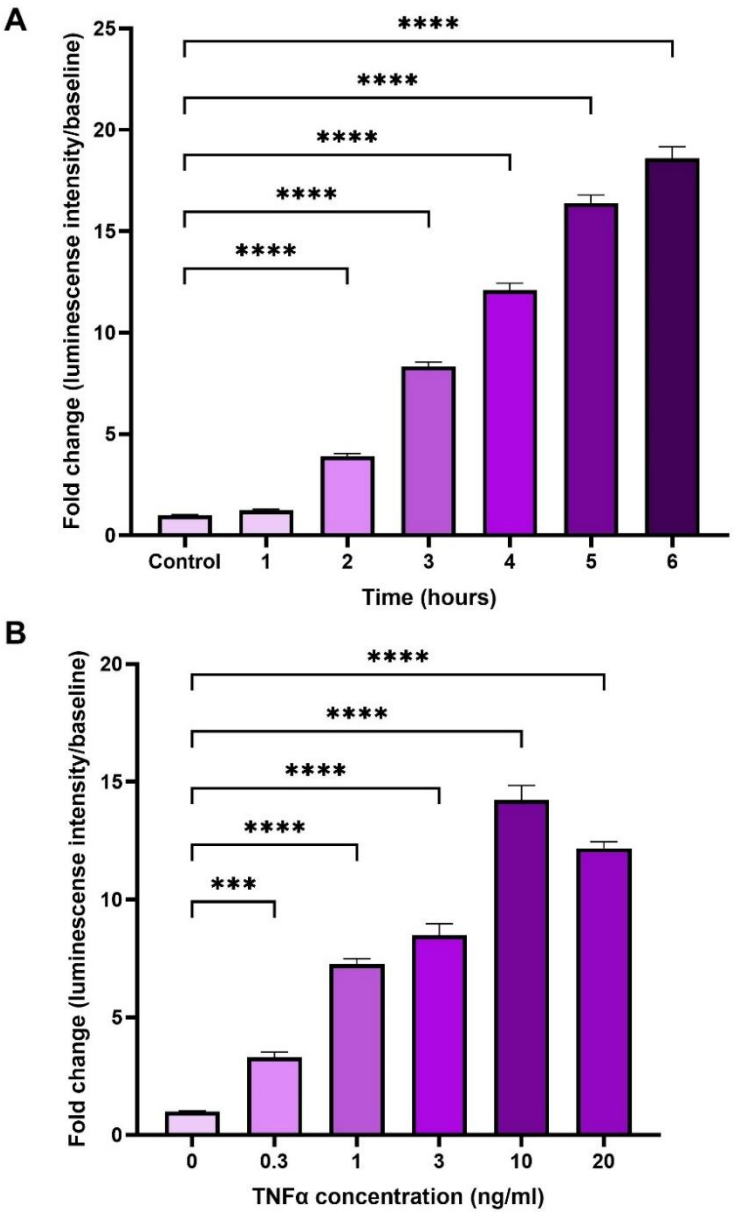

Figure 3.7: Time- and concentration-dependent activation of NF-κB reporter activity by TNFα in NCTC2544-hPAR2/NF-κB-L cells.

(A) Time-course of NF-κB reporter activation induced with 10 ng/mL TNFα, measured as fold change in luminescence intensity relative to baseline over 6 hours. **(B)** Concentration-response curve showing fold change in luminescence intensity triggered by increasing concentrations of TNFα (0.3 - 20 ng/mL). Graph shows representative data of 3-4 experiments, presented as mean ± SEM. Statistical analysis was performed by one-way ANOVA. Significant differences from baseline (control) are indicated: *** P< 0.001, ****P < 0.0001.

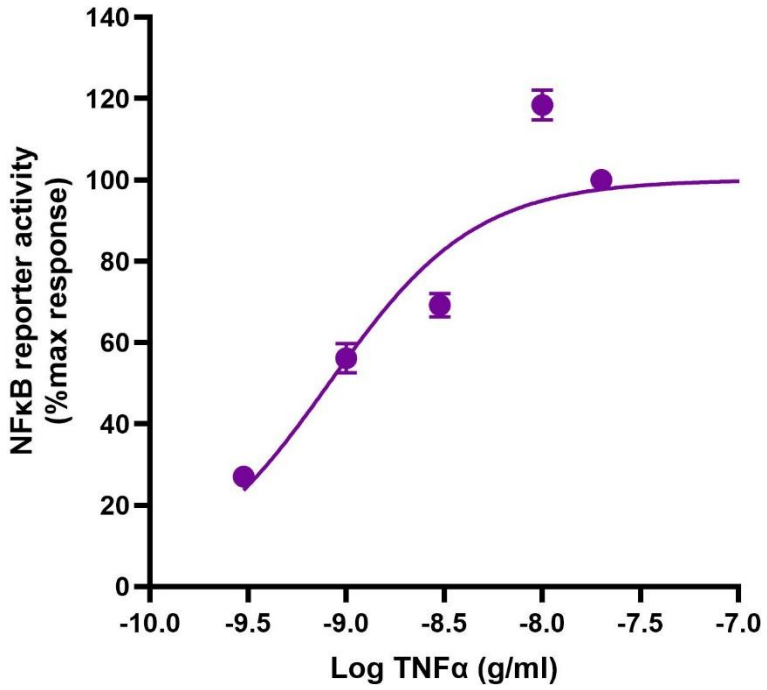

Figure 3.8: Concentration-response curve of TNFα induced NF-κB reporter activity in NCTC2544-hPAR2/NF-κB-L cells.
The curve illustrates NF-κB reporter activity as a % of maximal response versus concentration of TNFα (same data displayed in 3.7B). The EC_{50} value for TNFα is 0.818 ng/mL (95% CI: 0.661 to 1). Data were fitted using the Hill equation model in GraphPad Prism 10.3.1, n=4.

The effects of pre-treatment with increasing concentrations of AZ8838 (ranging from 0.1 to 30 μM) on TNFα-mediated NF-κB reporter activation in NCTC2544-hPAR2/NFκB-L cells are depicted in Figure 3.9. As observed previously, AZ8838 alone did not alter baseline activity (1.03 ± 0.03), and DMSO did not change the magnitude of NF-κB activation mediated by TNFα (TNFα 16.39 ± 0.99; TNFα plus DMSO 17.86 ± 1.2, n=4). The luminescence intensity, which indicates NF-κB reporter activity, remains relatively consistent across all tested concentrations of AZ8838 (even at highest tested concentration: 15.45 ± 0.74), suggesting no effects of AZ8838 on TNFα-induced NF-κB activation. In fact, the luminescence intensities are almost like those observed in the presence of TNFα alone, indicating that AZ8838 does not affect the TNFα signalling pathway in this context. This is also evident in the concentration-response curve (Figure 3.9B), which is relatively flat, further confirming that AZ8838

does not inhibit TNFα-induced NF-κB activation. In contrast, AZ8838 effectively inhibited 2fLIG and trypsin-stimulated NF-κB activity, as shown before (refer to subsection 3.2.2, Figure 3.5). This suggests a level of specific effect of AZ8838 for PAR2-mediated NF-κB activation.

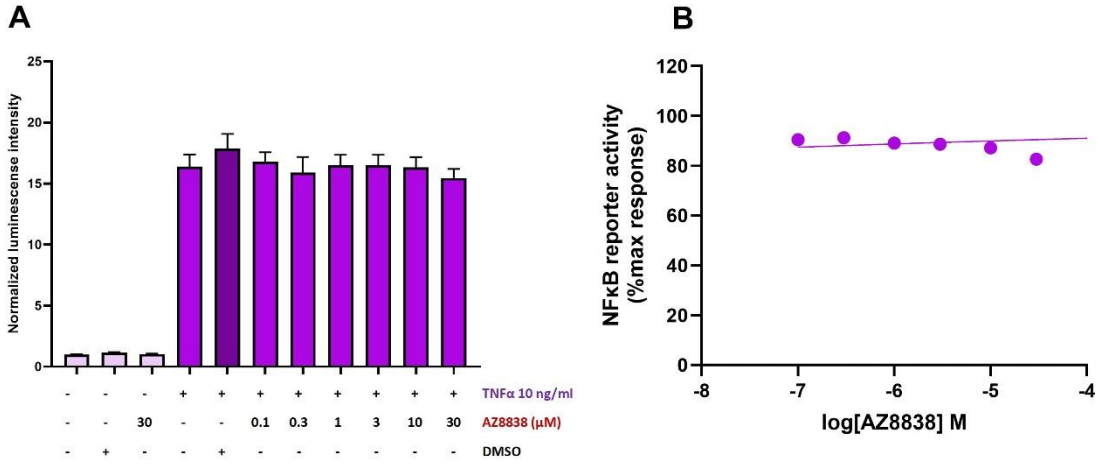

Figure 3.9: AZ8838 has no effect on TNFα-induced NF-κB activation in NCTC2544-hPAR2/NF-κB-L cells.

(A) Normalised luminescence intensity (normalised to control mean value) indicating NF-κB activation induced by 4 hours exposure with 10 ng/mL TNFα following 1 hour pre-treatment with increasing concentrations of AZ8838 (0.1 to 30 μM). **(B)** Concentration-response curve showing the percentage of maximal NF-κB reporter activity stimulated with 10 ng/mL TNFα and varying concentrations of AZ8838. Data were fitted using the Hill equation in GraphPad Prism 10.3.1. Graphs show representative data of four independent experiments, presented as mean ± SEM. Statistical analysis was performed using one-way ANOVA.

3.3 Effect of AZ8838 on PAR2-mediated p65 translocation in NCTC2544-hPAR2/NF-κB-L cells

Understanding the inhibitory effects of AZ8838 on PAR2-mediated NF-κB signalling pathways is essential for evaluating its selectivity as a targeted therapy for inflammatory diseases. One vital component of the NF-κB pathway is the p65 subunit, also known as RelA. This subunit is one component of the NF-κB family of transcription factors (normally activated as dimers), which, in its inactive state,

remains sequestered in the cytoplasm by inhibitor proteins known as IκBs. Upon activation by various stimuli or upstream receptors, IκBs get phosphorylated, ubiquitinated and eventually degraded. This allows the release of NF-κB dimers, predominantly p65/p50, facilitating their shuttling into the nucleus. In the nucleus, p65 binds to specific DNA sequences in promoter regions of target genes, turning on the transcriptional activity that directs later cellular processes (Liu et al., 2017, Guo et al., 2024). Since the activation of NF-κB pathway is associated with the intracellular localisation of NF-κB dimer, nuclear localisation is frequently utilised as an indicator of activation (Meier-Soelch et al., 2021). Therefore, inhibiting the nuclear translocation of p65 can serve as a measure of inhibition of NF-κB-mediated transcription and its downstream cellular responses.

To further elucidate the mechanism of AZ8838 inhibitory effect, immunofluorescence labelling was employed to track the localisation of p65 subunit (refer to Chapter 2, subsections 2.9.1 and 2.9.2). Visualising the nuclear translocation of p65 confirms the inhibitory effect of AZ8838 at the cellular level, one step ahead of the genetic activity, and correlates the reporter assay findings with direct observations of p65 dynamics.

3.3.1 The effect of 2fLIG on nuclear translocation of p65 in NCTC2544-hPAR2/NF-κB-L cells.

Initially, the specificity and accuracy of the immunofluorescence staining protocol were examined by testing any potential sources of background or non-specific signal. When cells are not incubated with antibodies, no background fluorescence was detectable in FITC channel (see Control, Figure 3.10), confirming that any signal seen later would be specific to the antibodies binding to the target protein. In the absence

of primary or secondary antibodies, there was no signal in the FITC channel. A distinct fluorescence signal in the FITC channel for p65 was observed only when cells were treated with both primary and secondary antibodies. In unstimulated cells, this signal was predominantly localised in the cytoplasm, with only small amounts detectable in the nucleus (1° Ab + 2° Ab, Figure 3.10).

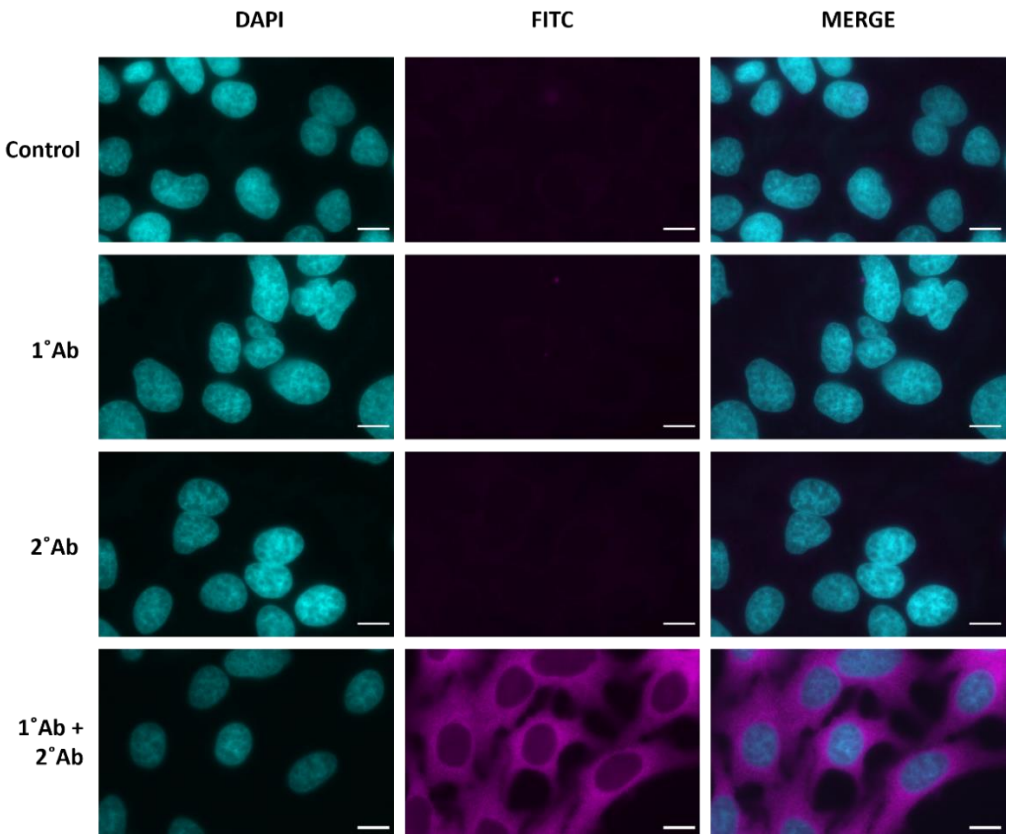

Figure 3.10: Control for immunofluorescence labelling of p65 in NCTC2544-hPAR2/NF-κB-L cells.
The first row (**Control**) shows the cells without any antibodies. The next rows, in order, display the result of incubating the cells with the primary antibody alone (**1° Ab**), with the secondary antibody alone (**2° Ab**), and with both primary and secondary antibodies (**1° Ab + 2° Ab**) showing the specific p65 labeling represented in FITC channel. n= 3, Scale bar = 20 µm.

Next, the kinetics of nuclear translocation of p65 following PAR2-activation with 2fLIG (10 µM) was examined. Figure 3.11 shows representative images of immunofluorescence studies. In control (untreated cells), p65 subunits were primarily located in the cytoplasm as indicated by the low FITC signal overlapping with DAPI.

This observation was supported by the colocalization analysis, where the mean Pearson's coefficient (PC) of FITC (p65) and DAPI signals was a low positive value (PC = 0.16 ± 0.03) and Mander's coefficient (MC), indicative of the fraction of p65 signal overlapping nuclear signal, was also low positive (MC = 0.23 ± 0.017). Upon 2fLIG treatment, a marked increase in the nuclear localisation of p65 was observed as early as 15 minutes of exposure, confirmed by the significant FITC signal overlapping with DAPI in representative images (Figure 3.11), indicating early activation of the NF-κB pathway. Between 15 and 30 minutes of stimulation, the p65 nuclear translocation continued to increase, reaching a peak around 30 minutes as visualised by the FITC signal (Figure 3.11) and confirmed by the colocalization analysis (Figure 3.12). Colocalization parameters, including PC and MC values, were significantly increased at 30 minutes post-stimulation (PC = 0.53 ± 0.07, $p < 0.0001$, MC = 0.38 ± 0.04, $p = 0.0011$) compared to baseline (PC = 0.16 ± 0.03, MC = 0.23 ± 0.01). Similarly, the percentage of FITC-positive nuclei from the cell population at 30 minutes post stimulation reached about 40% compared to none in the control (% 40.5 ± 6.15, $p = 0.003$). After 45 minutes, immunofluorescence (IF) representative images reveal a gradual decline in p65 FITC signal within the nucleus, with the majority relocating back to the cytoplasm. Colocalization parameters, including PC and MC values, dropped after 45 minutes post stimulation (at 120 minutes: PC = 0.33 ± 0.02, MC = 0.29 ± 0.01), approaching control values. Similarly, the percentage of FITC-positive nuclei from the cell population after 2 hours post-stimulation reached about 10% compared to 40% at 30 minutes (9 ± 5.2%). For investigating the effect of AZ8838, 30 minutes of stimulation with 10 μM 2fLIG was employed to ensure maximum p65 nuclear translocation.

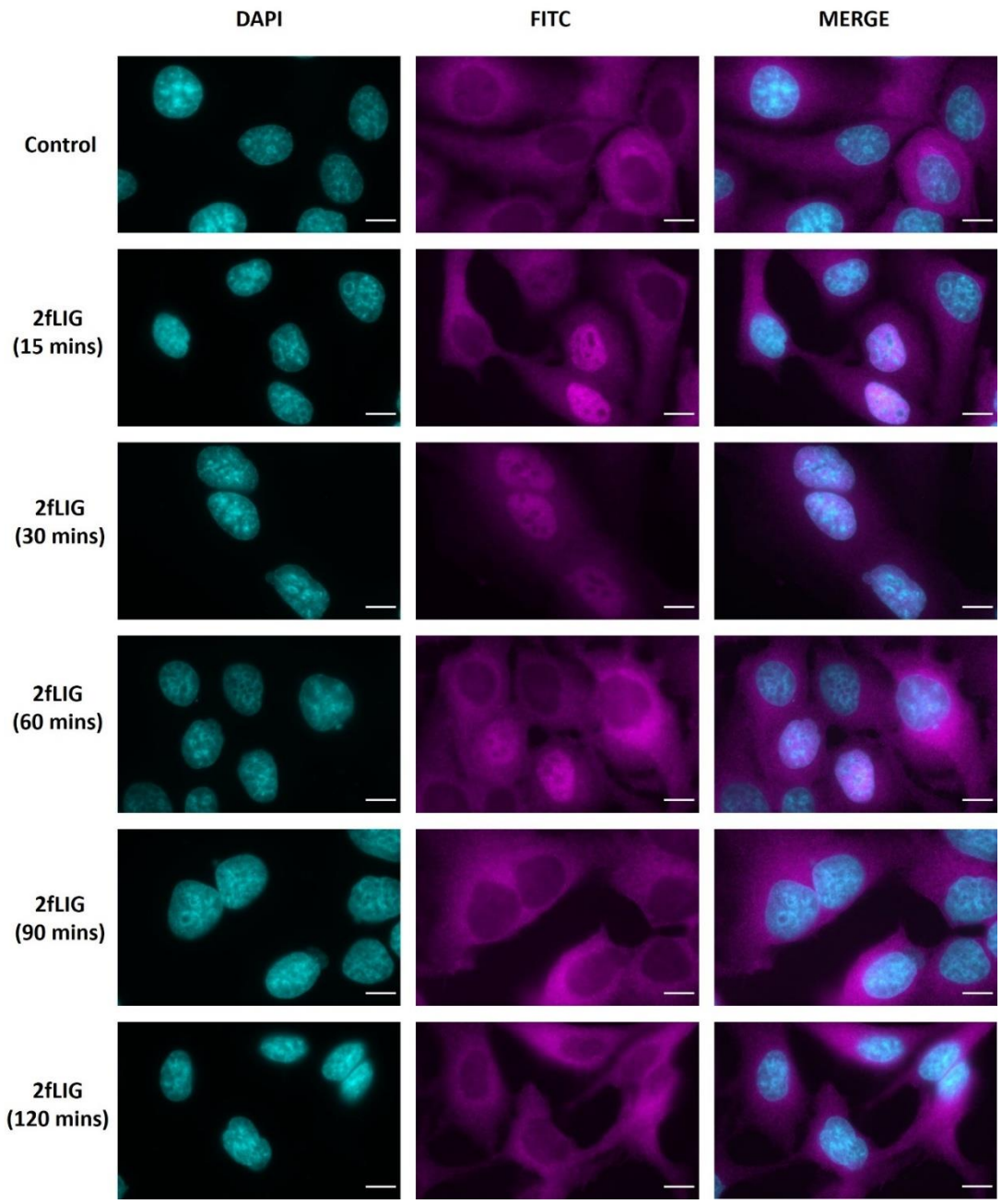

Figure 3.11: Time-course analysis of p65 nuclear translocation in NCTC2544-hPAR2/NF-κB-L cells following stimulation with 2fLIG.
Representative immunofluorescence micrographs showing the distribution of p65 at the indicated time points post-stimulation with 10 μM 2fLIG, with p65 indicated by FITC (magenta) and nuclei stained with DAPI (cyan) and overlap in merged images (blue intensity). n= 3, Scale bar = 20 μm.

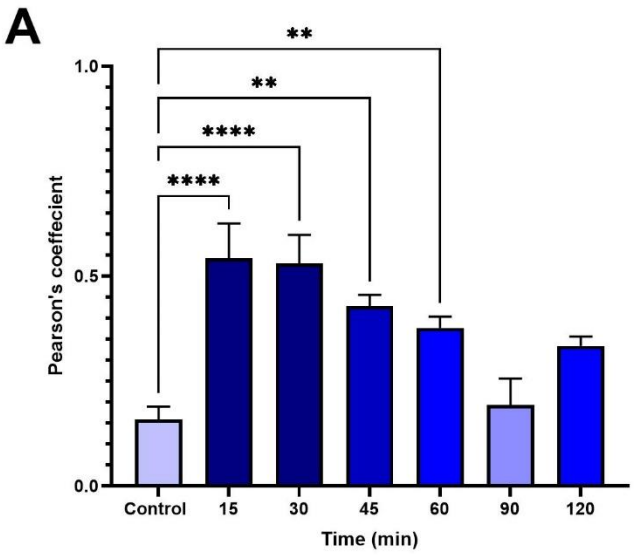
A
**
**
****
****
1.0
0.5
0.0
Pearson's coeffecient
Control
15
30
45
60
90
120
Time (min)

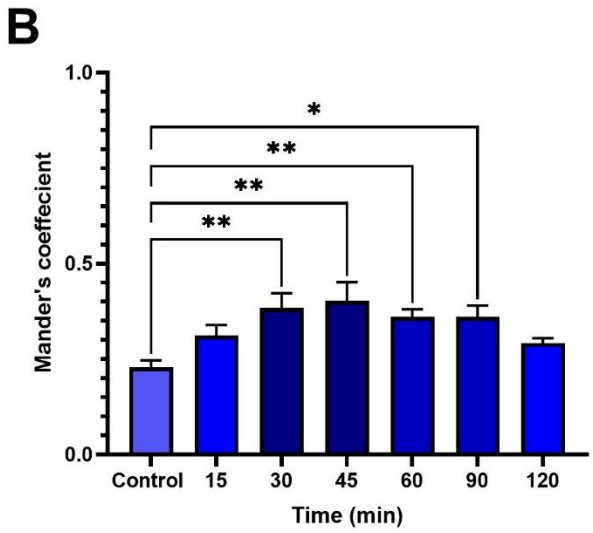
B
*
**
**
**
1.0
0.5
0.0
Mander's coeffecient
Control
15
30
45
60
90
120
Time (min)

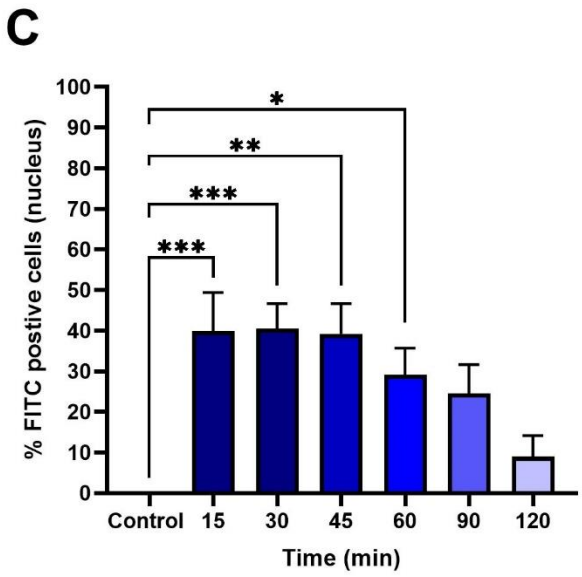
C
*
**
***
***
100
90
80
70
60
50
40
30
20
10
0
% FITC postive cells (nucleus)
Control
15
30
45
60
90
120
Time (min)

Figure 3.12: Quantitative colocalization analysis of nuclear localization of p65 in 2fLIG stimulated NCTC2544-hPAR2/NF-κB-L cells.
(A) Pearson's correlation coefficient (PC) indicates the degree of colocalization between DAPI and FITC channels, representing p65 nuclear translocation over time. **(B)** Mander's overlap coefficient (MC) quantifies the FITC signal overlapping DAPI at each time point. **(C)** The percentage of FITC-positive cells (nuclei) over the total cell population in each captured immunofluorescence image. Graphs show representative data of three independent experiments, presented as mean ± SEM. For each n, 4-7 images were analysed using ImageJ v1.54J equipped with the JACoP plugin, applying Costes's automatic threshold. Statistical analysis was performed using one-way ANOVA. Significant differences are indicated: *p<0.05, **p<0.01, ***p<0.001, and ****p<0.0001 compared to control (baseline) values.

3.3.2 Effect of AZ8838 on PAR2-induced p65 nuclear translocation in NCTC2544-hPAR2/NF-κB-L cells.

Confirming significant nuclear translocation of the p65 NF-κB subunit following 2fLIG stimulation for 30 minutes, the effect of AZ8838 pre-treatment was investigated. Figure 3.13 illustrates representative IF images of AZ8838 effects tested. Treating the cells with AZ8838 alone, without 2fLIG stimulation, did not influence the predominant p65 cytoplasmic localisation, similar to the control condition. This was confirmed with the colocalization quantitative analysis, as PC and MC values of AZ8838 treatment alone (PC = 0.12 ± 0.02, MC = 0.27 ± 0.01) were not different from those of control (PC = 0.19 ± 0.02, MC = 0.3 ± 0.01, $p > 0.999$). As observed before, stimulation of the cells with 10 μM 2fLIG for 30 minutes induced robust nuclear translocation (% FITC positive nuclei 74.2 ± 6.3) of p65 that was not significantly altered when cells were co-treated with DMSO (as a vehicle control, % FITC positive nuclei 58.8 ± 8, $p = 0.16$), confirming that DMSO does not interfere with the translocation process (Figure 3.13, Figure 3.14). The co-localisation analysis supported this observation (see Figure 3.14), where PC and MC values remained significantly different ($p < 0.0001$) from baseline values upon DMSO co-treatment (2fLIG: PC = 0.63 ± 0.02, MC = 0.54 ± 0.02; 2fLIG + DMSO: PC = 0.6 ± 0.03, MC = 0.54 ± 0.03). In contrast, when cells were pre-treated with AZ8838 at concentrations

of 10, 20, and 30 μM prior to 2fLIG stimulation, a concentration-dependent inhibition of p65 nuclear translocation was observed (Figure 3.14C). At 10 μM, p65 translocation was significantly reduced, reaching ~36% reduction of FITC positive nuclei (% FITC positive nuclei 21.9 ± 7.3, $p < 0.0001$) compared with the vehicle control. Further reduction was observed at higher AZ8838 concentrations (20 and 30 μM), where the FITC signal remains largely cytoplasmic (Figure 3.13), resembling the control condition. The colocalization analysis provided additional evidence of these findings, as indicators of p65 nuclear localisation exhibited a significant reduction to values close to control (at 30 μM AZ8838: PC = 0.23 ± 0.02, MC = 0.29 ± 0.01, $p < 0.0001$). However, it is important to note that the colocalisation parameter values did not exhibit a clear concentration-dependent pattern, as the trends observed in IF imaging and percent of FITC-positive nuclei. This suggests that the relationship between concentration and colocalization metrics may not be as straightforward, indicating the possible involvement of other regulatory mechanisms or variability in the cellular response. Nevertheless, these findings show that AZ8838 effectively inhibited 2fLIG-induced activation of NF-κB nuclear translocation.

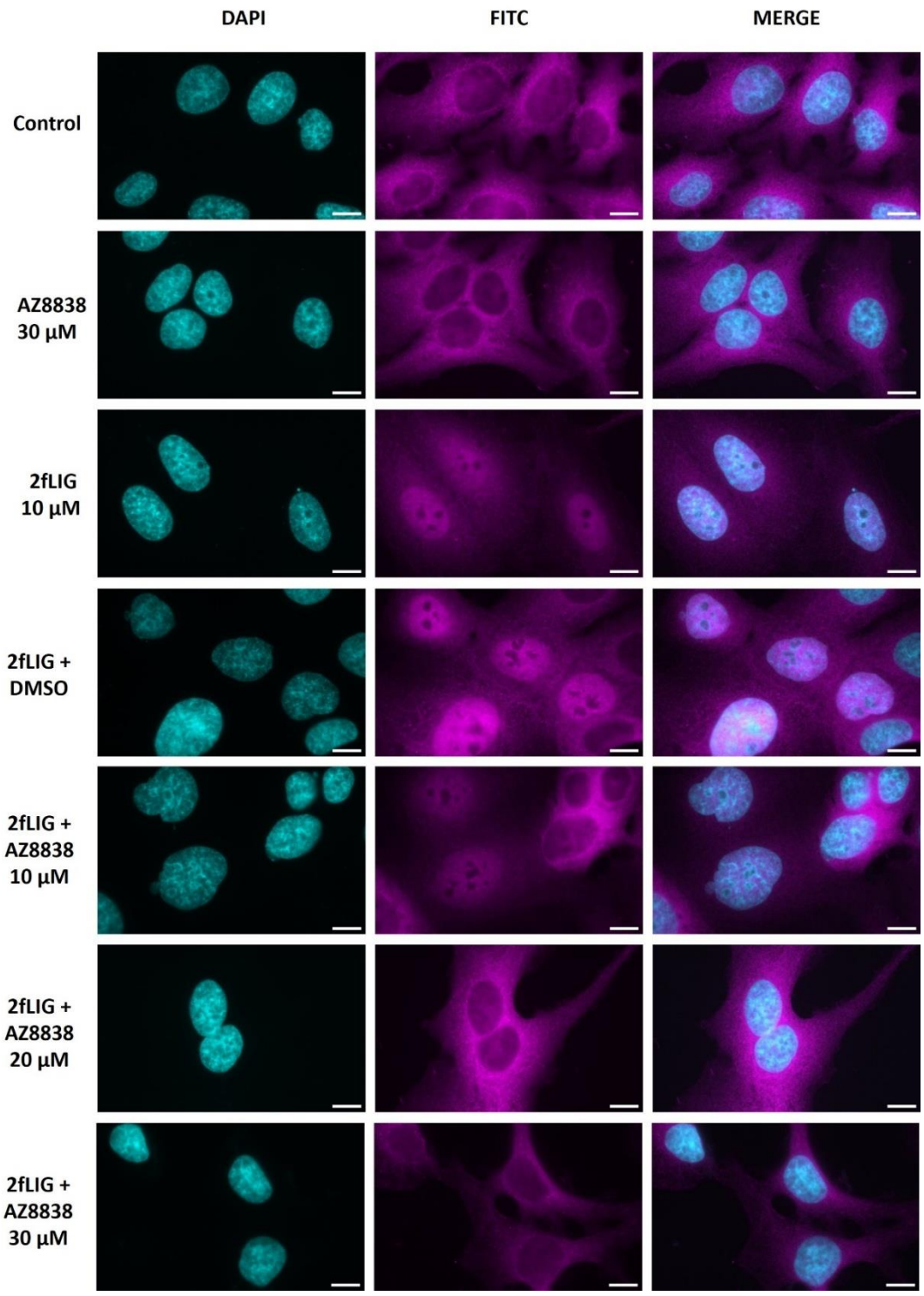

Figure 3.13: AZ8838 inhibits 2fLIG-induced p65 nuclear translocation in NCTC2544-hPAR2/NF-κB-L cells.

Representative micrographs showing the effect of pretreatment with increasing concentrations of AZ8838 (10 µM, 20 µM, 30 µM) 1 hour prior to stimulation of the cells with 10 µM 2fLIG for 30 minutes. The effects of AZ8838 (30 µM) incubation for one hour alone and the effect of vehicle (DMSO) on 2fLIG response were tested as controls. FITC channel represents p65 (magenta), and DAPI represents nuclei (cyan). The overlap level is shown in the merged images (blue intensity). n= 3, scale bar = 20 µm.

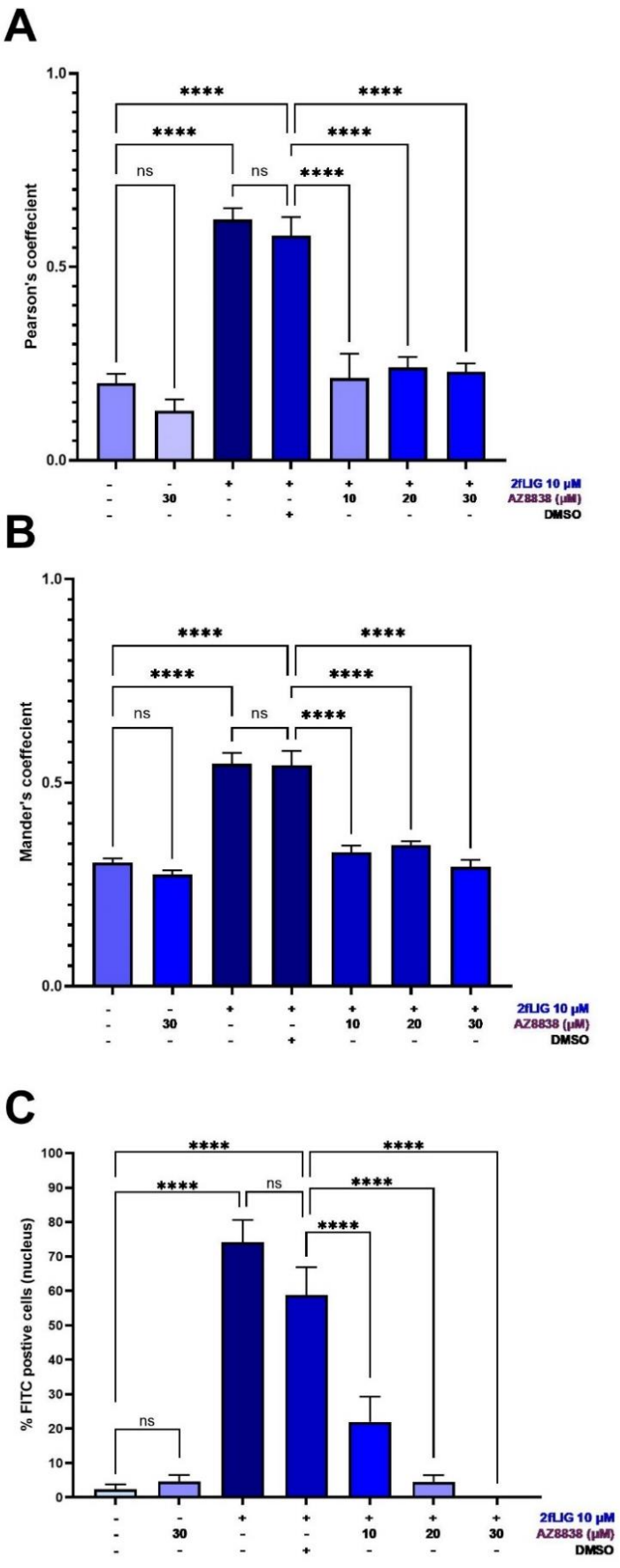
A
Pearson's coeffecient
1.0
0.5
0.0
****
****
****
****
****
ns
ns
2fLIG 10 µM
AZ8838 (µM)
DMSO
B
Mander's coeffecient
1.0
0.5
0.0
****
****
****
****
****
ns
ns
2fLIG 10 µM
AZ8838 (µM)
DMSO
C
% FITC postive cells (nucleus)
100
90
80
70
60
50
40
30
20
10
0
****
****
****
****
****
ns
ns
2fLIG 10 µM
AZ8838 (µM)
DMSO

Figure 3.14: Quantitative colocalization analysis of nuclear localization of p65 in NCTC2544-hPAR2/NF-κB-L cells in response to 2fLIG alone and AZ8838 co-treatment.

(A) Pearson's coefficient showing colocalization between p65 and DAPI. **(B)** Mander's coefficient for FITC signal overlapping DAPI. **(C)** The percentage of FITC-positive cells (nuclei) relative to the total cell count in captured IF images. Data represent 3 independent experiments as mean ± SEM. For each experiment, 4-7 images were analysed with ImageJ v1.54J, equipped with the JACoP plugin, and Costes's automatic threshold was applied. Statistical analysis was done using one-way ANOVA. Significant differences are indicated: *p < 0.05, **p < 0.01, ***p < 0.001, ****p < 0.0001, ns = not significant.

3.4 The effect of AZ8838 on PAR2-induced phosphorylation of ERK1/2.

Having established the profile of AZ8838 inhibition of PAR2-mediated NF-κB activity in NCTC2544-hPAR2/NF-κB-L cells, the effects of AZ8838 on extracellular signal-regulated kinases (ERK) phosphorylation were examined in the same cell line. As described earlier (see Chapter 1, section1.10.2), since the early characterisation of PAR2, it is well-established that activation of the receptor triggers mitogen-activated protein kinase (MAPK) signalling downstream of PAR2, leading to a rapid transient ERK1/2 phosphorylation (Belham et al., 1996, Déry et al., 1998, DeFea et al., 2000b). Initially, the kinetics and the concentration effects of the PAR2 agonists, 2fLIG and trypsin, on the phosphorylation of ERK1/2 were characterised using Western blotting (refer to chapter 2, section 2.5). Phosphorylated ERK1/2 was normalised against the total ERK1/2 in whole cell lysates of each sample.

3.4.1 Effects of 2fLIG and trypsin on ERK phosphorylation in NCTC2544-hPAR2/NF-κB-L cells.

The next set of experiments examined the kinetics of PAR2-mediated ERK1/2 phosphorylation in response to 2fLIG and trypsin. Understanding these dynamics is essential for subsequent inhibitor studies. As shown in Figure 3.15, 10 μM 2fLIG triggered a significant 5-fold increase of ERK1/2 phosphorylation at 2 minutes

exposure (mean fold 5.59 ± 0.93, p = 0.024) and reached a peak at 5 minutes, at ~7-fold of control values (mean fold 6.88 ± 1.44, p = 0.046). Phosphorylation levels then decreased rapidly, returning to near control levels by 60 minutes. Following similar kinetics (Figure 3.16), 0.1 μM trypsin induced a significant ~3.5-fold increase in pERK1/2 levels at 2 minutes (mean fold 3.29 ± 0.54, p = 0.04) and again reached a peak of about 4.5-fold of baseline at 5 minutes mean fold 4.57 ± 0.25, p = 0.0005). However, the decline in pERK levels was found to be slower compared to 2fLIG, with pERK1/2 levels remaining slightly above control levels at 60 minutes. This indicates a rapid transient effect of 2fLIG compared to a slightly more sustained phosphorylation of ERK1/2 by Trypsin, as depicted in Figure 3.17. For later experiments, five-minute exposure was employed for both agonists.

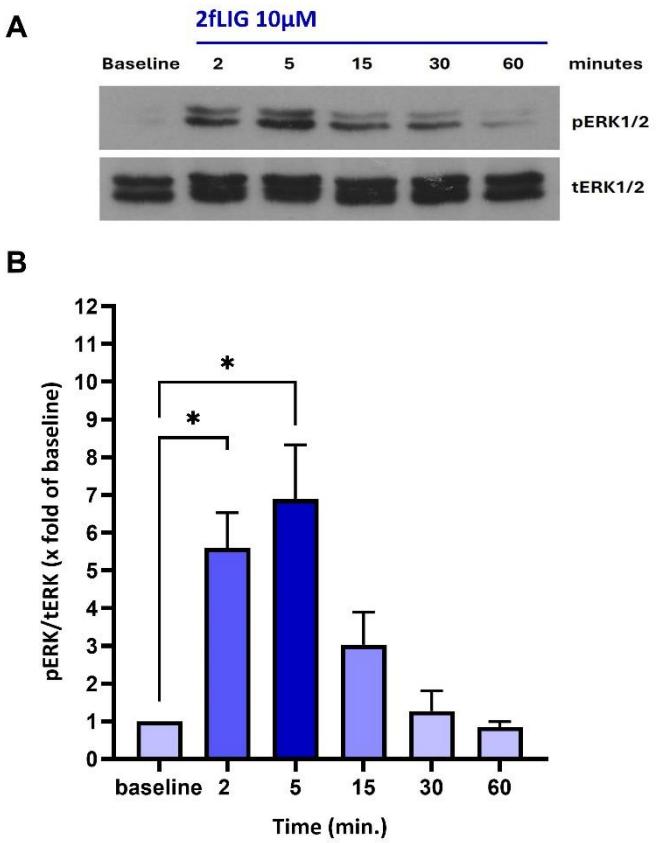

Figure 3.15: Time course of 2fLIG-induced ERK1/2 phosphorylation in NCTC2544-hPAR2/NF-κB-L cells.

(A) Representative immunoblots showing pERK1/2 and tERK1/2 in whole cell lysate treated with 10 µM 2fLIG over the indicated time points. **(B)** Band density semi-quantification of ERK1/2 phosphorylation time-course stimulated by 10 µM 2fLIG measured as the ratio of phosphorylated ERK1/2 (pERK1/2) to total ERK1/2 (tERK1/2) over 60 minutes. Graphs show representative data of 5-6 independent experiments, presented as mean ± SEM. Statistical analysis was performed by one-way ANOVA. Significant differences from control are indicated: *P< 0.05.

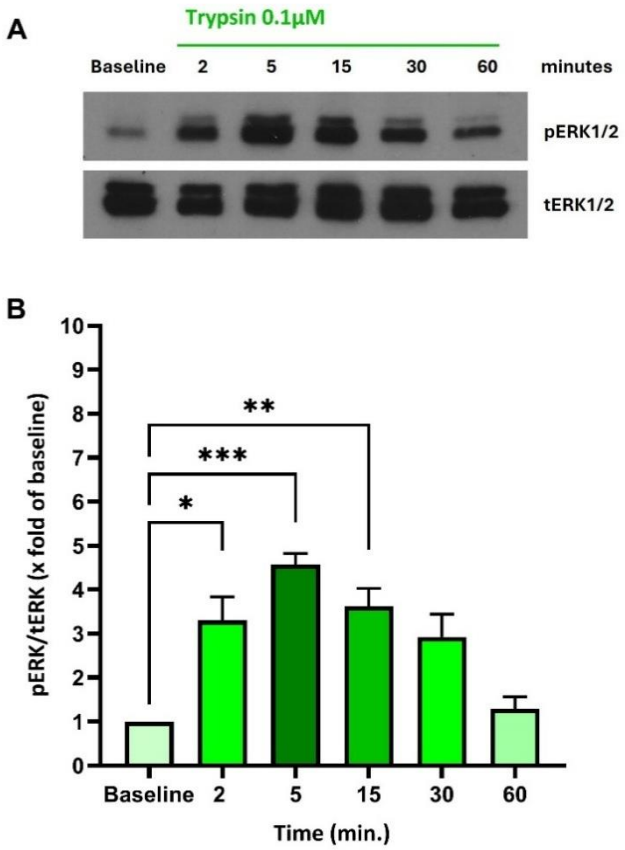

Figure 3.16: Time course of ERK1/2 of trypsin-induced phosphorylation in NCTC2544-hPAR2/NF-κB-L cells.

(A) Representative immunoblots showing pERK1/2 and tERK1/2 in whole cell lysate treated with 0.1 μM Trypsin over the indicated time points. **(B)** Band density semi-quantification of ERK1/2 phosphorylation time-course stimulated by 0.1 μM Trypsin measured as the ratio of phosphorylated ERK1/2 (pERK1/2) to total ERK1/2 (tERK1/2) over 60 minutes. Graphs show representative data of 5-6 independent experiments, presented as mean ± SEM. Statistical analysis was performed by one-way ANOVA. Significant differences from control are indicated: *P< 0.05, **P < 0.01, ***P < 0.001.

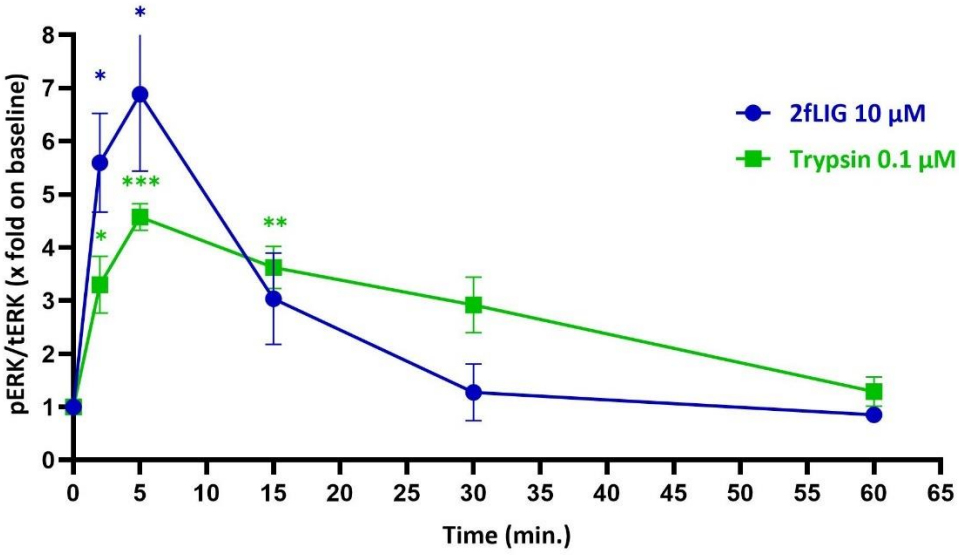

Figure 3.17: Kinetic analysis of PAR2-mediated ERK1/2 phosphorylation in NCTC2544-hPAR2/NF-κB-L cells.
Comparative time-course analysis of ERK1/2 phosphorylation between 2fLIG (blue) and trypsin (green) treatments. Each data point represents the mean of 5-6 independent experiments, presented as mean ± SEM. Statistical analysis was performed by one-way ANOVA. Significant differences from control are indicated: *P< 0.05, **P < 0.01, ***P < 0.001.

The next set of experiments assessed the concentration dependency of ERK phosphorylation following 5-minute stimulation by both agonists. As shown in Figure 3.18, 2fLIG induced a significant increase of pERK, starting from a concentration of 1 µM (3.8-fold increase ± 0.58, p = 0.02), with the highest activation observed at 30 µM (5-fold ± 0.89, p = 0.0003). Also, trypsin induced significant activation at concentrations as low as 10 nM (3.9-fold increase ± 0.55, p = 0.01), reaching a maximum activation of almost 30 nM (4.41-fold increase ± 0.65, p = 0.0023). Higher concentrations of trypsin did not further increase the response, suggesting saturation at nanomolar concentrations compared to 2fLIG (Figure 3.19).

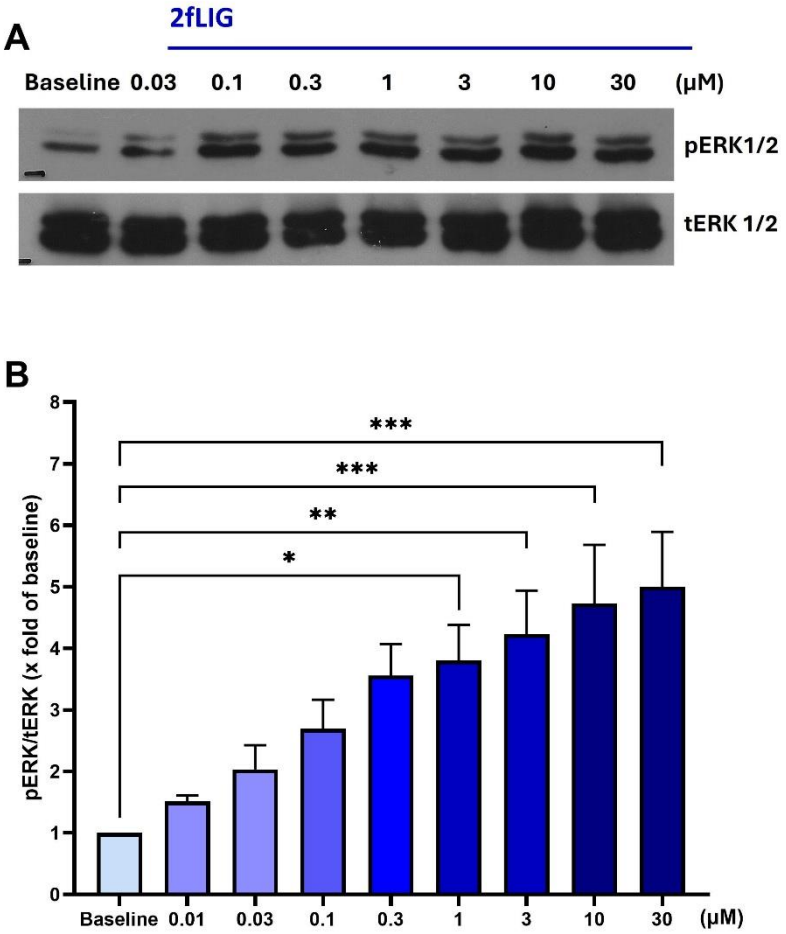

Figure 3.18: Concentration-dependent phosphorylation of ERK1/2 by 2fLIG in NCTC2544-hPAR2/NF-κB-L cells.

(A) Representative immunoblots showing pERK1/2 and tERK1/2 upon 5 minutes incubation with 2fLIG at the indicated concentrations. **(B)** Band density semi-quantification of ERK1/2 phosphorylation activated by increasing concentrations of 2fLIG (0.01 to 30 μM), measured as the ratio of phosphorylated ERK1/2 (pERK1/2) to total ERK1/2 (tERK1/2). Graphs show representative data of five independent experiments, presented as mean ± SEM. Statistical analysis was performed by one-way ANOVA. Significant differences from basal values are: *P < 0.05, **P < 0.01, ***P < 0.001.

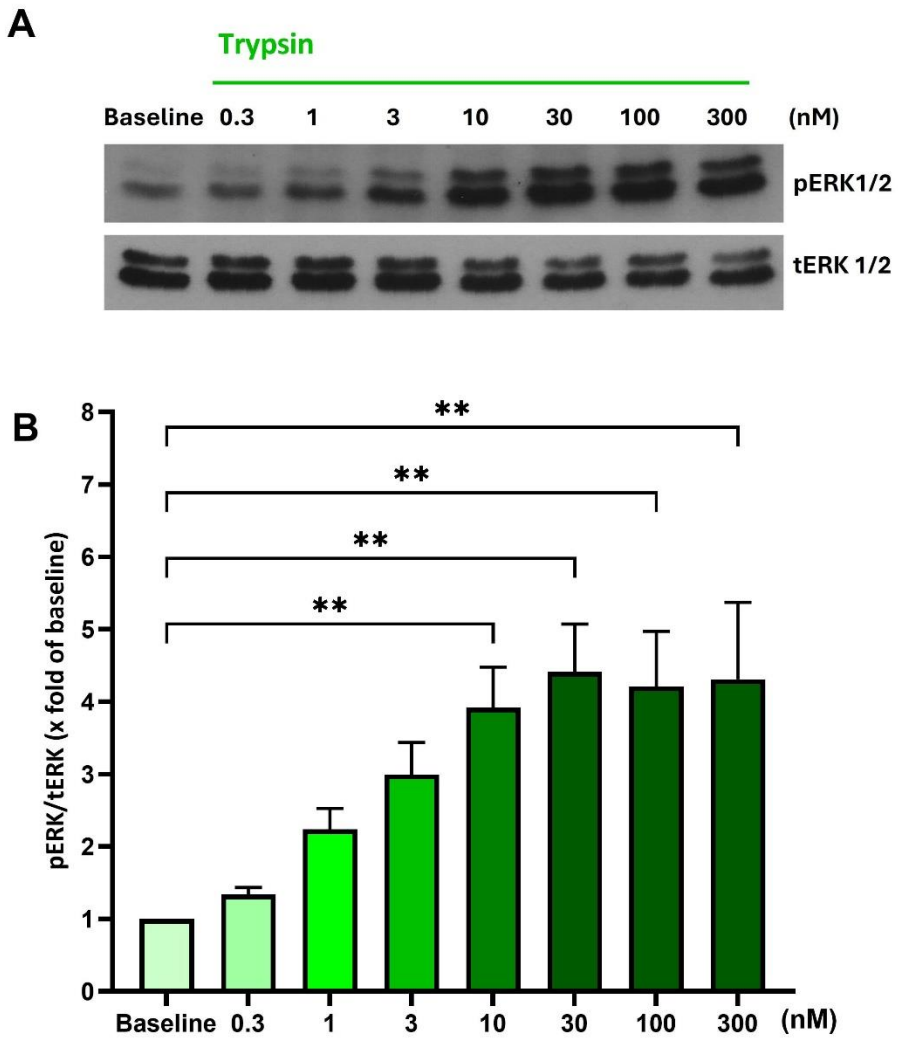

Figure 3.19: Concentration dependent phosphorylation of ERK1/2 by trypsin in NCTC2544-hPAR2/NF-κB-L cells.

(A) Representative immunoblots showing pERK1/2 and tERK1/2 upon 5 minutes incubation with trypsin at the indicated concentrations. **(B)** Band density semi-quantification of ERK1/2 phosphorylation activated by increasing concentrations of trypsin (0.3 to 300 nM), measured as the ratio of phosphorylated ERK1/2 (pERK1/2) to total ERK1/2 (tERK1/2). Graphs show representative data of five independent experiments, presented as mean ± SEM. Statistical analysis was performed by one-way ANOVA. Significant differences from basal values: *P < 0.05, **P < 0.01, ***P < 0.001.

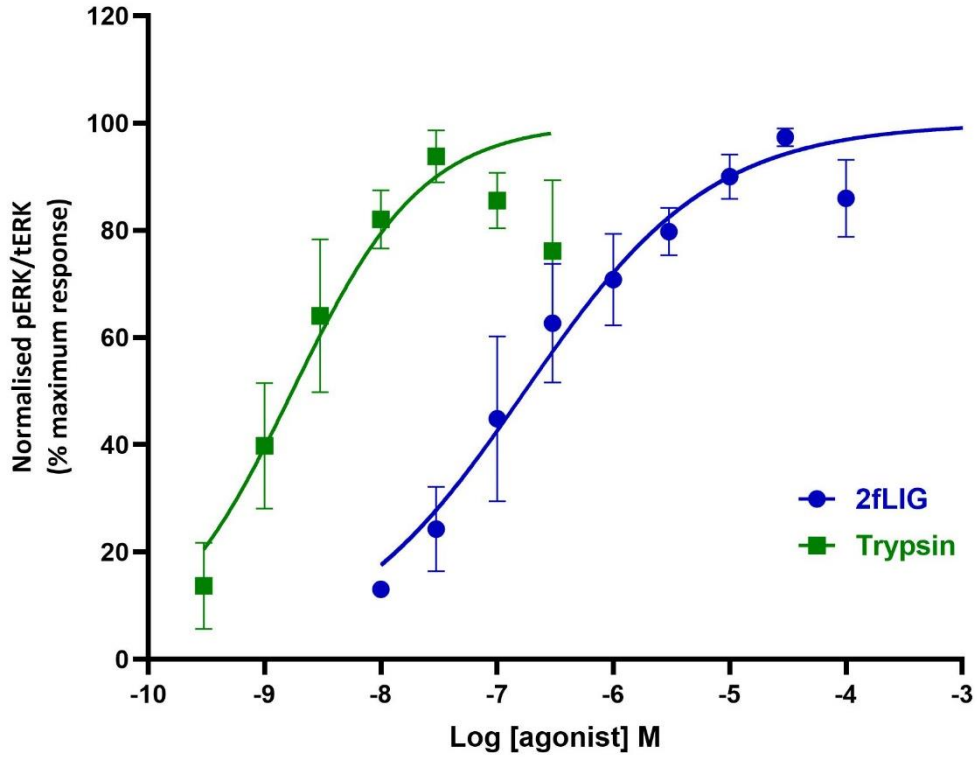

Figure 3.20: Concentration-response curves for PAR2-induced ERK1/2 phosphorylation in NCTC2544-hPAR2/NFκB-L cells.
Comparative concentration-response curves showing normalised pERK1/2 levels as a percentage of maximum response for 2fLIG (blue) and trypsin (green). The EC_{50} values for 2fLIG and trypsin are 0.1735 μM (95% CI 0.09 to 0.3) and 1.735 nM (95% CI 0.84 to 3.28), respectively. Data were fitted using the Hill equation in GraphPad Prism 10.3.1. Each data point represents the mean of five independent experiments, presented as mean ± SEM.

Comparative concentration-response curves for 2fLIG and trypsin, normalised to the maximum ERK1/2 activation are shown in Figure 3.20. The estimated EC_{50} for trypsin (1.735 nM, 50%CI: 0.84 to 3.28) is substantially lower than that for 2fLIG (0.173 μM: 50% CI: 0.09 to 0.3). For testing the AZ8838 effects on PAR2-induced phosphorylation of ERK, a concentration corresponding to the EC_{80} for both agonists were used for later experiments.

3.4.2 Effect of AZ8838 on PAR2-induced ERK phosphorylation in NCTC2544-hPAR2/NF-κB-L cells.

The effect of AZ8838 on 2fLIG- and trypsin-stimulated ERK1/2 phosphorylation in NCTC2544-hPAR2/NF-κB-L cells is shown in Figure 3.21. AZ8838 did not affect control pERK/ERK levels (Figure 3.21: fold change 0.83 ± 0.05, Figure 3.22: 1.01 ± 0.17). As examined earlier, both 0.1 μM 2fLIG and 30 nM trypsin induced a significant increase in phosphorylation of ERK (fold increase by 2fLIG: 5.6 ± 1.5; trypsin: 3.53 ± 0.6), which was not influenced significantly by the presence of the solvent, DMSO (fold increase by 2fLIG: 5.47 ± 1.25, $p > 0.99$; trypsin: 4 ± 0.8, $p = 0.98$). However, one-hour incubation of the cells with increasing concentrations of AZ8838 before stimulation with the agonists led to a concentration-dependent reduction of pERK levels. For 2fLIG, a significant inhibition was observed at AZ8838 concentrations of 10 μM (~2-fold ± 0.18, $p = 0.0147$) and 30 μM (1-fold ± 0.22, $p = 0.001$), almost to levels comparable to basal pERK levels (refer to Figure 3.21). With far less potency, AZ8838 significantly inhibited trypsin-stimulated phosphorylation of ERK only at the maximum tested concentration, that is, 30 μM (~ 1.8-fold of baseline ± 0.73, $p = 0.0161$, Figure 3.22). The concentration-response curves for the inhibition of ERK phosphorylation by AZ8838 induced by 0.1 μM 2fLIG (blue) and 30 nM trypsin (green) are shown in Figure 3.23. The IC_{50} values for AZ8838 were 9.83 μM (95% CI 6.82 to 14.6 μM) in 2fLIG-stimulated cells. The Hill curve did not fit in the case of trypsin ($r^2 = 0.48$). In contrast to 2fLIG, which produced reproducible inhibitory effects, the extent of inhibition achieved with the maximum concentration of AZ8838 varied across the four independent experiments. This could be attributed to the distinct mechanisms of PAR2 activation between these agonists.

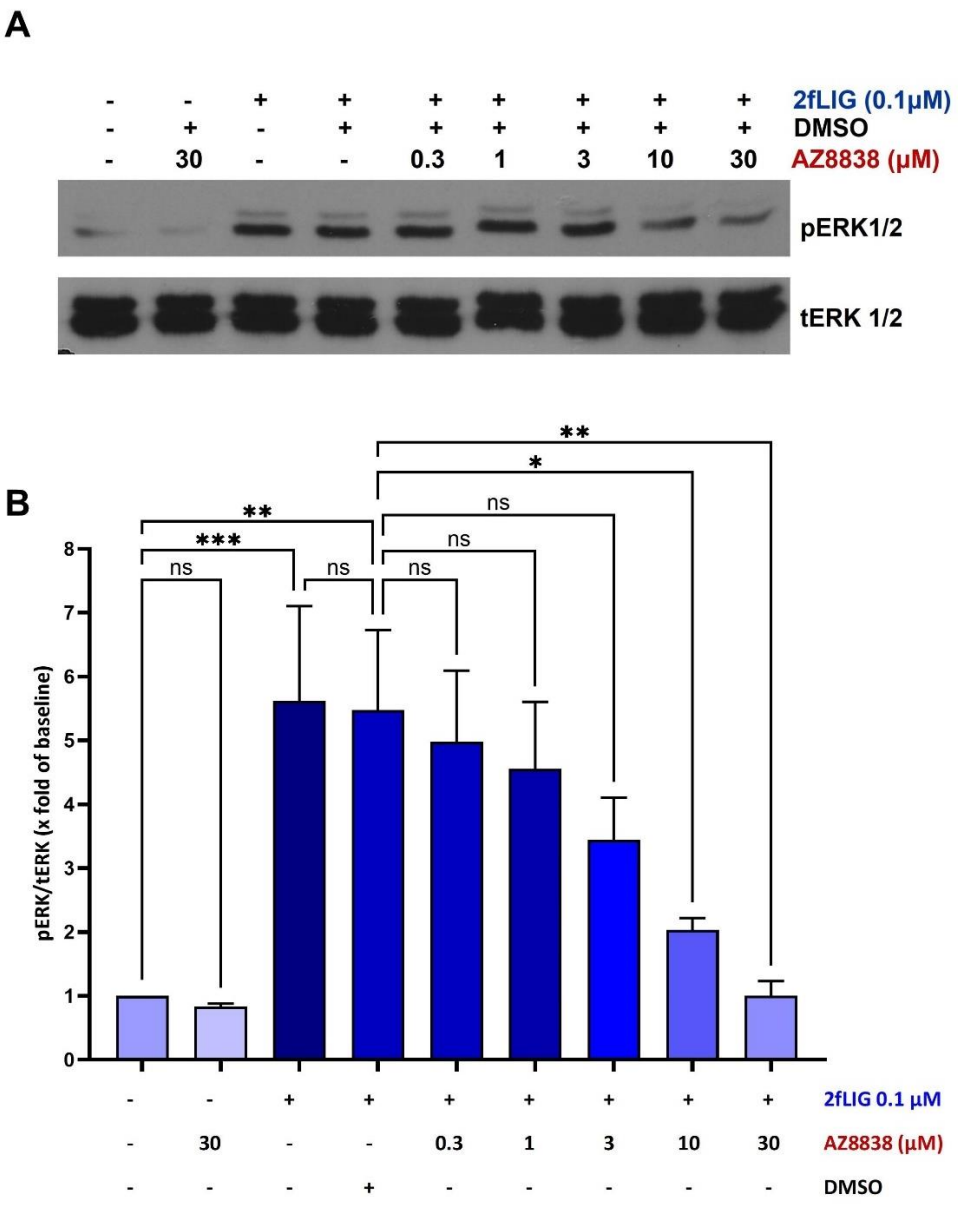

Figure 3.21: AZ8838 inhibits 2fLIG-induced ERK1/2 phosphorylation in NCTC2544-hPAR2/NF-κB-L cells.

(A) Representative immunoblots showing pERK1/2 and tERK1/2 bands upon 5-minute stimulation with 0.1µM 2fLIG in the presence of increasing concentrations of AZ8838. **(B)** Band density semi-quantification measured as the ratio of phosphorylated ERK1/2 (pERK1/2) to total ERK1/2 (tERK1/2), showing the effect of 0.1 µM 2fLIG with increasing concentrations of AZ8838 (0.3 to 30 µM) preincubated for 1hour. Graphs show representative data of four independent experiments, presented as mean ± SEM. Statistical analysis was performed using one-way ANOVA. Significant differences are indicated: *P < 0.05, **P < 0.01, ***P < 0.001. "ns" indicates no significant difference between the denoted compared data groups.

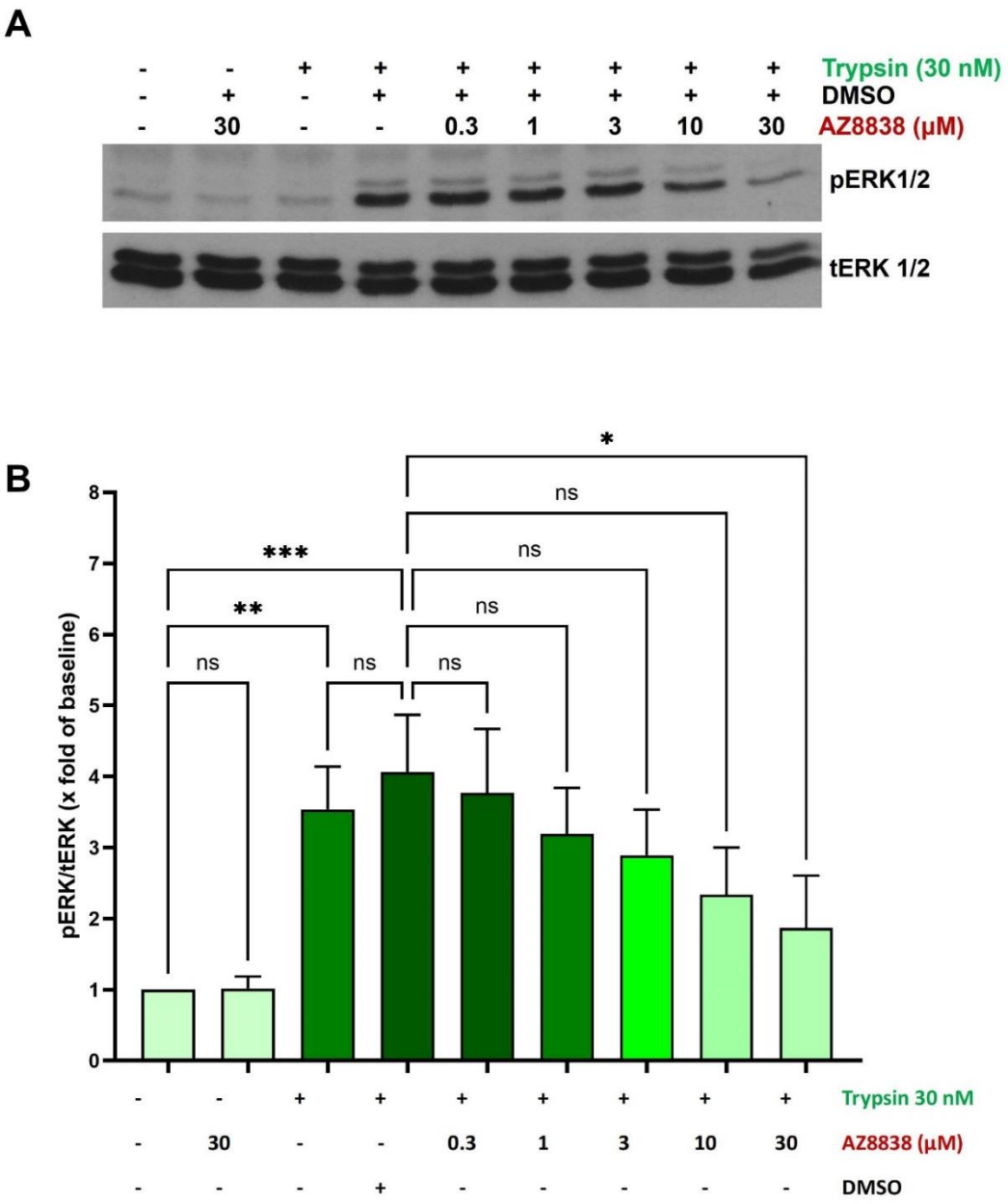

Figure 3.22: AZ8838 weakly inhibits trypsin-induced ERK1/2 phosphorylation in NCTC2544-hPAR2/NF-κB-L cells.

(A) Representative immunoblots showing pERK1/2 and tERK1/2 bands upon 5-minute stimulation with 30 nM trypsin in the presence of increasing concentrations of AZ8838. **(B)** Band density semi-quantification measured as the ratio of phosphorylated ERK1/2 (pERK1/2) to total ERK1/2 (tERK1/2) showing the effect of 30 nM trypsin with increasing concentrations of AZ8838 (0.3 to 30 µM) preincubated for 1hour. Graphs show representative data of four independent experiments, presented as mean ± SEM. Statistical analysis has been performed by one-way ANOVA. Significant differences are indicated: *P < 0.05, **P < 0.01, ***P < 0.001. "ns" indicates no significant difference between the denoted compared data groups.

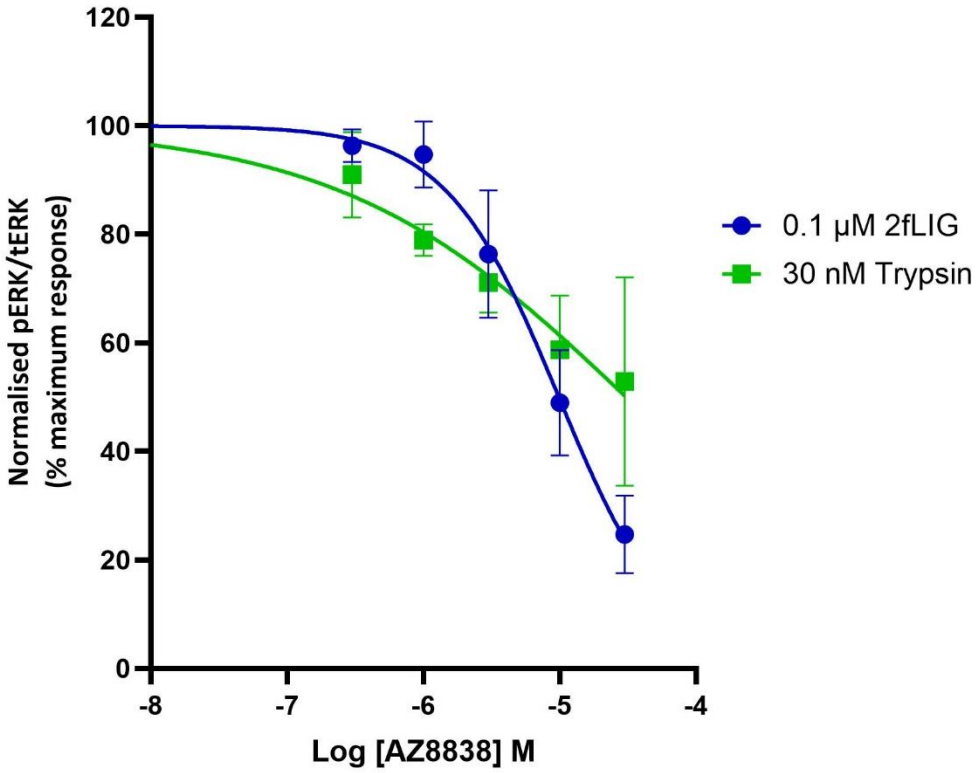

Figure 3.23: Concentration-response curves of AZ8838 against 2fLIG- and trypsin-induced ERK1/2 phosphorylation in NCTC2544-hPAR2/NF-κB-L cells.
Concentration-response curves showing normalised pERK1/2 levels as a percentage of maximum response for 2fLIG (blue) and trypsin (green) in the presence of varying concentrations of AZ8838. The estimated IC_{50} value for AZ8838 was 9.83 µM (95% CI 6.82 to 14.6) for 2fLIG. Data were fitted using the Hill equation in GraphPad Prism 10.3.1. Each data point represents the mean of four independent experiments, presented as mean ± SEM.

3.4.3 Effects of trypsin and 2fLIG on ERK phosphorylation in DU145 cells.

To determine if the variable effects of AZ8838 were a feature linked to ERK activation, the same experiments were conducted to test the effects of AZ8838 in a different cell type, DU145. This cell line is a prostate cancer cell line with epithelial morphology (Gingrich et al., 1991). It was selected to correlate with a later *in vivo* experimental prostate inflammatory model (see chapter 2, section 2.5).

Examining the dynamics of PAR2-mediated ERK1/2 phosphorylation in response to 2fLIG and trypsin in DU145, results are shown in Figure 3.24, Figure 3.25 and Figure

3.26. Similar to NCTC2544-hPAR2/NF-κB-L cells, 10 μM 2fLIG induced a rapid transient phosphorylation of ERK that reached maximum following 2-minute exposure to the agonist (4.8-fold increase over baseline ± 0.31, p = 0.0009, Figure 3.24). Phosphorylation levels rapidly declined to ~2-fold by 15 minutes, then to near-baseline levels by 60 minutes (fold increase 0.88 ± 0.16). Similarly, 0.1 μM trypsin (Figure 3.25) stimulated phosphorylation of ERK significantly, which reached a maximum of ~7-fold of basal values (mean value of 6.72 ± 1, p = 0.015) at 5 minutes exposure. Relatively, the decline in levels of ERK phosphorylation following trypsin stimulation was more gradual, compared to 2fLIG, and remained higher than basal values at 60 minutes (mean fold 1.77 ± 0.26). For subsequent experiments, 3 minutes was employed for 2fLIG, and 5 minutes for trypsin to capture the maximal pERK response.

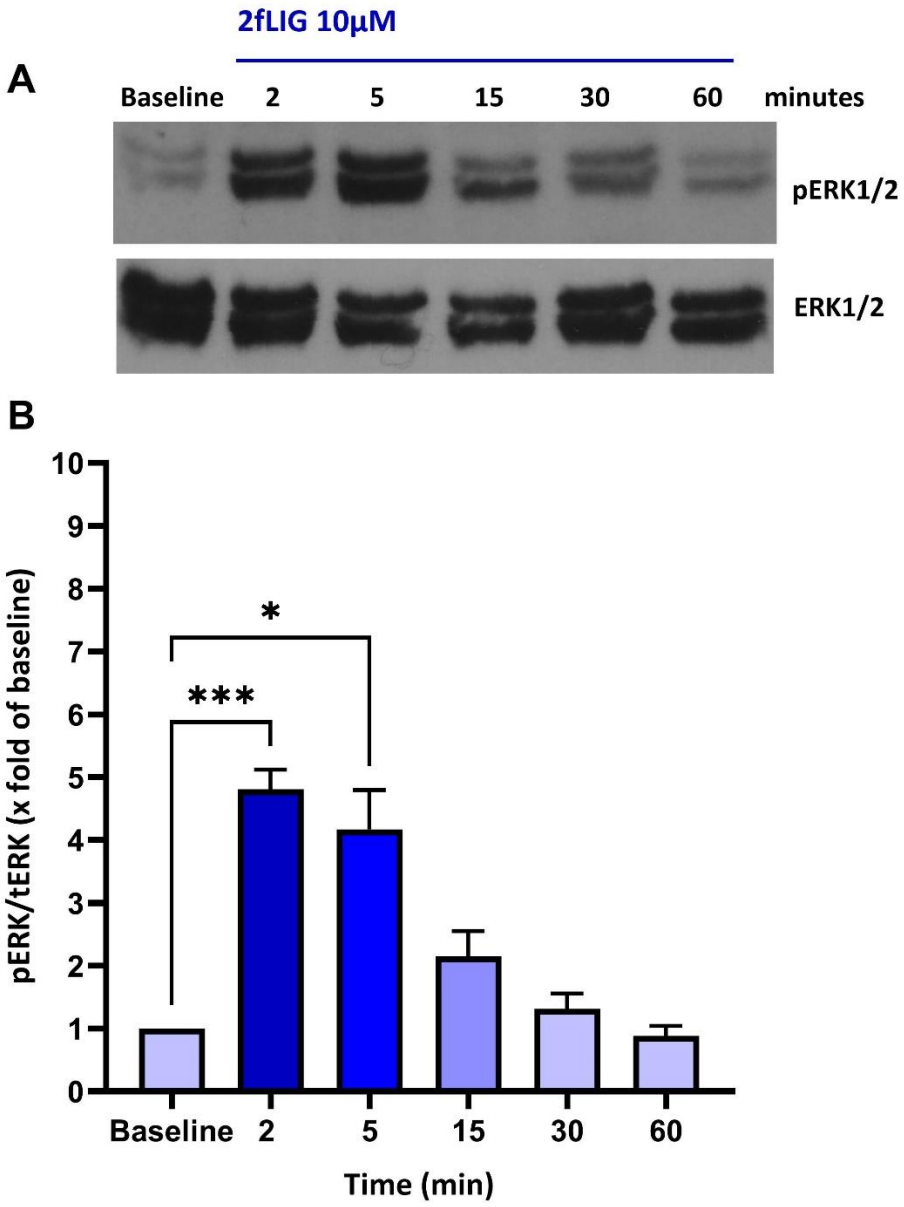

Figure 3.24: Time course of 2fLIG-stimulated ERK1/2 phosphorylation in DU145 cells
(A) Representative immunoblots showing pERK1/2 and tERK1/2 bands in whole cell lysate treated with 10 µM 2fLIG over the indicated time points. **(B)** Band semi-density quantification measured as the ratio of phosphorylated ERK1/2 (pERK1/2) to total ERK1/2 (tERK1/2). Graphs show representative data of 5 independent experiments, presented as mean ± SEM. Statistical analysis was performed using one-way ANOVA. Significant differences from baseline are indicated: *P< 0.05, **P < 0.01, ***P < 0.001.

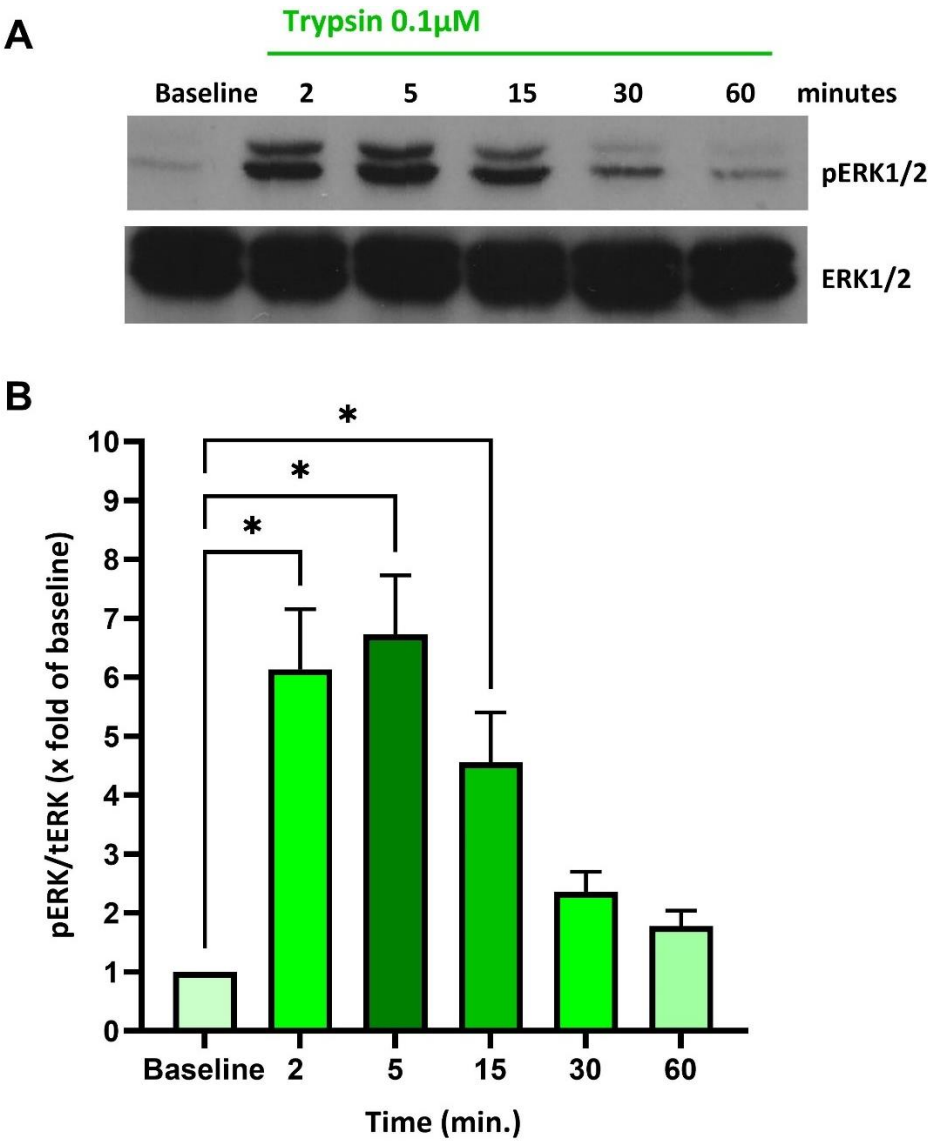

Figure 3.25: Time course of trypsin-stimulated ERK1/2 phosphorylation in DU145 cells **(A)** Representative immunoblots showing pERK1/2 and tERK1/2 bands in whole cell lysate treated with 0.1 µM trypsin over the indicated time points. **(B)** Band density semi-quantification measured as the ratio of phosphorylated ERK1/2 (pERK1/2) to total ERK1/2 (tERK1/2). Graphs show representative data of 5 independent experiments, presented as mean ± SEM. Statistical analysis was performed using one-way ANOVA. Significant differences from baseline are indicated: *P< 0.05.

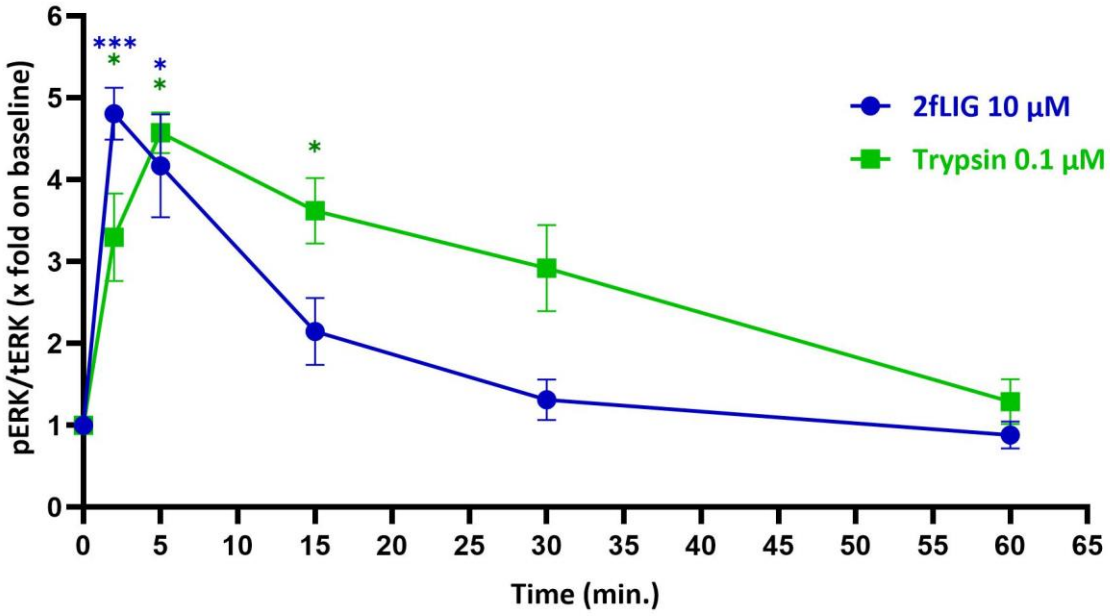

Figure 3.26: Kinetics of 2fLIG- and trypsin-stimulated ERK1/2 phosphorylation in DU145 cells
Comparative time-course analysis of ERK1/2 phosphorylation between 2fLIG (blue) and trypsin (green) treatments. Each data point represents the mean of 5 independent experiments, presented as mean ± SEM. Statistical analysis was performed using a two-way ANOVA. Significant differences from basal values are indicated: (*P< 0.05, **P < 0.01, ***P < 0.001).

Testing the concentration effect, both agonists displayed a concentration-dependent increase in pERK levels at the selected exposure times. Representative Western blots for pERK1/2 and tERK1/2 levels in DU145 cells treated with different concentrations (as indicated) of 2fLIG and trypsin are presented in Figure 3.27A and Figure 3.28A. Treatment with increasing concentrations of 2fLIG gradually stimulated a significant increase in pERK1/2 levels, normalised to tERK1/2, starting at a concentration of 1 µM (mean fold increase 6.85 ± 2, p = 0.031) and continuing to increase until the maximum tested concentration of 100 µM (mean fold increase 8.22 ± 3.1, p = 0.0054). This indicates a robust concentration-dependent stimulation of ERK1/2 by 2fLIG, with saturation occurring almost at 10 µM (Figure 3.27). Likewise, trypsin induced a concentration-dependent increase in pERK levels, showing a significant rise at 30 nM (4.17 ± 0.52, p = 0.0009) and reaching a peak at the maximum tested concentration of

300 nM (10.12 ± 2.52, $p < 0.0001$), as shown in Figure 3.28. Comparatively, trypsin stimulated a more potent activation of ERK, with an estimated EC_{50} value of 13.8 nM (95% CI 11.4 to 16.8), compared to 0.167 µM (95% CI 0.09 to 0.28) for 2fLIG. For testing the effects of AZ8838 on PAR2-mediated phosphorylation of ERK in these cell lines, a concentration around the EC_{75} for both agonists was used in later experiments.

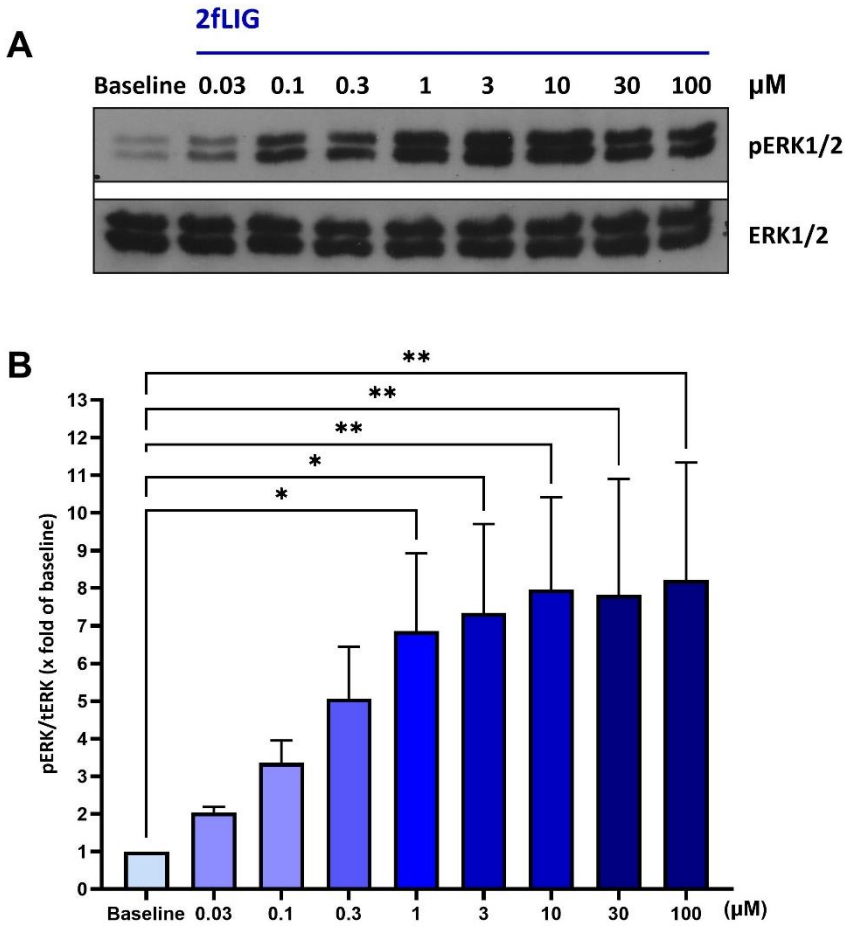

Figure 3.27: Concentration-dependent 2fLIG-stimulated ERK1/2 phosphorylation in DU145 cells.

(A) Representative immunoblots showing pERK1/2 and tERK1/2 bands upon 3 minutes stimulation with 2fLIG at the indicated concentrations. **(B)** Band density semi-quantification measured as the ratio of phosphorylated ERK1/2 (pERK1/2) to total ERK1/2 (tERK1/2). Graphs show representative data of 5 independent experiments, presented as mean ± SEM. Statistical analysis was performed using a two-way ANOVA. Significant differences from baseline are indicated: *P < 0.05, **P < 0.01.

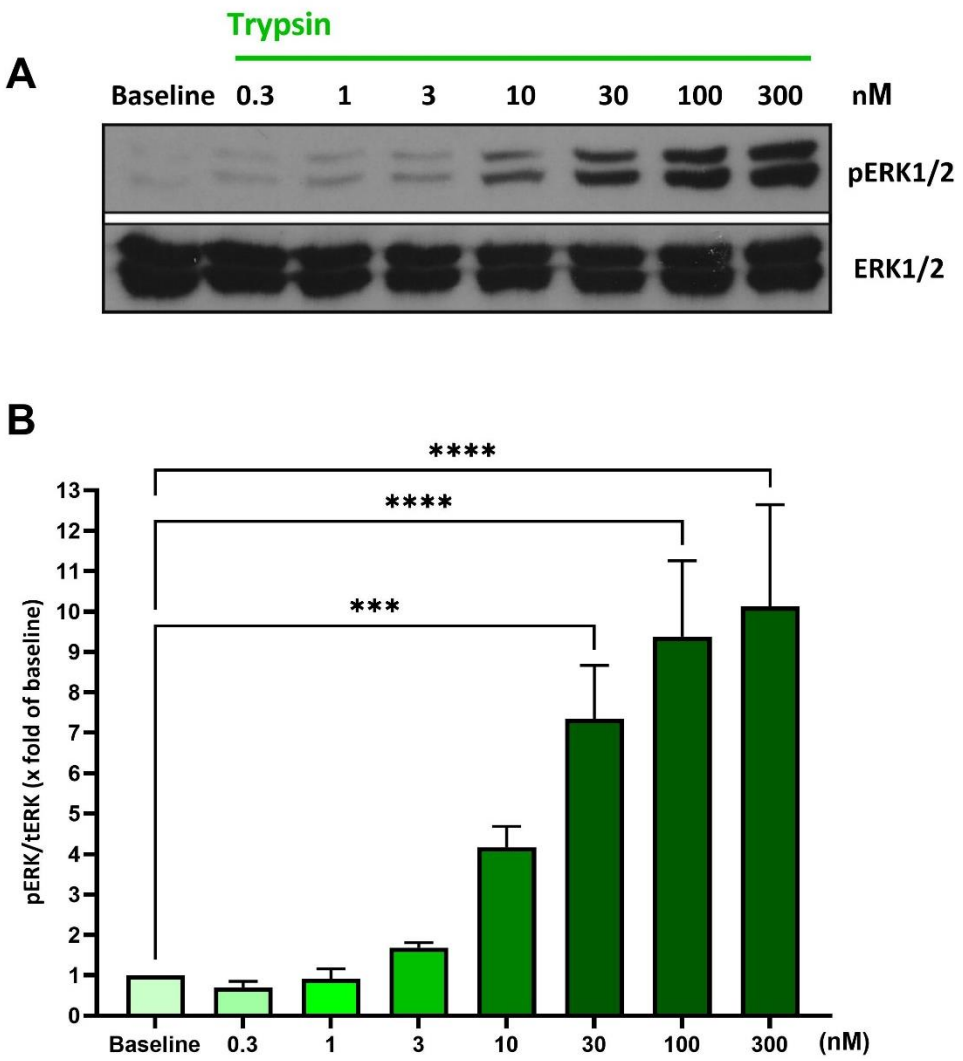

Figure 3.28: Concentration-dependent trypsin-stimulated ERK1/2 phosphorylation in DU145 cells.

(A) Representative immunoblots showing pERK1/2 and tERK1/2 levels upon 5 minutes incubation with trypsin at the indicated concentrations. **(B)** Band density quantification measured as the ratio of phosphorylated ERK1/2 (pERK1/2) to total ERK1/2 (tERK1/2). Graphs show representative data of 5 independent experiments, presented as mean ± SEM. Statistical analysis was performed using a two-way ANOVA. Significant differences from baseline are indicated: ***P < 0.001, ****P < 0.0001.

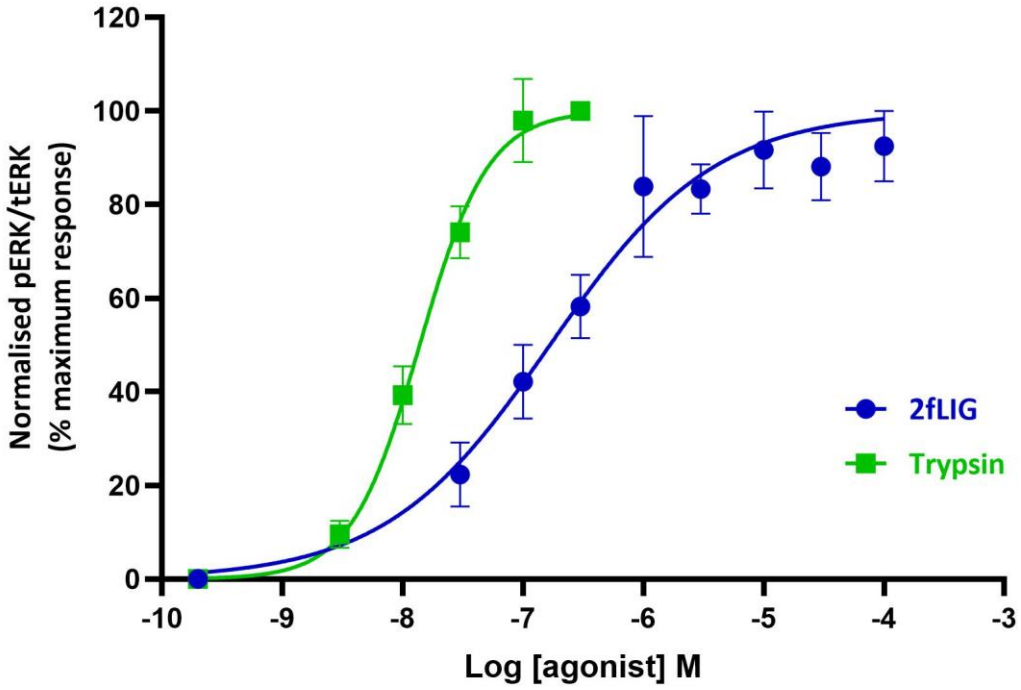

Figure 3.29: Comparative concentration-response curves for ERK1/2 phosphorylation by PAR2 agonists in DU145 cells.
Comparative concentration-response curves showing normalised pERK1/2 levels as a percentage of maximum response for 2fLIG (blue) and trypsin (green). The EC_{50} values for 2fLIG and trypsin were 0.167 µM (95% CI 0.09 to 0.28) and 13.8 nM (95% CI 11.4 to 16.8), respectively. Data were fitted using the Hill equation in GraphPad Prism 10.3.1. Graphs show the mean of 5 independent experiments, presented as mean ± SEM.

3.4.4 Effect of AZ8838 trypsin- and 2fLIG-induced ERK phosphorylation in DU145 cells.

As with NCTC2544-hPAR2/NF-κB-L cells, the effect of increasing concentrations of AZ8838 in the presence of 2fLIG and trypsin was tested in DU145. As observed previously, AZ8838 did not significantly impact control (baseline) pERK/ERK levels (Figure 3.30: fold change 1.37 ± 0.46, $p > 0.99$; Figure 3.31: 0.8 ± 0.14, $p > 0.99$). In addition, both 0.3 µM 2fLIG and 30 nM trypsin activated a significant increase in ERK phosphorylation (2fLIG: 3.64 ± 1, $p = 0.0006$; trypsin: 15 ± 3, $p = 0.0004$), which was not affected by DMSO (mean fold-increase 2fLIG: 4.07 ± 1.4, $p > 0.99$; trypsin: 15.13 ± 4, $p > 0.99$).

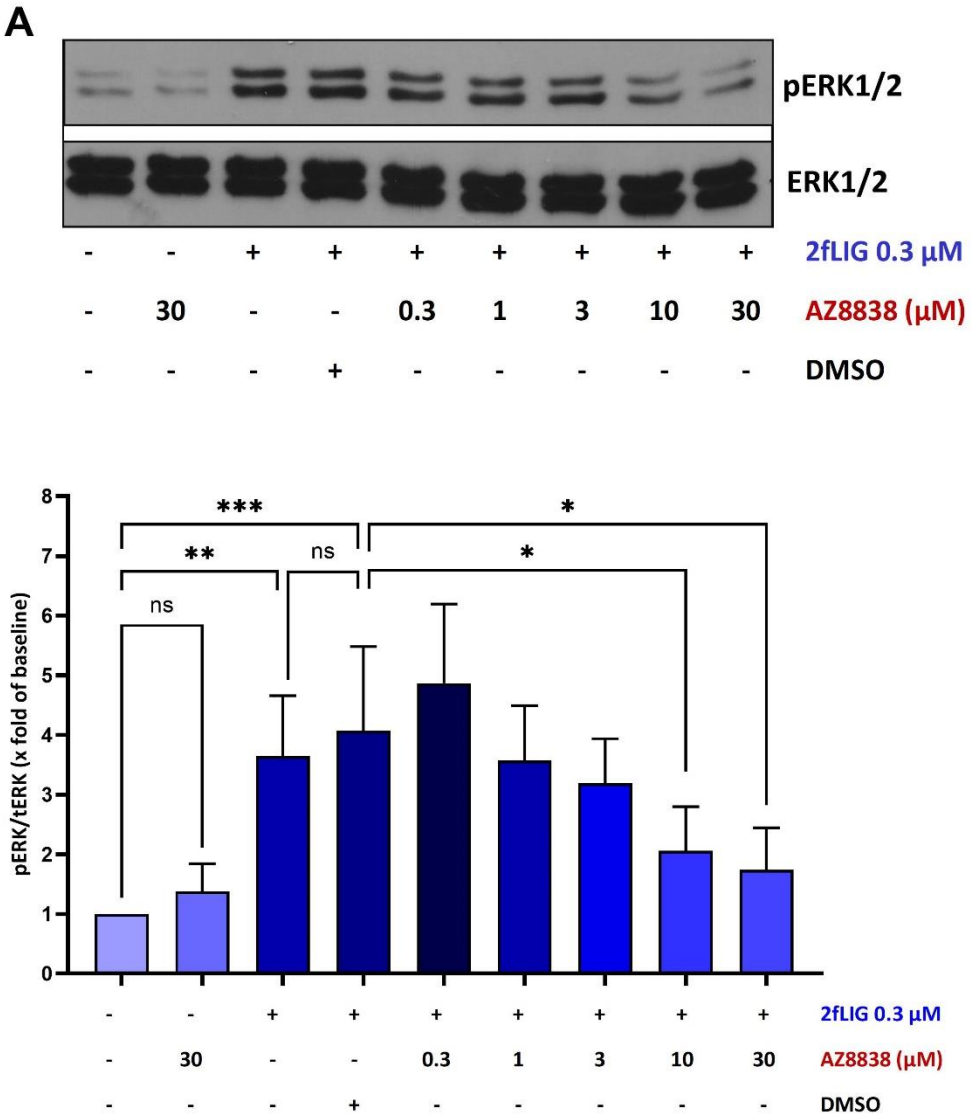

Figure 3.30: AZ8838 inhibits 2fLIG-induced ERK1/2 phosphorylation in DU145 cells.
(A) Representative immunoblots showing pERK1/2 and tERK1/2 bands following 3-minute stimulation with 0.3 µM 2fLIG in the presence of increasing concentrations of AZ8838. **(B)** Band density semi-quantification of ERK1/2 phosphorylation under the same conditions. Graphs show representative data of four independent experiments, presented as mean ± SEM. Statistical analysis was performed using a two-way ANOVA. Significant differences are indicated: *P < 0.05, **P < 0.01, ***P < 0.001. "ns" indicates no significant difference between the denoted compared data groups.

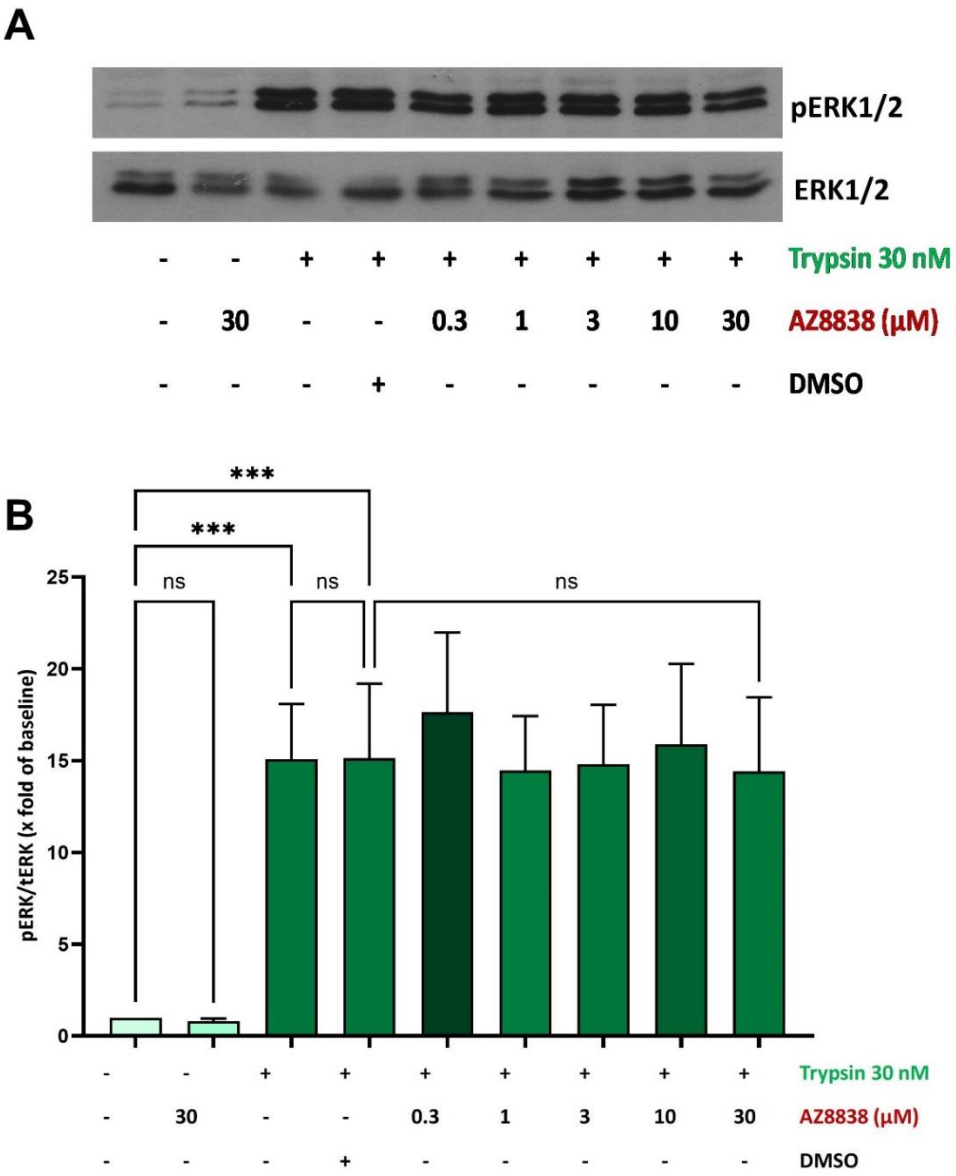

Figure 3.31: AZ8838 does not alter trypsin-induced ERK1/2 phosphorylation in DU145 cells. (**A**) Representative immunoblots showing pERK1/2 and tERK1/2 bands upon 5-minute stimulation with 30 nM trypsin in the presence of increasing concentrations of AZ8838. (**B**) Band density semi-quantification of ERK1/2 phosphorylation under the same conditions. Graphs show representative data of five independent experiments, presented as mean ± SEM. Statistical analysis was performed using a two-way ANOVA. Significant differences from baseline are indicated: ***P < 0.001. "ns" indicates no significant difference between the denoted compared data groups.

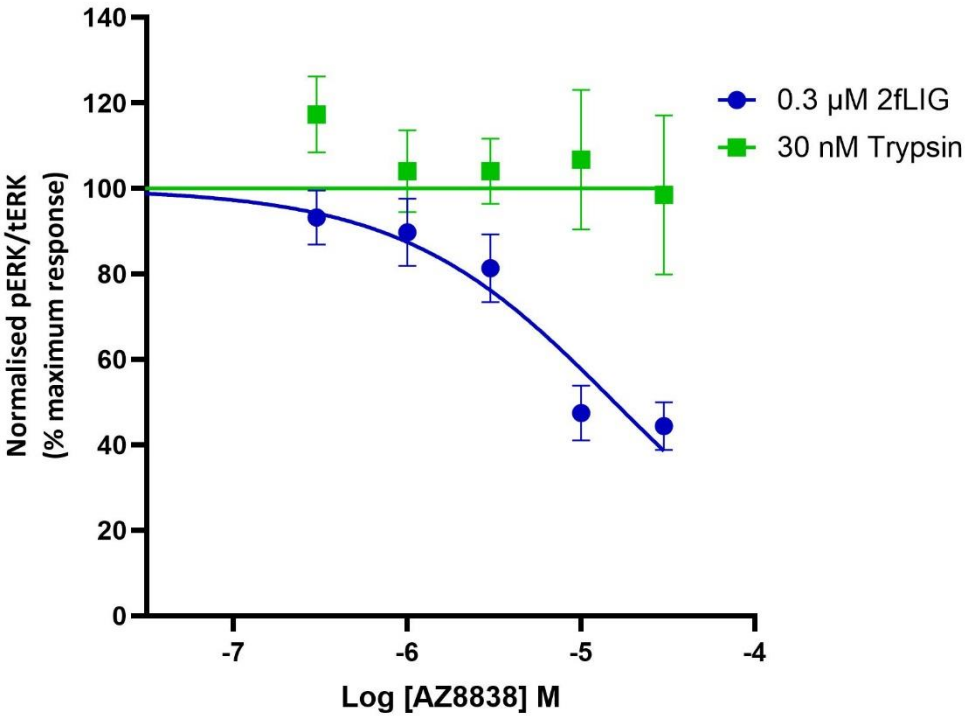

Figure 3.32: AZ8838 selectively inhibits 2fLIG-induced ERK1/2 phosphorylation in DU145 cells. Concentration-response curves showing normalised pERK1/2 levels as a percentage of maximum response for 2fLIG (blue) and trypsin (green) in the presence of varying concentrations of AZ8838. The estimated IC_{50} value for AZ8838 was 15.54 µM (95% CI 9.8 to 29.74) for 2fLIG. Data were fitted using the Hill equation in GraphPad Prism 10.3.1. Each data point represents the mean of 4-5 independent experiments, presented as mean ± SEM.

Pretreatment of DU145 cells for one hour with AZ8838 significantly inhibits 2fLIG-induced phosphorylation of ERK at concentrations of 10 µM (mean fold 2 ± 0.74, p = 0.0456) and 30 µM (mean fold 1.7 ± 0.7, p = 0.0132) by approximately 50% and 60% of maximal stimulation, respectively (Figure 3.30). Interestingly, AZ8838 did not inhibit trypsin-induced phosphorylation at all tested concentrations (Figure 3.31). Even at the maximum concentration, 30 µM, the fold increase in pERK levels was not affected by AZ8838 (mean fold, 14.42 ± 4). This is confirmed in the concentration-response curves for both agonists in the presence of AZ8838 (Figure 3.32). Trypsin data generated almost a flat curve, 2fLIG data could be fitted into a sigmoid concentration response curve (r^2= 0.7). The estimated IC_{50} value for AZ8838 in 2fLIG-treated DU145 cells was 15.54 µM (95% CI 9.8 to 29.74).

3.5 Effect of AZ8838 on PAR2-induced intracellular calcium mobilisation.

Like most of protease-activated receptors, stimulation of PAR2 is well-established to induce a surge in intracellular calcium levels. This is mediated through the coupling of PAR2 to $G\alpha_{q/11}$ proteins, which subsequently activate PLC, leading to the production of IP3 and the release of calcium from intracellular endoplasmic stores (Bohm et al., 1996a, Macfarlane et al., 2001, Chandrabalan and Ramachandran, 2021). In the upcoming section, the effects of AZ8838 (McGuire et al., 2004) on 2fLIG- and trypsin-stimulated intracellular calcium mobilisation (section2.6, Chapter 2) was examined. Human embryonic kidney cells (HEK293) were utilised, which naturally express PAR2.

3.5.1 Effects of 2fLIG and trypsin on intracellular calcium mobilisation.

Initially, the real-time dynamic changes of increasing concentrations of 2fLIG and trypsin on the levels of intracellular calcium were examined. According to the protocol, agonists are introduced at the 20-second mark from the start of recording. As shown in Figure 3.33A and Figure 3.34A, the peak relative fluorescence units (RFU) were reached within 30-40 seconds for both agonists. This indicated a sharp increase in intracellular calcium levels, peaking within 10 to 20 seconds after initial exposure to the agonists. Following peak response, 2fLIG and trypsin exhibited a gradual and slow decline in calcium levels, without returning to baseline RFU levels within the 120-second recording duration. Regarding the concentration effect, all panels in Figure 3.33 and Figure 3.34 display a concentration-dependent enhancement of intracellular calcium levels induced by 2fLIG and trypsin. As shown in Figure 3.33B, normalised peak RFU values to baseline (F_{max}/F_0) start to significantly differ from control (HBSS

treated wells) at 1 μM 2fLIG concentration (F_{max}/F_0: 2.12 ± 0.33, p = 0.0144) and continue to rise until the maximum concentration tested, 20 μM (F_{max}/F_0: 2.82 ± 0.34, p < 0.0001). Similarly, trypsin begins to display a significant increase in F_{max}/F_0 values at 1nM (2.03 ± 0.18, p = 0.0116), continuing up to the highest tested concentration of 100 nM (2.95 ± 0.25, p < 0.0001) (Figure 3.34B). Figure 3.35 illustrates the concentration-response curves for calcium response induced by 2fLIG and trypsin, normalised to the maximum response of each agonist. Using the Hill equation, the estimated EC_{50} value for trypsin, 1.22 nM (95% CI: 0.95 to 1.54), is significantly lower than that for 2fLIG, 0.54 μM (95% CI: 0.38 to 0.75). For testing the effect of AZ8838 on PAR2-mediated calcium flux, 2fLIG was used at a concentration slightly more than the estimated EC_{80} value.

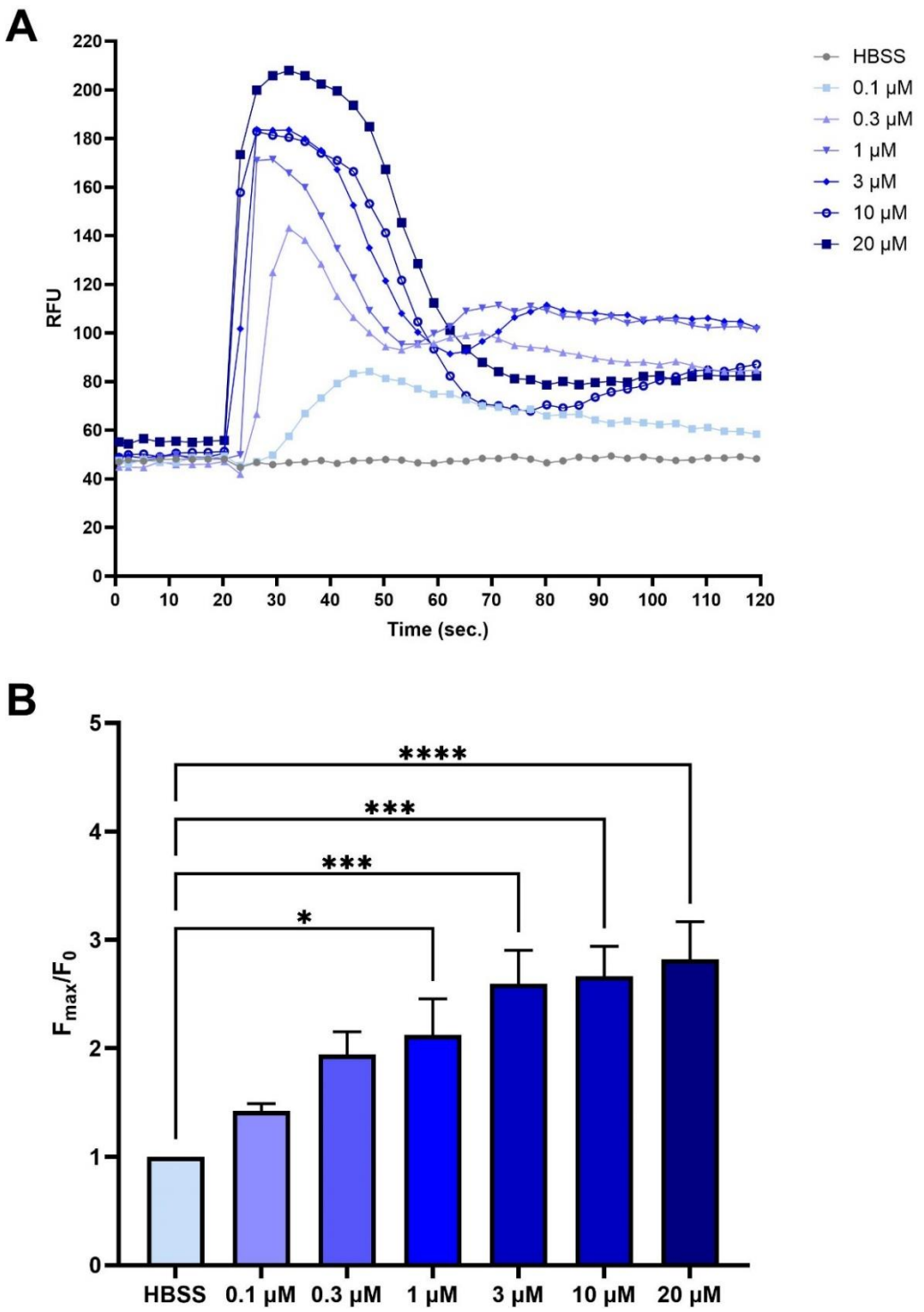

Figure 3.33: Concentration-dependent 2fLIG-stimulated intracellular Ca^{2+} mobilisation in HEK293 cells.

(A) Representative temporal profile of calcium flux in HEK293 cells treated with increasing concentrations of 2fLIG (0.1 to 20 µM), measured every three seconds over a period of 120 seconds. Agonists were added at 20 seconds. **(B)** Normalised peak RFU value to baseline (F_{max}/F_0) for calcium response induced by the tested concentrations of 2fLIG. The graph shows representative data of three independent experiments, presented as mean ± SEM. Statistical analysis was performed using a two-way ANOVA. Significant differences from baseline are indicated: *P < 0.05, **P < 0.01, ***P < 0.001, ****P < 0.0001.

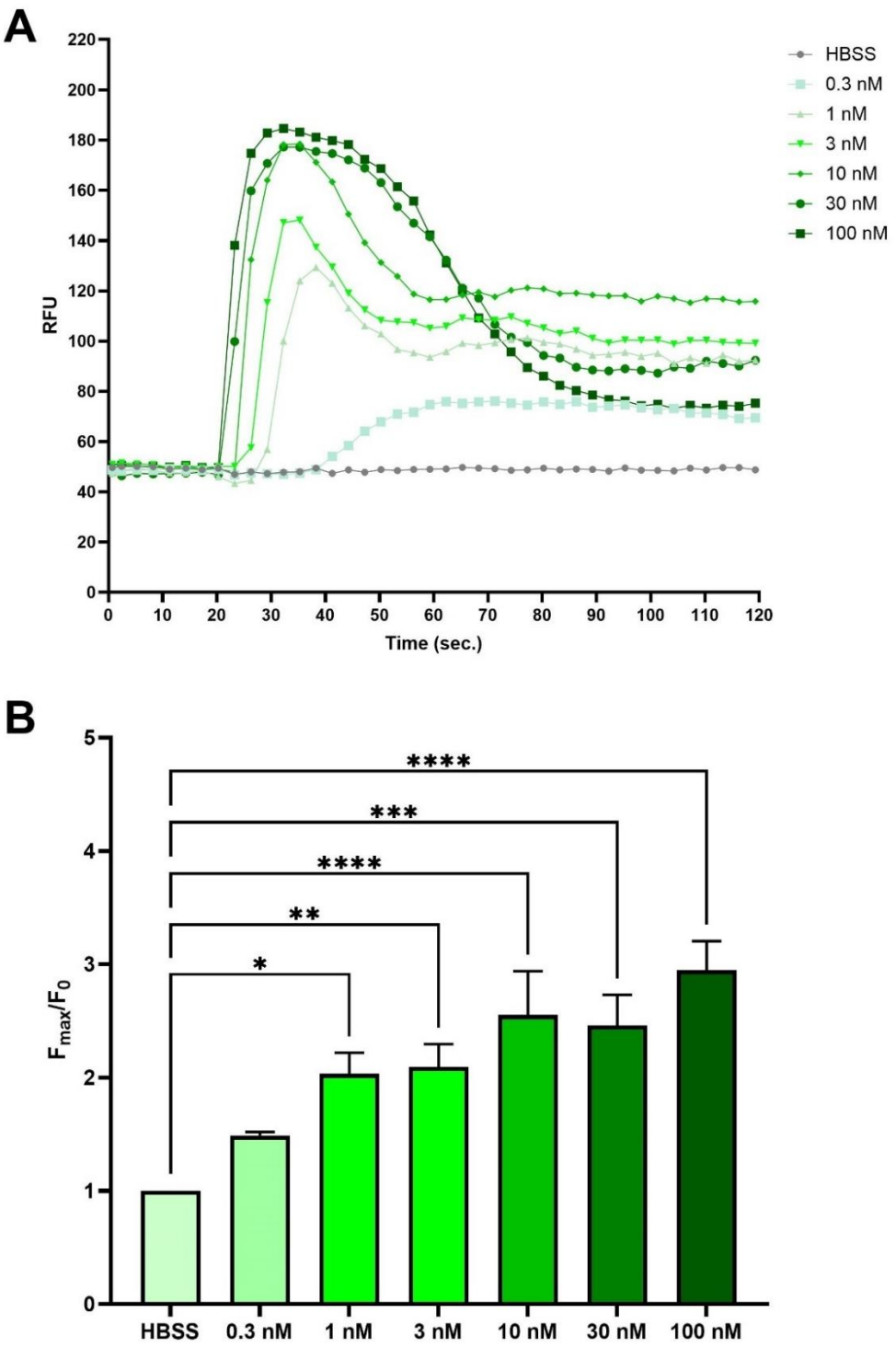

Figure 3.34: Concentration-dependent trypsin-stimulated intracellular Ca^{2+} mobilisation in HEK293 cells.

(A) Representative temporal profile of calcium flux in HEK293 cells treated with increasing concentrations of trypsin (0.3 nM to 100 nM), measured every three seconds over a period of 120 seconds. Agonists were added at 20 seconds. **(B)** Normalised peak RFU value to baseline (Fmax/F0) for calcium response induced by the tested concentrations of trypsin. The graph shows representative data of three independent experiments, presented as mean ± SEM. Statistical analysis was performed using a two-way ANOVA. Significant differences from baseline are indicated: *P < 0.05, **P < 0.01, ***P < 0.001, ****P < 0.0001.

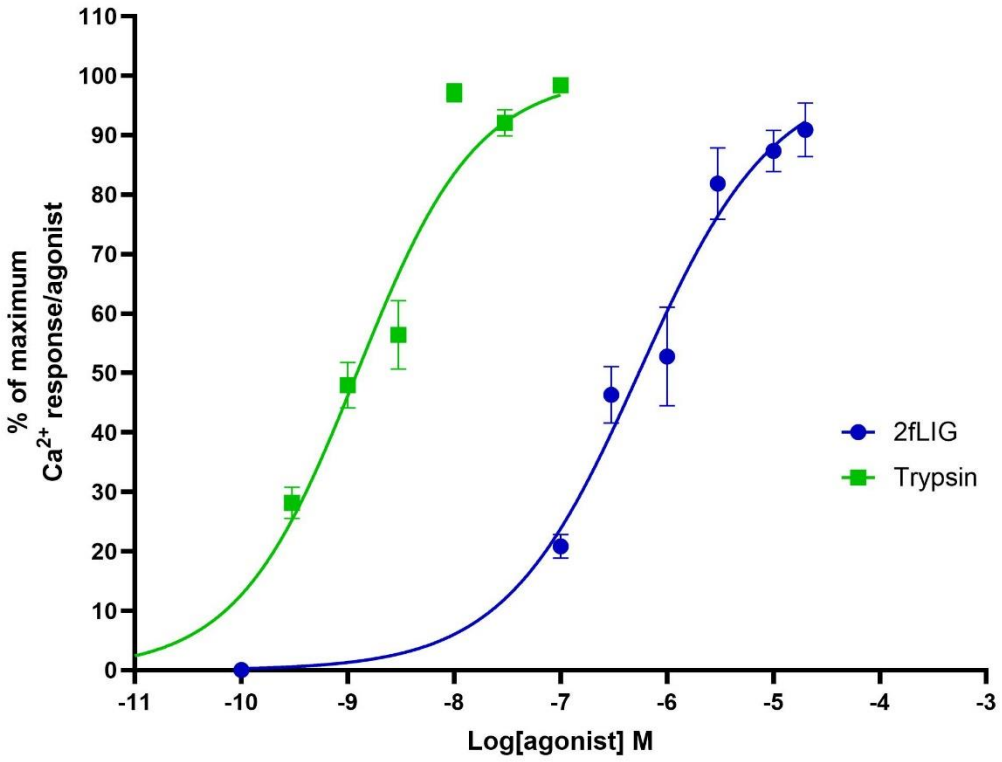

Figure 3.35: Comparative concentration-response curves for 2fLIG- and trypsin-stimulated intracellular Ca^{2+} mobilisation in HEK293.
Concentration-response curves showing the percentage of maximum calcium response for 2fLIG (blue) and trypsin (green). The EC_{50} values for 2fLIG and trypsin were 0.54 µM (95% CI: 0.38 to 0.75) and 1.22 nM (95%CI: 0.95 to 1.54), respectively. Data were fitted using the Hill equation in GraphPad Prism 10.3.1. Each data point represents the mean of three independent experiments, presented as mean ± SEM.

3.5.2 Effect of AZ8838 on 2fLIG-induced intracellular Ca^{2+} mobilisation.

In this experiment, the effect of one-hour pre-incubation of HEK293 with increasing concentrations of AZ8838 on the 2fLIG-triggered calcium response was examined (see, Figure 3.36).

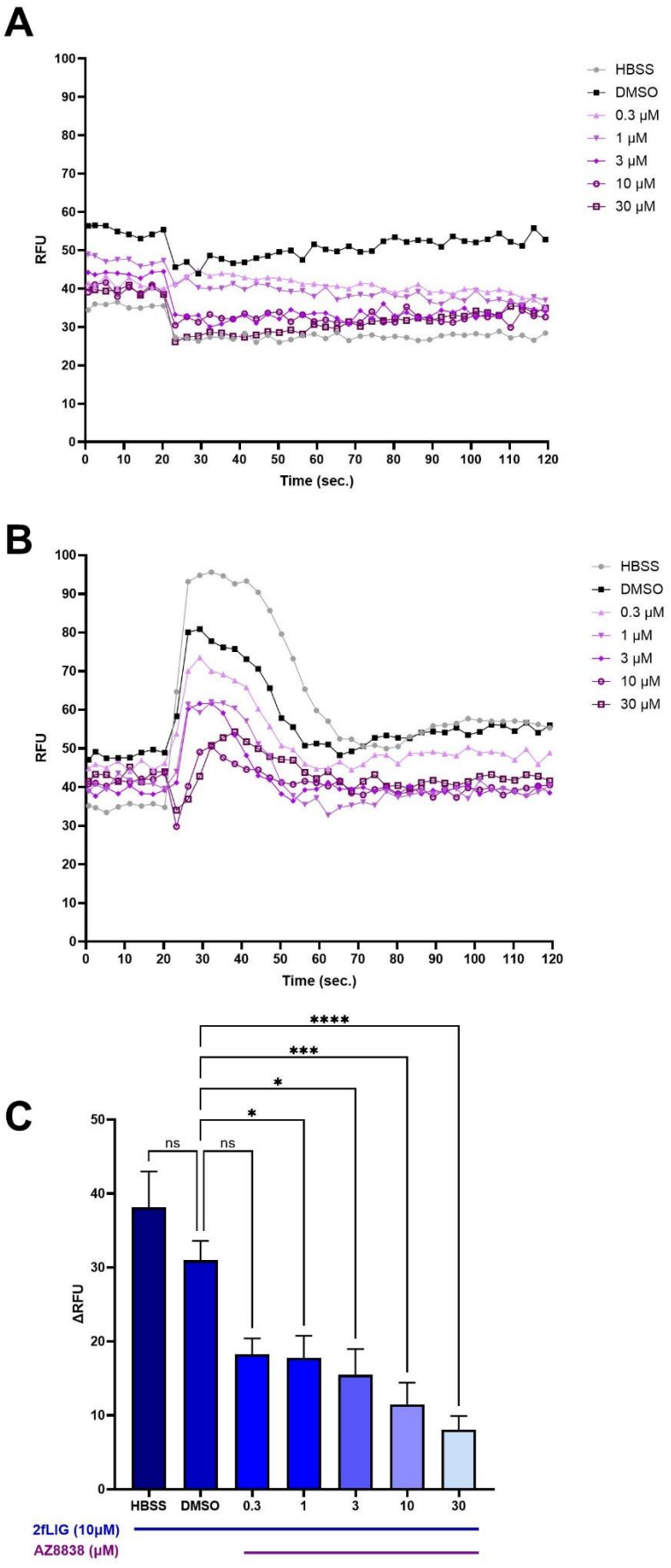
A
RFU
Time (sec.)
HBSS
DMSO
0.3 μM
1 μM
3 μM
10 μM
30 μM
B
RFU
Time (sec.)
HBSS
DMSO
0.3 μM
1 μM
3 μM
10 μM
30 μM
C
ΔRFU
****
***
*
*
ns
ns
HBSS
DMSO
0.3
1
3
10
30
2fLIG (10μM)
AZ8838 (μM)

Figure 3.36: Inhibition of 2fLIG-stimulated intracellular Ca^{2+} mobilisation by AZ8838 in HEK293 cells.
Representative temporal profile of Ca^{2+} flux in HEK293 cells incubated for one hour with increasing concentrations of **(A)** (0.3 to 30 µM) AZ8838 only and DMSO or **(B)** co-treated later with 10 µM 2fLIG, measured every three seconds over a period of 120 seconds. 2fLIG was added at 20 seconds. HBSS: Hank's Balanced Salt Solution represents the control. **(C)** Peak Ca^{2+} responses (ΔRFU) to 2fLIG alone and in combination with AZ8838, normalised to the DMSO control. Graphs show representative data of three independent experiments, presented as mean ± SEM. Statistical analysis has been performed by one-way ANOVA. Significant differences are indicated: *P < 0.05, **P < 0.01, ***P < 0.001, ****P < 0.0001.

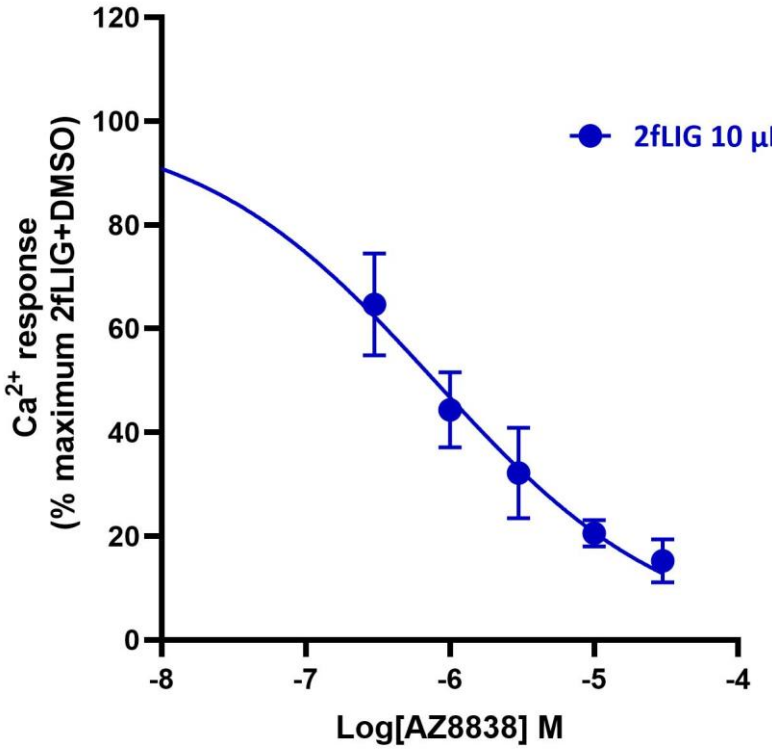

Figure 3.37: AZ8838 inhibits of 2fLIG-induced intracellular Ca^{2+} mobilisation in HEK293 cells.
Concentration-response curve showing the percentage of the maximum 2fLIG-induced Ca^{2+} response in the presence of AZ8838. The IC_{50} value for AZ8838 is 0.78 µM (95% CI 0.38 to 1.32). Data were fitted using the Hill equation in GraphPad Prism 10.3.1. Each data point represents the mean of three independent experiments, presented as mean ± SEM.

A one-hour incubation with AZ8838 did not significantly alter basal intracellular Ca^{2+} levels (Figure 3.36A). Consistent with the previous experiment, 10 µM 2fLIG induced a rapid increase of intracellular Ca^{2+} mobilisation (ΔRFU 38.14 ± 4.8), which was slightly, though insignificantly, reduced by DMSO (ΔRFU 31 ± 2.6, p = 0.586) (see Figure 3.36, B and C panels). AZ8838 exhibited a concentration-dependent inhibition of the maximum 2fLIG-induced Ca^{2+} response starting at 1 µM (ΔRFU 17.8 ± 2.9, p =

0.0406) and reaching 30 μM (ΔRFU 8 ± 1.8, $p < 0.0001$). Using Hill regression analysis, the estimated IC_{50} value for AZ8838 was 0.78 μM (95% CI 0.38 to 1.32) against the selective PAR2-agonist peptide 2fLIG (Figure 3.37), which is lower than the previously reported values against the maximum SLIGRL calcium response (2.3 ± 0.02 μM) (Cheng et al., 2017) and ~1.99 μM (Kennedy et al., 2020).

3.6 Effect of AZ8838 on PAR2 internalisation in DU145 cells.

To further explore the mechanisms underlying the inhibitory effect of AZ8838, we aimed to examine its effect on the PAR2 internalisation, a process typically mediated through β-arrestin recruitment (DeFea et al., 2000a, Chandrabalan and Ramachandran, 2021). This constitutes part of the non-G-protein-dependent activation pathway of PAR2, like other GPCRs, turning on other intracellular signalling elements (refer to Chapter 1, section 1.7.1). Previous studies reported the inhibitory effect of AZ8838 on β-arrestin recruitment, employing enzyme fragment complementation assays. The estimated pIC_{50} against SLIGRL-induced response was 6.1 ± 0.1, n=3 (IC_{50} ~0.8 μM) in U2OS-hPAR2 cells (Kennedy et al., 2020) and 0.63 μM IC_{50}, n=1 in 1321N1-hPAR2 cells (Cheng et al., 2017). The current investigation aimed to examine the effect of preincubation of the cells with AZ8838 on the visualised PAR2 cellular localisation stimulated by the selective agonist, 2fLIG, using transient transfection of the cells with PAR2-yellow fluorescent protein (YFP) (refer to Chapter 2, section 2.7).

3.6.1 Time and concentration effect on 2fLIG-mediated PAR2 internalisation.

To validate the transfection efficiency of PAR2-YFP in DU145 cells using polyethyleneimine (PEI) and to assess the response of transfected cells to 2fLIG stimulation, an initial control experiment was conducted. As illustrated in Figure 3.38,

control images show the DAPI staining clearly the nuclei (cyan), without any fluorescence observed in the FITC channel, indicating no background signal. Similar images were obtained for PEI-treated cells.

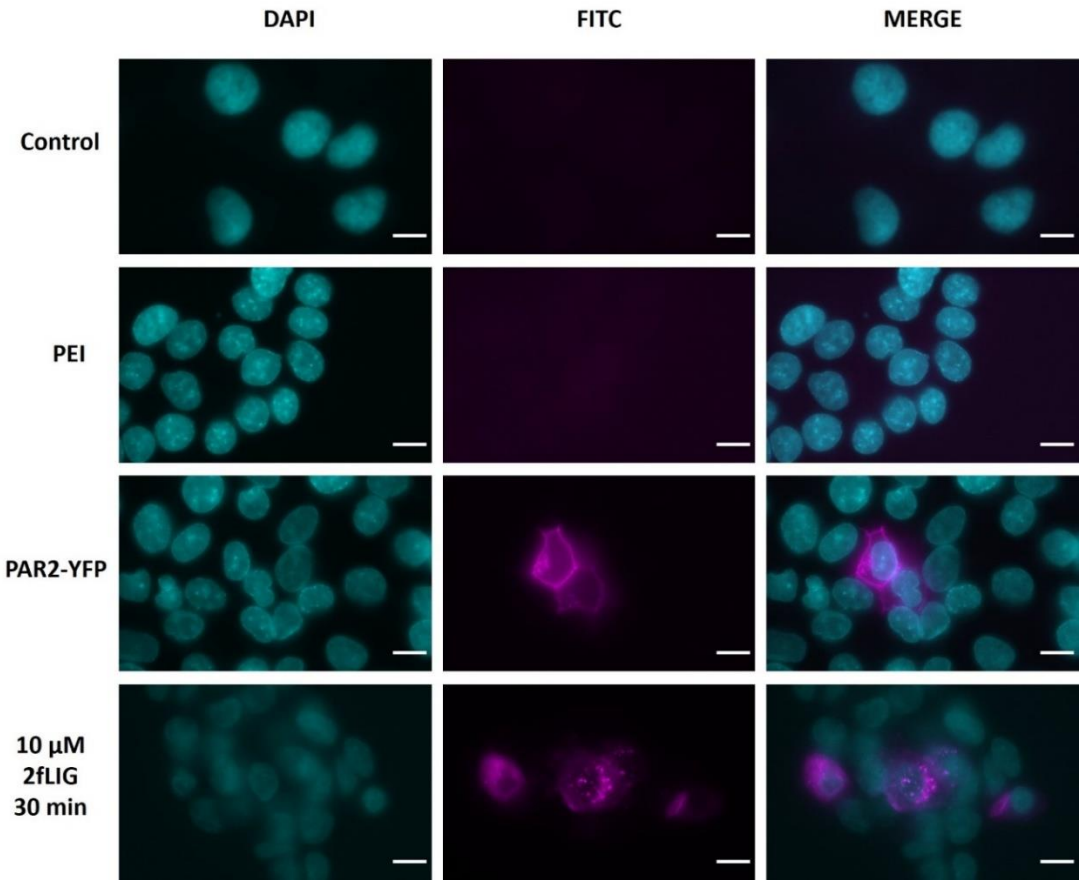

Figure 3.38: Validation of PAR2-YFP transfection in PAR2-YFP-transfected DU145 cells. Representative fluorescence microscopic images of DU145 cells (60x), from top row, showing **Control** cells without treatment (vehicle), cells treated with **PEI** only, cells transfected with **PAR2-YFP** using PEI, displaying successful expression of PAR2-YFP on the cell membrane and PAR2-YFP-transfected cells treated with **10 µM 2fLIG** for 30 minutes, showing 2fLIG-induced internalisation of PAR2-YFP. DAPI staining marks the nuclei (cyan), FITC channel shows PAR2-YFP (magenta), and the merge combines both channels. n=3, scale bar = 20 µm.

The PAR2-YFP images, cells were incubated with PEI plus PAR2-YFP, show clear YFP fluorescence (magenta), indicating successful expression of PAR2-YFP on the cell membrane. The merged image confirms the membrane localisation of PAR2-YFP in transfected cells. Testing the cells' responsiveness to agonist, treating the cells with 10 μM 2fLIG for 30 minutes induced redistribution of the detected fluorescence from the membrane to intracellular locations. This 2fLIG-induced internalisation is consistent with PAR2 activation, confirming the functionality of the transfected PAR2-YFP (see Figure 3.38, 3rd and 4th panels).

To understand the time-course and dynamics of PAR2 localisation upon agonist stimulation, the internalisation of PAR2 in PAR2-YFP-transfected DU145 cells over a 90-minute period following stimulation with 10 μM 2fLIG was investigated. A detailed visualisation of the time-dependent dynamics is shown in

Figure 3.39. The control panel shows membrane-associated PAR2-YFP fluorescence (magenta) in untreated cells. Upon 2fLIG stimulation, initial signs of PAR2 internalisation are detectable at 5 minutes of incubation. This continues to increase, reaching almost a maximum at 30 minutes, seen as fluorescence accumulating in intracellular compartments, and concurrent reduced membrane fluorescence. At 90 minutes, it appears that PAR2 started to be relocated again on the cell membrane, and intracellular localisation becomes relatively reduced, suggesting receptor recycling to the cell membrane. For later experiments, 30 minutes of stimulation was employed as it showed substantial PAR2-internalisation. The effect of 30 minutes of treatment of PAR2-YFP-transfected DU145 with various concentrations of 2fLIG on the PAR2 internalisation was tested. As demonstrated in

Figure 3.40The control panel represent untreated cells showing PAR2 membrane localisation. Starting from 0.3 μM 2fLIG stimulation, a small extent of intercellular PAR2 localisation increases in intensity with increased agonist concentrations. At both 10 μM and 30 μM, 2fLIG induced a substantial degree of internalisation of PAR2, as shown in

Figure 3.40. Subsequent experiments utilised 10μM 2fLIG as it was sufficient to induce a notable and consistent level of PAR2 internalisation in the majority of cells after 30 minutes of incubation.

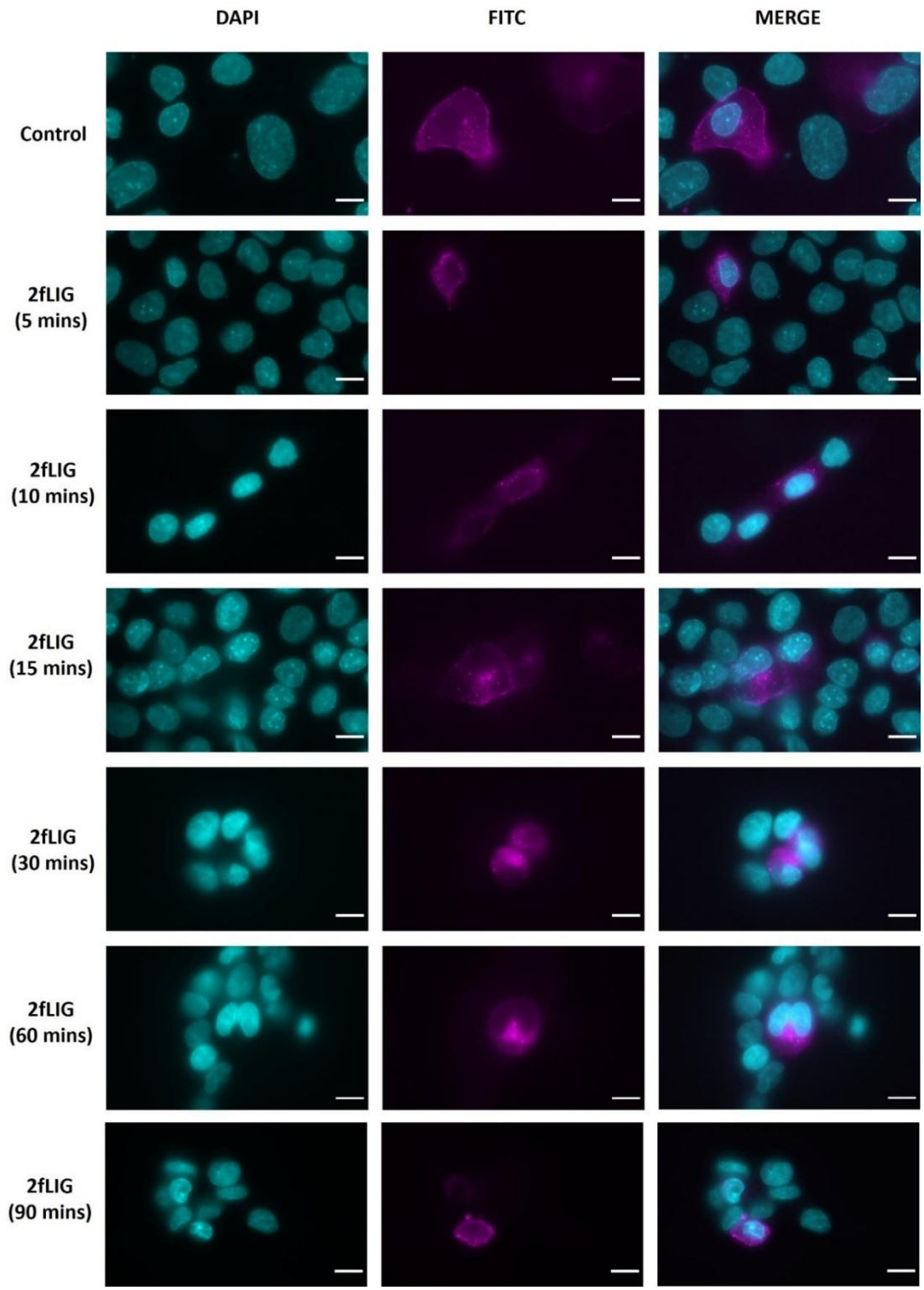

Figure 3.39: Time course of PAR2 internalization in PAR2-YFP-transfected DU145 cells upon 10 µM 2fLIG stimulation.
Representative fluorescence microscopic images showing the PAR2 internalisation over time in PAR2-YFP-transfected DU145 cells treated with 10 µM 2fLIG. **Control** cells without 2fLIG treatment. The following image rows represent cells treated with 10 µM 2fLIG for 5, 10, 15, 30, 60, and 90 minutes.

DAPI staining marks the nuclei (cyan), FITC channel shows PAR2-YFP (magenta), and the merge combines both channels. n=3, scale bar = 20 µm.

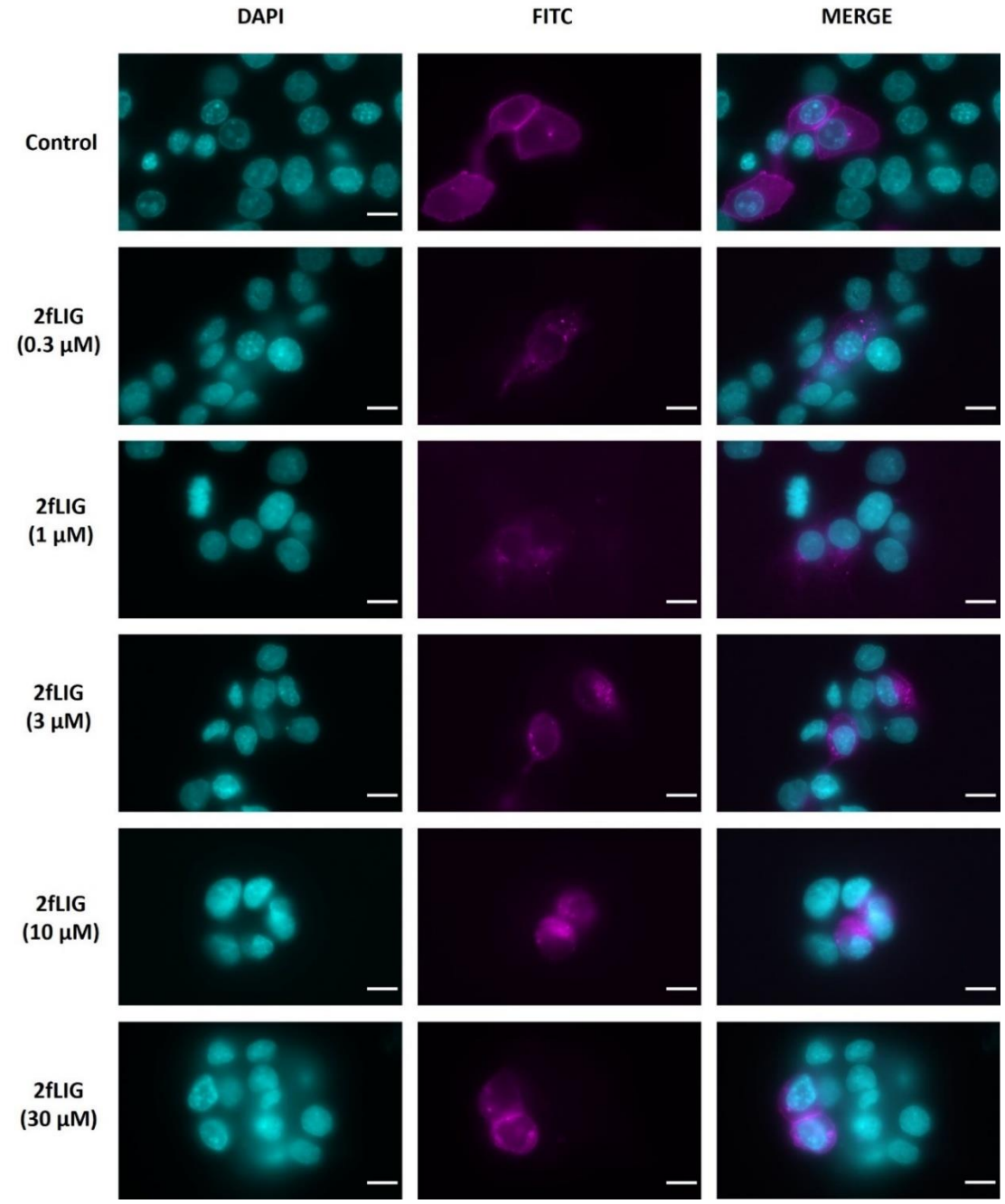

Figure 3.40: Concentration effect on PAR2 internalisation in PAR2-YFP-transfected DU145 cells following 30-minute 2fLIG treatment.

Representative fluorescence microscopic images showing the internalisation of PAR2 in PAR2-YFP-DU145 cells treated with increasing concentrations of 2fLIG (0.3 µM to 30 µM) for 30 minutes. The rows of the image below represent PAR2-YFP-transfected cells treated with the indicated concentrations of 2fLIG. DAPI staining marks the nuclei (cyan), FITC channel shows PAR2-YFP (magenta), and the merged image combines both channels. n=3, scale bar = 20 µm.

3.6.2 Effect of AZ8838 on 2fLIG-stimulated PAR2 internalization in PAR2-YFP-transfected DU145 cells.

Figure 3.41 illustrates representative micrographs of the impact of AZ8838 pre-treatment on the 2fLIG-mediated PAR2 internalisation in PAR2-YFP-DU145 cells. Baseline cell membrane localisation of PAR2 is shown in control images of unstimulated cells. Similarly, neither DMSO alone nor AZ8838 at maximum tested concentration (30μM) seem to affect baseline PAR2 cell membrane distribution. As seen before, 30-minute exposure to 10μM 2fLIG effectively translocated PAR2 to intracellular locations rather than the cell membrane, evidenced by redistribution of fluorescence from the membrane to the cytoplasm. DMSO 1-hour preincubation did not influence this 2fLIG-induced PAR2 internalisation. Interestingly, AZ8838 (30μM) pretreatment markedly limited 2fLIG-induced PAR2 internalisation at 10μM concentration and almost completely retained baseline PAR2 cellular distribution at 30μM as seen with the higher degree of membrane-associated fluorescence in the respective micrographs. These results further indicate that AZ8838 effectively inhibit 2fLIG-stimulated PAR2 internalisation, which is more pronounced at the higher concentration (30 μM).

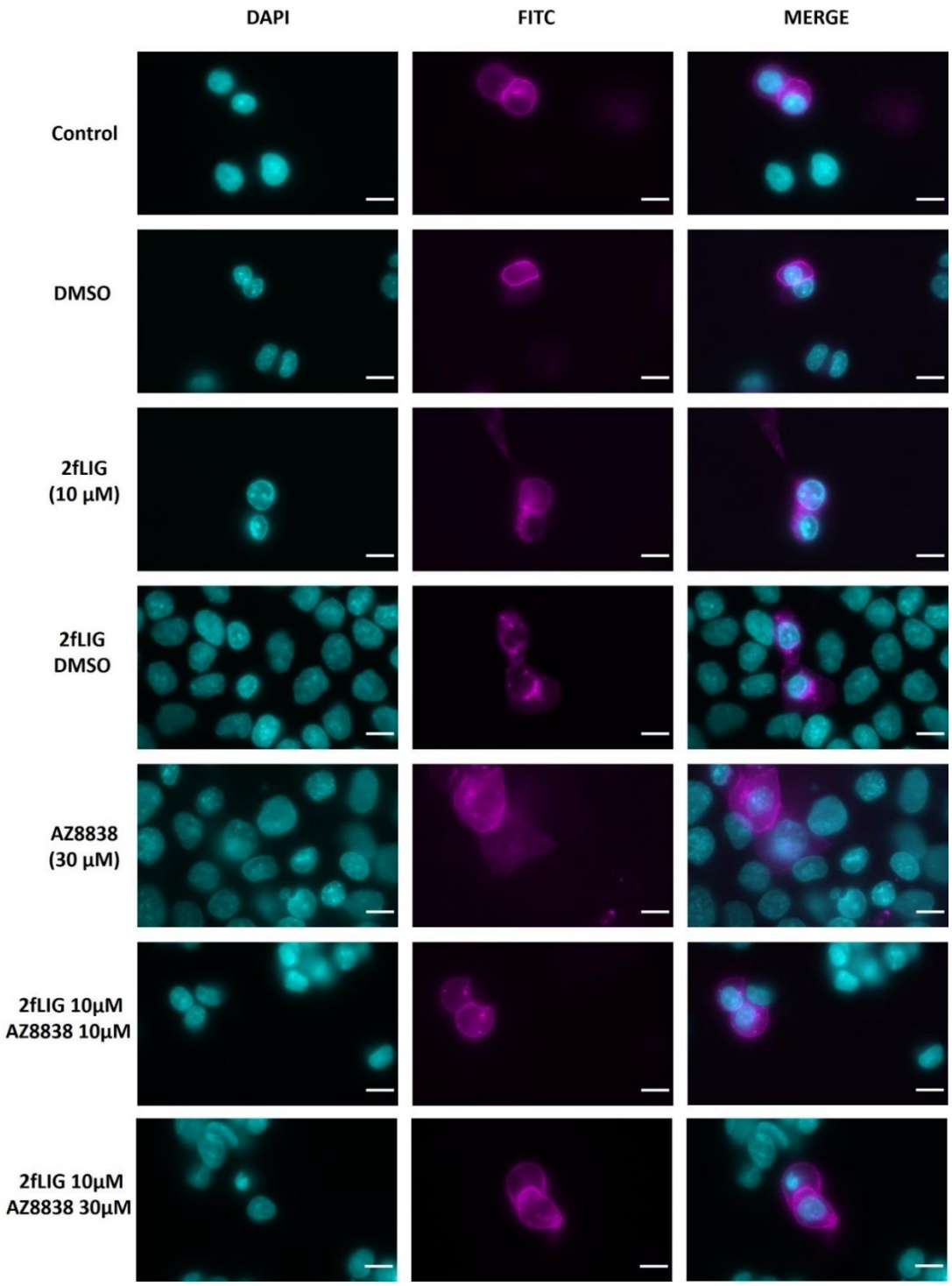

Figure 3.41: AZ8838 effects on 2fLIG-induced PAR2-internalisation in PAR2-YFP-DU145 cells. Representative fluorescence microscopic images showing the internalisation of PAR2-YFP under different conditions. From top to bottom rows: Control cells, cells treated with DMSO, 2fLIG only, 2fLIG plus DMSO, 30 µM AZ8838 only, 2fLIG plus 10 µM AZ8838 and 2fLIG plus 30 µM AZ8838. In the case of DMSO or AZ8838, cells were pretreated for one hour prior to each stimulation. For 2fLIG, cells were stimulated with 10µM for 30 min. DAPI staining marks the nuclei (cyan), FITC channel shows PAR2-YFP (magenta), and the merge combines both channels. n=4, scale bar = 20 µm.

3.7 Effects of AZ8838 on PAR2-mediated release of IL-8.

In the context of inflammatory processes across various tissues, PAR2 promotes inflammation by different mechanisms, including the release of pro-inflammatory cytokines. Interleukin-8 (IL-8) or C-X-C motif chemokine ligand 8 (CXCL8) is one of the chemotactic cytokines (chemokines) reported to be enhanced by PAR2 activation (refer to Chapter 1, section 1.10.5). It is the most potent human neutrophil-attracting and -activating chemokine, which also contributes to endothelial adhesion, chemotaxis, activation of other immune cells, as well as angiogenesis (Matsushima et al., 2022, Cambier et al., 2023). As demonstrated in earlier results, PAR2 stimulation induced NF-κB pathway and ERK1/2 phosphorylation (refer to subsections 3.2.1, 3.3.1 and 3.4.1), its effects on the expression of IL-8, one of the downstream chemokines responsive to these signalling pathways (Tanaka et al., 2008, Guo et al., 2024)AZ8388 was investigated, and AZ8388 effects on the release of this chemokine were assessed. All experiments were conducted using Enzyme-Linked Immunosorbent Assay (ELISA), with the cultured NCTC2544-hPAR2/NF-κB-L or DU145 cells incubated with treatments for 24 hours (refer to Chapter 2, section 2.8)

3.7.1 PAR2 activators' effect on IL-8 release in NCTC2544-hPAR2/NF-κB-L and DU145 cells.

Initially, the effects of several PAR2 agonists and proinflammatory mediators on levels of IL-8 in both NCTC2544-hPAR2/NF-κB-L and DU145 cells were screened. Figure 3.42 illustrates the changes in IL-8 levels induced by 24 hours of stimulation with 2fLIG (10 μM), TNFα (10 ng/mL), IL1β (10 ng/mL), and trypsin (100 nM). In NCTC2544-hPAR2/NF-κB-L cells, 10 μM 2fLIG significantly increased expression

levels of IL-8 to ~4.5 fold of baseline levels (untreated cells). TNFα also significantly enhanced IL-8 expression to almost three times the basal levels. Nevertheless, neither IL1β nor trypsin altered IL-8 levels in this cell type.

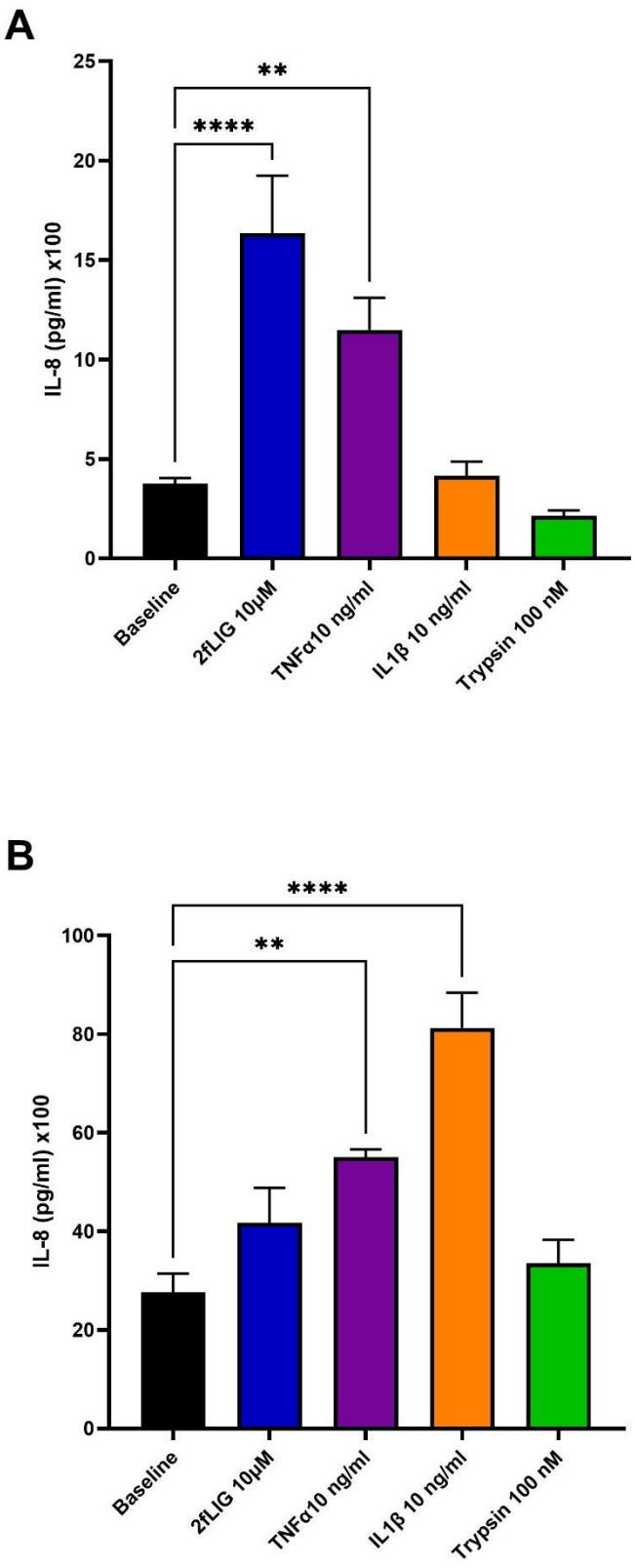

Figure 3.42: Effect of PAR2 agonists on IL-8 levels.
IL-8 levels in **(A)** NCTC2544-hPAR2/NF-κB-L cells and **(B)** DU145 cells were measured after 24 hours- treatment with 2fLIG (10 µM), TNFα (10 ng/ml), IL1β (10 ng/ml), and trypsin (100 nM). Data represent 3 independent experiments as mean ± SEM. Statistical analysis was done using one-way ANOVA, with significance levels indicated as: **p<0.01, ***p<0.001, ****p<0.0001.

In DU145 cells (Figure 3.42B), basal IL-8 levels were significantly greater (2.76 ± 0.38 ng/mL) than those observed in NCTC2544-hPAR2/NF-κB-L cells, more than seven-fold (0.37 ± 0.027 ng/mL, $p < 0.0001$). Despite that elevated baseline, IL1β (10 ng/mL) induced an approximate threefold enhancement in DU145 ($p < 0.0001$). Similarly, TNFα induced an approximate two-fold statistically significant increase in basal IL-8 levels ($p = 0.0049$). While both 2fLIG and trypsin also increased IL-8 levels, these changes were insignificant (2fLIG: $p = 0.73$, trypsin: $p = 0.93$).

Exploring further the concentration effect of 2fLIG on IL-8 levels in NCTC2544-hPAR2/NF-κB-L cells, an evident concentration-dependent enhancement was observed (see Figure 3.43). As the concentration of 2fLIG increases from 0.01 μM to 10 μM, an increase in IL-8 expression levels was observed that was significantly higher than baseline levels (0.47 ± 0.22 ng/mL) starting from 0.1 μM (2.41 ± 0.35 ng/mL, $p = 0.0017$). The peak IL-8 levels were observed at 10 μM 2fLIG stimulation (3.88 ± 0.44 ng/mL, $p < 0.0001$). As shown in Figure 3.43, Panel B presents the concentration-response curve for IL-8 levels induced by 2fLIG, normalised to the maximum response. Using the Hill equation, the estimated EC_{50} value for 2fLIG was 0.1 μM (95%CI: 0.08 to 0.12). A concentration close to EC_{80} was used for later experiments to investigate the inhibitor effects on levels of IL-8 in this cell type.

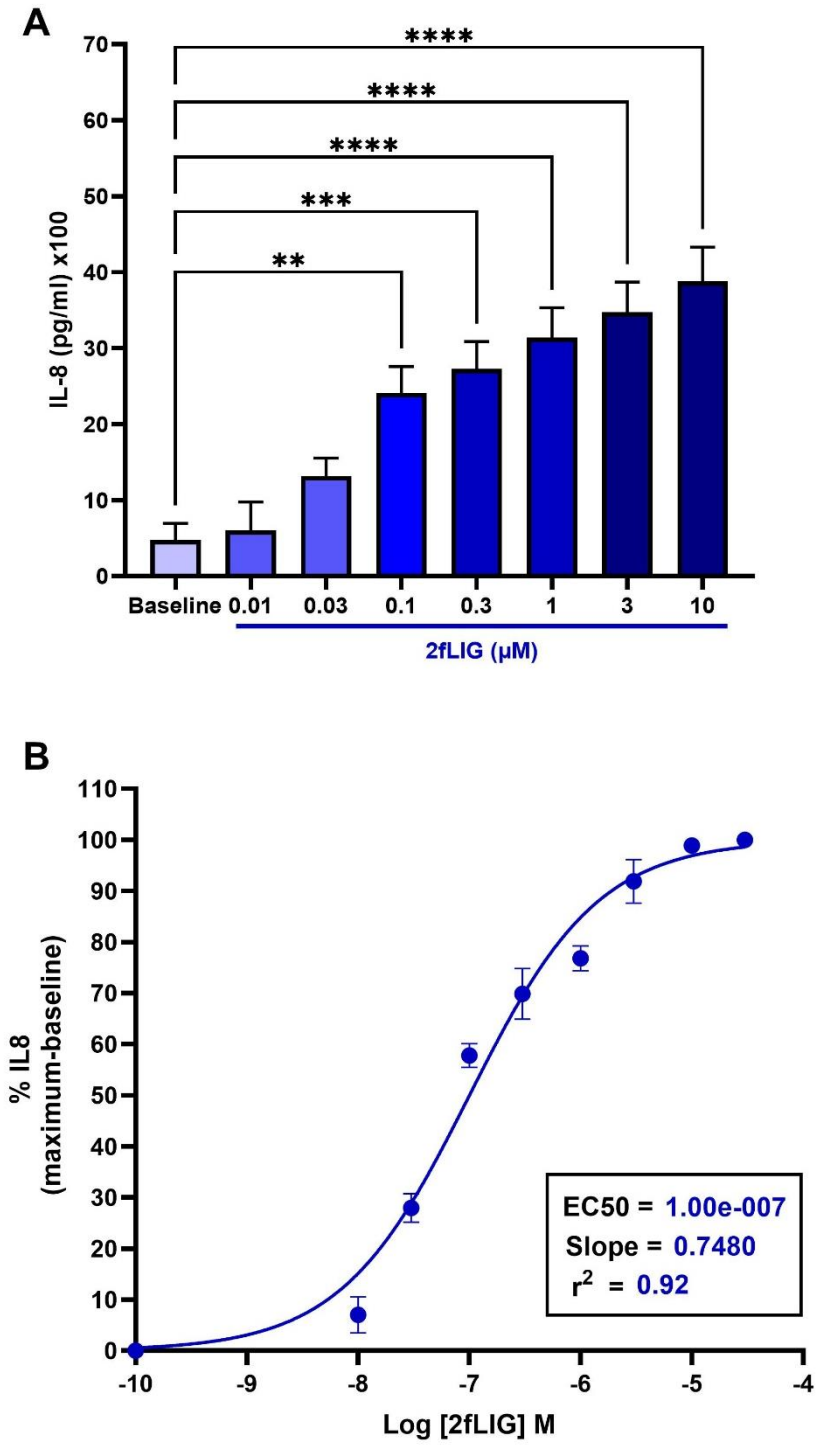

Figure 3.43: Concentration-dependent 2fLIG-induced IL-8 release in NCTC2544-hPAR2/NF-κB-L.

(A) Concentration-dependent effect of 24-hour stimulation with increasing concentrations of 2fLIG (0.01 µM to 10 µM) on IL-8 levels. IL-8 was measured by ELISA. **(B)** Concentration-response curve of IL-8 induction levels as % maximum against log molar concentration of 2fLIG. The EC_{50} was calculated to be 0.1 µM (95%CI: 0.08 to 0.12). Data were fitted using Hill equation in GraphPad prism 10.3.1. Data were presented as mean ± SEM n=5. Statistical analysis has been performed by one-way ANOVA. Significant differences from baseline are indicated: **P < 0.01, ***P < 0.001, ****P < 0.0001.

3.7.2 Effect of AZ8838 on PAR2-stimulated release of IL-8 NCTC2544-hPAR2/NF-κB-L cells.

The effect of AZ8838 on 2fLIG-stimulated release of IL-8 in NCTC2544-hPAR2/NF-κB-L cells over a 24-hour period is shown in Figure 3.44. As depicted in Panel A, treating the cells with AZ8838 alone did not alter baseline levels of IL-8. As seen before, 0.3 μM 2fLIG significantly increased IL-8 levels, exceeding an 11-fold increase from baseline. Notably, the maximum concentration of DMSO (equivalent to the maximum concentration of AZ8838) co-treatment with 0.3 μM 2fLIG caused a significant drop of IL-8 levels (~47% inhibition of 2fLIG response alone). Nevertheless, adding different concentrations of AZ8838 significantly further reduced the 2fLIG-induced IL-8 expression in a concentration-dependent manner. Starting at a concentration of 3 μM, AZ8838 pretreatment reduced IL-8 levels almost to baseline. The estimated IC_{50} value for AZ8838 was 0.63 μM (95% CI 0.15 to 1) against 2fLIG, underscoring its potency in this context.

These results are consistent with the previous observations, indicating that AZ8838 interferes with the PAR2 signalling pathway, namely, NF-κB pathway activation and ERK1/2 phosphorylation, which is known to be involved in the release of IL-8, contributing to the regulation of inflammatory responses. This indicates the potential of AZ8838 as a therapeutic candidate for conditions where excessive IL-8 production is implicated.

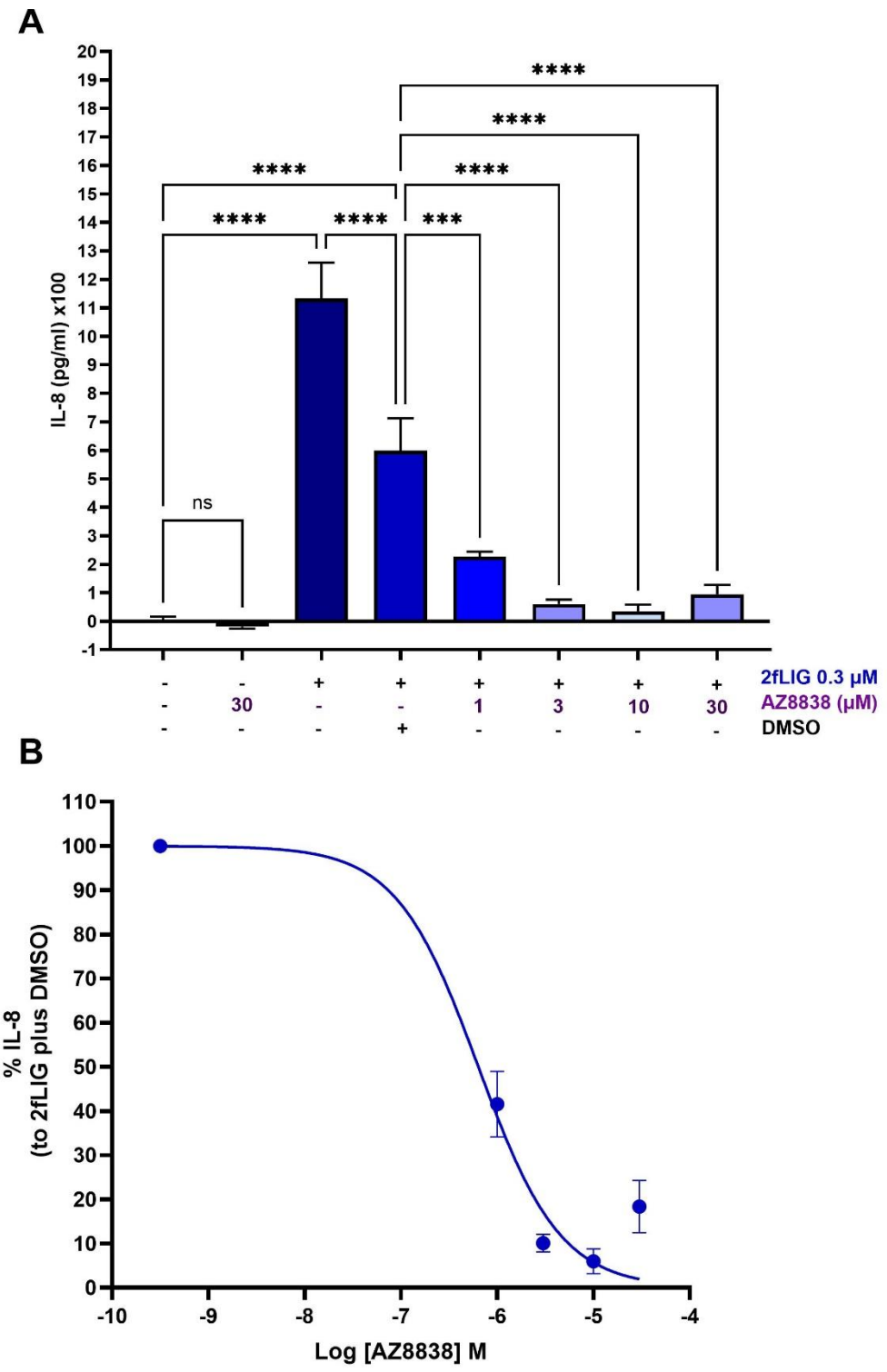

Figure 3.44: AZ8838 inhibits 2fLIG-induced IL-8 release in NCTC2544-hPAR2/NF-κB-L cells. **(A)** Effect of increasing concentrations of AZ8838 (1, 3, 10, and 30 µM) on 0.3 µM 2fLIG-induced IL-8 expression levels measured using ELISA. **(B)** Concentration-response curve showing % of 0.3 µM 2fLIG-induced IL-8 expression in the presence of DMSO (vehicle control) against log [AZ8838] M. The IC_{50} value for AZ8838 is 0.63 µM (95% CI 0.15 to 1). Data were fitted using the Hill equation in GraphPad Prism 10.3.1. Data presented as mean ± SEM, n = 3. Statistical analysis has been performed by one-way ANOVA. Significant differences are indicated: *P < 0.05, **P < 0.01, ***P < 0.001, ****P < 0.0001.

Table 3.1: *in vitro* pharmacology of AZ8838

Assay	IC_{50} (μM)	Agonist (μM)	*n*
NF-κB-luciferase reporter	0.38 (0.26 - 0.52)	2fLIG (1.0)	5
	0.06 (0.002-0.136)	Trypsin (0.1)	4
pERK Western blotting	9.83 (6.82 - 14.6)	2fLIG (0.1)	5
	15.54 (9.8 - 29.74)*	2fLIG (0.3)*	5
Ca^{2+} mobilization assay	0.78 (0.38 to 1.32)**	2fLIG (10)**	3
IL-8 expression ELISA	0.63 (0.15 to 1)	2fLIG (0.3)	3

In all assays, NCTC2544-hPAR2/NF-κB-L cells were used except results with asterisk. IC_{50} is presented as mean (95% confidence interval) based on *n* independent experiments. *DU145 cells and **HEK392

3.8 Discussion

This chapter explored the effects of AZ8838 (the active (S)-enantiomer) on PAR2-mediated intracellular signalling pathways, specifically focusing on its ability to modulate NF-κB activation, Ca^{2+} mobilisation, ERK1/2 phosphorylation (Mitogen-activated protein kinases (MAPKs) pathway), and IL-8 expression. Overall, the results consistently demonstrate that AZ8838 exerts significant inhibitory effects on PAR2 signalling, though the extent of inhibition for certain signalling responses depends on the mode of receptor activation. In the following sections, the results related to AZ8838 effects of the PAR2-mediated activation of the NF-κB pathway, ERK1/2 phosphorylation, and their downstream product, IL-8 levels, are discussed.

3.8.1 Modulation of PAR2-induced NF-κB pathway activation and Ca^{2+} mobilisation.

The NF-κB pathway can be activated downstream of PAR2 stimulation. In this study, the effects of AZ8838 on NF-κB reporter activity were investigated utilising the NCTC2544-hPAR2/NF-κB-L cells using luciferase-reporter assays, as well as its effects on the nuclear translocation of a key NF-κB subunit, p65, using immunofluorescence staining. In luciferase reporter assays, AZ8838 demonstrated significant concentration-dependent inhibition with an estimated IC_{50} value of 0.38

μM in 2fLIG-stimulated cells and 60.03 nM against trypsin (Figure 3.6). The more than 6-fold greater potency of AZ8838 against trypsin-induced NF-κB activation compared to 2fLIG suggests that AZ8838 may interact with the PAR2 receptor more effectively in the context of proteolytic activation of the receptor. This indicates that the inhibitor exerts a strong inhibitory effect in biological systems, as trypsin-induced activation serves as a model of endogenous PAR2 stimulation. This difference in potency could be attributed to differences in the receptor conformational states when activated by different agonists (Kennedy et al., 2018). Upstream of the eventual NF-κB genetic response inside the nucleus, the assessment of AZ8838's effect on nuclear translocation of NF-κB demonstrated consistent results. AZ8838 treatment diminished the p65 nuclear translocation, evident by the significantly reduced Pearson's and Mander's coefficients and representative immunofluorescence micrographs (Figure 3.13 and Figure 3.14). Previous research demonstrated that other PAR2 inhibitors also reduce NF-κB transcriptional activity (Goh et al., 2009, Kanke et al., 2009). For example, pretreatment with K-14585 (30 μM) inhibited PAR2-mediated p65 NF-κB phosphorylation and NF-κB-DNA binding, yet alone it stimulated NF-κB reporter activity to a level comparable to that induced by PAR2-AP (Goh et al., 2009). Also, Kanke *et al* showed that both K-12940 and K-14585 significantly inhibited PAR2-AP- and trypsin-induced NF-κB reporter activity in a concentration-dependent manner (Kanke et al., 2009). Compared to these PAR2 antagonists, AZ8838 exhibited superior potency in terms of inhibiting PAR2-mediated NF-κB activation, which is particularly relevant to the context of inflammation. Moreover, this potency was tested using 2fLIG, a highly potent selective PAR2 agonist peptide compared to other studies that used SLIGKV-NH2, which demonstrated less selectivity (McGuire et al., 2004).

Interestingly, AZ8838 was completely inactive against the TNF-α induced NF-κB transcriptional activity, which suggests a level of selectivity for PAR2 responsive elements, without any direct interference with downstream signalling pathways stimulated by other than the PAR2 receptor.

Earlier research has demonstrated that the PAR2-induced activation of NF-κB is dependent on the initial transient Ca^{2+} increase intracellularly (Macfarlane et al., 2005). Using the intracellularly permeable Ca^{2+} chelating agent, BAPTA-AM, it was evident that the PAR2-mediated activation of IKKα and IKKβ, NF-κB-DNA binding and NF-κB reporter activity are all dependent on PAR2-initiated enhanced cytoplasmic [Ca^{2+}] levels, in a way comparable to the direct activator of protein kinase C, Phorbol 12-myristate 13-acetate (PMA) (Macfarlane et al., 2005, Rallabhandi et al., 2008). PAR2 coupling to MAP kinase and TNF-α induced NF-κB activation was found to be Ca^{2+}-independent, further proposing selectivity of the AZ8838 effects. In this study, the effects of AZ8838 on PAR2-induced Ca^{2+} response were examined (see section 3.5.2). AZ8838 showed a concentration-dependent inhibition of the 2fLIG-induced intracellular Ca^{2+} mobilisation consistent with previous research. Using the Hill equation, the estimated IC_{50} value for AZ8838 was 0.78 μM (95% CI 0.38 to 1.32) against 2fLIG, which is less than the earlier estimations against the maximum SLIGRL-induced calcium response of Cheng *et al* (2.3 ± 0.02 μM) (Cheng et al., 2017) and Kennedy *et al* ~1.99 μM (Kennedy et al., 2020). This could be attributed to the potency and selectivity of 2fLIG stimulation of PAR2, which helps to generate sensitive and specific measurements of AZ8838 inhibition. Other possible factors are the exact assay methodology and experimental variations like the cell type, receptor expression levels and agonist concentration used. The benzimidazole PAR2

antagonist, AZ3451, showed higher potency in the same study against SLIGRL-induced Ca2+ mobilisation. This could be linked to the competitive binding assay results, which identified AZ8838 as an orthosteric competitive antagonist of PAR2, meaning it binds to the same site as the receptor's tethered ligand. In contrast, AZ3451 was characterised as an allosteric non-competitive antagonist of PAR2 interacting with the receptor at a site distinct from the tethered ligand binding site (Kennedy et al., 2020). Using Ca^{2+} mobilisation assays in that study, the concentration-response curves of 2fLIG and trypsin displayed the classical right shift in the presence of AZ8838, maximum response was reproducible with greater agonist concentrations, and the estimated Schild slope was 1.1 for 2fLIG and 0.9 for trypsin. All these data fit well with the molecular docking simulations. Collectively, these findings underscore the effectiveness and potency of AZ8838 as a selective PAR2 antagonist, inhibiting the early Ca2+ mobilisation and consequent NF-κB signalling activation. These data reinforce the therapeutic potential of AZ8838 in targeting PAR2-mediated inflammatory responses.

3.8.2 Modulation of MAP Kinase cascade (ERK1/2 phosphorylation) & PAR2 internalisation.

In addition to stimulation of the canonical Gq pathway, triggering Ca2+ mobilisation and the NF-κB pathway, PAR2 stimulation is known to activate signalling cascades resulting in phosphorylation of Extracellular signal-regulated kinase 1/2 (ERK1/2) and β-arrestin-mediated PAR2 internalisation (Chandrabalan and Ramachandran, 2021). ERK1/2 are members of MAP kinases that are mainly involved in cell proliferation, differentiation, growth, migration, metabolism and survival (Lavoie et al., 2020). PAR2-induced ERK1/2 phosphorylation was found to be mediated by β-arrestin

recruitment, which causes the internalisation of PAR2 and acts as a scaffold for MAPK activation (Déry et al., 1999, DeFea et al., 2000a).

Results of this study showed that AZ8838, at high concentrations (10 and 30 μM), effectively inhibits PAR2-induced ERK1/2 phosphorylation stimulated by 2fLIG, as assessed through Western blotting in two cell types: NCTC2544 stably expressing hPAR2 and DU145 endogenously expressing PAR2. The IC_{50} values were estimated to be 9.83 μM and 15.54 μM, respectively (see sections 3.4.2, 3.4.2 and 3.4.4). These values were notably higher compared to the reported IC_{50} by Kennedy *et al*, about 2 μM, possibly explained by differences in experimental factors like cell type and receptor expression levels used in the studies. In addition, the traditional Western blotting protocol was employed (Chapter 2, section 2.5) to assess phosphorylation of ERK1/2, while Kennedy *et al* used a phospho-ERK1/2 assay kit that measures pERK levels in cell lysate based on fluorescence emitted from tagged antibodies interacting with the pERK. In 2fLIG-induced pERK blots, preincubation with higher concentrations of AZ8838 displayed clear inhibition of pERK1/2 across both cell types (see Figure 3.21 and Figure 3.30). However, the AZ8838 inhibition was less consistent and showed more variation in the case of trypsin-induced ERK phosphorylation. This could be attributed to the difference in activation machinery by 2fLIG and trypsin. 2fLIG is a synthetic activating peptide that directly stimulates PAR2, while trypsin activates the receptor by proteolytic cleavage. This suggests that AZ8838 inhibition of PAR2-mediated pERK response is less efficient in the context of proteolytic activation of the receptor. It is worth noting that trypsin can also activate PAR4 in addition to PAR2. Although DU145 cells are not reported to endogenously express PAR4, a study by McIntosh et al demonstrated that NCTC2444 cells respond to the PAR4-specific

activating peptide, suggesting functional PAR4 expression in this cell line (McIntosh et al., 2010). Furthermore, PAR4 activation has been reported to stimulate ERK phosphorylation (Thibeault et al., 2020), raising the possibility that in trypsin-stimulated cells, the observed pERK response may be partially mediated by PAR4. As AZ8838 is a selective PAR2 antagonist, its weak inhibitory effect in NCTC2544 or lack of effect in DU145 cells on trypsin-induced ERK phosphorylation could be attributed to the contribution of PAR4 signalling. In contrast, in the case of trypsin-induced NF-κB activation, AZ8838 demonstrated efficient and potent inhibition, proposing possible pathway-selective effects of this inhibitor.

The trafficking of PAR2 in DU145 cells upon selective stimulation by 2fLIG was further investigated by transfecting the cells with human PAR2 tagged with Yellow Fluorescent protein (YFP). This approach allowed for the visual tracking of the receptor's localisation and movement within the cells in response to agonist stimulation, providing insights into the dynamic behaviour of PAR2 and further investigating the pERK inhibitory effects of AZ8838. Fluorescent microscopic images illustrated clear cell membrane localisation of PAR2-YFP in unstimulated cells (

Figure 3.39). While 2fLIG alone induces distinct internalisation of PAR2-YFP, treatment with AZ8838 reduces this internalisation, maintaining a higher proportion of the receptor at the membrane (see

Figure 3.41). This inhibitory effect highlights the ability of AZ8838 to modulate receptor internalisation, mostly mediated by β-arrestin recruitment (Déry et al., 1999, Stalheim et al., 2005, Heo et al., 2022), and subsequent signalling pathways. Results of this study are consistent with prior investigations examining SLIGRL-NH2-induced

β-arrestin recruitment employing chemiluminescence detection-based assays quantifying PAR2 interaction with β-arrestin. AZ8838 showed concentration-dependent inhibition of β-arrestin recruitment with the reported IC_{50} value between 0.63 - 0.8 μM (Cheng et al., 2017, Kennedy et al., 2020).

Several other PAR2 antagonists demonstrated similar inhibitory effects on MAPK signalling. In human hepatic stellate cells, 30 μM pepducin, PZ-235, efficiently inhibited SLIGRL- and trypsin-induced ERK phosphorylation relative to basal levels (Shearer et al., 2016). Similarly, the PAR2 peptidomimetic antagonist, C391, showed weak inhibition of ERK phosphorylation with an IC_{50} of 14.3 μM (Boitano et al., 2015), close to the estimated AZ8838 value of 15.5 μM in DU145 cells, while another report showed a potent inhibitory effect of 2fLIG-induced β-arrestin recruitment at a nanomolar level (Rivas et al., 2022). Recently, the same research group identified a novel MAPK/β-arrestin biased PAR2 antagonist, C781, that significantly reduced PAR2-mediated phosphorylation of ERK and β-arrestin binding, but did not alter Ca^{2+} mobilisation response (Kume et al., 2023b, Schiff et al., 2023). A different investigation employing pERK1/2 detection assay showed that the imidazopyridazine derivative, I-191, is capable of potently inhibiting 2fLIG- and trypsin-induced phosphorylation of ERK at nanomolar concentrations (Jiang et al., 2018). A recent study analysed I-287, a functionally selective PAR2 antagonist, and showed its effective anti-inflammatory effects *in vivo*. This inhibitor was capable of blocking Ca^{2+} mobilisation and PAR2-induced ERK phosphorylation without altering β-arrestin recruitment and PAR2 internalisation (Avet et al., 2020). The researchers showed that PAR2-induced pERK activation is not completely dependent on β-arrestin recruitment but could be mediated by $G_{q/11}$ and $G_{i/o}$ proteins, proposing that I-287 could inhibit

phosphorylation of ERK1/2 through the inhibition of G_q/DAG/Ca^{2+}/PKC cascade. In contrast, current results demonstrated that AZ8838 inhibited pERK generation and PAR2 internalisation, suggesting more comprehensive inhibitory effects of multiple downstream effects of PAR2 activation. These findings are consistent with this notion, potentially through AZ8838 interference with key upstream signalling events common to DAG/PKC, NF-κB, and ERK1/2 pathways and highlight its potential as a broad-spectrum anti-inflammatory agent.

3.8.3 Modulation of IL-8 levels.

Interleukin 8 (IL-8) is a key chemokine involved in the recruitment of neutrophils to sites of inflammation. NF-κB and MAPK pathways are one of the principal regulators of IL-8, acting through transcription factors NF-κB and activator protein -1 (AP-1) binding on the IL-8 promoter, making IL-8 a critical downstream target in the context of PAR2 signalling (Wang et al., 2006, Tanaka et al., 2008, Vesey et al., 2013). Robust increase in the release of IL-8 induced by 2fLIG in both NCTC2544 (EC_{50} = 0.1 μM) and DU145 cells, consistent with the activation of its upstream pathways. AZ8838 significantly reduced 2fLIG-stimulated IL-8 levels in a concentration-dependent manner, further confirming the compound's potential to mitigate PAR2-induced inflammatory responses. Studies investigating the effects of PAR2 antagonists have confirmed their inhibitory effects on IL-8 expression levels, including FSLLRY-NH2 (Lee et al., 2017), K-14585 (Goh et al., 2009), PZ-235 (Shearer et al., 2016), I-287 (Avet et al., 2020), GB88 (Wang et al., 2021) and AZ3451 (Sun et al., 2021). Consistently, current study findings demonstrated similar effects of AZ8838, with an estimated IC_{50} value of 0.63 μM (Figure 3.44). AZ8838 was examined in a bronchial epithelial cell line and showed significant inhibition of IL-8 at nanomolar

concentration ranges (Bailo et al., 2020). Moreover, the capacity of AZ8838 to reduce IL-8 levels to near-baseline at higher concentrations underscores its potential utility in therapeutic settings for pathologies associated with excessive IL-8 production , including prostate chronic inflammation and cancer, which is the focus of the current investigation (Khadra et al., 2006, McClelland et al., 2024).

3.9 Conclusion

Taken together, this chapter characterised the inhibitory effects of the small molecule PAR2 antagonist, AZ8838, providing compelling evidence of its effective inhibition and potency, focusing on multiple PAR2-mediated signalling pathways. The current study demonstrated that AZ8838 effectively inhibit PAR2-mediated NF-κB reporter activity as well as its nuclear translocation, ERK1/2 phosphorylation, PAR2 internalisation and IL-8 production. To ensure specific effects of AZ8838 to PAR2, the potent selective PAR2-activating peptide 2-furoyl-LIGRLO-NH2 (2fLIG) was employed in all investigations. Concentration-dependent effects of AZ8838 inhibition were observed in all studies, which highlights the potential for fine-tuning its therapeutic implications to achieve optimal outcomes in different disease settings. Furthermore, the broader inhibitory effects targeting multiple signalling pathways downstream of PAR2 strongly suggest that this compound would be a promising candidate for the treatment of chronic inflammatory conditions where PAR2 plays a pivotal role, and possibly oncological conditions. To our knowledge, limited research has investigated AZ8838 using *in vivo* disease models (Kennedy et al., 2020). As our understanding of PAR2 signalling under disease contexts continues to evolve, antagonists like AZ8838 could form a new treatment strategy that is effective and

selective for specific pathologies, minimising the incidence of side effects associated with traditional anti-inflammatory treatment.

Chapter 4

Investigation of AZ8838 *in vivo* effects in prostate inflammation model

4.1 Introduction

The aim of this chapter was to investigate PAR2 roles in mediating pain and inflammation in a rodent model of chronic prostatitis/ chronic pelvic pain syndrome (CP/CPPS). As discussed earlier (subsection 1.10.6), limited studies investigated the PAR2 involvement in prostate inflammatory conditions. In an experimental autoimmune prostatitis (EAP), researchers examined the role of PAR2 and observed significant inhibitory effects of pain elements, including intracellular Ca^{2+} levels in DRG and pain behaviour, resulting from PAR2 genetic deletion or treatment with the PAR2 neutralising antibody (SAM11) (Roman et al., 2014). The carrageenan-induced prostatitis (CIP) model was adopted, as reported to be a cost-effective, reproducible approach that induces a localised inflammatory response without significant tissue damage (He et al., 2023). This model has also been shown to exhibit early onset (after 24 hours) and extended hyperalgesic characteristics, including diminished heat and mechanical threshold in the pelvic region, along with the key inflammatory features, including inflammatory cell infiltration and tissue hyperplasia lasting up to 14 days post-induction (Zeng et al., 2014), resembling the main components of CP/CPPS. This allowed precise control over the onset of pain and inflammation, as well as facilitating investigations into behavioural and tissue-level molecular responses.

In light of the discussed evidence, it was hypothesised that PAR2 contributes to the development of prostatic inflammation and pain in the carrageenan-induced prostatitis model, and that pharmacological inhibition of PAR2 with AZ8838 would attenuate these responses.

4.2 Carrageenan-induced prostatitis (CIP) causes significant weight loss, prostate enlargement, and histological changes.

Carrageenan (CAR) treatment resulted in overall general and localised effects, presented as significant reductions in body weight and an increase in prostate size, besides local inflammatory features. The body weights recorded at 72 hours post-induction surgery of CIP rats were significantly reduced (mean change in body weight: -17.63 ± 6 grams) compared to controls (mean change: -0.81 ± 1.6 grams; Table 4.1), that may indicate systemic stress and inflammation. In contrast, treatment with Celecoxib (as a positive control) and AZ8838 partially mitigated this effect, showing less body weight reduction (-4.17 ± 0.3 g and -4.80 ± 0.91 g, respectively). The prostatic wet weight of the CAR/Vehicle group (360.3 ± 40 mg) was significantly increased in comparison to the control group (211.7 ± 19 mg, $P < 0.05$), representing over a 70% increase. Treatment with Celecoxib (307.5 ± 20.2 mg) and AZ8838 (298 ± 22.3 mg) reduced prostate weights relative to the untreated CAR/Vehicle group, suggesting attenuation of tissue swelling. Similarly, the prostatic index, normalised prostate weight to body weight, was significantly elevated in the CAR/ Vehicle group (1.47 ± 0.13 mg/g) relative to the control group (0.99 ± 0.07 mg/g, $P < 0.05$). Both Celecoxib and AZ8838 treatment groups showed slightly lower prostatic index values (1.35 ± 0.09 mg/g and 1.34 ± 0.10 mg/g, respectively).

Table 4.1: Effects of AZ8838 on carrageenan-intraprostatic injection-induced changes on body weight, prostatic wet weight, and the prostatic index.

Group	Body weight (g)	Body weight change (g)	Prostatic wet weight (mg)	Prostatic index (mg/g)
Control	233.6 ± 7.6	-0.81 ± 1.6	211.7± 19	0.99 ± 0.07
CAR/Vehicle	222.1 ± 9.5	-19.43 ± 6.7**	360.3 ± 40**	1.47 ±0.13*
CAR/Celecoxib	228.0 ± 3.9	-4.17 ± 0.3*	307.5 ± 20.2	1.35 ± 0.09
CAR/AZ8838	222.0 ± 1.8	-4.80 ± 0.91	298.0 ± 22.3	1.34 ± 0.1

Data are expressed as the mean ± SEM, *n* = 5-7 rats. Statistically significant differences compared to the control group or to carrageenan treated group are indicated as * if P< 0.05 and ** if P< 0.01.

To determine the optimal study endpoint, prostate tissue sections were evaluated after 24, 48 and 72 hours, as well as 7 days after CIP induction, to assess progression and severity of inflammation and to identify the approximate peak inflammatory response within the tissue. As shown in

Figure 4.1, visible peak inflammatory changes were observed at 72 hours post-induction and were used for subsequent treatment studies.

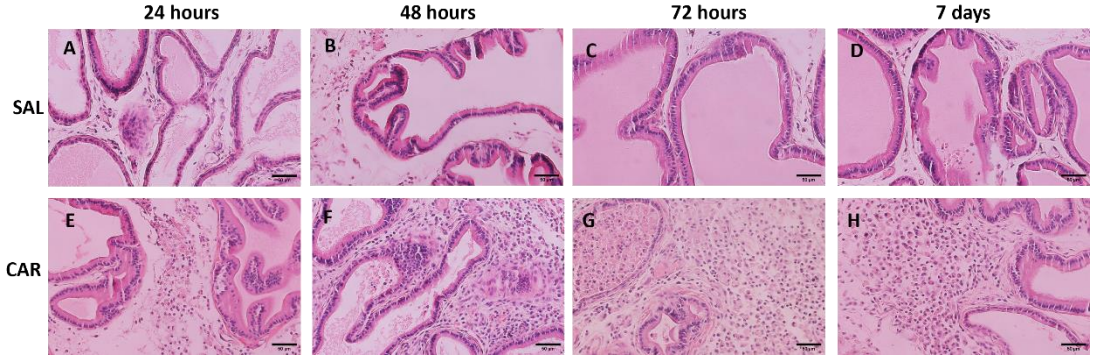

Figure 4.1: Histological evaluation of prostate tissue at different time points following CIP induction.
Representative H&E-stained prostate sections imaged at 20x magnification, isolated at different time points post-induction. Control (A–D) and CAR CIP model (E–H) groups were examined at the indicated time points. Scale bars = 50 µm.

Gross morphological evaluation of the excised prostate tissue revealed that CAR-injected prostate were visibly enlarged, and exhibited areas of hyperaemia, in contrast to the pale, healthy appearance in control prostates (

Figure 4.2, A&D). Results of Haematoxylin and Eosin (H&E) staining indicated that the control group presented with acini and typical histological characteristics of the gland, displaying the normal glandular architecture with absence of inflammation in the interstitial tissue. There was no stromal oedema nor abscess formation (

Figure 4.2B). The CAR group exhibited marked pathological alterations in the prostate consistent with acute and chronic inflammation. Acute inflammation was evident by the infiltration of neutrophils into interstitial spaces, with severity varying from mild to moderate and, in some cases, severe. Neutrophil infiltration was also observed in the glandular lumen, where in several instances, the accumulation of neutrophil cellular debris resulted in micro-abscess formation (

Figure 4.2E and Figure 4.3; B & F; yellow arrow heads). Additionally, interstitial oedema was present, as clear spaces between stromal cells (Figure 4.3; asterisk), and was scored across a spectrum of mild to severe. Evidence of chronic inflammation was noted by the marked presence of lymphoplasmacytic infiltrate and macrophage (Figure 4.3; B & F; black arrow heads) within the interstitium and, in some instances, inside the glandular lumen (Figure 4.3; B & F). Celecoxib/CAR prostates demonstrated preservation of glandular structure and a noticeable reduction in cellular infiltration and oedema (

Figure 4.2C, Figure 4.3 C&G), whereas AZ8838/CAR prostates showed a moderate reduction in inflammation, although the improvement was less marked compared to Celecoxib (

Figure 4.2G). High magnification images further confirm these observations (Figure 4.3 D&H).

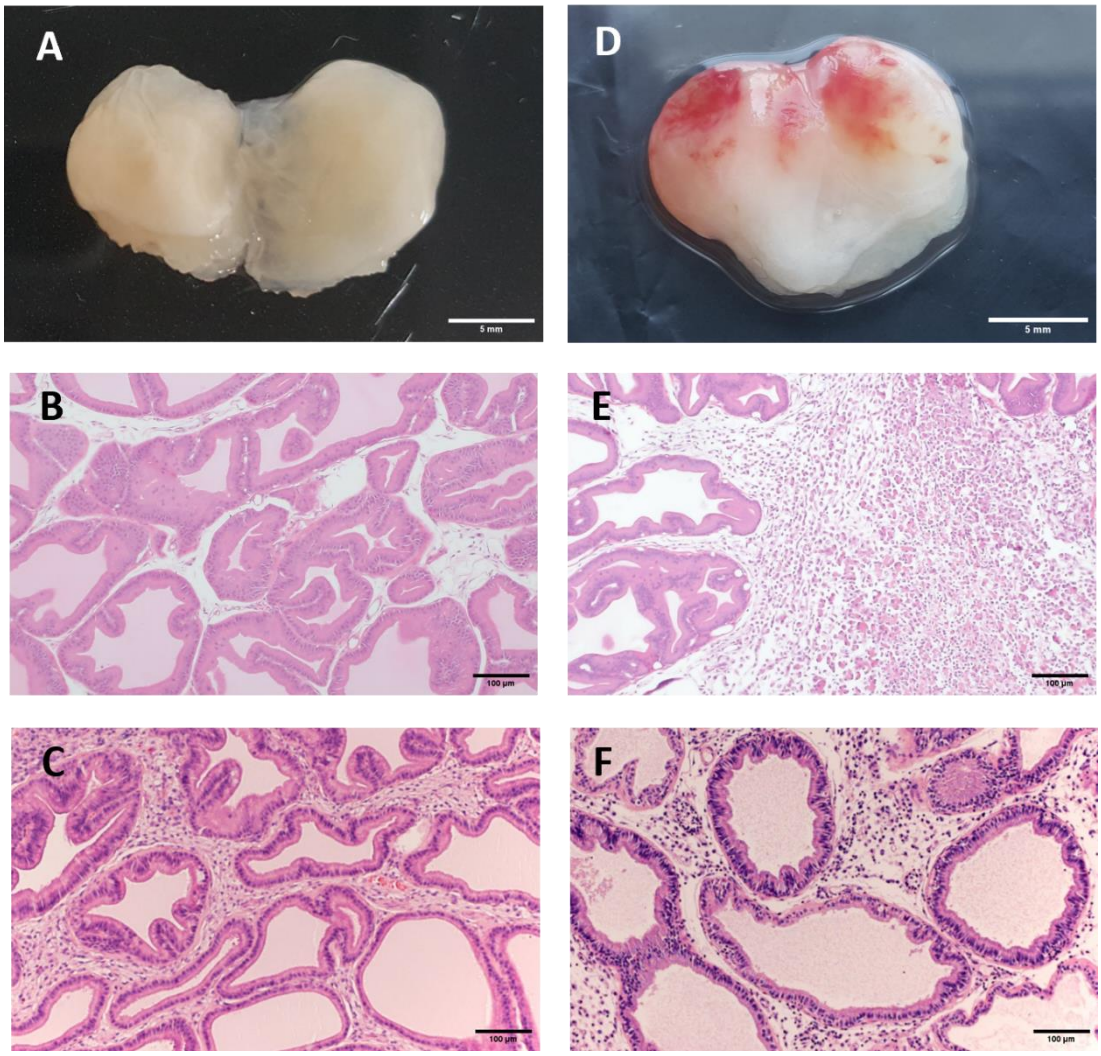

Figure 4.2: Gross morphologic and histologic changes in rat prostate (H&E stain, ×10). Representative gross images of prostate specimens from the control (A) and CAR group (D). Representative H&E-stained histology images from (B) Control, (E) Carrageenan (CAR)/Vehicle (C) Celecoxib/CAR and (F) AZ8838/CAR groups. Scale bars: gross images = 5 mm; histology images = 100 µm.

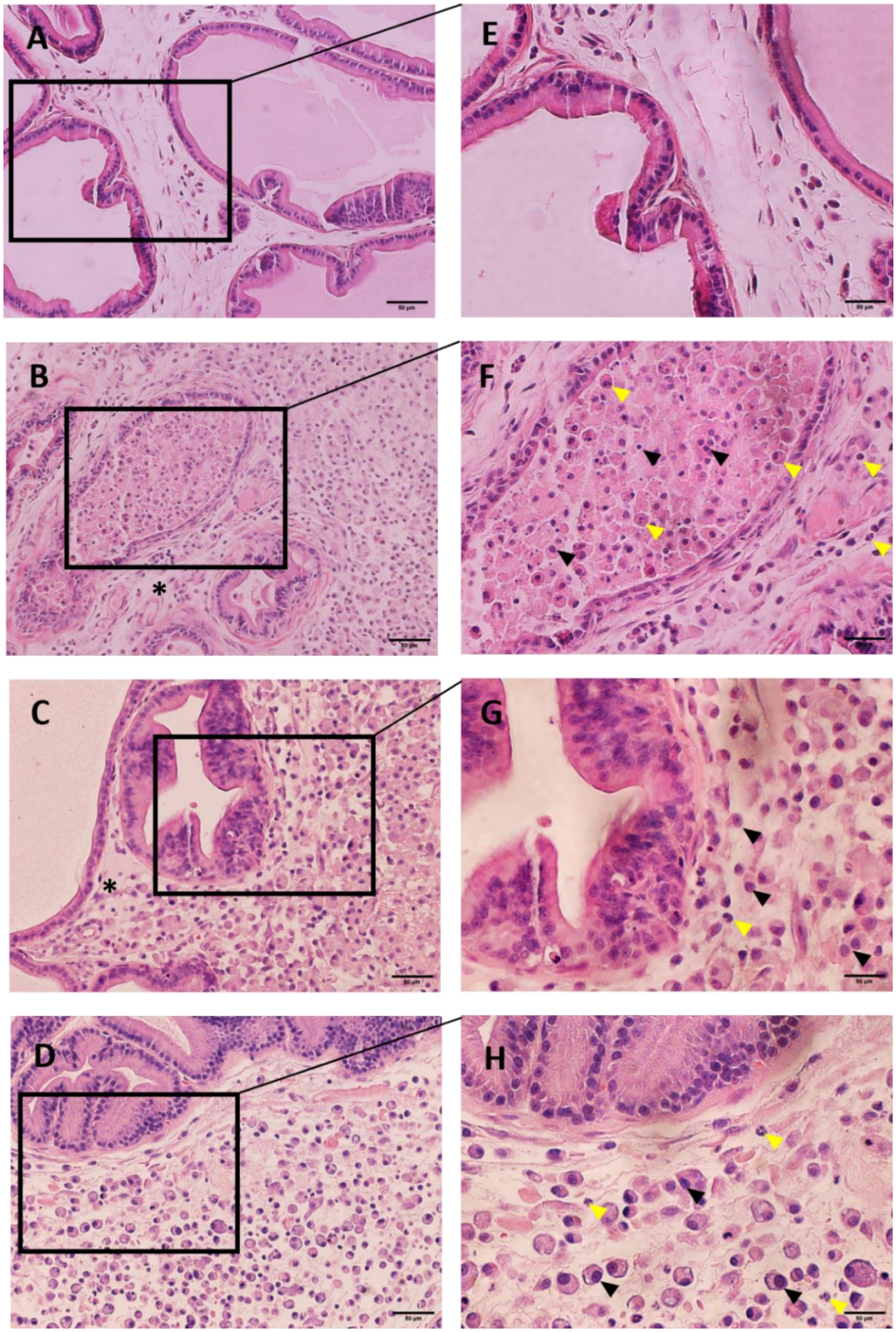

Figure 4.3: High-magnification histological images of prostate tissues from different treatment groups.

Representative H&E-stained images captured at (A-D) 20× magnification and (E-H) 40× magnification for (A, E) Control (Saline/Vehicle); (B, F) Carrageenan (CAR)-treated; (C, G) Celecoxib-treated; (D, H) AZ8838-treated groups. Yellow arrow heads indicate infiltrating neutrophils (acute inflammation),

black arrow heads indicate infiltrating lymphocyte/macrophages (chronic inflammation and an asterisk indicates oedema sites within the tissue section. Scale bars = 50 μm.

Semi-quantitative scoring (refer to Chapter 2, section 2.102.10) of individual inflammatory parameters confirmed a significant increase in neutrophil infiltration, abscess formation, oedema and lymphocyte/macrophage infiltration in CAR group relative to the control, in addition to the total inflammatory score (CAR: 7.57 ± 0.5, Control: 0.28 ± 0.3; see Figure 4.4). Both Celecoxib and AZ8838 pretreatment demonstrated a non-significant reduction of all inflammatory parameters and collectively the total inflammatory scores (CAR/Celecoxib: 5.83 ± 0.83, CAR/AZ8838: 6.6 ± 0.7; see Figure 4.4). Collectively, these findings confirm the inflammatory state of the CIP model and demonstrate that the weak anti-inflammatory

effects of AZ8838 were statistically insignificant.

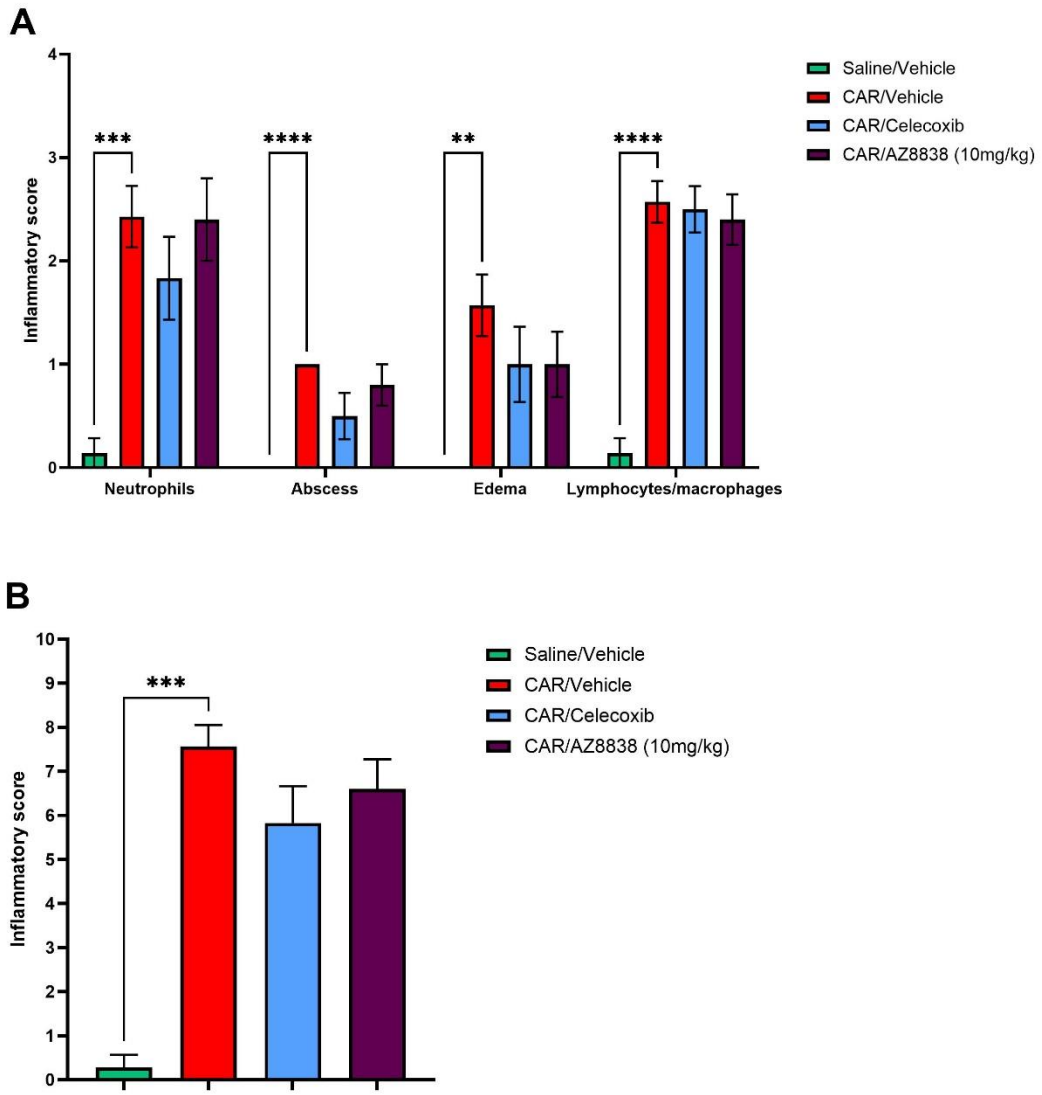

Figure 4.4: Histological evaluation of prostate inflammation reveals limited anti-inflammatory effect of AZ8838 pretreatment.

(**A**) Semi-quantification of individual inflammatory parameters (Neutrophil infiltration, presence of abscess, oedema, and lymphocyte/macrophage infiltration) based on histopathological scoring of prostate sections stained with H&E. Prior to induction, a single oral dose of Celecoxib (200 mg/kg), AZ8838 (10mg/kg) or vehicle were administered. (**B**) Total inflammatory score compiled from individual histological parameters in A. Data are presented as mean ± SEM. Statistical significance compared to Saline/Vehicle or CAR/Vehicle is indicated: **P < 0.01, ***P < 0.001, ****P < 0.0001.

4.3 Expression levels of PAR2 in prostate and lumbar/sacral DRGs:

4.3.1 Immunofluorescence reveals PAR2 upregulation in the prostate but not the DRG of CIP rats.

Initially, to confirm the identification of sensory neuron cell bodies within the DRG sections, the neuronal marker NeuN was used. NeuN is a well-established nuclear protein expressed in mature neurons and commonly used to distinguish neuronal from non-neuronal cell types in tissue sections. As shown in Figure 4.5, PAR2-positive cells were colocalised specifically to neuronal populations within DRG.

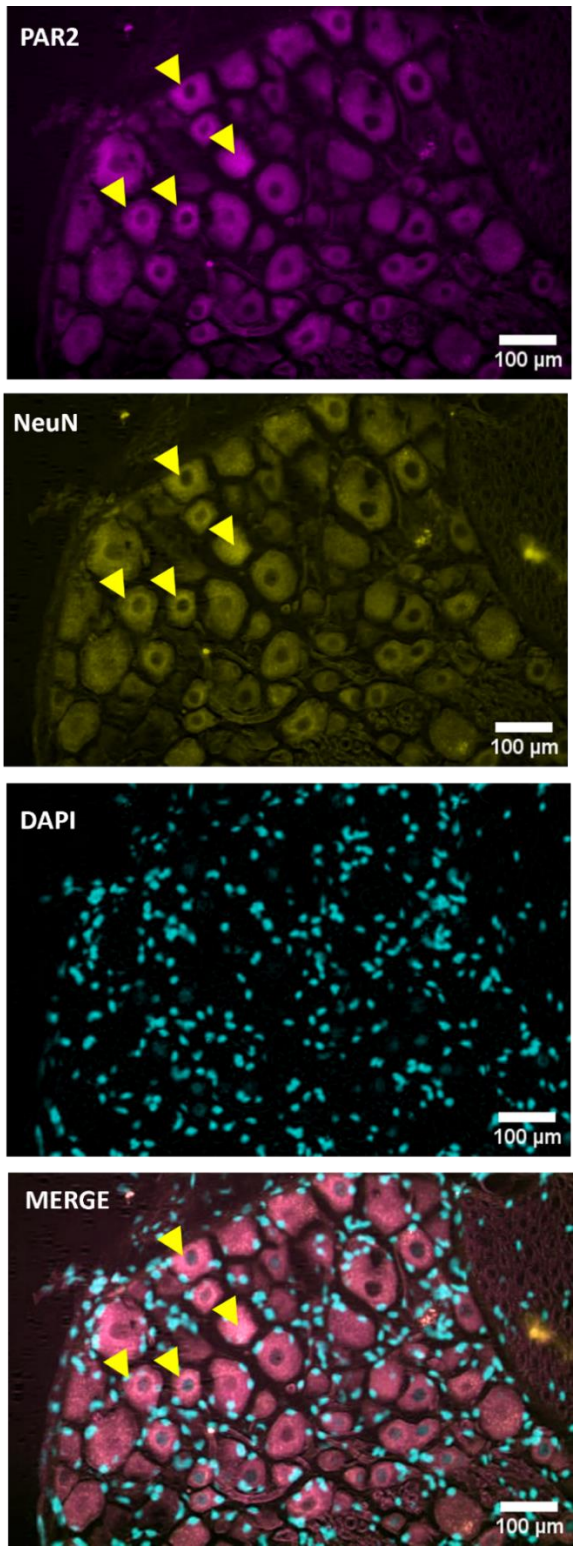

Figure 4.5: Confirmation of PAR2 expression in sensory neurons using NeuN in DRG sections. Representative immunofluorescence images showing PAR2 (magenta), NeuN (yellow), and DAPI (cyan) in DRG sections. Yellow arrowheads show the sample colocalised PAR2 with NeuN confirmed in the merged image. Scale bars = 100 µm.

To assess the expression of PAR2 in the lumbar (L5, L6) and sacral (S1) dorsal root ganglia (DRG) as well as in the prostate gland, immunofluorescence assays were employed. In DRG, PAR2 immunoreactivity was detectable predominantly at the plasma membrane and inside intracellular locations in the soma and axons of many DRG neurons (

Figure 4.6). A control experiment using only secondary antibodies verified the specificity of the antibodies in this study (image not shown). Quantitative analysis revealed no statistically significant difference between the groups (Figure 4.8); However, a non-significant trend towards increased PAR2 expression is noted in the model group (CAR-treated), especially in the L6 DRG ($p= 0.3954$). (

Figure 4.7). Despite having a smaller neuronal population (with an average of 29.5 ± 3 neurons per section, compared to 58.18 ± 6.7 for L5 and 66.2 ± 5.5 for L6), the S1 DRG displayed a higher proportion of PAR2 expression. The percentage of PAR2-positive neurons in S1 DRG was 34.8 ± 5.35 and 35.3 ± 5.7 for the sham (SAL) group and the CAR-treated group, respectively, surpassing both L5 (SAL: 18.67 ± 2.8; CAR: 23.41 ± 2.5) and L6 DRG (SAL: 17.8 ± 2.7; CAR: 25.8 ± 2.4). Generally, this finding may indicate that PAR2 expression in DRG neurons is relatively stable in response to prostate inflammation, or possible changes in PAR2 downstream signalling occur at post-receptor levels, not at the protein level. For that, further investigations may be required to assess functional changes of PAR2 activity or possibly sensitivity in response to local prostate inflammation.

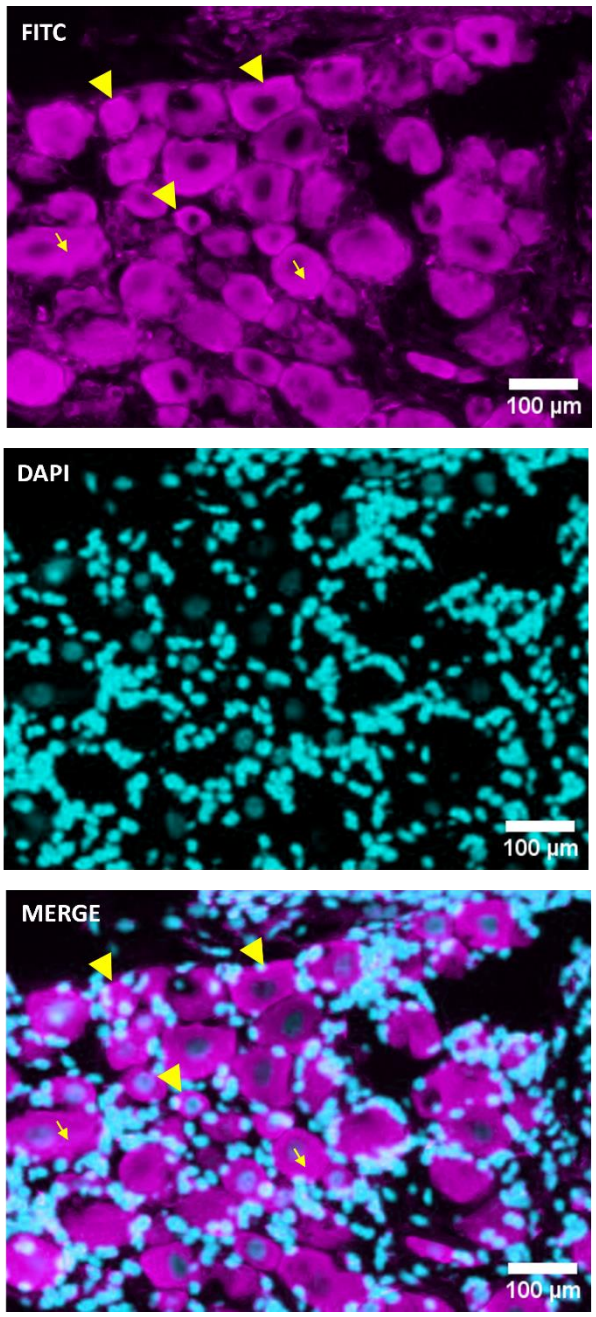

Figure 4.6: Localisation of PAR2 in the neurons of the dorsal root ganglia (DRG).
Representative immunofluorescence images displaying PAR2 localisation (FITC-top panel). PAR2 (magenta) was detectable at the plasma membrane and in intracellular locations (arrow heads) in the soma and in nerve fibres in the DRG cross-section (arrows). The DAPI staining (cyan) marks the nuclei (central panel). Scale bar = 100 µm.

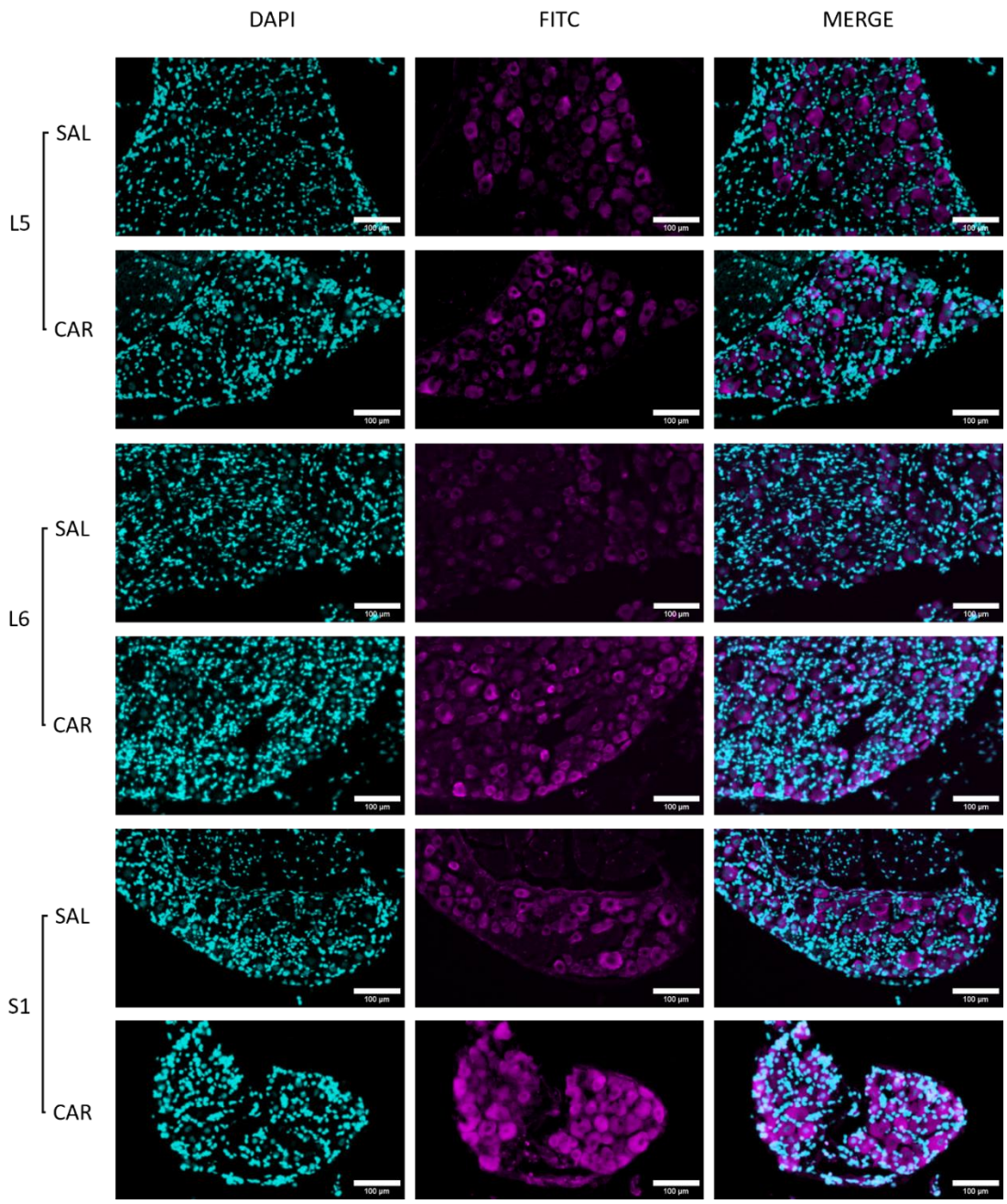

Figure 4.7: Carrageenan do not alter neuronal PAR2 expression compared to sham (SAL) group. Representative immunofluorescence images showing immunoreactive PAR2 in lumbar L5, L6 and sacral S1 DRG from both CAR and sham (SAL) groups. FITC (magenta) indicates PAR2 localisation, while DAPI (cyan) indicates the nuclei. Scale bar = 100 µm.

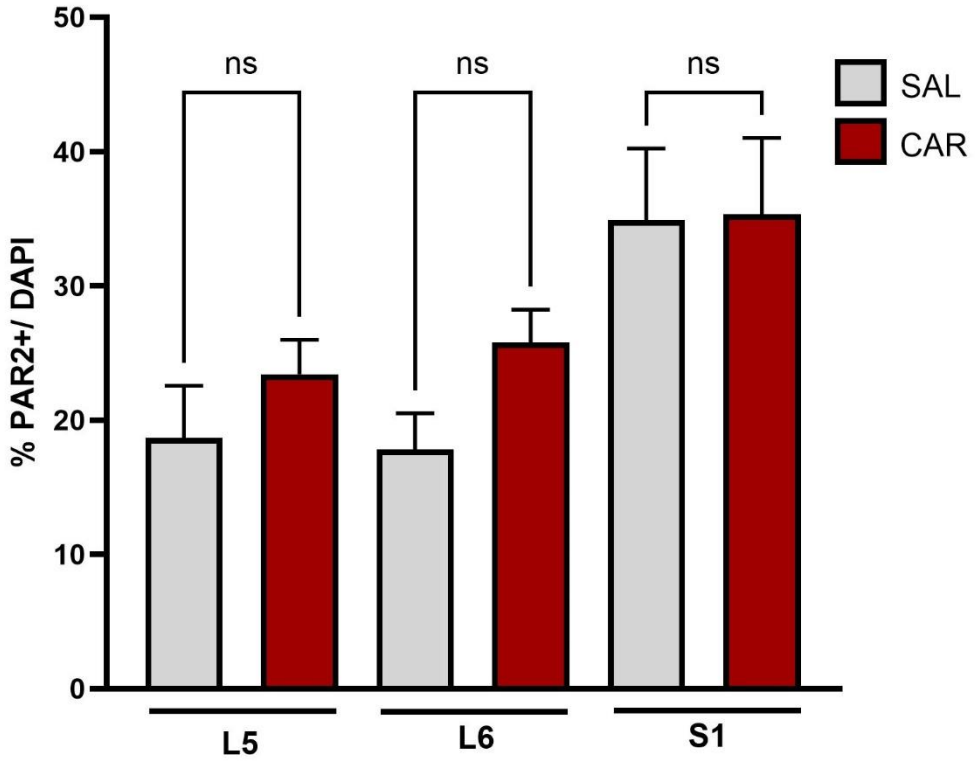

Figure 4.8: Semi-quantitative analysis of IF images showing no change in PAR2 expression in DRGs between the CAR-treated group and the sham (SAL) group.
Data displayed mean ± SEM of the % PAR2 positive cells relative to total neuron (DAPI), analysed via immunolabeling (n = 6, 5 DRG sections from each rat, sections were taken at varying depth). Statistical analysis has been performed by one-way ANOVA. No significant differences (ns) were indicated between the groups.

In prostate sections, PAR2 was localised predominantly at the apical plasma membrane or epithelial cells toward the secretory lumen (Figure 4.9). In contrast to DRG, quantitative analysis of PAR2 expression, measured as mean fluorescence intensity (MFI; refer to chapter 2, subsection 2.9.4), revealed a significant increase in PAR2 expression in the prostate tissue of the CAR-treated group compared to the sham (SAL) group, with approximately two-fold higher MFI values (SAL: 9.622 ± 1.6; CAR: 18.97 ± 2.6, p = 0.0137) (

Figure 4.10 and Figure 4.11).

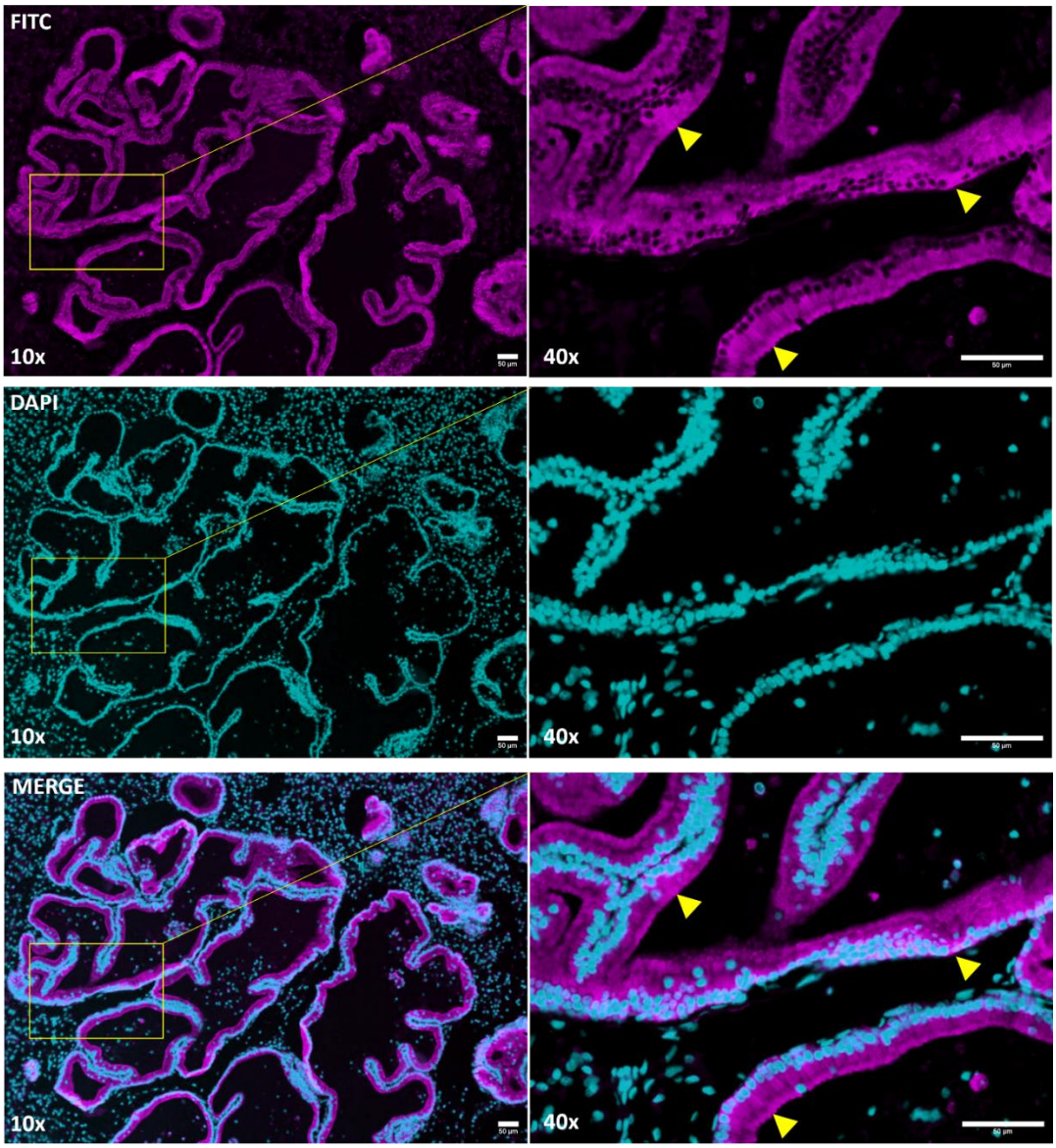

Figure 4.9: Localisation of PAR2 in rat prostate tissue sections.
Representative IF images displaying PAR2 localisation (FITC-top panel). PAR2 was detectable along the epithelial lining of the prostate gland (arrow heads). The DAPI staining (cyan) marks the nuclei (central panel). Scale bar = 50 µm.

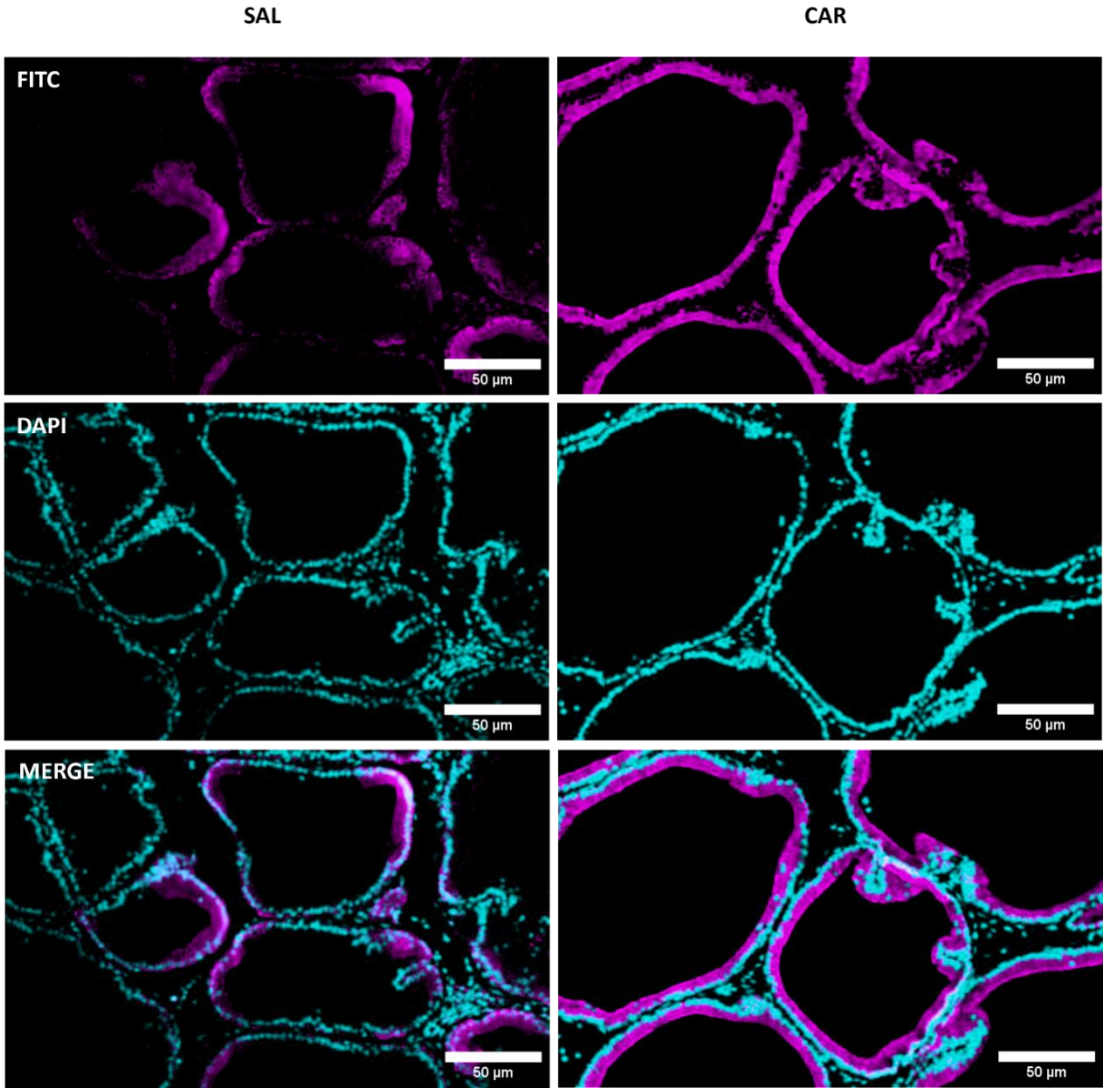

Figure 4.10: CAR-treatment enhanced PAR2 expression in prostate tissue compared to the sham (SAL) group.
Representative images showing IF staining for PAR2 (FITC) in prostate tissue from sham (SAL) & CAR-treated groups. Nuclei were counterstained with DAPI (cyan). Scale bar = 50 µm.

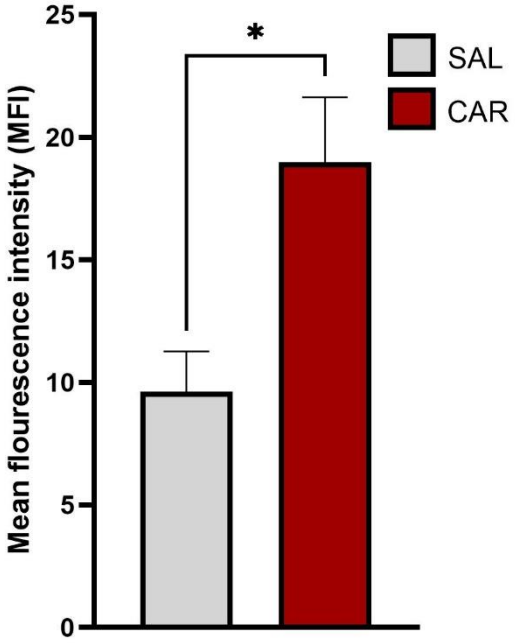

Figure 4.11: PAR2 expression increased in prostate tissue of the CAR-treated group compared to the sham (SAL) group, as investigated by immunofluorescence.
The graph shows mean fluorescence intensity (MFI) representing PAR2 expression in the saline-treated (SAL) and carrageenan-treated (CAR) groups. Data represent mean ± SEM measured from 5 sections/ specimen taken from each rat (n=6). Statistical analysis was performed using one-way ANOVA. Significant differences are indicated: *P < 0.05.

4.3.2 Significant changes in the expression of PAR2 in the prostate, not DRG, of CAR-treated rats using qRT-PCR and Western blotting.

To further investigate the potential effects of carrageenan-induced inflammation model on PAR2 expression levels, PAR2 gene (*F2rl1*) expression was analysed using a TaqMan probe detecting full-length *F2rl1* mRNA (Figure 4.12). CAR-induced inflammation did not significantly alter PAR2 expression in DRG compared to the sham (SAL) group. However, in the prostate, CAR treatment significantly decreased PAR2 gene expression relative to the SAL group (2-ΔΔCT for CAR 0.33 ± 0.67 compared to 1.2 ± 1.7 for the SAL group, p = 0.0062). This may indicate a localised regulatory response in the prostate because of an inflammatory response.

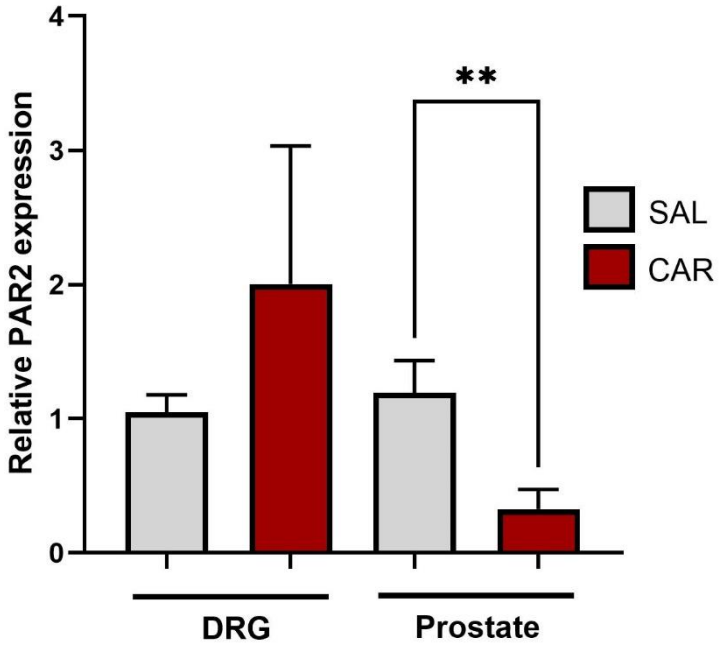

Figure 4.12: Carrageenan-induced inflammation decreases PAR2 mRNA expression, with no significant alterations in DRG.
The graph shows PAR2 gene expression quantified in DRG and prostate tissues as measured by quantitative RT-PCR in the saline (SAL)- and carrageenan (CAR)-treated groups. Gene expression is presented as relative PAR2 gene expression normalised to GAPDH in each sample expressed as $2^{-\Delta\Delta Ct}$. Data represent mean ± SEM measured from 3 replicates/specimen taken from each rat (n=6). Statistical analysis was performed using one-way ANOVA. Significant differences are indicated: *P < 0.05, **P < 0.001

Detected by immunoblotting, CAR treatment does not significantly alter PAR2 protein expression in DRG. In contrast to gene expression studies, CAR-induced inflammation caused a significant increase in PAR2 protein expression in prostate tissue, as shown in Figure 4.13, to reach about 2.75-fold of prostatic expression in the sham (SAL) group (β-actin normalised densitometry for CAR 1.36 ± 0.27 compared to 0.5 ± 0.08 for the SAL group. P = 0.0312). These results support the previously obtained findings from immunofluorescence studies, confirming enhanced PAR2 protein expression locally in the prostate but not in the lumbar/sacral DRG (Figure 4.11). Thus, these observations suggest that the PAR2 receptor may contribute to the inflammatory processes in the prostate of the carrageenan inflammation model.

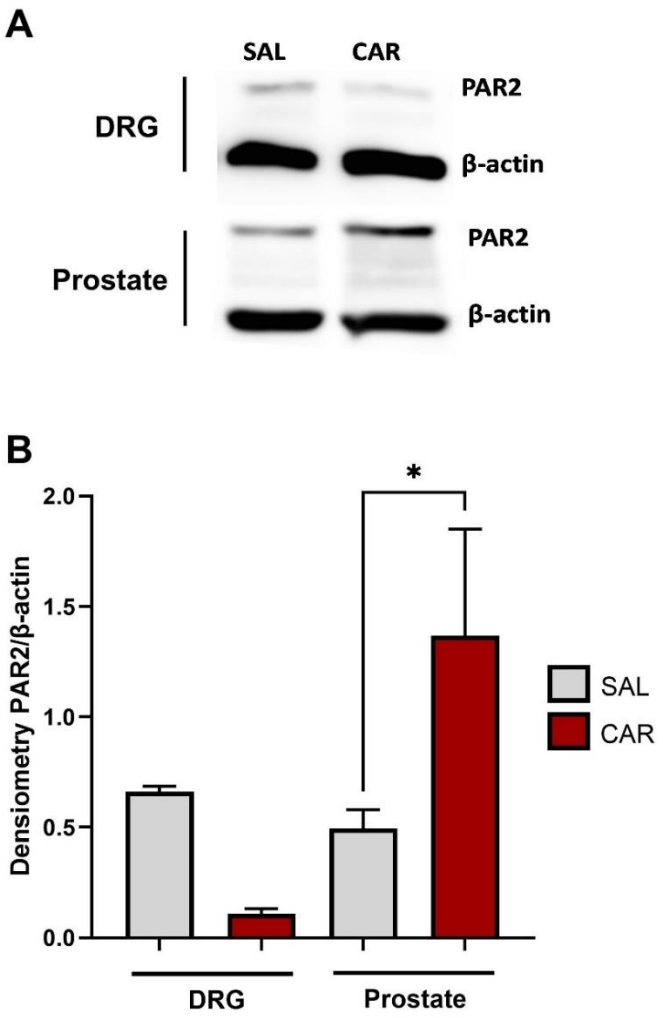

Figure 4.13: Carrageenan-treatment increases PAR2 protein expression in prostate, with no significant alterations in DRG.
(A) Representative immunoblots showing PAR2 levels and β-actin (as loading control) in DRG and prostate tissue lysates at 72 hours post-induction. **(B)** Band density semi-quantification of PAR2 relative to β-actin measured by ImageJ v1.54J. Data presented as mean ± SEM (8-10 rats per group). Statistical analysis has been performed by one-way ANOVA. Significant differences are indicated: (*P< 0.05).

4.4 Behavioural assessment of PAR2 antagonist, AZ8838.

Having established PAR2 expression in the prostate and related lumbar/sacral DRG, and the effect of carrageenan-induced prostate inflammation model on its expression levels, this study aimed to investigate the effects of PAR2 pharmacological inhibition. As discussed in Chapter 3, several *in vitro* assays demonstrated effective inhibition by

AZ8838 of multiple intracellular PAR2-specific responses. Based on these findings, the effects of AZ8838 were investigated *in vivo* using behavioural assessments to evaluate the potential in modulating pain responses associated with inflammatory conditions. Mechanical allodynia and thermal hyperalgesia were assessed in the rodent CAR-induced prostate inflammation model. Mechanical allodynia was tested using the von Frey filament test 2.12.1), and thermal hyperalgesia was measured through the Hargreaves (Plantar) test (Chapter 2, subsection 2.12.2). These tests allow a quantifiable evaluation of the possible analgesic effects of AZ8838 on pain behaviour associated with inflammation.

4.4.1 Mechanical allodynia assessment using von Frey filaments.

As described earlier, the mechanical nociceptive threshold was recorded for each rat at one, two, three, seven and 14 days after model induction surgery. As depicted in Figure 4.14A, nociceptive threshold (g) over time showed a significant reduction in mechanical sensitivity in CAR-treated groups compared to the saline control group (SAL/Vehicle). CAR-treated groups without AZ8838 pre-treatment showed a sharp decrease in nociceptive threshold by day 1, which persisted until day 14, indicating sustained mechanical allodynia. On days 1, 2, 3 and 7, the CAR treatment resulted in a significant decline of nociceptive threshold as shown in Figure 4.14. The decline reached its peak on day 3, with the CAR-vehicle-treated group showing a reduction to 7.8 ± 2.7 % of baseline and the CAR-none (untreated) group exhibiting a reduction to 11.28 ± 1.5 % of baseline in comparison to the sham (SAL) group (62.38 ± 19 % of baseline). AZ8838 at both 5 and 10 mg/kg doses mitigated CAR-induced reduction of nociceptive threshold, with statistically significant differences observed on Days 1, 2, 3, and 7 compared to untreated CAR groups (Figure 4.14 C). Animals treated with

AZ8838 exhibited a dose-dependent improvement of mechanical threshold. The higher dose, 10 mg/kg, mostly restored nociceptive threshold to levels comparable to the sham group (SAL/Vehicle) across all time points tested. Notably, on day 3, the 5 mg/kg dose of AZ8838 resulted in a mean relative mechanical threshold that is 48.7 ± 14 % of baseline, while the AZ8838 10 mg/kg dose recovered 79 ± 10.3% of baseline. These findings suggest that AZ8838 effectively alleviates CAR-induced mechanical allodynia in a dose-dependent manner in the murine prostate inflammation model.

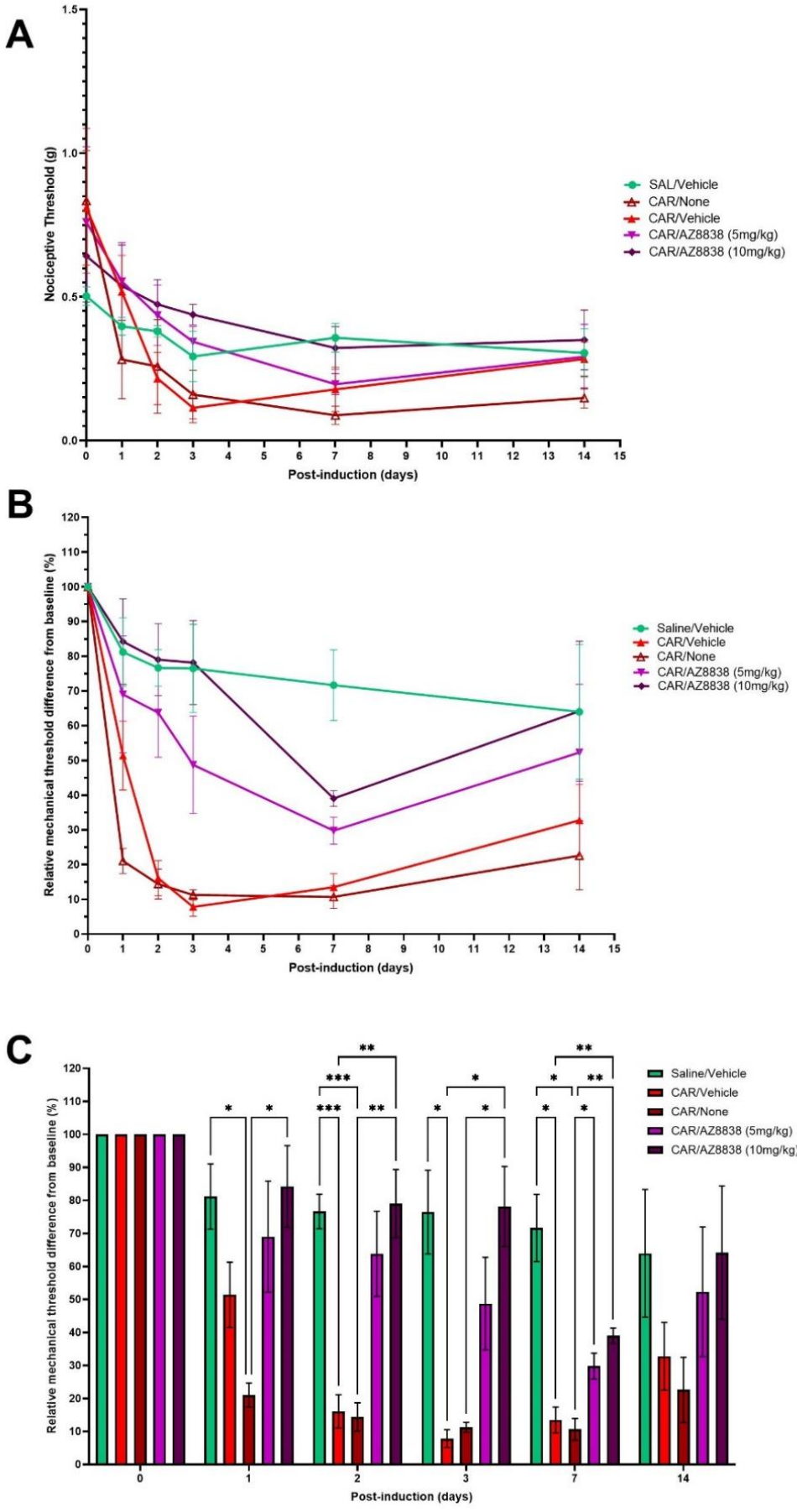
A
Nociceptive Threshold (g)
Post-induction (days)
SAL/Vehicle
CAR/None
CAR/Vehicle
CAR/AZ8838 (5mg/kg)
CAR/AZ8838 (10mg/kg)
B
Relative mechanical threshold difference from baseline (%)
Post-induction (days)
Saline/Vehicle
CAR/Vehicle
CAR/None
CAR/AZ8838 (5mg/kg)
CAR/AZ8838 (10mg/kg)
C
Relative mechanical threshold difference from baseline (%)
Post-induction (days)
Saline/Vehicle
CAR/Vehicle
CAR/None
CAR/AZ8838 (5mg/kg)
CAR/AZ8838 (10mg/kg)

Figure 4.14: AZ8838 treatment alleviates carrageenan (CAR)-induced mechanical allodynia in the prostate inflammation model.
(**A**) Nociceptive threshold (g) assessed using von Frey filaments over 14 days post-induction (mean ± SEM, $n = 5$). AZ8838 (5 mg/kg and 10 mg/kg) was administered orally one hour before induction. (**B**) Mechanical threshold relative to baseline (%), quantified over the test period. (**C**) Relative threshold differences at the tested time points post-induction, illustrating significant improvements in AZ8838-treated groups compared to untreated CAR groups. Data are presented as mean ± SEM, $n = 5$. Statistical analysis was performed using two-way ANOVA (*$p < 0.05$, **$p < 0.01$, ***$p < 0.001$).

4.4.2 Thermal hyperalgesia assessment using Hargreave's (Plantar) test.

In parallel with the mechanical allodynia assessment, the rat groups underwent thermal hyperalgesia assessment using Hargreave's test, ensuring a 15-minute interval between the two tests for each rat. As shown in Figure 4.15A, latency measurements (in seconds) over time showed an overall reduction in thermal sensitivity in CAR-treated groups compared to the saline control group (SAL/Vehicle). CAR-treated groups that are AZ8838 untreated (CAR/None and CAR/Vehicle) exhibited a marked reduction in latency values, indicative of thermal hyperalgesia. Significant reductions were observed on day 3 and continued through day 14 compared to the saline-treated control group (SAL/Vehicle). On day 3, the CAR-vehicle treated group showed a reduction to 86.8 ± 10 % of baseline latency and CAR-none (untreated) group exhibited a reduction to 64.5 ± 7.3 % of baseline in comparison to the sham group (124.7 ± 20 % of baseline). AZ8838 effectively alleviated thermal hyperalgesia in a dose-dependent manner. Notably, on both day 3 and 14, the 10 mg/kg dose restored latency values close to those observed in the SAL/Vehicle group, reaching 135.3 ± 21 % and 133 ± 22.8% of baseline, respectively, Figure 4.15C. These findings confirm that AZ8838 effectively alleviates CAR-induced thermal hyperalgesia in a dose-dependent manner in the murine prostate inflammation model, supporting its potential role as a therapeutic agent targeting PAR2-mediated inflammatory pain. The reduction

in allodynia and hyperalgesia by AZ8838 suggests its effectiveness in modulating pain pathways activated during inflammation.

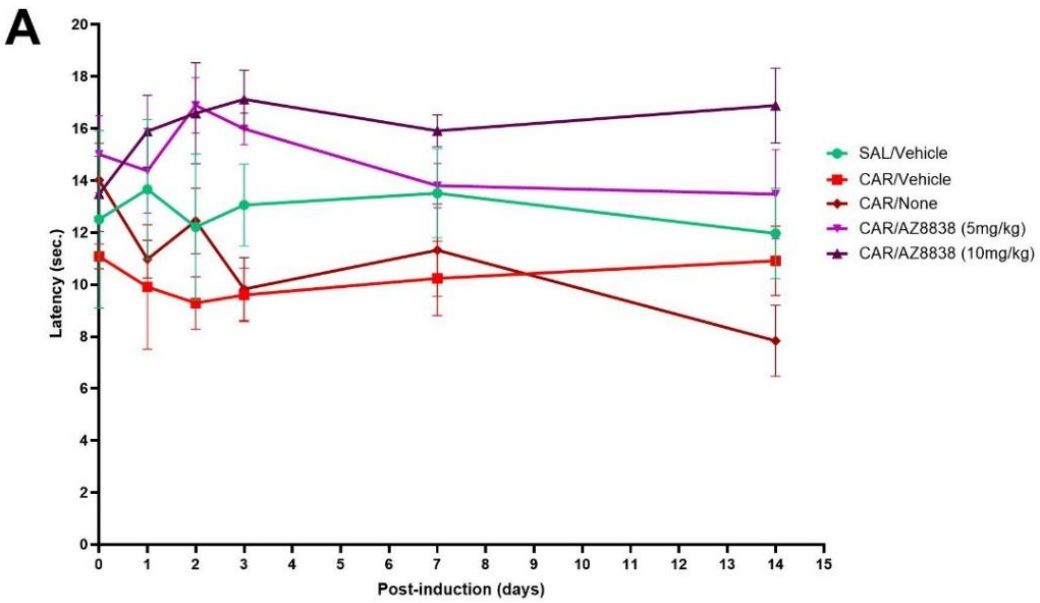
A
Latency (sec.)
Post-induction (days)
SAL/Vehicle
CAR/Vehicle
CAR/None
CAR/AZ8838 (5mg/kg)
CAR/AZ8838 (10mg/kg)

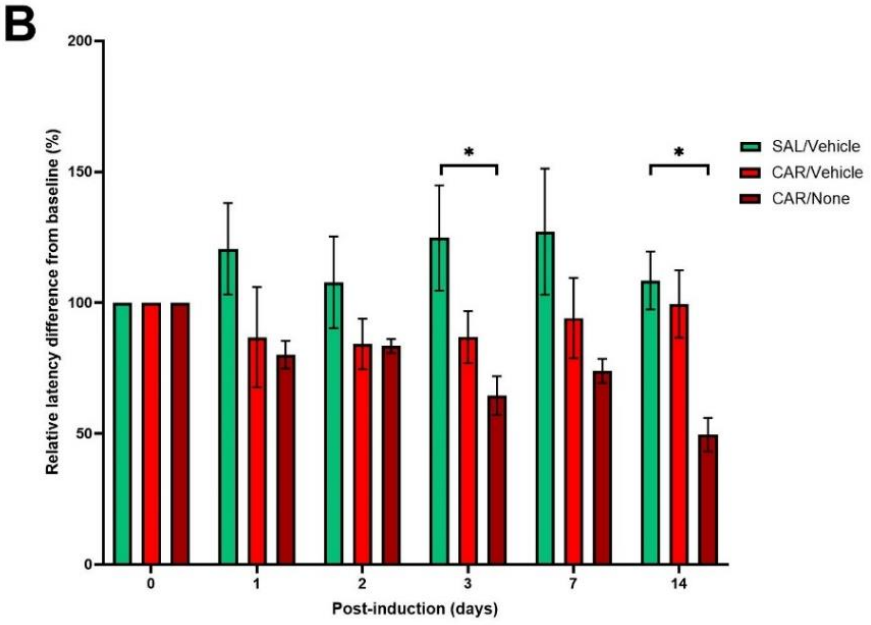
B
Relative latency difference from baseline (%)
Post-induction (days)
SAL/Vehicle
CAR/Vehicle
CAR/None
*
*

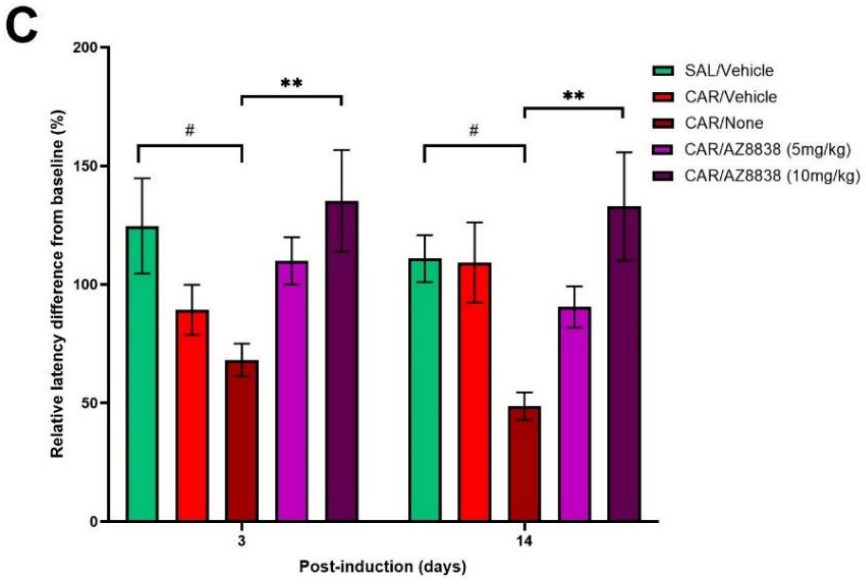
C
Relative latency difference from baseline (%)
Post-induction (days)
SAL/Vehicle
CAR/Vehicle
CAR/None
CAR/AZ8838 (5mg/kg)
CAR/AZ8838 (10mg/kg)
#
**
#
**

Figure 4.15: AZ8838 reduces carrageenan (CAR)-induced thermal hyperalgesia assessed by the Hargreaves test.
(**A**) Latency to heat stimuli over 14 days post-induction across treatment groups. (**B**) Relative latency difference from baseline in the CAR-treated and SAL-treated groups, showing persistent hyperalgesia, particularly in the CAR/None (vehicle untreated) group. (**C**) Comparison of relative latency differences at days 3 and 14, demonstrating dose-dependent effects of AZ8838. Data are presented as mean ± SEM, $n = 5$. Statistical analysis was performed using two-way ANOVA (*P < 0.05, **P < 0.01).

4.5 Discussion.

CP/CPPS is a complex condition characterised by inflammation and pain, with a limited understanding of its underlying mechanisms and effective treatments. PAR2 is a receptor known for its pivotal roles in mediating inflammation, and CP/CPPS is not an exception. Aiming to investigate the involvement of PAR2 in a murine model of this condition, initially, the inflammatory features in prostate tissue of carrageenan-induced prostatitis (CIP) were established. Additionally, this study aimed to investigate the changes in PAR2 expression level both locally in prostatic tissue and within the nociceptive afferents in lumbar/sacral dorsal root ganglia (L5, L6 and S1) in relation to the confirmed inflammatory state.

4.5.1 Carrageenan-induced prostatitis (CIP): inflammatory and pain components

Carrageenan-induced prostatitis (CIP) represents an established model to simulate the chronic inflammatory and pain characteristics of CP/CPPS, where inflammation is thought to be the main cause of the persistent pelvic pain (Radhakrishnan and Nallu, 2009). Several murine models were developed to study prostatitis, including spontaneous, infectious, immune-induced, hormone-associated and chemical-induced models, reviewed in (Vykhovanets et al., 2007, Wang et al., 2018). The CIP model was adopted in this study, being a well-validated representative model of chronic non-

infectious prostatitis associated with chronic pelvic pain, resembling category IIIA prostatitis according to NIH classification (see Chapter 1: section 1.5). A single intraprostatic injection of 3% λ carrageenan has been shown to induce prostate inflammation, without major tissue damage, associated with sustained pelvic pain for at least one week (Radhakrishnan and Nallu, 2009), with Zeng *et al* confirming this response for up to 14 days (Zeng et al., 2014). Carrageenan, a linear sulfated polysaccharide extracted from red seaweed (De Ruiter and Rudolph, 1997), is widely employed as an inflammogen in various *in vivo* animal models of localised tissue inflammation, including paw oedema, pleurisy, peritonitis, and muscle inflammation (Thomson and Fowler, 1981, Kehl et al., 2000, Morris, 2003, Necas and Bartosikova, 2013). Carrageenan is known to induce reproducible non-immunogenic inflammation, without systemic or severe organ pathology. In this study, the 72-hour post-surgical induction time point was found to display significant inflammatory morphologic and histological features in the initial pilot experiments and was followed for all later experiments (see Table 4.1 &

Figure 4.1).

Several *in vitro* studies suggested that carrageenan triggers inflammation through activation of Toll-like receptors (TLRs) and downstream NF-κB signalling pathways, leading to the release of inflammatory mediators such as prostaglandins, cytokines, and chemokines (Borthakur et al., 2007, Bhattacharyya et al., 2008). On the contrary, other studies, using HEK293-TLR4 reporter systems, reported that carrageenan, in all its forms, does not directly bind or activate TLR4 in this specific *in vitro* model (McKim, 2014, McKim et al., 2015). These findings suggest that carrageenans' *in vitro* effects might be cell type-specific or require cofactors. Supporting the role of TLR4 in

carrageenan-induced activation of NF-κB, a recent report demonstrated that TLR4 genetic deletion, CD14, besides intracellular adapter proteins MyD88 and TRIF, abolished carrageenan-induced IL-1β release through the NF-κB pathway in peritoneal (Lopes et al., 2020). Despite the ongoing debate over its direct interaction with TLR4, carrageenan consistently induces hallmark inflammatory features *in vivo*, including immune cell infiltration, oedema, NF-κB activation and elevated cytokine levels, across various animal models. These models have been widely utilised to screen anti-inflammatory properties of synthetic compounds and phytochemicals (Patil et al., 2019). Although carrageenan's direct binding to TLR4 might be cell-type-dependent or involve secondary pathways, its ability to induce robust induction of cyclooxygenase-2 (COX2), NF-κB and cell infiltration, has been has been consistently reported across multiple studies (Guo et al., 2023, Interdonato et al., 2023, Javed et al., 2024).

The CIP model shares these features and has been validated for persistent hyperalgesia and inflammation for up to 14 days post-induction (Zeng et al., 2014). Additional studies have revealed that carrageenan intraprostatic injection caused upregulation of mitochondrial integrity markers, including dynamin-related protein 1 (Drp-1), mitofusin-2 (MFN-2), NOD-like receptor family pyrin domain containing 3 (NLRP3), as well as neurogenic peptides, including substance P, and CGRP-receptor component protein (CGRP-RCP), potentially contributing to pain persistence (Wu et al., 2023). Even after 35 days post-induction, rat prostate tissue displayed increased expression of TLR4 and phosphorylation of p65 and p38, mirroring the LPS-induced inflammatory response in the human prostate epithelial cell line, suggesting the involvement of TLR4/MAPK p38/NF-κB signalling axis (Li et al., 2021). This

subsection will analyse inflammatory features within the prostate tissue in the CIP model. Special emphasis will be placed on the histological changes, PAR2 expression dynamics, and inflammatory pain that defines this model.

4.5.1.1 Inflammatory features in the CIP model

In the current study, the CIP model was successfully established by surgical intraprostatic injection of 3% carrageenan. At 72 hours post-induction, rats exhibited significant body weight loss, increased prostatic wet weight, and elevated prostatic index compared to sham controls (Table 4.1). These outcomes may reflect systemic stress and local prostate enlargement associated with inflammation. Histopathological analysis of prostate tissue sections revealed characteristic features of acute and chronic inflammation. Acute inflammation was evident by substantial neutrophil infiltration into the interstitial tissue and glandular lumens, occasionally progressing to abscess formation. Chronic inflammation was evident by the presence of lymphocytes and macrophages, suggesting sustained immune activation. Zeng *et al* confirmed the sustained inflammatory cell infiltration in this model, which was evident even at 14 days after induction (Zeng et al., 2014). Interestingly, a recent immunohistochemistry investigation demonstrated neurogenic inflammatory features within prostate tissue in the CIP model through the enhanced expression of substance P and CGRP-receptor component protein, a protein whose expression correlates with the biological efficacy of CGRP *in vivo*, that was evident for one to two weeks after induction (Wu et al., 2023).

4.5.1.2 Differential expression of PAR2 in DRG and prostate tissue

In this study, the expression of PAR2 in DRGs and the prostate was investigated within the CIP model. Study findings revealed a significant upregulation of PAR2 in the

prostate tissue of carrageenan-treated rats, as confirmed by immunofluorescence and Western blot analysis. No notable changes were observed in PAR2 expression within the lumbar and sacral DRGs (section 4.3). Interestingly, qRT-PCR demonstrated a significant reduction of PAR2 mRNA levels in the prostate (Figure 4.12), contrasting with the observed protein upregulation. Although mRNA and protein levels generally correlate, discrepancies have been documented and may result from post-transcriptional receptor modifications, alterations in protein stability, or translational regulation (Koussounadis et al., 2015, Buccitelli and Selbach, 2020). While most studies investigating PAR2 expression have reported consistent changes between mRNA and protein levels (Lee et al., 2018, Liu et al., 2022b, Quarta et al., 2024), mismatches have been reported. For instance, in macrophages, PAR2 activation led to elevated PAR2 mRNA expression, yet, unpredictably, reduced PAR2 protein expression was observed (Silva et al., 2023). This discrepancy suggests the involvement of complex regulatory mechanisms that may include irreversible receptor activation, β-arrestin-mediated endocytosis, and proteolytic degradation pathways, particularly in inflammatory settings. Moreover, methodological factors, like the semi-quantitative nature of Western blotting and the antibody-dependent specificity of immunofluorescence, can influence apparent expression levels. This emphasises the necessity of integrating data using various experimental approaches to provide a comprehensive insight into PAR2 dynamics under study conditions.

The findings of this study regarding elevated PAR2 protein expression in the prostate are consistent with previous studies using localised inflammatory models. For example, intra-articular carrageenan injection in rodents induced increased local expression of PAR2 in joints and associated nociceptors (Kelso et al., 2006, Denadai-

Souza et al., 2012). PAR2 antagonists have also been shown to attenuate inflammatory features of carrageenan-induced paw oedema, reducing both swelling and inflammatory markers (Lohman et al., 2012). These studies, along with the current results, suggest a key role of PAR2 in mediating inflammatory responses within carrageenan-induced preclinical models.

In humans, studies demonstrated functional expression of PAR2 in primary prostate cell cultures and prostate cell lines (Cottrell et al., 2004a, Myatt and Hill, 2005, Mannowetz et al., 2010, Paul et al., 2019, Noh et al., 2021). Mannowetz *et al*. showed PAR2 expression in both normal and pathological human prostate tissues using immunofluorescence staining. In normal human prostate samples, PAR2 expression was localised specifically to the apical margins of epithelial cells. In contrast, this pattern was shifted to the entire cell in cases of atypical prostatic hyperplasia and prostate cancer. Interestingly, benign prostatic hyperplasia specimens exhibited PAR2 expression exclusively within the stroma rather than the epithelia (Mannowetz et al., 2010).

In rodents, research investigating endogenous expression of PAR2 in the prostate is limited. Roman *et al* reported increased PAR2 expression in prostate tissue from NOD mice with experimental autoimmune prostatitis (EAP), which was induced by subcutaneous injection of rat prostate antigen (Roman et al., 2014). Notably, micro-dissection revealed that both epithelial and stromal compartments showed upregulated PAR2, with higher expression in stromal cells. Using immunofluorescence staining and co-localisation, Paul *et al* identified that prostate smooth muscle cells of stroma are the stromal cell type expressing PAR2, not fibroblasts (Paul et al., 2019).

In this study, Wistar rats' normal prostate tissue showed PAR2 expression restricted to epithelial cells, rather than stroma, which was significantly increased following carrageenan-induced inflammation (Figure 4.9). This displays a common endogenous expression of PAR2 within normal prostate among species, with potential variations in cell-type localisation and functional roles during inflammation.

In the neural compartment, PAR2 expression in DRG has been investigated in several rat pain models. Early studies identified PAR2 localisation on the plasma membrane and intracellular compartments of rat DRG neuronal soma and nerve fibre, linking PAR2 neural expression and neurogenic pain and inflammation (Steinhoff et al., 2000a). PAR2 mRNA has been detected in rat lumbar L4- L6 DRG but not in corresponding spinal cord segments, and confirmed direct involvement of peripheral PAR2 specifically in thermal, but not mechanical hyperalgesia (Kawabata et al., 2001, Zhu et al., 2005). Current findings confirmed basal endogenous expression of PAR2 in lumbosacral neurons of DRG, primarily on the plasma membrane and intracellularly (

Figure 4.6), but remained unchanged following prostate inflammation.

Few studies have explored changes in PAR2 expression level in pain and inflammation models within DRG neurons. Liu *et al* reported a time-dependent increase in PAR2 expression in DRG sections and tissue lysate within a cancer bone pain model induced in mice by tumour cell implantation (Liu et al., 2014b). Similarly, a neuropathic pain model induced by chronic constriction of a major nerve in rats resulted in PAR2 overexpression within the DRG neurons, confirmed through Western blot and immunostaining (Zhang et al., 2018). Increased PAR2 expression was also reported in rodent DRG tissue of limbs affected in a femoral artery ligation model (Xing and Li,

2017). Few studies have explored whether peripheral inflammation alters PAR2 in associated DRGs. Interestingly, a study specifically investigated the role of neural PAR2 in pain behaviours by employing conditional PAR2 knockout in DRG sensory neurons only within a paw-inflammation model induced by PAR2-AP and neutrophil elastase (Hassler et al., 2020). The study revealed that mechanical hyperalgesia and facial grimacing were dependent on neural PAR2, whereas thermal hyperalgesia remained unaffected.

The results of the current study showed that PAR2 levels in DRG neurons remained unchanged despite prostate inflammation, suggesting that inflammatory tissue injury does not necessarily alter PAR2 expression within associated neural tissue.

4.5.2 AZ8838 ameliorates carrageenan-induced pain, with insignificant anti-inflammatory effects

This study showed that AZ8838 significantly reduced pain-related behaviours associated with the CIP model. However, its impact on prostatic inflammation was minimal, as evidenced by histological assessments (

Figure 4.2 and Figure 4.4). A similar dosing approach was applied in the PAR2-induced paw oedema model, where AZ8838 demonstrated a significant anti-inflammatory profile, including reduced oedema, neutrophil activation, mast cell degranulation, and myeloperoxidase (MPO) activity (Kennedy et al., 2020). In the current study, similar to AZ8838, mild anti-inflammatory effects were observed for Celecoxib, which despite its well-documented anti-inflammatory properties (Pinheiro and Calixto, 2002, Choi et al., 2020), also showed modest histological protection in this model, indicating potential limitations in tissue penetration and model-specific

responsiveness. Importantly, prostate tissue penetration is a known pharmacokinetic challenge. Celecoxib has shown the highest prostate tissue penetration and retention among four other NSAIDs (naproxen, ibuprofen, and diclofenac) following single oral treatment in healthy rats (Yellepeddi et al., 2018). Despite this, celecoxib's mild anti-inflammatory effect in the current study might reflect differences in model-specific factors like inflammation severity, differential penetration under inflammatory conditions or insufficient dosing relative to tissue accumulation under disease conditions. Despite AZ8838's analgesic effect in this model, its weak anti-inflammatory effects may be linked to dosing limitations or dynamic tissue-specific pharmacokinetics that need to be addressed.

Regarding *in vivo* pain behavioural studies, AZ8838 demonstrated significant mitigation of carrageenan-induced mechanical allodynia and thermal hyperalgesia in a dose-dependent manner, as assessed through von Frey filaments and Hargreaves tests (Figure 4.14 and Figure 4.15). The observed results with AZ8838 treatment are consistent with the established role of PAR2 in modulating pain pathways, as evidenced by numerous studies demonstrating effective inhibition of pain behaviour by other PAR2 antagonists. Carrageenan-evoked pain has been shown to be associated with PAR2 activity, as demonstrated in multiple *in vivo* studies. Using PAR2-knockout mice, a significant reduction of carrageenan-induced inflammatory pain was evident, highlighting PAR2's role in mediating pain (Vergnolle et al., 2001a). This involvement was consistently reported with several studies specifically investigating the role of spinal PAR2, via intrathecal administration of PAR2-AP, and showed that it causes exacerbation of carrageenan-induced thermal hyperalgesia (Mrozkova et al., 2021), indicating the pain-potentiating effects of PAR2 within the CNS. Notably, the same

study reported that PAR2 peptide antagonist intrathecal treatment alleviated carrageenan-induced thermal hyperalgesia, reducing pain sensitivity by over 30 % compared to untreated controls. Similarly, spinal PAR2 blocking (GB83), or the use of PAR2 knockout mice, significantly diminished pain sensitivity in chronic arthritis models (Muley et al., 2016, Muley et al., 2017, Lucena and McDougall, 2020). Moreover, disarming proteases (e.g. calpain I) demonstrated a significant increase in withdrawal thresholds in both carrageenan- and tryptase-induced joint inflammation models (McDougall et al., 2021). Comparable outcomes have been reported across other inflammatory pain models, including those stimulating visceral pain (Cattaruzza et al., 2011, Shah et al., 2020, Manoj, 2023), bladder pain (Chen et al., 2016, Tsubota et al., 2018) and pelvic pain (Roman et al., 2014).

To our knowledge, this is the first *in vivo* investigation of AZ8838 effects employing an inflammatory pain model. Earlier work demonstrated its anti-inflammatory potential in a rodent paw oedema model. AZ8838 reduced paw swelling by 60%, neutrophil and mast cell activity by 50% and normalised myeloperoxidase (MPO) activity in 2fLIG-induced paw oedema (Kennedy et al., 2020). The observed pain-alleviating effect of AZ8838 in the current study could be attributed to disrupting the role of PAR2 to sensitise several reported ion channels in sensory nociceptors like transient receptor potential vanilloid 1 (TRPV1). PAR2 activation by endogenous proteases such as trypsin and mast cell tryptase triggers downstream signalling cascades involving PKC and PKA, ultimately leading to enhancing nociceptor excitability (Mrozkova et al., 2016). In the context of inflammatory pain, PAR2 has been shown to sensitise TRPV4 channels through adenylyl cyclase- and PKA-dependent mechanisms, causing neuronal hyperexcitability and sustained mechanical

hyperalgesia (Poole et al., 2013, Zhao et al., 2015). Other studies reported similar PAR2-sensitising effects of other pain-sensing ion channels, including TRPV1 (Mrozkova et al., 2021, Scheff et al., 2022), TRPA1 (Chen et al., 2016, Ceuleers et al., 2018), acid-sensing ion channel 3 (ASIC3) (Wu et al., 2017) and ATP receptors P2X3 (Wang et al., 2012). Furthermore, PAR2 activation during chronic inflammation has been linked to neurogenic inflammation through the release of pro-inflammatory neuropeptides such as substance P and CGRP, further amplifying inflammatory and pain responses (Shah et al., 2020). In prostate inflammation models, one study demonstrated that PAR2 sensitises TRPV1 channels, evidenced by the enhanced capsaicin-induced TRPV1 activation and elevated intracellular Ca2+ levels in DRG neurons from EAP mice, which was abolished in PAR2 KO mice, highlighting PAR2's role in sensitising TRPV1in a pelvic pain model (Roman et al., 2014).

Interestingly, a recent study using a β-arrestin biased PAR2 antagonist, C781, showed that carrageenan-induced nociceptive effects were not altered in male and female mice pre-treated with C781 (Kume et al., 2023b). C781was shown to effectively reduce β-arrestin recruitment and MAPK phosphorylation, while having no effects on the Gq/Ca^{2+} signalling pathway induced by various concentrations of selective PAR2-AP (Schiff et al., 2023). Results of the current study demonstrated effective Gq/Ca^{2+} mobilisation inhibition by AZ8838 (Figure 3.36 and Figure 3.37), potentially contributing to the observed significant inhibition of pain behaviour in the *in vivo* study. By antagonising PAR2, AZ8838 likely inhibits these signalling pathways, thereby reducing peripheral and spinal sensitisation to inflammatory stimuli.

4.5.3 Implications, study limitations and future directions

The present findings underscore PAR2's role in inflammatory pain responses within the context of carrageenan-induced prostatitis (CIP). The unique mechanism of PAR2 activation, involving protease-mediated tethered ligand exposure, along with conformational diversity and potential dimerisation or crosstalk with other receptors, presents significant challenges in the development of effective PAR2 modulators. These complexities, besides the difficulty in isolating condition-specific endogenous protease activators and the consequent receptor states, complicate pharmacological targeting strategies and have slowed the translation of PAR2 antagonists into clinical applications (McIntosh et al., 2020). The ability of AZ8838 to attenuate nociceptive behaviours identify its therapeutic potential for managing chronic pelvic pain in CP/CPPS. The significant inhibition of both mechanical allodynia and thermal hyperalgesia in the current study aligns with prior research showing the effectiveness of PAR2 antagonists in various inflammatory pain models, including carrageenan-induced paw oedema, arthritis, and visceral pain. The discrepancy between PAR2 mRNA and protein expression levels in the prostate tissue and insignificant changes in the associated DRG require further investigation of post-transcriptional and translational mechanisms regulating PAR2 expression during inflammation. While AZ8838's analgesic effects in the CIP model were evident, its weak anti-inflammatory effects present certain limitations in this study design. The effect of a single pre-induction dose was investigated, which may not have provided a sustained effect throughout the inflammatory process. Moreover, tissue-specific pharmacokinetics and possible limited drug penetration into the prostate could have constrained its anti-inflammatory impact in this model. Additionally, while AZ8838 effectively inhibited

PAR2 activity in the prostate inflammation, its broader impact on local and systemic inflammatory mediators, pain and inflammatory effects in other organ inflammatory pain models remains unclear. Carrageenan-induced prostate inflammation is one of the multiple preclinical prostate inflammation models that could be investigated to provide further insights into PAR2's role in the aetiology of pelvic pain (He et al., 2023).

Future research could focus on optimising the dosing regimen of AZ8838, including repeated or post-induction administration, to address the possibility of insufficient tissue-level concentrations. Additionally, a detailed evaluation of AZ8838's tissue distribution and retention within the prostate is necessary to confirm its local bioavailability and support its anti-inflammatory potential. Also, Future research is required to understand the molecular mechanisms by which PAR2 antagonism modulates nociceptive pathways, possible interactions with pain-sensing ion channels such as TRPV1 and TRPA1 and the involvement of neuropeptides like CGRP. High-resolution imaging, cellular transcriptomics, and proteomics could help to visualise the spatial and time-based dynamics of PAR2 expression/signalling in inflamed tissues. Clinical translation necessitates pharmacokinetic and safety profiling of AZ8838, along with investigations into its effects in advanced humanised models of inflammation and pain (Lebonvallet et al., 2021).

4.6 Conclusion

This study provides compelling evidence that PAR2 plays a pivotal role in the pathophysiology of CIP, driving nociceptive responses. AZ8838 effectively mitigated pain responses, supporting its potential as a therapeutic candidate for chronic pelvic pain and inflammation. By targeting PAR2, AZ8838 not only offers symptom relief but also highlights the potential of PAR2 antagonism as a broader therapeutic strategy.

These findings may support future studies on the continued development of PAR2 antagonists as therapeutic agents and highlight the need for further investigations aiming to understand PAR2 signalling in chronic inflammatory diseases.

Chapter 5

General Discussion

5.1 Introduction

Chronic pain and inflammation are hallmark features of chronic prostatitis/chronic pelvic pain syndrome (CP/CPPS), a condition with poorly understood pathophysiology and limited effective treatment options. Among the key molecular players implicated in pain sensitisation in the context of inflammation, PAR2 has emerged as a critical mediator across multiple preclinical models of inflammatory pain involving the prostate, skin, GI tract, and other peripheral tissues (Roman et al., 2014, Kido et al., 2021, Mrozkova et al., 2021, Barra et al., 2022, Mason et al., 2023). Endogenous stimulation of PAR2 by proteases, such as trypsin, mast cell tryptase, and neutrophil elastase, has been shown to drive pro-inflammatory signalling cascades (de Almeida et al., 2020), increase nociceptor sensitivity (Mrozkova et al., 2021), and modulate pain perception via neuroimmune interactions (Zhao et al., 2015, Fan et al., 2024). Understanding the role of PAR2 in the context of prostate inflammation and pain signalling is therefore essential for identifying new therapeutic targets for CP/CPPS and related conditions.

Despite the extensive *in vitro* evidence demonstrating the contribution of PAR2 to inflammatory signalling, its specific role in the context of *in vivo* prostate inflammatory models remains largely unexplored. Previous studies have reported that PAR2 enhances neurogenic inflammation, promotes cytokine and chemokine release, and sensitises nociceptive ion channels such as TRPV1, TRPV4, and ASIC3, leading to enhanced pain perception (refer to subsections 1.10.5 and 1.10.5). However, the extent to which PAR2 inhibition can ameliorate prostate-associated pain and inflammation has not been systematically investigated (1.10.6). This thesis aimed to

bridge this gap by integrating cellular and preclinical models to examine the role of PAR2 in CP/CPPS.

The key findings of this work demonstrated significant upregulation of PAR2 in prostate tissue following carrageenan-induced inflammation (CIP model) (

Figure 4.10), accompanied by pain hypersensitivity. Surprisingly, despite the critical role of PAR2 in nociceptive signalling, its expression remained unchanged in sensory neurons of DRG. However, pharmacological inhibition of PAR2 using AZ8838 significantly alleviated mechanical allodynia and thermal hyperalgesia (Figure 4.14, Figure 4.15), underscoring PAR2's involvement in inflammatory pain processing in this model. AZ8838 *in vitro* studies conducted in this work showed significant potential of this molecule to inhibit PAR2-mediated signalling pathways, including NF-κB activation, its nuclear translocation, ERK1/2 phosphorylation, PAR2 internalisation and IL-8 production. These findings underscore the complex interplay between peripheral inflammation, neuronal sensitisation, and receptor signalling, providing novel insights into the potential therapeutic benefits of targeting PAR2 in CP/CPPS.

This chapter will discuss the correlation between in vitro and in vivo studies, compare them to other inflammatory pain models used to examine PAR2 roles, explore the biological and clinical relevance of PAR2 signalling, examine study limitations and future challenges, and investigate the therapeutic implications of PAR2 antagonism in inflammatory pain conditions.

5.2 Mechanistic insights from *in vitro* and *in vivo* findings

In vitro studies investigating the molecular mechanisms of PAR2 activation in DU145 prostate epithelial cells confirmed functional receptor responsiveness. These studies demonstrated that DU145 endogenously express PAR2 and responds to its activation, leading to ERK phosphorylation (Figure 3.29) and receptor internalisation in PAR2-YFP-transfected cells (

Figure 3.40). Both effects are key downstream responses of inflammation. Notably, AZ8838, a potent PAR2 antagonist, effectively blocked these responses (Figure 3.30 and

Figure 3.41), reinforcing the pro-inflammatory role of PAR2 in prostate cells. These results correlated with the enhanced PAR2 expression in prostate tissue following carrageenan-induced inflammation in the *in vivo* studies (

Figure 4.10, Figure 4.11 and Figure 4.13). It is noteworthy that, despite robust inhibition of PAR2 signalling in vitro, AZ8838 did not reduce total inflammatory cell infiltrate in CIP. This may reflect PAR2-independent drivers of carrageenan inflammation, agonist heterogeneity *in vivo*, limited prostatic exposure, or limited sensitivity of H&E counts for detecting changes in the inflammatory state.

To gain deeper insights into PAR2 involvement in this prostate inflammation model, future studies could utilise PAR2 knockout (KO) animals to assess the inflammatory and behavioural consequences of PAR2 deficiency and correlate with specific PAR2 roles. This approach has been previously applied in an autoimmune prostatitis (EAP) model of CP/CPPS, where wild-type (WT) mice exhibited a significant increase in ERK phosphorylation in sacral DRGs 30 days post-induction, while PAR2 KO mice

showed a response equivalent to baseline (Roman et al., 2014). Additionally, the same study reported that capsaicin (TRPV1 agonist)-induced calcium mobilisation in DRG neurons was abolished in naïve and PARK2 KO-EAP mice, suggesting that EAP-induced neuronal hypersensitivity is dependent on PAR2. However, histological analysis of the prostate revealed no significant difference in inflammatory cell infiltration or mast cell activation between wild-type and the PAR2 KO-EAP mice, indicating that PAR2 mainly contribute to pain rather than prostatic inflammation.

Beyond the ERK1/2 pathway, PAR2 activation has also demonstrated significant activation of NF-κB signalling, a critical pathway in inflammation and immune responses. The *in vitro* findings of this study demonstrated that stimulation of PAR2 with 2fLIG and trypsin significantly enhanced NF-κB transcriptional activity (Figure 3.4), which was effectively inhibited by AZ8838 (Figure 3.6). Previous studies examining PAR2 antagonists have demonstrated their ability to inhibit NF-κB signalling and suppress pro-inflammatory IL-8 expression (Goh et al., 2009). NF-κB inhibitory capability of these PAR2 antagonists has been linked to their *in vivo* anti-inflammatory effects, including the reduction of PAR2-induced vascular permeability, further supporting the potential implication of PAR2 antagonists in inflammatory conditions (Kanke et al., 2009). These findings have strong implications for the *in vivo* CIP model, as chronic inflammation is often driven by NF-κB signalling in prostate tissues, which regulates the expression of pro-inflammatory cytokines such as IL-8. Studies employing the autoimmune prostatitis model *in vivo* have shown elevated phosphorylated p65 (p-p65) levels in prostate tissue of EAP animals compared to controls, indicating enhanced NF-κB activation in the inflamed prostate (Zhang et al., 2020b, Liu et al., 2022a). Additionally, a report identified a cooperative interaction

between platelet-activating factor (PAF) and PAR2 in the context of inflammation and demonstrated that PAR2 antagonism exhibited inhibition of PAF-mediated pro-inflammatory effects through inhibition of NF-κB activity (Silva et al., 2023). This effect was examined *in vivo*, showing a significant inhibition in neutrophil recruitment, leukocyte rolling and adhesion, local tissue inflammation and chemokine release, all induced by a PAF analogue. This evidence highlights the potential of PAR2 inhibition to exert broader anti-inflammatory effects by interfering with other synergistic pathways in inflammation.

5.3 AZ8838 as a PAR2 antagonist: mechanism of action in pain and inflammation

As discussed earlier (section 3.8), data from the current study present AZ8838 as a potent small molecule PAR2 antagonist effectively inhibiting key cellular response elements induced by endogenous protease (trypsin) or selective PAR2-AP (2fLIG). AZ8838 *in vivo* study also demonstrated effective inhibition of pain behaviour in the CIP model. In a similar pattern, several previous studies have examined the effects of PAR2 antagonists on inflammatory signalling and pain modulation. C391, a partial PAR2 agonist, effectively antagonised PAR2-mediated MAP kinase signalling (14.3 μM) and intracellular calcium mobilisation (IC_{50} 1.3 μM). In the *in vivo* model of mast cell degranulation-induced paw inflammation, C391 significantly reduced thermal hyperalgesia, indicating that PAR2 antagonists capable of inhibiting cellular Ca^{2+} mobilisation and MAPK can potentially modulate inflammation-associated pain (Boitano et al., 2015). Another selective PAR2 antagonist, ENMD-1068, that has been shown to inhibit PAR2-induced calcium mobilisation in vitro (Kelso et al., 2006), was found recently to briefly minimise post-operative incisional pain in a murine model,

particularly during the early post-surgical period (Kido et al., 2021). In line with these investigations of PAR2 antagonists, C781 was identified as a biased PAR2 antagonist that selectively inhibits β-arrestin/MAPK pathway without significantly affecting Gq/Ca^{2+} signalling (Schiff et al., 2023). In preclinical models, C781 effectively prevented and reversed mechanical and spontaneous nociceptive behaviours in response to PAR2-AP (2-aminothiazole-LIGR-NH2), mast cell activators, and neutrophil elastase (Kume et al., 2023b). Current findings on AZ8838's inhibition of PAR2-specific cellular responses and its pain-minimising effects in the *in vivo* CIP prostate inflammation model align with these studies, suggesting the therapeutic potential of this compound in mitigating PAR2-driven inflammation and pain.

Studies have explored the mechanisms of PAR2-mediated pain responses and demonstrated its ability to sensitise transient receptor potential (TRP) channels, such as TRPV1 and TRPV4. As discussed earlier (subsection 4.5.2) this interaction has been shown to be dependent on the activity of PKC, PKA, and Rho kinase downstream of PAR2 activation. These studies have confirmed that the intracellular calcium mobilisation induced by PAR2 activation in sensory neurons occurs via these kinases, ultimately resulting in enhanced pain sensitivity. It is worth mentioning that a study by Linley *et al.* (2008) indicated that the activation of PAR2 in nociceptive neurons strongly inhibits M-type potassium currents (Kv7 channels), leading to neuronal depolarisation and increased excitability. This effect was also dependent on PLC activation, which triggered intracellular calcium mobilisation and PIP2 depletion (Linley et al., 2008). The study assessed the cellular effects in an *in vivo* paw-inflammation model and reported that pharmacological blockade of Kv7 channels using XE991 mimicked the effects of PAR2 activation. Future studies may confirm

PAR2-mediated inhibition of these channels utilized a specific Kv7 channel activator, such as flupirtine, to counteract this effect, thereby verifying the role of PAR2 in modulating Kv7 channel activity in inflammatory pain.

In the following sections, the limitations of this study will be critically evaluated, addressing methodological constraints, potential confounding factors, and challenges encountered during the experimental process. Additionally, future research directions will be explored, emphasising key areas for further investigation that could enhance our understanding of PAR2-mediated inflammation and pain, as well as the therapeutic potential of AZ8838 in CP/CPPS and other inflammatory conditions.

5.4 Study limitations, challenges and future directions

5.4.1 Study limitations and challenges in targeting PAR2 as a therapeutic strategy

Since its initial discovery of the receptor (Nystedt et al., 1994), and despite its well-established role in inflammation and pain signalling, over 30 years of investigations have yet to yield a clinically approved drug targeting this receptor. This is largely attributed to the several challenges associated with developing PAR2-targeted therapy (McIntosh et al., 2020). One of the primary challenges is the receptor's unique activation mechanism, involving proteolytic cleavage of the receptor itself, exposing a specific amino acid sequence (tethered ligand) capable of interacting with the rest of the receptor and turning on its intracellular signalling cascades. Unlike classical GPCRs (1.6.2), competitive agonists or antagonists could specifically target that at their orthosteric binding sites, PAR2 lacks a freely circulating endogenous ligand, making its pharmacological modulation particularly complex.

Another major challenge is the ability of multiple proteases to activate PAR2 at different cleavage sites, leading to diverse and context-dependent signalling outcomes. This presents a challenging design of a single antagonist that can effectively inhibit all modes of endogenous PAR2 activation. Additionally, receptor capability of dimerisation and crosstalk with other GPCRs contributes to the complexity of its signalling. For instance, studies have demonstrated that PAR1 and PAR2 form functional heterodimers in vascular and inflammatory contexts, making selective inhibition of PAR2 a significant pharmacological challenge (Lee-Rivera et al., 2022).

Bioavailability, metabolic stability, and receptor selectivity offered an initial challenge in the process of developing small-molecule PAR2 inhibitors. *In vivo* investigations of peptide-based inhibitors such as FSLLRY-NH2 and ENMD-1068 demonstrated issues related to their stability and potency despite their capacity to inhibit PAR2 signalling *in vitro* (McIntosh et al., 2020). Non-peptide inhibitors, such as AZ8838 and AZ3451, have the advantage of improved pharmacokinetic properties, but further *in vivo* investigations and optimisation are needed for clinical translation. It is worth mentioning that PAR2 is exerting both pro-inflammatory and tissue-protective responses that may add a layer of complexity; complete inhibition of PAR2 signalling might not be desirable in certain contexts (Piran et al., 2016).

Despite these challenges, advancements in structural biology have provided valuable insights into the ligand-binding sites of PAR2, enabling the rational design of antagonists. The development of monoclonal antibodies targeting PAR2, such as MEDI0618, is currently in phase II clinical trials (ClinicalTrials.gov, 2024) after completing two pharmacokinetics, safety and tolerability clinical trials in healthy volunteers (ClinicalTrials.gov, 2019, ClinicalTrials.gov, 2022), highlights the

potential of biologic therapies to overcome some of these pharmacological hurdles. Nevertheless, further research is required to determine the long-term safety and efficacy of small-molecule PAR2 inhibitors in relevant chronic inflammatory diseases, including CP/CPPS.

5.4.2 Implications for CP/CPPS and future directions

The findings from this study underscore the critical role of PAR2 in prostate inflammatory pain, reinforcing the potential of PAR2 antagonism as a therapeutic strategy for CP/CPPS. Future research could focus on specifically understanding the role of PAR2 in the CIP model, utilising genetic approaches, such as PAR KO rats. Emerging techniques, including CRISPR-based genome editing, have been proposed to modulate PAR2 expression in inflammatory conditions. A recent study demonstrated that delivering CRISPR-Cas9 systems via nanosized albumin carriers effectively downregulated PAR2 expression, reducing inflammation through modulation of the TLR4/NF-κB axis (Li et al., 2025). Specifically, Li et al (2025) reported that these albumin-based CRISPR-Cas9-PAR2 nanoparticles achieved up to an 80-90% reduction in pro-inflammatory cytokines, including IL-6, IL-1β and CCL5, by suppressing TLR4/NF-κB/ERK/(stimulator of interferon genes) STING signalling cascade, beside alleviation of systemic inflammation and improving survival in cytokine-storm and sepsis models, showing the therapeutic promise of PAR2 gene silencing in inflammatory conditions. Applying this approach to prostate inflammation models could offer a convenient tool to isolate PAR2-driven inflammatory effects in CP/CPPS. Furthermore, looking at specific PAR2-specific downstream signalling elements within the CIP model could provide deeper mechanistic insight into PAR2

involvement in the disease. Detailed profiling of the anti-inflammatory effects of AZ8838 could reveal its therapeutic potential for this disease.

One interesting avenue for future research is the exploration of nanomedicine-based delivery systems for PAR2 antagonists. Recent studies have demonstrated the feasibility of utilising receptor-mediated endocytosis of PAR2 to facilitate targeted drug delivery to inflamed tissues. For instance, a recent study demonstrated the use of PAR2 as a probe, utilising PAR2 activation-triggered receptor endocytosis, to direct targeted delivery systems to the relevant PAR2-expressing cells (Chen et al., 2024). In the context of CP/CPPS, designing nanoparticles loaded with PAR2 inhibitors like AZ8838 could provide a means of achieving sustained inhibition of PAR2-mediated inflammation within the prostate tissue. Nanomedicine-based delivery of PAR2 antagonist, AZ3451, to internalised PAR2 inside organelles provides sustained pain relief in the colon inflammation model (Teng et al., 2024).

Finally, additional research is needed to assess the broader systemic effects of PAR2 inhibition. While AZ8838 has shown efficacy in mitigating prostate pain *in vivo*, it remains unclear whether long-term PAR2 inhibition might impact other physiological processes, such as immune homeostasis, tissue repair, or vascular function. Comprehensive pharmacokinetic and toxicological studies will be essential for advancing AZ8838 and other PAR2-targeted therapeutics to clinical application.

5.5 General conclusion

This study provides evidence supporting the role of PAR2 in mediating prostate inflammatory pain responses in CP/CPPS. The study's in vitro findings confirmed the existing evidence that PAR2 activation leads to NF-κB signalling, intracellular Ca2+

mobilisation, ERK phosphorylation and receptor internalisation at the molecular level. The *in vivo* data further confirmed that PAR2 is upregulated in inflamed prostate tissues, and its inhibition using AZ8838 effectively mitigates pain behaviours and inflammatory features within affected tissue. These findings establish a foundation for further research into PAR2-targeted therapies for chronic prostate inflammatory conditions.

Despite the progress made, several challenges remain in translating these findings into clinical applications. The unique activation mechanism of PAR2, its crosstalk with other inflammatory and pain pathways, and the complexities of protease-mediated signalling necessitate further exploration of selective and potent PAR2 antagonists. Future research should focus on investigating the possible crosstalk between PAR2 and other key inflammatory and pain mediators involved in the studied condition, optimising drug delivery methods, exploring pharmacokinetic characteristics, and conducting long-term studies to evaluate the safety and therapeutic potential of PAR2 inhibition in CP/CPPS and other inflammatory diseases.

In conclusion, targeting PAR2 represents a promising approach for managing chronic prostate inflammatory pain syndromes. The findings from this study contribute to a growing body of evidence supporting the therapeutic potential of PAR2 antagonists and provide valuable insights for developing novel strategies to manage pain and inflammation. Further investigations will be crucial in translating these discoveries into effective clinical treatments for CP/CPPS and related conditions.

References

ACTOR, J. K. 2019. Chapter 2 - The Inflammatory Response. *In:* ACTOR, J. K. (ed.) *Introductory Immunology (Second Edition).* Academic Press.

ADAM, E., HANSEN, K. K., ASTUDILLO, O. F., COULON, L., BEX, F., DUHANT, X., JAUMOTTE, E., HOLLENBERG, M. D. & JACQUET, A. 2006. The house dust mite allergen Der p 1, unlike Der p 3, stimulates the expression of interleukin-8 in human airway epithelial cells via a proteinase-activated receptor-2-independent mechanism. *Journal of Biological Chemistry,* 281**,** 6910-6923.

ADAMS, M. N., RAMACHANDRAN, R., YAU, M. K., SUEN, J. Y., FAIRLIE, D. P., HOLLENBERG, M. D. & HOOPER, J. D. 2011. Structure, function and pathophysiology of protease activated receptors. *Pharmacol Ther,* 130**,** 248-82.

AKERS, I. A., PARSONS, M., HILL, M. R., HOLLENBERG, M. D., SANJAR, S., LAURENT, G. J. & MCANULTY, R. J. 2000. Mast cell tryptase stimulates human lung fibroblast proliferation via protease-activated receptor-2. *American Journal of Physiology-Lung Cellular and Molecular Physiology,* 278**,** L193-L201.

AL-ANI, B., SAIFEDDINE, M. & HOLLENBERG, M. D. 1995. Detection of functional receptors for the proteinase-activated-receptor-2-activating polypeptide, SLIGRL-NH2, in rat vascular and gastric smooth muscle. *Canadian journal of physiology and pharmacology,* 73**,** 1203-1207.

AL-ANI, B., SAIFEDDINE, M., WIJESURIYA, S. J. & HOLLENBERG, M. D. 2002. Modified proteinase-activated receptor-1 and-2 derived peptides inhibit proteinase-activated receptor-2 activation by trypsin. *Journal of Pharmacology and Experimental Therapeutics,* 300**,** 702-708.

AMADESI, S., COTTRELL, G. S., DIVINO, L., CHAPMAN, K., GRADY, E. F., BAUTISTA, F., KARANJIA, R., BARAJAS-LOPEZ, C., VANNER, S., VERGNOLLE, N. & BUNNETT, N. W. 2006. Protease-activated receptor 2 sensitizes TRPV1 by protein kinase Cepsilon- and A-dependent mechanisms in rats and mice. *J Physiol,* 575**,** 555-71.

AMADESI, S., NIE, J., VERGNOLLE, N., COTTRELL, G. S., GRADY, E. F., TREVISANI, M., MANNI, C., GEPPETTI, P., MCROBERTS, J. A., ENNES, H., DAVIS, J. B., MAYER, E. A. & BUNNETT, N. W. 2004. Protease-activated receptor 2 sensitizes the capsaicin receptor transient receptor potential vanilloid receptor 1 to induce hyperalgesia. *J Neurosci,* 24**,** 4300-12.

ASADUZZAMAN, M., DAVIDSON, C., NAHIRNEY, D., FITEIH, Y., PUTTAGUNTA, L. & VLIAGOFTIS, H. 2018. Proteinase-activated receptor-2 blockade inhibits changes seen in a chronic murine asthma model. *Allergy,* 73**,** 416-420.

ASADUZZAMAN, M., NADEEM, A., ARIZMENDI, N., DAVIDSON, C., NICHOLS, H. L., ABEL, M., IONESCU, L. I., PUTTAGUNTA, L., THEBAUD, B., GORDON, J., DEFEA, K., HOLLENBERG, M. D. & VLIAGOFTIS, H. 2015. Functional inhibition of PAR2 alleviates allergen-induced airway hyperresponsiveness and inflammation. *Clin Exp Allergy,* 45**,** 1844-55.

ATRETKHANY, K. N., GOGOLEVA, V. S., DRUTSKAYA, M. S. & NEDOSPASOV, S. A. 2020. Distinct modes of TNF signaling through its two receptors in health and disease. *J Leukoc Biol,* 107**,** 893-905.

AVET, C., STURINO, C., GRASTILLEUR, S., GOUILL, C. L., SEMACHE, M., GROSS, F., GENDRON, L., BENNANI, Y., MANCINI, J. A., SAYEGH, C. E. & BOUVIER, M. 2020. The PAR2 inhibitor I-287 selectively targets Gα(q) and Gα(12/13) signaling and has anti-inflammatory effects. *Commun Biol,* 3**,** 719.

BAE, J. S., KIM, Y. U., PARK, M. K. & REZAIE, A. R. 2009. Concentration dependent dual effect of thrombin in endothelial cells via Par-1 and Pi3 Kinase. *J Cell Physiol,* 219**,** 744-51.

BAILO, M., DUNNING, L., BRZESZCZYNSKA, J., MCINTOSH, K., PLEVIN, R., MARTIN, S. L., SERGEANT, G. P., GOODYEAR, C. S., LITHERLAND, G. S., LOCKHART, J. C. & CRILLY, A. 2020. Protease activated receptor 2 (PAR2) antagonism reduces pro-inflammatory cytokine production in bronchial epithelial cells. *European Respiratory Journal,* 56**,** 2292.

BANDARA, M. & MACNAUGHTON, W. K. 2022. Protease-activated receptor-2 activation enhances epithelial wound healing via epidermal growth factor receptor. *Tissue Barriers,* 10**,** 1968763.

BANG, E., KIM, D. H. & CHUNG, H. Y. 2021. Protease-activated receptor 2 induces ROS-mediated inflammation through Akt-mediated NF-κB and FoxO6 modulation during skin photoaging. *Redox Biol,* 44**,** 102022.

BAO, Y., GAO, Y., HOU, W., YANG, L., KONG, X., ZHENG, H., LI, C. & HUA, B. 2015a. Engagement of signaling pathways of protease-activated receptor 2 and mu-opioid receptor in bone cancer pain and morphine tolerance. *Int J Cancer,* 137**,** 1475-83.

BAO, Y., HOU, W., YANG, L., KONG, X., DU, M., ZHENG, H., GAO, Y. & HUA, B. 2015b. Protease-activated receptor 2 antagonist potentiates analgesic effects of systemic morphine in a rat model of bone cancer pain. *Reg Anesth Pain Med,* 40**,** 158-65.

BAO, Y., HOU, W., YANG, L., LIU, R., GAO, Y., KONG, X., SHI, Z., LI, W., ZHENG, H., JIANG, S. & HUA, B. 2015c. Increased expression of protease-activated receptor 2 and 4 within dorsal root ganglia in a rat model of bone cancer pain. *J Mol Neurosci,* 55**,** 706-14.

BAO, Y., HUA, B., HOU, W., SHI, Z., LI, W., LI, C., CHEN, C., LIU, R. & QIN, Y. 2014. Involvement of protease-activated receptor 2 in nociceptive behavior in a rat model of bone cancer. *J Mol Neurosci,* 52**,** 566-76.

BARAL, P., UDIT, S. & CHIU, I. M. 2019. Pain and immunity: implications for host defence. *Nature Reviews Immunology,* 19**,** 433-447.

BARR, T. P., GARZIA, C., GUHA, S., FLETCHER, E. K., NGUYEN, N., WIESCHHAUS, A. J., FERRER, L., COVIC, L. & KULIOPULOS, A. 2019. PAR2 Pepducin-Based Suppression of Inflammation and Itch in Atopic Dermatitis Models. *J Invest Dermatol,* 139**,** 412-421.

BARRA, A., BRASIL, A. F., FERREIRA, T. L., FERNANDES-BRAGA, W., MARCONATO, D. G., FARIA-PINTO, P., ALVAREZ-LEITE, J. I., DOS SANTOS AGGUM CAPETTINI, L. & KLEIN, A. 2022. Protease-activated receptor 2 enhances innate and inflammatory mechanisms induced by lipopolysaccharide in macrophages from C57BL/6 mice. *Inflamm Res,* 71**,** 439-448.

BARRY, G. D., LE, G. T. & FAIRLIE, D. P. 2006. Agonists and antagonists of protease activated receptors (PARs). *Current medicinal chemistry,* 13**,** 243-265.

BARRY, G. D., SUEN, J. Y., LE, G. T., COTTERELL, A., REID, R. C. & FAIRLIE, D. P. 2010. Novel agonists and antagonists for human protease activated receptor 2. *Journal of medicinal chemistry,* 53**,** 7428-7440.

BASBAUM, A. I., BAUTISTA, D. M., SCHERRER, G. & JULIUS, D. 2009. Cellular and molecular mechanisms of pain. *Cell,* 139**,** 267-84.

BEECHER, K. L., ANDERSEN, T. T., FENTON, J. W., 2ND & FESTOFF, B. W. 1994. Thrombin receptor peptides induce shape change in neonatal murine astrocytes in culture. *J Neurosci Res,* 37**,** 108-15.

BELHAM, C. M., TATE, R. J., SCOTT, P. H., PEMBERTON, A. D., MILLER, H. R., WADSWORTH, R. M., GOULD, G. W. & PLEVIN, R. 1996. Trypsin stimulates

proteinase-activated receptor-2-dependent and -independent activation of mitogen-activated protein kinases. *Biochem J,* 320 (Pt 3)**,** 939-46.
BHATTACHARYYA, S., GILL, R., CHEN, M. L., ZHANG, F., LINHARDT, R. J., DUDEJA, P. K. & TOBACMAN, J. K. 2008. Toll-like Receptor 4 Mediates Induction of the Bcl10-NFκB-Interleukin-8 Inflammatory Pathway by Carrageenan in Human Intestinal Epithelial Cells *. *Journal of Biological Chemistry,* 283**,** 10550-10558.
BLACK, A. R. & BLACK, J. D. 2012. Protein kinase C signaling and cell cycle regulation. *Front Immunol,* 3**,** 423.
BLACKHART, B. D., EMILSSON, K., NGUYEN, D., TENG, W., MARTELLI, A. J., NYSTEDT, S., SUNDELIN, J. & SCARBOROUGH, R. M. 1996. Ligand cross-reactivity within the protease-activated receptor family. *Journal of Biological Chemistry,* 271**,** 16466-16471.
BLOW, D. M., BIRKTOFT, J. J. & HARTLEY, B. S. 1969. Role of a buried acid group in the mechanism of action of chymotrypsin. *Nature,* 221**,** 337-40.
BOCKAERT, J. & PIN, J. P. 1999. Molecular tinkering of G protein-coupled receptors: an evolutionary success. *Embo j,* 18**,** 1723-9.
BOHM, S. K., KHITIN, L. M., GRADY, E. F., APONTE, G., PAYAN, D. G. & BUNNETT, N. W. 1996a. Mechanisms of desensitization and resensitization of proteinase-activated receptor-2. *J Biol Chem,* 271**,** 22003-16.
BOHM, S. K., KONG, W., BROMME, D., SMEEKENS, S. P., ANDERSON, D. C., CONNOLLY, A., KAHN, M., NELKEN, N. A., COUGHLIN, S. R., PAYAN, D. G. & BUNNETT, N. W. 1996b. Molecular cloning, expression and potential functions of the human proteinase-activated receptor-2. *Biochem J,* 314 (Pt 3)**,** 1009-16.
BOITANO, S., HOFFMAN, J., FLYNN, A. N., ASIEDU, M. N., TILLU, D. V., ZHANG, Z., SHERWOOD, C. L., RIVAS, C. M., DEFEA, K. A., VAGNER, J. & PRICE, T. J. 2015. The novel PAR2 ligand C391 blocks multiple PAR2 signalling pathways in vitro and in vivo. *Br J Pharmacol,* 172**,** 4535-4545.
BOLTE, S. & CORDELIÈRES, F. P. 2006. A guided tour into subcellular colocalization analysis in light microscopy. *J Microsc,* 224**,** 213-32.
BORISSOFF, J. I., SPRONK, H. M. & TEN CATE, H. 2011. The hemostatic system as a modulator of atherosclerosis. *N Engl J Med,* 364**,** 1746-60.
BORTHAKUR, A., BHATTACHARYYA, S., DUDEJA, P. K. & TOBACMAN, J. K. 2007. Carrageenan induces interleukin-8 production through distinct Bcl10 pathway in normal human colonic epithelial cells. *Am J Physiol Gastrointest Liver Physiol,* 292**,** G829-38.
BOTHAM, A., GUO, X., XIAO, Y. P., MORICE, A. H., COMPTON, S. J. & SADOFSKY, L. R. 2011. Palmitoylation of human proteinase-activated receptor-2 differentially regulates receptor-triggered ERK1/2 activation, calcium signalling and endocytosis. *Biochem J,* 438**,** 359-67.
BRAGA, A. D., MIRANDA, J. P., FERREIRA, G. M., BILHEIRO, R. P., DUARTE, I. D., FRANCISCHI, J. N. & KLEIN, A. 2010. Blockade of proteinase-activated receptor-4 inhibits the eosinophil recruitment induced by eotaxin-1 in the pleural cavity of mice. *Pharmacology,* 86**,** 224-30.
BRESER, M. L., MOTRICH, R. D., SANCHEZ, L. R. & RIVERO, V. E. 2017. Chronic Pelvic Pain Development and Prostate Inflammation in Strains of Mice With Different Susceptibility to Experimental Autoimmune Prostatitis. *The Prostate,* 77**,** 94-104.
BROWN, D. G., BROWN, G. A., CENTRELLA, P., CERTEL, K., COOKE, R. M., CUOZZO, J. W., DEKKER, N., DUMELIN, C. E., FERGUSON, A., FIEZ-VANDAL, C., GESCHWINDNER, S., GUIÉ, M. A., HABESHIAN, S., KEEFE, A. D., SCHLENKER, O., SIGEL, E. A., SNIJDER, A., SOUTTER, H. T., SUNDSTRÖM, L., TROAST, D. M., WIGGIN, G., ZHANG, J., ZHANG, Y. &

CLARK, M. A. 2018. Agonists and Antagonists of Protease-Activated Receptor 2 Discovered within a DNA-Encoded Chemical Library Using Mutational Stabilization of the Target. *SLAS Discov,* 23**,** 429-436.
BUCCITELLI, C. & SELBACH, M. 2020. mRNAs, proteins and the emerging principles of gene expression control. *Nat Rev Genet,* 21**,** 630-644.
BUENO, L. 2008. Protease activated receptor 2: a new target for IBS treatment. *Eur Rev Med Pharmacol Sci,* 12 Suppl 1**,** 95-102.
BUNNETT, N. W. 2006. Protease-activated receptors: how proteases signal to cells to cause inflammation and pain. *Semin Thromb Hemost,* 32 Suppl 1**,** 39-48.
BURGER, M. M. 1970. Proteolytic enzymes initiating cell division and escape from contact inhibition of growth. *Nature,* 227**,** 170-1.
BUSHELL, T. J., PLEVIN, R., COBB, S. & IRVING, A. J. 2006. Characterization of proteinase-activated receptor 2 signalling and expression in rat hippocampal neurons and astrocytes. *Neuropharmacology,* 50**,** 714-725.
CAI, T., ALIDJANOV, J., PALAGIN, I., MEDINA-POLO, J., NICKEL, J. C. & WAGENLEHNER, F. M. E. 2024. Chronic prostatitis/chronic pelvic pain syndrome (CP/CPPS): look to the future. *Prostate Cancer and Prostatic Diseases,* 27**,** 239-241.
CAMBIER, S., GOUWY, M. & PROOST, P. 2023. The chemokines CXCL8 and CXCL12: molecular and functional properties, role in disease and efforts towards pharmacological intervention. *Cellular & Molecular Immunology,* 20**,** 217-251.
CAMERER, E., HUANG, W. & COUGHLIN, S. R. 2000. Tissue factor-and factor X-dependent activation of protease-activated receptor 2 by factor VIIa. *Proceedings of the National Academy of Sciences,* 97**,** 5255-5260.
CAMPBELL, A. P. & SMRCKA, A. V. 2018. Targeting G protein-coupled receptor signalling by blocking G proteins. *Nature Reviews Drug Discovery,* 17**,** 789-803.
CAO, B., XU, Q., SHI, Y., ZHAO, R., LI, H., ZHENG, J., LIU, F., WAN, Y. & WEI, B. 2024. Pathology of pain and its implications for therapeutic interventions. *Signal Transduction and Targeted Therapy,* 9**,** 155.
CASTRO, M. L., FRANCO, G. C., BRANCO-DE-ALMEIDA, L. S., ANBINDER, A. L., COGO-MULLER, K., CORTELLI, S. C., DUARTE, S., SAXENA, D. & ROSALEN, P. L. 2016. Downregulation of Proteinase-Activated Receptor-2, Interleukin-17, and Other Proinflammatory Genes by Subantimicrobial Doxycycline Dose in a Rat Periodontitis Model. *J Periodontol,* 87**,** 203-10.
CATTARUZZA, F., LYO, V., JONES, E., PHAM, D., HAWKINS, J., KIRKWOOD, K., VALDEZ-MORALES, E., IBEAKANMA, C., VANNER, S. J., BOGYO, M. & BUNNETT, N. W. 2011. Cathepsin S is activated during colitis and causes visceral hyperalgesia by a PAR2-dependent mechanism in mice. *Gastroenterology,* 141**,** 1864-74.e1-3.
CEDERQVIST, K., HAGLUND, C., HEIKKILA, P., HOLLENBERG, M. D., KARIKOSKI, R. & ANDERSSON, S. 2005. High expression of pulmonary proteinase-activated receptor 2 in acute and chronic lung injury in preterm infants. *Pediatr Res,* 57**,** 831-6.
CENAC, N., ANDREWS, C. N., HOLZHAUSEN, M., CHAPMAN, K., COTTRELL, G., ANDRADE-GORDON, P., STEINHOFF, M., BARBARA, G., BECK, P., BUNNETT, N. W., SHARKEY, K. A., FERRAZ, J. G., SHAFFER, E. & VERGNOLLE, N. 2007. Role for protease activity in visceral pain in irritable bowel syndrome. *J Clin Invest,* 117**,** 636-47.
CENAC, N., COELHO, A. M., NGUYEN, C., COMPTON, S., ANDRADE-GORDON, P., MACNAUGHTON, W. K., WALLACE, J. L., HOLLENBERG, M. D., BUNNETT, N. W., GARCIA-VILLAR, R., BUENO, L. & VERGNOLLE, N. 2002. Induction of intestinal inflammation in mouse by activation of proteinase-activated receptor-2. *Am J Pathol,* 161**,** 1903-15.

CEULEERS, H., HANNING, N., HEIRBAUT, J., VAN REMOORTEL, S., JOOSSENS, J., VAN DER VEKEN, P., FRANCQUE, S. M., DE BRUYN, M., LAMBEIR, A.-M., DE MAN, J. G., TIMMERMANS, J.-P., AUGUSTYNS, K., DE MEESTER, I. & DE WINTER, B. Y. 2018. Newly developed serine protease inhibitors decrease visceral hypersensitivity in a post-inflammatory rat model for irritable bowel syndrome. *British Journal of Pharmacology,* 175**,** 3516-3533.

CEULEERS, H., VAN SPAENDONK, H., HANNING, N., HEIRBAUT, J., LAMBEIR, A. M., JOOSSENS, J., AUGUSTYNS, K., DE MAN, J. G., DE MEESTER, I. & DE WINTER, B. Y. 2016. Visceral hypersensitivity in inflammatory bowel diseases and irritable bowel syndrome: The role of proteases. *World J Gastroenterol,* 22**,** 10275-10286.

CHAMBERS, L. S., BLACK, J. L., PORONNIK, P. & JOHNSON, P. R. 2001. Functional effects of protease-activated receptor-2 stimulation on human airway smooth muscle. *American Journal of Physiology-Lung Cellular and Molecular Physiology,* 281**,** L1369-L1378.

CHANDRABALAN, A. & RAMACHANDRAN, R. 2021. Molecular mechanisms regulating Proteinase-Activated Receptors (PARs). *The FEBS Journal,* 288**,** 2697-2726.

CHE, T. & ROTH, B. L. 2023. Molecular basis of opioid receptor signaling. *Cell,* 186**,** 5203-5219.

CHEN, C. H., PAING, M. M. & TREJO, J. 2004. Termination of protease-activated receptor-1 signaling by beta-arrestins is independent of receptor phosphorylation. *J Biol Chem,* 279**,** 10020-31.

CHEN, D., CARPENTER, A., ABRAHAMS, J., CHAMBERS, R. C., LECHLER, R. I., MCVEY, J. H. & DORLING, A. 2008. Protease-activated receptor 1 activation is necessary for monocyte chemoattractant protein 1-dependent leukocyte recruitment in vivo. *J Exp Med,* 205**,** 1739-46.

CHEN, D., LIU, N., LI, M. & LIANG, S. 2016. Blocking PAR2 Alleviates Bladder Pain and Hyperactivity via TRPA1 Signal. *Transl Neurosci,* 7**,** 133-138.

CHEN, J., REN, T., XIE, L., HU, H., LI, X., MAITUSONG, M., ZHOU, X., HU, W., XU, D., QIAN, Y., CHENG, S., YU, K., WANG, J. A. & LIU, X. 2024. Enhancing aortic valve drug delivery with PAR2-targeting magnetic nano-cargoes for calcification alleviation. *Nat Commun,* 15**,** 557.

CHEN, L., BIAN, Z., CHEN, J., MENG, J., ZHANG, M. & LIANG, C. 2021. Immunological alterations in patients with chronic prostatitis/chronic pelvic pain syndrome and experimental autoimmune prostatitis model: A systematic review and meta-analysis. *Cytokine,* 141**,** 155440.

CHEN, L. B. & BUCHANAN, J. M. 1975. Mitogenic activity of blood components. I. Thrombin and prothrombin. *Proc Natl Acad Sci U S A,* 72**,** 131-5.

CHEN, Y., YANG, C. & WANG, Z. J. 2011. Proteinase-activated receptor 2 sensitizes transient receptor potential vanilloid 1, transient receptor potential vanilloid 4, and transient receptor potential ankyrin 1 in paclitaxel-induced neuropathic pain. *Neuroscience,* 193**,** 440-51.

CHENG, R. K. Y., FIEZ-VANDAL, C., SCHLENKER, O., EDMAN, K., AGGELER, B., BROWN, D. G., BROWN, G. A., COOKE, R. M., DUMELIN, C. E., DORE, A. S., GESCHWINDNER, S., GREBNER, C., HERMANSSON, N. O., JAZAYERI, A., JOHANSSON, P., LEONG, L., PRIHANDOKO, R., RAPPAS, M., SOUTTER, H., SNIJDER, A., SUNDSTROM, L., TEHAN, B., THORNTON, P., TROAST, D., WIGGIN, G., ZHUKOV, A., MARSHALL, F. H. & DEKKER, N. 2017. Structural insight into allosteric modulation of protease-activated receptor 2. *Nature,* 545**,** 112-115.

CHINELLATO, M., GASPAROTTO, M., QUARTA, S., RUVOLETTO, M., BIASIOLO, A., FILIPPINI, F., SPIEZIA, L., CENDRON, L. & PONTISSO, P. 2023. 1-

Piperidine Propionic Acid as an Allosteric Inhibitor of Protease Activated Receptor-2. *Pharmaceuticals,* 16**,** 1486.
CHIU, L.-L., PERNG, D.-W., YU, C.-H., SU, S.-N. & CHOW, L.-P. 2007. Mold allergen, pen C 13, induces IL-8 expression in human airway epithelial cells by activating protease-activated receptor 1 and 2. *The Journal of Immunology,* 178**,** 5237-5244.
CHOI, J. S., LEE, D. H., AHN, J. B., SIM, S., HEO, K. S., MYUNG, C. S. & PARK, J. S. 2020. Therapeutic effects of celecoxib polymeric systems in rat models of inflammation and adjuvant-induced rheumatoid arthritis. *Mater Sci Eng C Mater Biol Appl,* 114**,** 111042.
CIRINO, G., CICALA, C., BUCCI, M. R., SORRENTINO, L., MARAGANORE, J. M. & STONE, S. R. 1996. Thrombin functions as an inflammatory mediator through activation of its receptor. *Journal of Experimental Medicine,* 183**,** 821-827.
CIRINO, G., NAPOLI, C., BUCCI, M. & CICALA, C. 2000. Inflammation–coagulation network: are serine protease receptors the knot? *Trends in pharmacological sciences,* 21**,** 170-172.
CITRON, B. A., AMEENUDDIN, S., UCHIDA, K., SUO, W. Z., SANTACRUZ, K. & FESTOFF, B. W. 2016. Membrane lipid peroxidation in neurodegeneration: Role of thrombin and proteinase-activated receptor-1. *Brain Res,* 1643**,** 10-7.
CLEMENS, J. Q., CALHOUN, E. A., LITWIN, M. S., MCNAUGHTON-COLLINS, M., DUNN, R. L., CROWLEY, E. M. & LANDIS, J. R. 2009. Rescoring the NIH chronic prostatitis symptom index: nothing new. *Prostate Cancer Prostatic Dis,* 12**,** 285-7.
CLINICALTRIALS.GOV 2019. A Randomised, Double-blind, Placebo-controlled Study of the Safety, Tolerability, and Pharmacokinetics of Single Ascending Doses of MEDI0618 in Healthy Male and Female Volunteers.
CLINICALTRIALS.GOV 2022. A Randomised, Double-blind, Placebo-controlled Study of the Safety, Tolerability, and Pharmacokinetics of Multiple Ascending Doses of MEDI0618 in Healthy Male and Female Volunteers.
CLINICALTRIALS.GOV 2024. A Phase 2, Randomised, Multicentre, Parallel-Group Treatment, Double-Blind Study to Investigate the Safety and Efficacy of Subcutaneous MEDI0618 in the Reduction of Migraine Headache Days Compared to Placebo in Adult Participants With Episodic Migraine.
COCKS, T. M., FONG, B., CHOW, J. M., ANDERSON, G. P., FRAUMAN, A. G., GOLDIE, R. G., HENRY, P. J., CARR, M. J., HAMILTON, J. R. & MOFFATT, J. D. 1999. A protective role for protease-activated receptors in the airways. *Nature,* 398**,** 156-60.
COELHO, A. M., VERGNOLLE, N., GUIARD, B., FIORAMONTI, J. & BUENO, L. 2002. Proteinases and proteinase-activated receptor 2: a possible role to promote visceral hyperalgesia in rats. *Gastroenterology,* 122**,** 1035-47.
COFFIELD, V. M., HELMS, W. S., JIANG, Q. & SU, L. 2004. Galpha13 mediates a signal that is essential for proliferation and survival of thymocyte progenitors. *J Exp Med,* 200**,** 1315-24.
COHEN, S. P., VASE, L. & HOOTEN, W. M. 2021. Chronic pain: an update on burden, best practices, and new advances. *The Lancet,* 397**,** 2082-2097.
COMPTON, S. J., RENAUX, B., WIJESURIYA, S. J. & HOLLENBERG, M. D. 2001. Glycosylation and the activation of proteinase-activated receptor 2 (PAR(2)) by human mast cell tryptase. *Br J Pharmacol,* 134**,** 705-18.
COMPTON, S. J., SANDHU, S., WIJESURIYA, S. J. & HOLLENBERG, M. D. 2002. Glycosylation of human proteinase-activated receptor-2 (hPAR2): role in cell surface expression and signalling. *Biochem J,* 368**,** 495-505.
CONFLITTI, P., LYMAN, E., SANSOM, M. S. P., HILDEBRAND, P. W., GUTIÉRREZ-DE-TERÁN, H., CARLONI, P., ANSELL, T. B., YUAN, S., BARTH, P., ROBINSON, A. S., TATE, C. G., GLORIAM, D., GRZESIEK, S., EDDY, M. T.,

PROSSER, S. & LIMONGELLI, V. 2025. Functional dynamics of G protein-coupled receptors reveal new routes for drug discovery. *Nature Reviews Drug Discovery*.
COTTRELL, G. S., AMADESI, S., GRADY, E. F. & BUNNETT, N. W. 2004a. Trypsin IV, a novel agonist of protease-activated receptors 2 and 4. *Journal of Biological Chemistry,* 279**,** 13532-13539.
COTTRELL, G. S., AMADESI, S., GRADY, E. F. & BUNNETT, N. W. 2004b. Trypsin IV, a novel agonist of protease-activated receptors 2 and 4. *J Biol Chem,* 279**,** 13532-9.
COUGHLIN, S. R. 2001. Protease-activated receptors in vascular biology. *Thromb Haemost,* 86**,** 298-307.
COUGHLIN, S. R. 2005. Protease-activated receptors in hemostasis, thrombosis and vascular biology. *J Thromb Haemost,* 3**,** 1800-14.
CRILLY, A., PALMER, H., NICKDEL, M. B., DUNNING, L., LOCKHART, J. C., PLEVIN, R., MCINNES, I. B. & FERRELL, W. R. 2012. Immunomodulatory role of proteinase-activated receptor-2. *Ann Rheum Dis,* 71**,** 1559-66.
CUNNINGHAM, M. R. 2010. *The molecular pharmacology of proteinase-activated receptor 4 (PAR4).* Thesis [PhD] --University of Strathclyde, 2010.
CUNNINGHAM, M. R., MCINTOSH, K. A., PEDIANI, J. D., ROBBEN, J., COOKE, A. E., NILSSON, M., GOULD, G. W., MUNDELL, S., MILLIGAN, G. & PLEVIN, R. 2012. Novel role for proteinase-activated receptor 2 (PAR2) in membrane trafficking of proteinase-activated receptor 4 (PAR4). *J Biol Chem,* 287**,** 16656-69.
DAHLHAMER, J., LUCAS, J., ZELAYA, C., NAHIN, R., MACKEY, S., DEBAR, L., KERNS, R., VON KORFF, M., PORTER, L. & HELMICK, C. 2018. Prevalence of Chronic Pain and High-Impact Chronic Pain Among Adults - United States, 2016. *MMWR Morb Mortal Wkly Rep,* 67**,** 1001-1006.
DAI, Y., MORIYAMA, T., HIGASHI, T., TOGASHI, K., KOBAYASHI, K., YAMANAKA, H., TOMINAGA, M. & NOGUCHI, K. 2004. Proteinase-activated receptor 2-mediated potentiation of transient receptor potential vanilloid subfamily 1 activity reveals a mechanism for proteinase-induced inflammatory pain. *J Neurosci,* 24**,** 4293-9.
DAINES, M., ZHU, L., PEREIRA, R., ZHOU, X., BONDY, C., PRYOR, B. M., ZHOU, J. & CHEN, Y. 2020. Alternaria induces airway epithelial cytokine expression independent of protease-activated receptor. *Respirology,* 25**,** 502-510.
DALESIO, N. M., BARRETO ORTIZ, S. F., PLUZNICK, J. L. & BERKOWITZ, D. E. 2018. Olfactory, Taste, and Photo Sensory Receptors in Non-sensory Organs: It Just Makes Sense. *Frontiers in Physiology,* 9.
DANAHAY, H., WITHEY, L., POLL, C. T., VAN DE GRAAF, S. F. & BRIDGES, R. J. 2001. Protease-activated receptor-2-mediated inhibition of ion transport in human bronchial epithelial cells. *American Journal of Physiology-Cell Physiology,* 280**,** C1455-C1464.
DARMOUL, D., GRATIO, V., DEVAUD, H. & LABURTHE, M. 2004. Protease-activated receptor 2 in colon cancer: trypsin-induced MAPK phosphorylation and cell proliferation are mediated by epidermal growth factor receptor transactivation. *J Biol Chem,* 279**,** 20927-34.
DAVIS NG, S. M. 2025. *Acute Bacterial Prostatitis.* [Online]. Treasure Island (FL): StatPearls Publishing. Available: https://www.ncbi.nlm.nih.gov/books/NBK459257/ [Accessed Feb 2025].
DE ALMEIDA, A. D., SILVA, I. S., FERNANDES-BRAGA, W., LIMAFILHO, A. C. M., FLORENTINO, R. O. M., BARRA, A., DE OLIVEIRA ANDRADE, L., LEITE, M. F., CASSALI, G. D. & KLEIN, A. 2020. A role for mast cells and mast cell tryptase in driving neutrophil recruitment in LPS-induced lung inflammation via protease-activated receptor 2 in mice. *Inflamm Res,* 69**,** 1059-1070.

DE LOGU, F. & GEPPETTI, P. 2019. Ion Channel Pharmacology for Pain Modulation. *In:* BARRETT, J. E., PAGE, C. P. & MICHEL, M. C. (eds.) *Concepts and Principles of Pharmacology: 100 Years of the Handbook of Experimental Pharmacology.* Cham: Springer International Publishing.

DE OLIVEIRA, P. G., RAMOS, M. L. S., AMARO, A. J., DIAS, R. A. & VIEIRA, S. I. 2019. Gi/o-Protein Coupled Receptors in the Aging Brain. *Frontiers in Aging Neuroscience,* 11.

DE RUITER, G. A. & RUDOLPH, B. 1997. Carrageenan biotechnology. *Trends in Food Science & Technology,* 8**,** 389-395.

DEFEA, K. 2008. β-arrestins and heterotrimeric G-proteins: collaborators and competitors in signal transduction. *British Journal of Pharmacology,* 153**,** S298-S309.

DEFEA, K., ZALEVSKY, J., THOMA, M., DERY, O., MULLINS, R. & BUNNETT, N. 2000a. β-Arrestin–dependent endocytosis of proteinase-activated receptor 2 is required for intracellular targeting of activated ERK1/2. *The Journal of cell biology,* 148**,** 1267-1282.

DEFEA, K. A., ZALEVSKY, J., THOMA, M. S., DERY, O., MULLINS, R. D. & BUNNETT, N. W. 2000b. beta-arrestin-dependent endocytosis of proteinase-activated receptor 2 is required for intracellular targeting of activated ERK1/2. *J Cell Biol,* 148**,** 1267-81.

DENADAI-SOUZA, A., MARTIN, L., DE PAULA, M. A., DE AVELLAR, M. C., MUSCARÁ, M. N., VERGNOLLE, N. & CENAC, N. 2012. Role of transient receptor potential vanilloid 4 in rat joint inflammation. *Arthritis Rheum,* 64**,** 1848-58.

DÉRY, O., CORVERA, C. U., STEINHOFF, M. & BUNNETT, N. W. 1998. Proteinase-activated receptors: novel mechanisms of signaling by serine proteases. *American Journal of Physiology-Cell Physiology,* 274**,** C1429-C1452.

DÉRY, O., THOMA, M. S., WONG, H., GRADY, E. F. & BUNNETT, N. W. 1999. Trafficking of proteinase-activated receptor-2 and beta-arrestin-1 tagged with green fluorescent protein. beta-Arrestin-dependent endocytosis of a proteinase receptor. *J Biol Chem,* 274**,** 18524-35.

DEUIS, J. R., DVORAKOVA, L. S. & VETTER, I. 2017. Methods Used to Evaluate Pain Behaviors in Rodents. *Front Mol Neurosci,* 10**,** 284.

DEWENTER, M., VON DER LIETH, A., KATUS, H. A. & BACKS, J. 2017. Calcium Signaling and Transcriptional Regulation in Cardiomyocytes. *Circulation Research,* 121**,** 1000-1020.

DOMEIER, T. L., ZIMA, A. V., MAXWELL, J. T., HUKE, S., MIGNERY, G. A. & BLATTER, L. A. 2008. IP3 receptor-dependent Ca2+ release modulates excitation-contraction coupling in rabbit ventricular myocytes. *Am J Physiol Heart Circ Physiol,* 294**,** H596-604.

DOYEN, P. J., BECKERS, P., BROOK, G. A. & HERMANS, E. 2020. Regulators of G protein signalling as pharmacological targets for the treatment of neuropathic pain. *Pharmacological Research,* 160**,** 105148.

DULON, S., CANDÉ, C., BUNNETT, N. W., HOLLENBERG, M. D., CHIGNARD, M. & PIDARD, D. 2003. Proteinase-activated receptor-2 and human lung epithelial cells: disarming by neutrophil serine proteinases. *American journal of respiratory cell and molecular biology,* 28**,** 339-346.

DULON, S., LEDUC, D., COTTRELL, G. S., D'ALAYER, J., HANSEN, K. K., BUNNETT, N. W., HOLLENBERG, M. D., PIDARD, D. & CHIGNARD, M. 2005. Pseudomonas aeruginosa elastase disables proteinase-activated receptor 2 in respiratory epithelial cells. *American journal of respiratory cell and molecular biology,* 32**,** 411-419.

EFTEKHARI, R., EWANCHUK, B. W., RAWJI, K. S., YATES, R. M., NOORBAKHSH, F., KUIPERS, H. F. & HOLLENBERG, M. D. 2024. Blockade of Proteinase-

Activated Receptor 2 (PAR2) Attenuates Neuroinflammation in Experimental Autoimmune Encephalomyelitis. *J Pharmacol Exp Ther,* 388**,** 12-22.
EICHEL, K. & VON ZASTROW, M. 2018. Subcellular Organization of GPCR Signaling. *Trends Pharmacol Sci,* 39**,** 200-208.
ENOMOTO, A., YOSHIHISA, Y., YAMAKOSHI, T., UR REHMAN, M., NORISUGI, O., HARA, H., MATSUNAGA, K., MAKINO, T., NISHIHIRA, J. & SHIMIZU, T. 2011. UV-B radiation induces macrophage migration inhibitory factor-mediated melanogenesis through activation of protease-activated receptor-2 and stem cell factor in keratinocytes. *Am J Pathol,* 178**,** 679-87.
FALCONER, A. M. D., CHAN, C. M., GRAY, J., NAGASHIMA, I., HOLLAND, R. A., SHIMIZU, H., PICKFORD, A. R., ROWAN, A. D. & WILKINSON, D. J. 2019. Collagenolytic matrix metalloproteinases antagonize proteinase-activated receptor-2 activation, providing insights into extracellular matrix turnover. *J Biol Chem,* 294**,** 10266-10277.
FAN, M., FAN, X., LAI, Y., CHEN, J., PENG, Y., PENG, Y., XIANG, L. & MA, Y. 2024. Protease-Activated Receptor 2 in inflammatory skin disease: current evidence and future perspectives. *Front Immunol,* 15**,** 1448952.
FEISTRITZER, C., LENTA, R. & RIEWALD, M. 2005. Protease-activated receptors-1 and -2 can mediate endothelial barrier protection: role in factor Xa signaling. *J Thromb Haemost,* 3**,** 2798-805.
FERRELL, W. R., LOCKHART, J. C., KELSO, E. B., DUNNING, L., PLEVIN, R., MEEK, S. E., SMITH, A. J., HUNTER, G. D., MCLEAN, J. S., MCGARRY, F., RAMAGE, R., JIANG, L., KANKE, T. & KAWAGOE, J. 2003. Essential role for proteinase-activated receptor-2 in arthritis. *J Clin Invest,* 111**,** 35-41.
FINLEY, C. R., CHAN, D. S., GARRISON, S., KOROWNYK, C., KOLBER, M. R., CAMPBELL, S., EURICH, D. T., LINDBLAD, A. J., VANDERMEER, B. & ALLAN, G. M. 2018. What are the most common conditions in primary care? Systematic review. *Can Fam Physician,* 64**,** 832-840.
FITZCHARLES, M.-A., COHEN, S. P., CLAUW, D. J., LITTLEJOHN, G., USUI, C. & HÄUSER, W. 2021. Nociplastic pain: towards an understanding of prevalent pain conditions. *The Lancet,* 397**,** 2098-2110.
FLEISCHER, M., SZEPANOWSKI, R. D., PESARA, V., BIHORAC, J. S., OEHLER, B., DOBREV, D., KLEINSCHNITZ, C. & FENDER, A. C. 2024. Direct neuronal protection by the protease-activated receptor PAR4 antagonist ML354 after experimental stroke in mice. *Br J Pharmacol,* 181**,** 3364-3379.
FOGH, B. S., MULTHAUPT, H. A. & COUCHMAN, J. R. 2014. Protein kinase C, focal adhesions and the regulation of cell migration. *J Histochem Cytochem,* 62**,** 172-84.
FRANCIS, N., SANAEI, R., AYODELE, B. A., O'BRIEN-SIMPSON, N. M., FAIRLIE, D. P., WIJEYEWICKREMA, L. C., PIKE, R. N., MACKIE, E. J. & PAGEL, C. N. 2023. Effect of a protease-activated receptor-2 antagonist (GB88) on inflammation-related loss of alveolar bone in periodontal disease. *J Periodontal Res,* 58**,** 544-552.
GARCÍA-GONZÁLEZ, G., SÁNCHEZ-GONZÁLEZ, A., HERNÁNDEZ-BELLO, R., GONZÁLEZ, G. M., FRANCO-MOLINA, M. A., CORONADO-CERDA, E. E. & PALMA-NICOLÁS, J. P. 2019. Triggering of protease-activated receptors (PARs) induces alternative M2 macrophage polarization with impaired plasticity. *Molecular Immunology,* 114**,** 278-288.
GARDELL, L. R., MA, J.-N., SEITZBERG, J. G., KNAPP, A. E., SCHIFFER, H. H., TABATABAEI, A., DAVIS, C. N., OWENS, M., CLEMONS, B. & WONG, K. K. 2008. Identification and characterization of novel small-molecule protease-activated receptor 2 agonists. *Journal of Pharmacology and Experimental Therapeutics,* 327**,** 799-808.

GBD2019IMIDCOLLABORATORS 2023. Global, regional, and national incidence of six major immune-mediated inflammatory diseases: findings from the global burden of disease study 2019. *EClinicalMedicine,* 64**,** 102193.
GINGRICH, J. R., TUCKER, J. A., WALTHER, P. J., DAY, J. W., POULTON, S. H. & WEBB, K. S. 1991. Establishment and characterization of a new human prostatic carcinoma cell line (DuPro-1). *J Urol,* 146**,** 915-9.
GOH, F. G., NG, P. Y., NILSSON, M., KANKE, T. & PLEVIN, R. 2009. Dual effect of the novel peptide antagonist K-14585 on proteinase-activated receptor-2-mediated signalling. *Br J Pharmacol,* 158**,** 1695-704.
GOMIDES, L. F., DUARTE, I. D., FERREIRA, R. G., PEREZ, A. C., FRANCISCHI, J. N. & KLEIN, A. 2012. Proteinase-activated receptor-4 plays a major role in the recruitment of neutrophils induced by trypsin or carrageenan during pleurisy in mice. *Pharmacology,* 89**,** 275-82.
GOMIDES, L. F., LIMA, O. C., MATOS, N. A., FREITAS, K. M., FRANCISCHI, J. N., TAVARES, J. C. & KLEIN, A. 2014. Blockade of proteinase-activated receptor 4 inhibits neutrophil recruitment in experimental inflammation in mice. *Inflamm Res,* 63**,** 935-41.
GOODWIN, G. & MCMAHON, S. B. 2021. The physiological function of different voltage-gated sodium channels in pain. *Nat Rev Neurosci,* 22**,** 263-274.
GRANT, A. D., COTTRELL, G. S., AMADESI, S., TREVISANI, M., NICOLETTI, P., MATERAZZI, S., ALTIER, C., CENAC, N., ZAMPONI, G. W., BAUTISTA-CRUZ, F., LOPEZ, C. B., JOSEPH, E. K., LEVINE, J. D., LIEDTKE, W., VANNER, S., VERGNOLLE, N., GEPPETTI, P. & BUNNETT, N. W. 2007. Protease-activated receptor 2 sensitizes the transient receptor potential vanilloid 4 ion channel to cause mechanical hyperalgesia in mice. *J Physiol,* 578**,** 715-33.
GREENBERG, D. L., MIZE, G. J. & TAKAYAMA, T. K. 2003. Protease-activated receptor mediated RhoA signaling and cytoskeletal reorganization in LNCaP cells. *Biochemistry,* 42**,** 702-709.
GUENTHER, F. & MELZIG, M. F. 2015. Protease-activated receptors and their biological role - focused on skin inflammation. *J Pharm Pharmacol,* 67**,** 1623-33.
GUO, J., SHANG, X., CHEN, P. & HUANG, X. 2023. How does carrageenan cause colitis? A review. *Carbohydr Polym,* 302**,** 120374.
GUO, P., TAI, Y., WANG, M., SUN, H., ZHANG, L., WEI, W., XIANG, Y. K. & WANG, Q. 2022. Gα12 and Gα13: Versatility in Physiology and Pathology. *Frontiers in Cell and Developmental Biology,* 10.
GUO, Q., JIN, Y., CHEN, X., YE, X., SHEN, X., LIN, M., ZENG, C., ZHOU, T. & ZHANG, J. 2024. NF-κB in biology and targeted therapy: new insights and translational implications. *Signal Transduction and Targeted Therapy,* 9**,** 53.
GUREVICH, V. V. & GUREVICH, E. V. 2019. Plethora of functions packed into 45 kDa arrestins: biological implications and possible therapeutic strategies. *Cell Mol Life Sci,* 76**,** 4413-4421.
HABIBI, A., RUF, W. & SCHURGERS, L. 2025. Protease-activated receptors in vascular smooth muscle cells: a bridge between thrombo-inflammation and vascular remodelling. *Cell Commun Signal,* 23**,** 57.
HAGRAS, M. M. & KAMEL, F. O. 2020. Effect of Protease-Activated Receptor-2-Activating Peptide on Guinea Pig Airway Resistance and Isolated Tracheal Strips. *J Microsc Ultrastruct,* 8**,** 7-13.
HAMILTON, J. R. & COCKS, T. M. 2000. Heterogeneous mechanisms of endothelium-dependent relaxation for thrombin and peptide activators of protease-activated receptor-1 in porcine isolated coronary artery. *Br J Pharmacol,* 130**,** 181-8.
HAMILTON, J. R., MOFFATT, J. D., FRAUMAN, A. G. & COCKS, T. M. 2001. Protease-activated receptor (PAR) 1 but not PAR2 or PAR4 mediates endothelium-dependent

relaxation to thrombin and trypsin in human pulmonary arteries. *J Cardiovasc Pharmacol,* 38**,** 108-19.
HAMM, H. E. 2001. How activated receptors couple to G proteins. *Proceedings of the National Academy of Sciences,* 98**,** 4819-4821.
HAN, X. & NIEMAN, M. T. 2020. The domino effect triggered by the tethered ligand of the protease activated receptors. *Thromb Res,* 196**,** 87-98.
HAN, Y., TIAN, L., MA, F., TESCH, G., VESEY, D. A., GOBE, G. C., LOHMAN, R. J., MORAIS, C., SUEN, J. Y., FAIRLIE, D. P. & NIKOLIC-PATERSON, D. J. 2019. Pharmacological inhibition of protease-activated receptor-2 reduces crescent formation in rat nephrotoxic serum nephritis. *Clin Exp Pharmacol Physiol,* 46**,** 456-464.
HANSEN, K. K., SAIFEDDINE, M. & HOLLENBERG, M. D. 2004. Tethered ligand-derived peptides of proteinase-activated receptor 3 (PAR3) activate PAR1 and PAR2 in Jurkat T cells. *Immunology,* 112**,** 183-90.
HANSEN, K. K., SHERMAN, P. M., CELLARS, L., ANDRADE-GORDON, P., PAN, Z., BARUCH, A., WALLACE, J. L., HOLLENBERG, M. D. & VERGNOLLE, N. 2005. A major role for proteolytic activity and proteinase-activated receptor-2 in the pathogenesis of infectious colitis. *Proceedings of the National Academy of Sciences,* 102**,** 8363-8368.
HARGREAVES, K., DUBNER, R., BROWN, F., FLORES, C. & JORIS, J. 1988. A new and sensitive method for measuring thermal nociception in cutaneous hyperalgesia. *Pain,* 32**,** 77-88.
HASDEMIR, B., BUNNETT, N. W. & COTTRELL, G. S. 2007. Hepatocyte growth factor-regulated tyrosine kinase substrate (HRS) mediates post-endocytic trafficking of protease-activated receptor 2 and calcitonin receptor-like receptor. *Journal of biological chemistry,* 282**,** 29646-29657.
HASDEMIR, B., MURPHY, J. E., COTTRELL, G. S. & BUNNETT, N. W. 2009a. Endosomal deubiquitinating enzymes control ubiquitination and down-regulation of protease-activated receptor 2. *Journal of Biological Chemistry,* 284**,** 28453-28466.
HASDEMIR, B., MURPHY, J. E., COTTRELL, G. S. & BUNNETT, N. W. 2009b. Endosomal deubiquitinating enzymes control ubiquitination and down-regulation of protease-activated receptor 2. *J Biol Chem,* 284**,** 28453-66.
HASHIMOTO, T., OKUZAWA, M., OKUNO, S. & SATOH, T. 2023. Mast cell protease/protease-activated receptor-2 axis: Another mechanism of pigmentation in cutaneous lesions of mastocytosis. *J Eur Acad Dermatol Venereol,* 37**,** e529-e531.
HAUSER, A. S., CHAVALI, S., MASUHO, I., JAHN, L. J., MARTEMYANOV, K. A., GLORIAM, D. E. & BABU, M. M. 2018. Pharmacogenomics of GPCR Drug Targets. *Cell,* 172**,** 41-54.e19.
HE, H., LUO, H., XU, H., QIAN, B., ZOU, X., ZHANG, G., ZENG, F. & ZOU, J. 2023. Preclinical models and evaluation criteria of prostatitis. *Front Immunol,* 14**,** 1183895.
HE, L., MA, Y., LI, W., HAN, W., ZHAO, X. & WANG, H. 2018. Protease-activated receptor 2 signaling modulates susceptibility of colonic epithelium to injury through stabilization of YAP in vivo. *Cell Death Dis,* 9**,** 949.
HELYES, Z., SANDOR, K., BORBELY, E., TEKUS, V., PINTER, E., ELEKES, K., TOTH, D. M., SZOLCSANYI, J. & MCDOUGALL, J. J. 2010. Involvement of transient receptor potential vanilloid 1 receptors in protease-activated receptor-2-induced joint inflammation and nociception. *Eur J Pain,* 14**,** 351-8.
HEO, Y., YANG, E., LEE, Y., SEO, Y., RYU, K., JEON, H. & NAMKUNG, W. 2022. GB83, an Agonist of PAR2 with a Unique Mechanism of Action Distinct from Trypsin and PAR2-AP. *Int J Mol Sci,* 23.
HER, J. Y., LEE, Y., KIM, S. J., HEO, G., CHOO, J., KIM, Y., HOWE, C., RHEE, S. H., YU, H. S., CHUNG, H. Y., POTHOULAKIS, C. & IM, E. 2021. Blockage of

protease-activated receptor 2 exacerbates inflammation in high-fat environment partly through autophagy inhibition. *Am J Physiol Gastrointest Liver Physiol,* 320**,** G30-g42.
HEUBERGER, D. M., FRANCHINI, A. G., MADON, J. & SCHUEPBACH, R. A. 2019. Thrombin cleaves and activates the protease-activated receptor 2 dependent on thrombomodulin co-receptor availability. *Thromb Res,* 177**,** 91-101.
HEUBERGER, D. M. & SCHUEPBACH, R. A. 2019. Protease-activated receptors (PARs): mechanisms of action and potential therapeutic modulators in PAR-driven inflammatory diseases. *Thromb J,* 17**,** 4.
HLEIHIL, M., VAAS, M., BHAT, M. A., BALAKRISHNAN, K. & BENKE, D. 2021. Sustained Baclofen-Induced Activation of GABAB Receptors After Cerebral Ischemia Restores Receptor Expression and Function and Limits Progressing Loss of Neurons. *Frontiers in Molecular Neuroscience,* Volume 14 - 2021.
HOLLENBERG, M. D., MIHARA, K., POLLEY, D., SUEN, J. Y., HAN, A., FAIRLIE, D. P. & RAMACHANDRAN, R. 2014. Biased signalling and proteinase-activated receptors (PARs): targeting inflammatory disease. *Br J Pharmacol,* 171**,** 1180-94.
HOLLENBERG, M. D., SAIFEDDINE, M. & AL-ANI, B. 1996. Proteinase-activated receptor-2 in rat aorta: structural requirements for agonist activity of receptor-activating peptides. *Mol Pharmacol,* 49**,** 229-33.
HOLLENBERG, M. D., SAIFEDDINE, M., AL-ANI, B. & KAWABATA, A. 1997. Proteinase-activated receptors: structural requirements for activity, receptor cross-reactivity, and receptor selectivity of receptor-activating peptides. *Can J Physiol Pharmacol,* 75**,** 832-41.
HOLZ, G. G., KANG, G., HARBECK, M., ROE, M. W. & CHEPURNY, O. G. 2006. Cell physiology of cAMP sensor Epac. *J Physiol,* 577**,** 5-15.
HONG, J. H., HONG, J. Y., PARK, B., LEE, S.-I., SEO, J. T., KIM, K.-E., SOHN, M. H. & SHIN, D. M. 2008. Chitinase activates protease-activated receptor-2 in human airway epithelial cells. *American journal of respiratory cell and molecular biology,* 39**,** 530-535.
HOULE, S., PAPEZ, M. D., FERAZZINI, M., HOLLENBERG, M. D. & VERGNOLLE, N. 2005. Neutrophils and the kallikrein-kinin system in proteinase-activated receptor 4-mediated inflammation in rodents. *Br J Pharmacol,* 146**,** 670-8.
HOWELLS, G. L., MACEY, M. G., CHINNI, C., HOU, L., FOX, M. T., HARRIOTT, P. & STONE, S. R. 1997. Proteinase-activated receptor-2: expression by human neutrophils. *Journal of Cell Science,* 110**,** 881-887.
HU, G.-M., MAI, T.-L. & CHEN, C.-M. 2017. Visualizing the GPCR Network: Classification and Evolution. *Scientific Reports,* 7**,** 15495.
HUANG, J., GADOTTI, V. M., CHEN, L., SOUZA, I. A., HUANG, S., WANG, D., RAMAKRISHNAN, C., DEISSEROTH, K., ZHANG, Z. & ZAMPONI, G. W. 2019. A neuronal circuit for activating descending modulation of neuropathic pain. *Nat Neurosci,* 22**,** 1659-1668.
HUANG, J. & ZAMPONI, G. W. 2017. Regulation of voltage gated calcium channels by GPCRs and post-translational modification. *Current Opinion in Pharmacology,* 32**,** 1-8.
HUANG, Z. J., LI, H. C., COWAN, A. A., LIU, S., ZHANG, Y. K. & SONG, X. J. 2012. Chronic compression or acute dissociation of dorsal root ganglion induces cAMP-dependent neuronal hyperexcitability through activation of PAR2. *Pain,* 153**,** 1426-37.
HUESA, C., ORTIZ, A. C., DUNNING, L., MCGAVIN, L., BENNETT, L., MCINTOSH, K., CRILLY, A., KUROWSKA-STOLARSKA, M., PLEVIN, R., VAN 'T HOF, R. J., ROWAN, A. D., MCINNES, I. B., GOODYEAR, C. S., LOCKHART, J. C. & FERRELL, W. R. 2016. Proteinase-activated receptor 2 modulates OA-related pain, cartilage and bone pathology. *Ann Rheum Dis,* 75**,** 1989-1997.

HUMPHRIES, T. L. R., SHEN, K., IYER, A., JOHNSON, D. W., GOBE, G. C., NIKOLIC-PATERSON, D., FAIRLIE, D. P. & VESEY, D. A. 2021. PAR2-Induced Tissue Factor Synthesis by Primary Cultures of Human Kidney Tubular Epithelial Cells Is Modified by Glucose Availability. *Int J Mol Sci,* 22.

IASP, I. A. F. T. S. O. P. 2021. *Terminology* [Online]. Available: https://www.iasp-pain.org/resources/terminology/ [Accessed 12/02/2025 2025].

INTERDONATO, L., FERRARIO, G., CORDARO, M., D'AMICO, R., SIRACUSA, R., FUSCO, R., IMPELLIZZERI, D., CUZZOCREA, S., ALDINI, G. & DI PAOLA, R. 2023. Targeting Nrf2 and NF-κB Signaling Pathways in Inflammatory Pain: The Role of Polyphenols from Thinned Apples. *Molecules,* 28.

ISHII, K., CHEN, J., ISHII, M., KOCH, W. J., FREEDMAN, N. J., LEFKOWITZ, R. J. & COUGHLIN, S. R. 1994. Inhibition of thrombin receptor signaling by a G-protein coupled receptor kinase. Functional specificity among G-protein coupled receptor kinases. *J Biol Chem,* 269**,** 1125-30.

ISHIKAWA, C., TSUDA, T., KONISHI, H., NAKAGAWA, N. & YAMANISHI, K. 2009. Tetracyclines modulate protease-activated receptor 2-mediated proinflammatory reactions in epidermal keratinocytes. *Antimicrob Agents Chemother,* 53**,** 1760-5.

ITTO, R., OE, Y., IMARUOKA, K., SATO, E., SEKIMOTO, A., YAMAKAGE, S., KUMAKURA, S., SATO, H., ITO, S. & TAKAHASHI, N. 2019. Glomerular Injury Is Exacerbated in Lupus-Prone MRL/lpr Mice Treated with a Protease-Activated Receptor 2 Antagonist. *Tohoku J Exp Med,* 249**,** 127-133.

JACKSON, T., THOMAS, S., STABILE, V., SHOTWELL, M., HAN, X. & MCQUEEN, K. 2016. A systematic review and meta-analysis of the global burden of chronic pain without clear etiology in low-and middle-income countries: trends in heterogeneous data and a proposal for new assessment methods. *Anesthesia & Analgesia,* 123**,** 739-748.

JACOB, C., COTTRELL, G. S., GEHRINGER, D., SCHMIDLIN, F., GRADY, E. F. & BUNNETT, N. W. 2005. c-Cbl mediates ubiquitination, degradation, and down-regulation of human protease-activated receptor 2. *Journal of Biological Chemistry,* 280**,** 16076-16087.

JACQUES, S. L. & KULIOPULOS, A. 2003. Protease-activated receptor-4 uses dual prolines and an anionic retention motif for thrombin recognition and cleavage. *The Biochemical journal,* 376**,** 733-740.

JAIRAMAN, A., YAMASHITA, M., SCHLEIMER, R. P. & PRAKRIYA, M. 2015. Store-Operated Ca2+ Release-Activated Ca2+ Channels Regulate PAR2-Activated Ca2+ Signaling and Cytokine Production in Airway Epithelial Cells. *J Immunol,* 195**,** 2122-33.

JAVED, A., SONG, B. R., LEE, C. H., ALAM, M. B., KIM, S. L. & LEE, S. H. 2024. Glycoprotein from Sargassum fusiforme exhibiting anti-inflammatory responses in vitro and in vivo via modulation of TLR4/MyD88 and NF-κB signaling. *Int J Biol Macromol,* 272**,** 132574.

JEAN-CHARLES, P. Y., KAUR, S. & SHENOY, S. K. 2017. G Protein-Coupled Receptor Signaling Through β-Arrestin-Dependent Mechanisms. *J Cardiovasc Pharmacol,* 70**,** 142-158.

JESIK, C. J., HOLLAND, J. M. & LEE, C. 1982. An anatomic and histologic study of the rat prostate. *Prostate,* 3**,** 81-97.

JIANG, Y., LIM, J., WU, K. C., XU, W., SUEN, J. Y. & FAIRLIE, D. P. 2021. PAR2 induces ovarian cancer cell motility by merging three signalling pathways to transactivate EGFR. *Br J Pharmacol,* 178**,** 913-932.

JIANG, Y., YAU, M. K., LIM, J., WU, K. C., XU, W., SUEN, J. Y. & FAIRLIE, D. P. 2018. A Potent Antagonist of Protease-Activated Receptor 2 That Inhibits Multiple Signaling Functions in Human Cancer Cells. *J Pharmacol Exp Ther,* 364**,** 246-257.

JIMENEZ-VARGAS, N. N., PATTISON, L. A., ZHAO, P., LIEU, T., LATORRE, R., JENSEN, D. D., CASTRO, J., AURELIO, L., LE, G. T., FLYNN, B., HERENBRINK, C. K., YEATMAN, H. R., EDGINGTON-MITCHELL, L., PORTER, C. J. H., HALLS, M. L., CANALS, M., VELDHUIS, N. A., POOLE, D. P., MCLEAN, P., HICKS, G. A., SCHEFF, N., CHEN, E., BHATTACHARYA, A., SCHMIDT, B. L., BRIERLEY, S. M., VANNER, S. J. & BUNNETT, N. W. 2018. Protease-activated receptor-2 in endosomes signals persistent pain of irritable bowel syndrome. *Proc Natl Acad Sci U S A,* 115**,** E7438-e7447.

JOBE, A. & VIJAYAN, R. 2024. Orphan G protein-coupled receptors: the ongoing search for a home. *Frontiers in Pharmacology,* 15.

KANEIDER, N. C., LEGER, A. J., AGARWAL, A., NGUYEN, N., PERIDES, G., DERIAN, C., COVIC, L. & KULIOPULOS, A. 2007. 'Role reversal' for the receptor PAR1 in sepsis-induced vascular damage. *Nat Immunol,* 8**,** 1303-12.

KANKE, T., KABEYA, M., KUBO, S., KONDO, S., YASUOKA, K., TAGASHIRA, J., ISHIWATA, H., SAKA, M., FURUYAMA, T., NISHIYAMA, T., DOI, T., HATTORI, Y., KAWABATA, A., CUNNINGHAM, M. R. & PLEVIN, R. 2009. Novel antagonists for proteinase-activated receptor 2: inhibition of cellular and vascular responses in vitro and in vivo. *Br J Pharmacol,* 158**,** 361-71.

KANKE, T., MACFARLANE, S. R., SEATTER, M. J., DAVENPORT, E., PAUL, A., MCKENZIE, R. C. & PLEVIN, R. 2001. Proteinase-activated receptor-2-mediated activation of stress-activated protein kinases and inhibitory kappa B kinases in NCTC 2544 keratinocytes. *J Biol Chem,* 276**,** 31657-66.

KAPLAN, J. G. & BONA, C. 1974. Proteases as mitogens. The Effect of trypsin and pronase on mouse and human lymphocytes. *Exp Cell Res,* 88**,** 388-94.

KAUFMANN, R., SCHULZE, B., KRAUSE, G., MAYR, L. M., SETTMACHER, U. & HENKLEIN, P. 2005. Proteinase-activated receptors (PARs)--the PAR3 Neo-N-terminal peptide TFRGAP interacts with PAR1. *Regul Pept,* 125**,** 61-6.

KAWABATA, A. 2003. Gastrointestinal functions of proteinase-activated receptors. *Life Sci,* 74**,** 247-54.

KAWABATA, A., KANKE, T., YONEZAWA, D., ISHIKI, T., SAKA, M., KABEYA, M., SEKIGUCHI, F., KUBO, S., KURODA, R. & IWAKI, M. 2004. Potent and metabolically stable agonists for protease-activated receptor-2: evaluation of activity in multiple assay systems in vitro and in vivo. *Journal of Pharmacology and Experimental Therapeutics,* 309**,** 1098-1107.

KAWABATA, A., KAWAO, N., KURODA, R., TANAKA, A., ITOH, H. & NISHIKAWA, H. 2001. Peripheral PAR-2 triggers thermal hyperalgesia and nociceptive responses in rats. *Neuroreport,* 12**,** 715-9.

KAWABATA, A., KURODA, R., MINAMI, T., KATAOKA, K. & TANEDA, M. 1998. Increased vascular permeability by a specific agonist of protease-activated receptor-2 in rat hindpaw. *British journal of pharmacology,* 125**,** 419-422.

KAWABATA, A., MATSUNAMI, M. & SEKIGUCHI, F. 2008. Gastrointestinal roles for proteinase-activated receptors in health and disease. *Br J Pharmacol,* 153 Suppl 1**,** S230-40.

KAWAI, K., KAWAI, A. T., WOLLAN, P. & YAWN, B. P. 2017. Adverse impacts of chronic pain on health-related quality of life, work productivity, depression and anxiety in a community-based study. *Family Practice,* 34**,** 656-661.

KAWANO, N., OSAWA, H., ITO, T., NAGASHIMA, Y., HIRAHARA, F., INAYAMA, Y., NAKATANI, Y., KIMURA, S., KITAJIMA, H. & KOSHIKAWA, N. 1997. Expression of gelatinase A, tissue inhibitor of metalloproteinases-2, matrilysin, and trypsin (ogen) in lung neoplasms: an immunohistochemical study. *Human pathology,* 28**,** 613-622.

KAWATKAR, A., SCHEFTER, M., HERMANSSON, N. O., SNIJDER, A., DEKKER, N., BROWN, D. G., LUNDBÄCK, T., ZHANG, A. X. & CASTALDI, M. P. 2019.

CETSA beyond Soluble Targets: a Broad Application to Multipass Transmembrane Proteins. *ACS Chem Biol,* 14**,** 1913-1920.
KAYSSI, A., AMADESI, S., BAUTISTA, F., BUNNETT, N. W. & VANNER, S. 2007. Mechanisms of protease-activated receptor 2-evoked hyperexcitability of nociceptive neurons innervating the mouse colon. *J Physiol,* 580**,** 977-91.
KEHL, L. J., TREMPE, T. M. & HARGREAVES, K. M. 2000. A new animal model for assessing mechanisms and management of muscle hyperalgesia. *Pain,* 85**,** 333-343.
KELSO, E. B., FERRELL, W. R., LOCKHART, J. C., ELIAS-JONES, I., HEMBROUGH, T., DUNNING, L., GRACIE, J. A. & MCINNES, I. B. 2007. Expression and proinflammatory role of proteinase-activated receptor 2 in rheumatoid synovium: ex vivo studies using a novel proteinase-activated receptor 2 antagonist. *Arthritis Rheum,* 56**,** 765-71.
KELSO, E. B., LOCKHART, J. C., HEMBROUGH, T., DUNNING, L., PLEVIN, R., HOLLENBERG, M. D., SOMMERHOFF, C. P., MCLEAN, J. S. & FERRELL, W. R. 2006. Therapeutic promise of proteinase-activated receptor-2 antagonism in joint inflammation. *J Pharmacol Exp Ther,* 316**,** 1017-24.
KENAKIN, T. 2011. Functional selectivity and biased receptor signaling. *J Pharmacol Exp Ther,* 336**,** 296-302.
KENNEDY, A. J., BALLANTE, F., JOHANSSON, J. R., MILLIGAN, G., SUNDSTRÖM, L., NORDQVIST, A. & CARLSSON, J. 2018. Structural Characterization of Agonist Binding to Protease-Activated Receptor 2 through Mutagenesis and Computational Modeling. *ACS Pharmacol Transl Sci,* 1**,** 119-133.
KENNEDY, A. J., SUNDSTRÖM, L., GESCHWINDNER, S., POON, E. K. Y., JIANG, Y., CHEN, R., COOKE, R., JOHNSTONE, S., MADIN, A., LIM, J., LIU, Q., LOHMAN, R.-J., NORDQVIST, A., FRIDÉN-SAXIN, M., YANG, W., BROWN, D. G., FAIRLIE, D. P. & DEKKER, N. 2020. Protease-activated receptor-2 ligands reveal orthosteric and allosteric mechanisms of receptor inhibition. *Communications Biology,* 3**,** 782.
KHADRA, A., FLETCHER, P., LUZZI, G., SHATTOCK, R. & HAY, P. 2006. Interleukin-8 levels in seminal plasma in chronic prostatitis/chronic pelvic pain syndrome and nonspecific urethritis. *BJU Int,* 97**,** 1043-6.
KIDO, K., KATAGIRI, N., KAWANA, H., SUGINO, S., YAMAUCHI, M. & MASAKI, E. 2021. Nociceptive Sensitization by Activation of Protease-Activated Receptor 2 in a Rat Model of Incisional Pain. *Brain Sci,* 11.
KIM, H. N., TRIPLET, E. M., RADULOVIC, M., BOUCHAL, S., KLEPPE, L. S., SIMON, W. L., YOON, H. & SCARISBRICK, I. A. 2021. The thrombin receptor modulates astroglia-neuron trophic coupling and neural repair after spinal cord injury. *Glia,* 69**,** 2111-2132.
KIM, J. J., KIM, N., CHOI, Y. J., KIM, J. S. & JUNG, H. C. 2016. Increased TRPV1 and PAR2 mRNA expression levels are associated only with the esophageal reflux symptoms, but not with the extraesophageal reflux symptoms. *Medicine (Baltimore),* 95**,** e4387.
KIRKUP, A. J., JIANG, W., BUNNETT, N. W. & GRUNDY, D. 2003. Stimulation of proteinase-activated receptor 2 excites jejunal afferent nerves in anaesthetised rats. *J Physiol,* 552**,** 589-601.
KISELEVA, E., SIDOROVA, M., GORBACHEVA, L. & STRUKOVA, S. 2015. Peptide-agonist of protease-activated receptor (PAR1) stimulates keratinocyte proliferation and epithelial layer wound healing similarly to activated protein C. *Biochemistry (Moscow) Supplement Series B: Biomedical Chemistry,* 9**,** 199-204.
KLARENBACH, S. W., CHIPIUK, A., NELSON, R. C., HOLLENBERG, M. D. & MURRAY, A. G. 2003. Differential actions of PAR2 and PAR1 in stimulating human endothelial cell exocytosis and permeability: the role of Rho-GTPases. *Circulation research,* 92**,** 272-278.

KONG, W., MCCONALOGUE, K., KHITIN, L. M., HOLLENBERG, M. D., PAYAN, D. G., BOHM, S. K. & BUNNETT, N. W. 1997. Luminal trypsin may regulate enterocytes through proteinase-activated receptor 2. *Proc Natl Acad Sci U S A,* 94**,** 8884-9.

KOOISTRA, A. J., MORDALSKI, S., PÁNDY-SZEKERES, G., ESGUERRA, M., MAMYRBEKOV, A., MUNK, C., KESERŰ, G. M. & GLORIAM, D. E. 2021. GPCRdb in 2021: integrating GPCR sequence, structure and function. *Nucleic Acids Res,* 49**,** D335-d343.

KOPRUSZINSKI, C. M., LINLEY, J. E., THORNTON, P., WALKER, A. S., NEWTON, P., PODICHETTY, S., RUPAREL, R. H., MOREIRA DE SOUZA, L. H., NAVRATILOVA, E., MENO-TETANG, G., GURRELL, I., DODICK, D. W., DOBSON, C., CHESSELL, T., PORRECA, F. & CHESSELL, I. 2025. Efficacy of MEDI0618, a pH-dependent monoclonal antibody targeting PAR2, in preclinical models of migraine. *Brain*.

KOUSSOUNADIS, A., LANGDON, S. P., UM, I. H., HARRISON, D. J. & SMITH, V. A. 2015. Relationship between differentially expressed mRNA and mRNA-protein correlations in a xenograft model system. *Scientific Reports,* 5**,** 10775.

KRIEGER, J. N., LEE, S. W., JEON, J., CHEAH, P. Y., LIONG, M. L. & RILEY, D. E. 2008. Epidemiology of prostatitis. *Int J Antimicrob Agents,* 31 Suppl 1**,** S85-90.

KULIOPULOS, A. & COVIC, L. 2003. Blocking receptors on the inside: pepducin-based intervention of PAR signaling and thrombosis. *Life Sci,* 74**,** 255-62.

KUME, M., AHMAD, A., DEFEA, K. A., VAGNER, J., DUSSOR, G., BOITANO, S. & PRICE, T. J. 2023a. Protease-Activated Receptor 2 (PAR2) Expressed in Sensory Neurons Contributes to Signs of Pain and Neuropathy in Paclitaxel Treated Mice. *J Pain,* 24**,** 1980-1993.

KUME, M., AHMAD, A., SHIERS, S., BURTON, M. D., DEFEA, K. A., VAGNER, J., DUSSOR, G., BOITANO, S. & PRICE, T. J. 2023b. C781, a β-Arrestin Biased Antagonist at Protease-Activated Receptor-2 (PAR2), Displays in vivo Efficacy Against Protease-Induced Pain in Mice. *The Journal of Pain,* 24**,** 605-616.

LAEDERMANN, C. J., ABRIEL, H. & DECOSTERD, I. 2015. Post-translational modifications of voltage-gated sodium channels in chronic pain syndromes. *Frontiers in Pharmacology,* 6.

LAM, D. K., DANG, D., ZHANG, J., DOLAN, J. C. & SCHMIDT, B. L. 2012. Novel animal models of acute and chronic cancer pain: a pivotal role for PAR2. *J Neurosci,* 32**,** 14178-83.

LAM, D. K. & SCHMIDT, B. L. 2010. Serine proteases and protease-activated receptor 2-dependent allodynia: a novel cancer pain pathway. *Pain,* 149**,** 263-72.

LAN, R. S., STEWART, G. A. & HENRY, P. J. 2000. Modulation of airway smooth muscle tone by protease activated receptor-1,-2,-3 and -4 in trachea isolated from influenza A virus-infected mice. *Br J Pharmacol,* 129**,** 63-70.

LAN, R. S., STEWART, G. A. & HENRY, P. J. 2002. Role of protease-activated receptors in airway function: a target for therapeutic intervention? *Pharmacology & Therapeutics,* 95**,** 239-257.

LANDMARK, L., SUNDE, H. F., FORS, E. A., KENNAIR, L. E. O., SAYADIAN, A., BACKELIN, C. & REME, S. E. 2024. Associations between pain intensity, psychosocial factors, and pain-related disability in 4285 patients with chronic pain. *Scientific Reports,* 14**,** 13477.

LATORRACA, N. R., VENKATAKRISHNAN, A. J. & DROR, R. O. 2017. GPCR Dynamics: Structures in Motion. *Chem Rev,* 117**,** 139-155.

LATREMOLIERE, A. & WOOLF, C. J. 2009. Central sensitization: a generator of pain hypersensitivity by central neural plasticity. *J Pain,* 10**,** 895-926.

LAVOIE, H., GAGNON, J. & THERRIEN, M. 2020. ERK signalling: a master regulator of cell behaviour, life and fate. *Nat Rev Mol Cell Biol,* 21**,** 607-632.

LEBONVALLET, N., FLUHR, J. W., LE GALL-IANOTTO, C., LESCHIERA, R., TALAGAS, M., REUX, A., BATAILLE, A., BRUN, C., ODDOS, T., PENNEC, J. P., CARRÉ, J. L. & MISERY, L. 2021. A re-innervated in vitro skin model of non-histaminergic itch and skin neurogenic inflammation: PAR2-, TRPV1- and TRPA1-agonist induced functionality. *Skin Health Dis,* 1**,** e66.

LEE-RIVERA, I., LÓPEZ, E. & LÓPEZ-COLOMÉ, A. M. 2022. Diversification of PAR signaling through receptor crosstalk. *Cellular & Molecular Biology Letters,* 27**,** 77.

LEE, K.-H., LEE, J., JEONG, J., WOO, J., LEE, C.-H. & YOO, C.-G. 2018. Cigarette smoke extract enhances neutrophil elastase-induced IL-8 production via proteinase-activated receptor-2 upregulation in human bronchial epithelial cells. *Experimental & Molecular Medicine,* 50**,** 79.

LEE, S. E., KIM, J. M., JEONG, S. K., JEON, J. E., YOON, H. J., JEONG, M. K. & LEE, S. H. 2010. Protease-activated receptor-2 mediates the expression of inflammatory cytokines, antimicrobial peptides, and matrix metalloproteinases in keratinocytes in response to Propionibacterium acnes. *Arch Dermatol Res,* 302**,** 745-56.

LEE, Y. J., KIM, S. J., KWON, K. W., LEE, W. M., IM, W. J. & SOHN, U. D. 2017. Inhibitory effect of FSLLRY-NH2 on inflammatory responses induced by hydrogen peroxide in HepG2 cells. *Archives of Pharmacal Research,* 40**,** 854-863.

LEFKOWITZ, R. J. 2013. A brief history of G-protein coupled receptors (Nobel Lecture). *Angewandte Chemie International Edition,* 52.

LI, B., ZOU, Z., MENG, F., RAZ, E., HUANG, Y., TAO, A. & AI, Y. 2019. Dust mite-derived Der f 3 activates a pro-inflammatory program in airway epithelial cells via PAR-1 and PAR-2. *Mol Immunol,* 109**,** 1-11.

LI, C.-X., LIN, X.-Y., LI, H.-Y., XU, L., WU, L., YE, P.-L., LI, H., ZHOU, L.-C. & QIN, G.-Z. 2021. Qinshi Shimiao San Enhances Autophagy Via TLR4/p38MAPK/NF-κB Signaling Pathway in Treating Chronic Prostatitis. *Available at SSRN 3989479*.

LI, J., ZHENG, D., QI, S., MAO, C. & JIANG, Y. 2025. Dual-functional Nanosized Albumin Facilitates CRISPR-Cas9-PAR2 to Mitigate Cytokine Storm via TLR4 and Pyroptosis Signaling. *Small,* 21**,** 2405593.

LI, Y., HUANG, H., CHEN, X., YU, N., YE, X., CHEN, L. & HUANG, Z. 2022. PAR2 promotes tumor-associated angiogenesis in lung adenocarcinoma through activating EGFR pathway. *Tissue Cell,* 79**,** 101918.

LIEU, T., SAVAGE, E., ZHAO, P., EDGINGTON-MITCHELL, L., BARLOW, N., BRON, R., POOLE, D. P., MCLEAN, P., LOHMAN, R. J., FAIRLIE, D. P. & BUNNETT, N. W. 2016. Antagonism of the proinflammatory and pronociceptive actions of canonical and biased agonists of protease-activated receptor-2. *Br J Pharmacol,* 173**,** 2752-65.

LIN, C., VON DER THÜSEN, J., DAALHUISEN, J., TEN BRINK, M., CRESTANI, B., VAN DER POLL, T., BORENSZTAJN, K. & SPEK, C. A. 2015. Protease-activated receptor (PAR)-2 is required for PAR-1 signalling in pulmonary fibrosis. *J Cell Mol Med,* 19**,** 1346-56.

LIN, H. & TREJO, J. 2013. Transactivation of the PAR1-PAR2 heterodimer by thrombin elicits beta-arrestin-mediated endosomal signaling. *J Biol Chem,* 288**,** 11203-15.

LINLEY, J. E., ROSE, K., PATIL, M., ROBERTSON, B., AKOPIAN, A. N. & GAMPER, N. 2008. Inhibition of M Current in Sensory Neurons by Exogenous Proteases: A Signaling Pathway Mediating Inflammatory Nociception. *The Journal of Neuroscience,* 28**,** 11240-11249.

LITWIN, M. S., MCNAUGHTON-COLLINS, M., FOWLER, F. J., JR., NICKEL, J. C., CALHOUN, E. A., PONTARI, M. A., ALEXANDER, R. B., FARRAR, J. T. & O'LEARY, M. P. 1999. The National Institutes of Health chronic prostatitis symptom index: development and validation of a new outcome measure. Chronic Prostatitis Collaborative Research Network. *J Urol,* 162**,** 369-75.

LIU, H., LESSIEUR, E. M., SAADANE, A., LINDSTROM, S. I., TAYLOR, P. R. & KERN, T. S. 2019. Neutrophil elastase contributes to the pathological vascular permeability characteristic of diabetic retinopathy. *Diabetologia,* 62**,** 2365-2374.

LIU, H., WANG, Z., XIE, Q., CHI, A., LI, Y., DAI, J., ZHANG, M., DENG, C. & LIU, G. 2022a. Ningmitai capsules have anti-inflammatory and pain-relieving effects in the chronic prostatitis/chronic pelvic pain syndrome mouse model through systemic immunity. *Front Pharmacol,* 13**,** 949316.

LIU, P., SUN, L., ZHAO, X. L., ZHANG, P., ZHAO, X. M. & ZHANG, J. 2014a. PAR2-mediated epigenetic upregulation of alpha-synuclein contributes to the pathogenesis of Parkinsons disease. *Brain Res,* 1565**,** 82-9.

LIU, S., LIU, Y. P., YUE, D. M. & LIU, G. J. 2014b. Protease-activated receptor 2 in dorsal root ganglion contributes to peripheral sensitization of bone cancer pain. *Eur J Pain,* 18**,** 326-37.

LIU, S. C., JEN, Y. M., JIANG, S. S., CHANG, J. L., HSIUNG, C. A., WANG, C. H. & JUANG, J. L. 2009. G(alpha)12-mediated pathway promotes invasiveness of nasopharyngeal carcinoma by modulating actin cytoskeleton reorganization. *Cancer Res,* 69**,** 6122-30.

LIU, T., ZHANG, L., JOO, D. & SUN, S. C. 2017. NF-κB signaling in inflammation. *Signal Transduct Target Ther,* 2**,** 17023-.

LIU, X. J., MU, Z. L., ZHAO, Y. & ZHANG, J. Z. 2016. Topical Tetracycline Improves MC903-induced Atopic Dermatitis in Mice through Inhibition of Inflammatory Cytokines and Thymic Stromal Lymphopoietin Expression. *Chin Med J (Engl),* 129**,** 1483-90.

LIU, Y., LI, H., HU, J., WU, Z., MENG, J., HAYASHI, Y., NAKANISHI, H., QING, H. & NI, J. 2022b. Differential Expression and Distinct Roles of Proteinase-Activated Receptor 2 in Microglia and Neurons in Neonatal Mouse Brain After Hypoxia-Ischemic Injury. *Mol Neurobiol,* 59**,** 717-730.

LIVAK, K. J. & SCHMITTGEN, T. D. 2001. Analysis of relative gene expression data using real-time quantitative PCR and the 2(-Delta Delta C(T)) Method. *Methods,* 25**,** 402-8.

LOCKWOOD, S. & DICKENSON, A. H. 2020. What goes up must come down: insights from studies on descending controls acting on spinal pain processing. *J Neural Transm (Vienna),* 127**,** 541-549.

LOEW, D., PERRAULT, C., MORALES, M., MOOG, S., RAVANAT, C., SCHUHLER, S., ARCONE, R., PIETROPAOLO, C., CAZENAVE, J.-P. & VAN DORSSELAER, A. 2000. Proteolysis of the exodomain of recombinant protease-activated receptors: prediction of receptor activation or inactivation by MALDI mass spectrometry. *Biochemistry,* 39**,** 10812-10822.

LOHMAN, R. J., COTTERELL, A. J., BARRY, G. D., LIU, L., SUEN, J. Y., VESEY, D. A. & FAIRLIE, D. P. 2012. An antagonist of human protease activated receptor-2 attenuates PAR2 signaling, macrophage activation, mast cell degranulation, and collagen-induced arthritis in rats. *Faseb j,* 26**,** 2877-87.

LOPES, A. H., SILVA, R. L., FONSECA, M. D., GOMES, F. I., MAGANIN, A. G., RIBEIRO, L. S., MARQUES, L. M. M., CUNHA, F. Q., ALVES-FILHO, J. C., ZAMBONI, D. S., LOPES, N. P., FRANKLIN, B. S., GOMBAULT, A., RAMALHO, F. S., QUESNIAUX, V. F. J., COUILLIN, I., RYFFEL, B. & CUNHA, T. M. 2020. Molecular basis of carrageenan-induced cytokines production in macrophages. *Cell Communication and Signaling,* 18**,** 141.

LORENOWICZ, M. J., FERNANDEZ-BORJA, M., KOOISTRA, M. R. H., BOS, J. L. & HORDIJK, P. L. 2008. PKA and Epac1 regulate endothelial integrity and migration through parallel and independent pathways. *European Journal of Cell Biology,* 87**,** 779-792.

LOUIS, R., LAU, L. C., BRON, A. O., ROLDAAN, A. C., RADERMECKER, M. & DJUKANOVIC, R. 2000. The relationship between airways inflammation and asthma severity. *American journal of respiratory and critical care medicine,* 161**,** 9-16.

LUCENA, F. & MCDOUGALL, J. J. 2020. Pain responses to protease-activated receptor-2 stimulation in the spinal cord of naïve and arthritic rats. *Neurosci Lett,* 739**,** 135391.

LUO, J., WU, X., LIU, H., CUI, W., GUO, W., GUO, K., GUO, H., TAO, K., LI, F., SHI, Y., FENG, D., YAN, H., GAO, G. & QU, Y. 2021. Antagonism of Protease-Activated Receptor 4 Protects Against Traumatic Brain Injury by Suppressing Neuroinflammation via Inhibition of Tab2/NF-κB Signaling. *Neurosci Bull,* 37**,** 242-254.

LÜSCHER, C. & SLESINGER, P. A. 2010. Emerging roles for G protein-gated inwardly rectifying potassium (GIRK) channels in health and disease. *Nat Rev Neurosci,* 11**,** 301-15.

MA, L. & DORLING, A. 2012. The roles of thrombin and protease-activated receptors in inflammation. *Semin Immunopathol,* 34**,** 63-72.

MA, X., LAO, Y., BAI, Y., GUAN, X., JIANG, J., CUI, M. & DONG, Z. 2025. Study progress of etiologic mechanisms of chronic prostatitis/chronic pelvic pain syndrome. *International Immunopharmacology,* 148**,** 114128.

MACFARLANE, S. R., SEATTER, M. J., KANKE, T., HUNTER, G. D. & PLEVIN, R. 2001. Proteinase-activated receptors. *Pharmacol Rev,* 53**,** 245-82.

MACFARLANE, S. R., SLOSS, C. M., CAMERON, P., KANKE, T., MCKENZIE, R. C. & PLEVIN, R. 2005. The role of intracellular Ca2+ in the regulation of proteinase-activated receptor-2 mediated nuclear factor kappa B signalling in keratinocytes. *Br J Pharmacol,* 145**,** 535-44.

MACKIE, E. J., PAGEL, C. N., SMITH, R., DE NIESE, M. R., SONG, S. J. & PIKE, R. N. 2002. Protease-activated receptors: a means of converting extracellular proteolysis into intracellular signals. *IUBMB Life,* 53**,** 277-81.

MANNING, D. R. & BLUMENTHAL, D. K. 2023. Pharmacodynamics: Molecular Mechanisms of Drug Action. *In:* BRUNTON, L. L. & KNOLLMANN, B. C. (eds.) *Goodman & Gilman's: The Pharmacological Basis of Therapeutics, 14th Edition.* New York, NY: McGraw-Hill Education.

MANNOWETZ, N., WÜRDINGER, R., ZIPPEL, A., AUMÜLLER, G. & WENNEMUTH, G. 2010. Expression of proteinase-activated receptor-2 (PAR2) is androgen-dependent in stromal cell line (hPCPs) from benign prostatic hyperplasia. *The Prostate,* 70**,** 1350-1358.

MANOJ, S. 2023. Intervention of PAR-2 Mediated CGRP in Animal Model of Visceral Hyperalgesia. *In:* MAHMUT, K., VOLKAN, G. & ABDULSAMED, K. (eds.) *Animal Models and Experimental Research in Medicine.* Rijeka: IntechOpen.

MAREK-JOZEFOWICZ, L., NEDOSZYTKO, B., GROCHOCKA, M., ŻMIJEWSKI, M. A., CZAJKOWSKI, R., CUBAŁA, W. J. & SLOMINSKI, A. T. 2023. Molecular Mechanisms of Neurogenic Inflammation of the Skin. *International Journal of Molecular Sciences,* 24**,** 5001.

MARSZALEK, M., WEHRBERGER, C., HOCHREITER, W., TEMML, C. & MADERSBACHER, S. 2007. Symptoms suggestive of chronic pelvic pain syndrome in an urban population: prevalence and associations with lower urinary tract symptoms and erectile function. *J Urol,* 177**,** 1815-9.

MASON, B. N., HASSLER, S. N., DEFEA, K., BOITANO, S., VAGNER, J., PRICE, T. J. & DUSSOR, G. 2023. PAR2 activation in the dura causes acute behavioral responses and priming to glyceryl trinitrate in a mouse migraine model. *The Journal of Headache and Pain,* 24**,** 42.

MATSUDA, M., HUH, Y. & JI, R. R. 2019. Roles of inflammation, neurogenic inflammation, and neuroinflammation in pain. *J Anesth,* 33**,** 131-139.

MATSUSHIMA, K., YANG, D. & OPPENHEIM, J. J. 2022. Interleukin-8: An evolving chemokine. *Cytokine,* 153**,** 155828.
MCCLELLAND, S., MAXWELL, P. J., BRANCO, C., BARRY, S. T., EBERLEIN, C. & LABONTE, M. J. 2024. Targeting IL-8 and Its Receptors in Prostate Cancer: Inflammation, Stress Response, and Treatment Resistance. *Cancers (Basel),* 16.
MCDOUGALL, J. J., MCCONNELL, M. & REID, A. R. 2021. Intracellular versus extracellular inhibition of calpain I causes differential effects on pain in a rat model of joint inflammation. *Mol Pain,* 17**,** 17448069211016141.
MCDOUGALL, J. J., ZHANG, C., CELLARS, L., JOUBERT, E., DIXON, C. M. & VERGNOLLE, N. 2009. Triggering of proteinase-activated receptor 4 leads to joint pain and inflammation in mice. *Arthritis Rheum,* 60**,** 728-37.
MCGUIRE, J. J., SAIFEDDINE, M., TRIGGLE, C. R., SUN, K. & HOLLENBERG, M. D. 2004. 2-furoyl-LIGRLO-amide: a potent and selective proteinase-activated receptor 2 agonist. *Journal of Pharmacology and Experimental Therapeutics,* 309**,** 1124-1131.
MCINTOSH, K., CUNNINGHAM, M. R., CADALBERT, L., LOCKHART, J., BOYD, G., FERRELL, W. R. & PLEVIN, R. 2010. Proteinase-activated receptor-2 mediated inhibition of TNFalpha-stimulated JNK activation - A novel paradigm for G(q/11) linked GPCRs. *Cell Signal,* 22**,** 265-73.
MCINTOSH, K. A., CUNNINGHAM, M. R., BUSHELL, T. & PLEVIN, R. 2020. The development of proteinase-activated receptor-2 modulators and the challenges involved. *Biochem Soc Trans,* 48**,** 2525-2537.
MCKIM, J. M. 2014. Food additive carrageenan: Part I: A critical review of carrageenan in vitro studies, potential pitfalls, and implications for human health and safety. *Critical Reviews in Toxicology,* 44**,** 211-243.
MCKIM, J. M., JR., WILGA, P. C., PREGENZER, J. F. & BLAKEMORE, W. R. 2015. The common food additive carrageenan is not a ligand for Toll-Like- Receptor 4 (TLR4) in an HEK293-TLR4 reporter cell-line model. *Food Chem Toxicol,* 78**,** 153-8.
MEIER-SOELCH, J., MAYR-BURO, C., JULI, J., LEIB, L., LINNE, U., DREUTE, J., PAPANTONIS, A., SCHMITZ, M. L. & KRACHT, M. 2021. Monitoring the Levels of Cellular NF-κB Activation States. *Cancers,* 13**,** 5351.
MELLON, P. L., CLEGG, C. H., CORRELL, L. A. & MCKNIGHT, G. S. 1989. Regulation of transcription by cyclic AMP-dependent protein kinase. *Proc Natl Acad Sci U S A,* 86**,** 4887-91.
MENON, J., DOEBELE, R. C., GOMES, S., BEVILACQUA, E., REINDL, K. M. & ROSNER, M. R. 2012. A novel interplay between Rap1 and PKA regulates induction of angiogenesis in prostate cancer. *PLoS One,* 7**,** e49893.
MENOU, A., DUITMAN, J., FLAJOLET, P., SALLENAVE, J. M., MAILLEUX, A. A. & CRESTANI, B. 2017. Human airway trypsin-like protease, a serine protease involved in respiratory diseases. *Am J Physiol Lung Cell Mol Physiol,* 312**,** L657-l668.
MICHAEL, E. S., KULIOPULOS, A., COVIC, L., STEER, M. L. & PERIDES, G. 2013. Pharmacological inhibition of PAR2 with the pepducin P2pal-18S protects mice against acute experimental biliary pancreatitis. *Am J Physiol Gastrointest Liver Physiol,* 304**,** G516-26.
MIIKE, S., MCWILLIAM, A. S. & KITA, H. 2001. Trypsin Induces Activation and Inflammatory Mediator Release from Human Eosinophils Through Protease-Activated Receptor-21. *The Journal of Immunology,* 167**,** 6615-6622.
MIKI, M., NAKAMURA, Y., TAKAHASHI, A., NAKAYA, Y., EGUCHI, H., MASEGI, T., YONEDA, K., YASUOKA, S. & SONE, S. 2003. Effect of human airway trypsin-like protease on intracellular free Ca^ 2^+ concentration in human bronchial epithelial cells. *Journal of Medical Investigation,* 50**,** 95-107.

MINETT, M. S., QUICK, K. & WOOD, J. N. 2011. Behavioral Measures of Pain Thresholds. *Curr Protoc Mouse Biol,* 1**,** 383-412.
MIRAKHUR, M. & DIENER, M. 2022. Proteinase-activated receptors regulate intestinal functions in a segment-dependent manner in rats. *European Journal of Pharmacology,* 933**,** 175264.
MIZE, G. J., WANG, W. & TAKAYAMA, T. K. 2008. Prostate-specific kallikreins-2 and-4 enhance the proliferation of DU-145 prostate cancer cells through protease-activated receptors-1 and-2. *Molecular Cancer Research,* 6**,** 1043-1051.
MOLINO, M., BARNATHAN, E. S., NUMEROF, R., CLARK, J., DREYER, M., CUMASHI, A., HOXIE, J. A., SCHECHTER, N., WOOLKALIS, M. & BRASS, L. F. 1997. Interactions of mast cell tryptase with thrombin receptors and PAR-2. *Journal of Biological Chemistry,* 272**,** 4043-4049.
MOLLIVER, D. C. 2009. G-Protein Coupled Receptors in Sensory Neuron Function and Pain. *In:* BINDER, M. D., HIROKAWA, N. & WINDHORST, U. (eds.) *Encyclopedia of Neuroscience.* Berlin, Heidelberg: Springer Berlin Heidelberg.
MOREIRAS, H., BENTO-LOPES, L., NETO, M. V., ESCREVENTE, C., CABAÇO, L. C., HALL, M. J., RAMALHO, J. S., SEABRA, M. C. & BARRAL, D. C. 2022. Melanocore uptake by keratinocytes occurs through phagocytosis and involves protease-activated receptor-2 internalization. *Traffic,* 23**,** 331-345.
MORRIS, C. J. 2003. Carrageenan-Induced Paw Edema in the Rat and Mouse. *In:* WINYARD, P. G. & WILLOUGHBY, D. A. (eds.) *Inflammation Protocols.* Totowa, NJ: Humana Press.
MOSNIER, L. O., SINHA, R. K., BURNIER, L., BOUWENS, E. A. & GRIFFIN, J. H. 2012. Biased agonism of protease-activated receptor 1 by activated protein C caused by noncanonical cleavage at Arg46. *Blood,* 120**,** 5237-46.
MOUDIO, S., WILLIS, A., PYTKA, K., ABULKASSIM, R., BRETT, R. R., WEBSTER, J. F., WOZNY, C., BARBOUR, M., JIANG, H. R., WATSON, D. G., VAN KRALINGEN, J. C., MACKENZIE, S. M., DANIELS, M., MCCOLL, B. W., SOSSICK, S., NUTHALL, H. N. & BUSHELL, T. J. 2022. Protease-activated receptor 2 activation induces behavioural changes associated with depression-like behaviour through microglial-independent modulation of inflammatory cytokines. *Psychopharmacology (Berl),* 239**,** 229-242.
MROZKOVA, P., PALECEK, J. & SPICAROVA, D. 2016. The role of protease-activated receptor type 2 in nociceptive signaling and pain. *Physiol Res,* 65**,** 357-67.
MROZKOVA, P., SPICAROVA, D. & PALECEK, J. 2021. Spinal PAR2 Activation Contributes to Hypersensitivity Induced by Peripheral Inflammation in Rats. *International Journal of Molecular Sciences,* 22**,** 991.
MULEY, M. M., KRUSTEV, E., REID, A. R. & MCDOUGALL, J. J. 2017. Prophylactic inhibition of neutrophil elastase prevents the development of chronic neuropathic pain in osteoarthritic mice. *J Neuroinflammation,* 14**,** 168.
MULEY, M. M., REID, A. R., BOTZ, B., BOELCSKEI, K., HELYES, Z. & MCDOUGALL, J. J. 2016. Neutrophil elastase induces inflammation and pain in mouse knee joints via activation of proteinase-activated receptor-2. *British journal of pharmacology,* 173**,** 766-777.
MURATSPAHIĆ, E., FREISSMUTH, M. & GRUBER, C. W. 2019. Nature-Derived Peptides: A Growing Niche for GPCR Ligand Discovery. *Trends Pharmacol Sci,* 40**,** 309-326.
MYATT, A. & HILL, S. J. 2005. Trypsin stimulates the phosphorylation of p42,44 mitogen-activated protein kinases via the proteinase-activated receptor-2 and protein kinase C epsilon in human cultured prostate stromal cells. *Prostate,* 64**,** 175-85.
NAGARAJA, S., TEWARI, S. G. & REIFMAN, J. 2023. Identification of key factors driving inflammation-induced sensitization of muscle sensory neurons. *Front Neurosci,* 17**,** 1147437.

NAKANISHI-MATSUI, M., ZHENG, Y. W., SULCINER, D. J., WEISS, E. J., LUDEMAN, M. J. & COUGHLIN, S. R. 2000. PAR3 is a cofactor for PAR4 activation by thrombin. *Nature,* 404**,** 609-13.

NANEVICZ, T., WANG, L., CHEN, M., ISHII, M. & COUGHLIN, S. R. 1996. Thrombin Receptor Activating Mutations Alteration of an Extracellular Agonist Recognition Domain Causes Constitutive Signaling. *Journal of Biological Chemistry,* 271**,** 702-706.

NAPOLI, C., CICALA, C., WALLACE, J. L., DE NIGRIS, F., SANTAGADA, V., CALIENDO, G., FRANCONI, F., IGNARRO, L. J. & CIRINO, G. 2000. Protease-activated receptor-2 modulates myocardial ischemia-reperfusion injury in the rat heart. *Proc Natl Acad Sci U S A,* 97**,** 3678-83.

NATIONAL RESEARCH, C. & INSTITUTE FOR LABORATORY ANIMAL, R. 2011. Guide for the care and use of laboratory animals. 8th ed ed. Washington, D.C.: National Academies Press.

NECAS, J. & BARTOSIKOVA, L. 2013. Carrageenan: a review. *Veterinarni medicina,* 58.

NEURATH, H. & WALSH, K. A. 1976. Role of proteolytic enzymes in biological regulation (a review). *Proc Natl Acad Sci U S A,* 73**,** 3825-32.

NGUYEN, C., COELHO, A. M., GRADY, E., COMPTON, S. J., WALLACE, J. L., HOLLENBERG, M. D., CENAC, N., GARCIA-VILLAR, R., BUENO, L., STEINHOFF, M., BUNNETT, N. W. & VERGNOLLE, N. 2003. Colitis induced by proteinase-activated receptor-2 agonists is mediated by a neurogenic mechanism. *Can J Physiol Pharmacol,* 81**,** 920-7.

NHU, Q. M., SHIREY, K., TEIJARO, J. R., FARBER, D. L., NETZEL-ARNETT, S., ANTALIS, T. M., FASANO, A. & VOGEL, S. N. 2010. Novel signaling interactions between proteinase-activated receptor 2 and Toll-like receptors in vitro and in vivo. *Mucosal Immunol,* 3**,** 29-39.

NHU, Q. M., SHIREY, K. A., PENNINI, M. E., STILTZ, J. & VOGEL, S. N. 2012. Proteinase-activated receptor 2 activation promotes an anti-inflammatory and alternatively activated phenotype in LPS-stimulated murine macrophages. *Innate Immun,* 18**,** 193-203.

NICKEL, J. C. & SHOSKES, D. A. 2010. Phenotypic approach to the management of the chronic prostatitis/chronic pelvic pain syndrome. *BJU Int,* 106**,** 1252-63.

NIDDK, N. I. O. D. A. D. A. K. D. 2014. *Prostatitis: Inflammation of the Prostate* [Online]. Available: https://www.niddk.nih.gov/health-information/urologic-diseases/prostate-problems/prostatitis-inflammation-prostate#prostatitis [Accessed February 2025].

NIKOLAKOPOULOU, A. M., GEORGAKOPOULOS, A. & ROBAKIS, N. K. 2016. Presenilin 1 promotes trypsin-induced neuroprotection via the PAR2/ERK signaling pathway. Effects of presenilin 1 FAD mutations. *Neurobiol Aging,* 42**,** 41-9.

NISHIMOTO, R., KODAMA, C., YAMASHITA, H. & HATTORI, F. 2023. Human Induced Pluripotent Stem Cell-Derived Keratinocyte-Like Cells for Research on Protease-Activated Receptor 2 in Nonhistaminergic Cascades of Atopic Dermatitis *J Pharmacol Exp Ther,* 384**,** 248-253.

NOH, C. S., CHUNG, H. Y., HAN, I. H., KIM, J. H., KIM, Y. M. & RYU, J. S. 2021. Mast cell tryptase-PAR2 pathway in proliferation of prostatic stromal cells reacted with Trichomonas vaginalis. *Parasite Immunol,* 43**,** e12868.

NOORBAKHSH, F., TSUTSUI, S., VERGNOLLE, N., BOVEN, L. A., SHARIAT, N., VODJGANI, M., WARREN, K. G., ANDRADE-GORDON, P., HOLLENBERG, M. D. & POWER, C. 2006. Proteinase-activated receptor 2 modulates neuroinflammation in experimental autoimmune encephalomyelitis and multiple sclerosis. *J Exp Med,* 203**,** 425-35.

NYSTEDT, S., EMILSSON, K., LARSSON, A. K., STROMBECK, B. & SUNDELIN, J. 1995a. Molecular cloning and functional expression of the gene encoding the human proteinase-activated receptor 2. *Eur J Biochem,* 232**,** 84-9.

NYSTEDT, S., EMILSSON, K., WAHLESTEDT, C. & SUNDELIN, J. 1994. Molecular cloning of a potential proteinase activated receptor. *Proc Natl Acad Sci U S A,* 91**,** 9208-12.
NYSTEDT, S., LARSSON, A.-K., ÅBERG, H. & SUNDELIN, J. 1995b. The Mouse Proteinase-activated Receptor-2 cDNA and Gene MOLECULAR CLONING AND FUNCTIONAL EXPRESSION. *Journal of Biological Chemistry,* 270**,** 5950-5955.
NYSTEDT, S., RAMAKRISHNAN, V. & SUNDELIN, J. 1996. The proteinase-activated receptor 2 is induced by inflammatory mediators in human endothelial cells. Comparison with the thrombin receptor. *J Biol Chem,* 271**,** 14910-5.
O'CALLAGHAN, K., KULIOPULOS, A. & COVIC, L. 2012. Turning receptors on and off with intracellular pepducins: new insights into G-protein-coupled receptor drug development. *J Biol Chem,* 287**,** 12787-96.
OE, Y., FUSHIMA, T., SATO, E., SEKIMOTO, A., KISU, K., SATO, H., SUGAWARA, J., ITO, S. & TAKAHASHI, N. 2019. Protease-activated receptor 2 protects against VEGF inhibitor-induced glomerular endothelial and podocyte injury. *Scientific Reports,* 9**,** 2986.
OELKE, M. 2020. Physiology and Pharmacology of the Prostate. *In:* CHAPPLE, C. R., STEERS, W. D. & EVANS, C. P. (eds.) *Urologic Principles and Practice.* Cham: Springer International Publishing.
OIKONOMOPOULOU, K., HANSEN, K. K., CHAPMAN, K., VERGNOLLE, N., DIAMANDIS, E. P. & HOLLENBERG, M. D. 2007. Kallikrein-mediated activation of PARs in inflammation and nociception. *Inflammation Research,* 56**,** S499-S502.
OIKONOMOPOULOU, K., HANSEN, K. K., SAIFEDDINE, M., TEA, I., BLABER, M., BLABER, S. I., SCARISBRICK, I., ANDRADE-GORDON, P., COTTRELL, G. S. & BUNNETT, N. W. 2006. Proteinase-activated receptors, targets for kallikrein signaling. *Journal of Biological Chemistry,* 281**,** 32095-32112.
OLDHAM, W. M. & HAMM, H. E. 2007. How do receptors activate G proteins? *Adv Protein Chem,* 74**,** 67-93.
OLDHAM, W. M. & HAMM, H. E. 2008. Heterotrimeric G protein activation by G-protein-coupled receptors. *Nat Rev Mol Cell Biol,* 9**,** 60-71.
OSSOVSKAYA, V. S. & BUNNETT, N. W. 2004. Protease-activated receptors: contribution to physiology and disease. *Physiological reviews,* 84**,** 579-621.
OSTROWSKA, E. & REISER, G. 2008. The protease-activated receptor-3 (PAR-3) can signal autonomously to induce interleukin-8 release. *Cell Mol Life Sci,* 65**,** 970-81.
OUYANG, X., REIHILL, J. A., DOUGLAS, L. E. J., DUNNE, O. M., SERGEANT, G. P. & MARTIN, S. L. 2024. House dust mite allergens induce Ca(2+) signalling and alarmin responses in asthma airway epithelial cells. *Biochim Biophys Acta Mol Basis Dis,* 1870**,** 167079.
PAINE, C., SHARLOW, E., LIEBEL, F., EISINGER, M., SHAPIRO, S. & SEIBERG, M. 2001. An alternative approach to depigmentation by soybean extracts via inhibition of the PAR-2 pathway. *J Invest Dermatol,* 116**,** 587-95.
PAING, M. M., STUTTS, A. B., KOHOUT, T. A., LEFKOWITZ, R. J. & TREJO, J. 2002. β-Arrestins regulate protease-activated receptor-1 desensitization but not internalization or down-regulation. *Journal of Biological Chemistry,* 277**,** 1292-1300.
PANETTIERI JR, R. A., HALL, I. P., MAKI, C. S. & MURRAY, R. K. 1995. alpha-Thrombin increases cytosolic calcium and induces human airway smooth muscle cell proliferation. *American Journal of Respiratory Cell and Molecular Biology,* 13**,** 205-216.
PARK, J. & LUO, Z. D. 2010. Calcium channel functions in pain processing. *Channels (Austin),* 4**,** 510-7.
PATIL, K. R., MAHAJAN, U. B., UNGER, B. S., GOYAL, S. N., BELEMKAR, S., SURANA, S. J., OJHA, S. & PATIL, C. R. 2019. Animal Models of Inflammation

for Screening of Anti-inflammatory Drugs: Implications for the Discovery and Development of Phytopharmaceuticals. *International Journal of Molecular Sciences,* 20**,** 4367.
PAUL, A., DOHERTY, K. & PLEVIN, R. 1997. Differential regulation by protein kinase C isoforms of nitric oxide synthase induction in RAW 264.7 macrophages and rat aortic smooth muscle cells. *Br J Pharmacol,* 120**,** 940-6.
PAUL, M., MURPHY, S. F., HALL, C., SCHAEFFER, A. J. & THUMBIKAT, P. 2019. Protease-activated receptor 2 activates CRAC-mediated Ca2+ influx to cause prostate smooth muscle contraction. *FASEB Bioadv,* 1**,** 255-264.
PBD, R. 2024. *Ligand: 8TZ* [Online]. Available: https://www.rcsb.org/ligand/8TZ [Accessed].
PEACH, C. J., EDGINGTON-MITCHELL, L. E., BUNNETT, N. W. & SCHMIDT, B. L. 2023. Protease-activated receptors in health and disease. *Physiological Reviews,* 103**,** 717-785.
PETERSEN, R. K., MADSEN, L., PEDERSEN, L. M., HALLENBORG, P., HAGLAND, H., VISTE, K., DØSKELAND, S. O. & KRISTIANSEN, K. 2008. Cyclic AMP (cAMP)-mediated stimulation of adipocyte differentiation requires the synergistic action of Epac- and cAMP-dependent protein kinase-dependent processes. *Mol Cell Biol,* 28**,** 3804-16.
PIELES, O. & MORSCZECK, C. 2024. The Role of Protein Kinase C During the Differentiation of Stem and Precursor Cells into Tissue Cells. *Biomedicines,* 12.
PINHEIRO, R. M. & CALIXTO, J. B. 2002. Effect of the selective COX-2 inhibitors, celecoxib and rofecoxib in rat acute models of inflammation. *Inflamm Res,* 51**,** 603-10.
PIRAN, R., LEE, S.-H., KUSS, P., HAO, E., NEWLIN, R., MILLÁN, J. L. & LEVINE, F. 2016. PAR2 regulates regeneration, transdifferentiation, and death. *Cell Death & Disease,* 7**,** e2452-e2452.
POLACKWICH, A. S. & SHOSKES, D. A. 2016. Chronic prostatitis/chronic pelvic pain syndrome: a review of evaluation and therapy. *Prostate Cancer and Prostatic Diseases,* 19**,** 132-138.
PONTARI, M. 2025. Chronic prostatitis and chronic pelvic pain syndrome. Mar 29, 2024 ed.
PONTAROLLO, G., MANN, A., BRANDÃO, I., MALINARICH, F., SCHÖPF, M. & REINHARDT, C. 2020. Protease-activated receptor signaling in intestinal permeability regulation. *Febs j,* 287**,** 645-658.
POOLE, D. P., AMADESI, S., VELDHUIS, N. A., ABOGADIE, F. C., LIEU, T., DARBY, W., LIEDTKE, W., LEW, M. J., MCINTYRE, P. & BUNNETT, N. W. 2013. Protease-activated receptor 2 (PAR2) protein and transient receptor potential vanilloid 4 (TRPV4) protein coupling is required for sustained inflammatory signaling. *J Biol Chem,* 288**,** 5790-802.
POTTS, J. & PAYNE, R. E. 2007. Prostatitis: Infection, neuromuscular disorder, or pain syndrome? Proper patient classification is key. *Cleve Clin J Med,* 74 Suppl 3**,** S63-71.
PREDESCU, D. V., CREȚOIU, S. M., CREȚOIU, D., PAVELESCU, L. A., SUCIU, N., RADU, B. M. & VOINEA, S. C. 2019. G Protein-Coupled Receptors (GPCRs)-Mediated Calcium Signaling in Ovarian Cancer: Focus on GPCRs activated by Neurotransmitters and Inflammation-Associated Molecules. *Int J Mol Sci,* 20.
PRICE, R., MERCURI, N. B. & LEDONNE, A. 2021. Emerging Roles of Protease-Activated Receptors (PARs) in the Modulation of Synaptic Transmission and Plasticity. *Int J Mol Sci,* 22.
PRINCE KASONGO, M., PHILIPPA, E., FABIENNE, W. H., MARYLYNE, Y. & BEHNAZIR, M. 2024. The histological prevalence of prostatitis at Potchefstroom Hospital: a cross-sectional study. *Pan Afr Med J,* 47**,** 8.

QUARTA, S., SANDRE, M., RUVOLETTO, M., CAMPAGNOLO, M., EMMI, A., BIASIOLO, A., PONTISSO, P. & ANTONINI, A. 2024. Inhibition of Protease-Activated Receptor-2 Activation in Parkinson's Disease Using 1-Piperidin Propionic Acid. *Biomedicines,* 12.

RADHAKRISHNAN, R. & NALLU, R. S. 2009. Development and characterisation of a novel animal model of prostate inflammation-induced chronic pelvic pain. *Inflammopharmacology,* 17**,** 23-8.

RAHMAN, M. T., GHOSH, C., HOSSAIN, M., LINFIELD, D., REZAEE, F., JANIGRO, D., MARCHI, N. & VAN BOXEL-DEZAIRE, A. H. H. 2018. IFN-γ, IL-17A, or zonulin rapidly increase the permeability of the blood-brain and small intestinal epithelial barriers: Relevance for neuro-inflammatory diseases. *Biochem Biophys Res Commun,* 507**,** 274-279.

RAJA, S. N., CARR, D. B., COHEN, M., FINNERUP, N. B., FLOR, H., GIBSON, S., KEEFE, F. J., MOGIL, J. S., RINGKAMP, M., SLUKA, K. A., SONG, X. J., STEVENS, B., SULLIVAN, M. D., TUTELMAN, P. R., USHIDA, T. & VADER, K. 2020. The revised International Association for the Study of Pain definition of pain: concepts, challenges, and compromises. *Pain,* 161**,** 1976-1982.

RAJAGOPAL, S. & SHENOY, S. K. 2018. GPCR desensitization: Acute and prolonged phases. *Cell Signal,* 41**,** 9-16.

RAJPUT, P. S., LAMB, J., KOTHARI, S., PEREIRA, B., SOETKAMP, D., WANG, Y., TANG, J., VAN EYK, J. E., MULLINS, E. S. & LYDEN, P. D. 2020. Neuron-generated thrombin induces a protective astrocyte response via protease activated receptors. *Glia,* 68**,** 246-262.

RALLABHANDI, P., NHU, Q. M., TOSHCHAKOV, V. Y., PIAO, W., MEDVEDEV, A. E., HOLLENBERG, M. D., FASANO, A. & VOGEL, S. N. 2008. Analysis of proteinase-activated receptor 2 and TLR4 signal transduction: a novel paradigm for receptor cooperativity. *J Biol Chem,* 283**,** 24314-25.

RAMACHANDRAN, R., MIHARA, K., CHUNG, H., RENAUX, B., LAU, C. S., MURUVE, D. A., DEFEA, K. A., BOUVIER, M. & HOLLENBERG, M. D. 2011. Neutrophil elastase acts as a biased agonist for proteinase-activated receptor-2 (PAR2). *J Biol Chem,* 286**,** 24638-48.

RAMACHANDRAN, R., MIHARA, K., MATHUR, M., ROCHDI, M. D., BOUVIER, M., DEFEA, K. & HOLLENBERG, M. D. 2009. Agonist-biased signaling via proteinase activated receptor-2: differential activation of calcium and mitogen-activated protein kinase pathways. *Mol Pharmacol,* 76**,** 791-801.

RAMACHANDRAN, R., NOORBAKHSH, F., DEFEA, K. & HOLLENBERG, M. D. 2012. Targeting proteinase-activated receptors: therapeutic potential and challenges. *Nat Rev Drug Discov,* 11**,** 69-86.

RAYMOND, D. R., WILSON, L. S., CARTER, R. L. & MAURICE, D. H. 2007. Numerous distinct PKA-, or EPAC-based, signalling complexes allow selective phosphodiesterase 3 and phosphodiesterase 4 coordination of cell adhesion. *Cell Signal,* 19**,** 2507-18.

REED, C. E. & KITA, H. 2004. The role of protease activation of inflammation in allergic respiratory diseases. *J Allergy Clin Immunol,* 114**,** 997-1008; quiz 1009.

REES, J., ABRAHAMS, M., DOBLE, A. & COOPER, A. 2015. Diagnosis and treatment of chronic bacterial prostatitis and chronic prostatitis/chronic pelvic pain syndrome: a consensus guideline. *BJU Int,* 116**,** 509-25.

RICCIARDOLO, F. L., STEINHOFF, M., AMADESI, S., GUERRINI, R., TOGNETTO, M., TREVISANI, M., CREMINON, C., BERTRAND, C., BUNNETT, N. W. & FABBRI, L. M. 2000. Presence and bronchomotor activity of protease-activated receptor-2 in guinea pig airways. *American Journal of Respiratory and Critical Care Medicine,* 161**,** 1672-1680.

RICKS, T. K. & TREJO, J. 2009a. Phosphorylation of protease-activated receptor-2 differentially regulates desensitization and internalization. *J Biol Chem,* 284**,** 34444-57.
RICKS, T. K. & TREJO, J. 2009b. Phosphorylation of protease-activated receptor-2 differentially regulates desensitization and internalization. *Journal of Biological Chemistry,* 284**,** 34444-34457.
RITCHIE, E., SAKA, M., MACKENZIE, C., DRUMMOND, R., WHEELER-JONES, C., KANKE, T. & PLEVIN, R. 2007. Cytokine upregulation of proteinase-activated-receptors 2 and 4 expression mediated by p38 MAP kinase and inhibitory kappa B kinase beta in human endothelial cells. *Br J Pharmacol,* 150**,** 1044-54.
RIVAS, C. M., YEE, M. C., ADDISON, K. J., LOVETT, M., PAL, K., LEDFORD, J. G., DUSSOR, G., PRICE, T. J., VAGNER, J., DEFEA, K. A. & BOITANO, S. 2022. Proteinase-activated receptor-2 antagonist C391 inhibits Alternaria-induced airway epithelial signalling and asthma indicators in acute exposure mouse models. *British Journal of Pharmacology,* 179**,** 2208-2222.
ROMAN, K., DONE, J. D., SCHAEFFER, A. J., MURPHY, S. F. & THUMBIKAT, P. 2014. Tryptase-PAR2 axis in experimental autoimmune prostatitis, a model for chronic pelvic pain syndrome. *Pain,* 155**,** 1328-38.
ROMAN, K., MURPHY, S. F., DONE, J. D., MCKENNA, K. E., SCHAEFFER, A. J. & THUMBIKAT, P. 2016. Role of PAR2 in the Development of Lower Urinary Tract Dysfunction. *J Urol,* 196**,** 588-98.
ROSENBAUM, D. M., RASMUSSEN, S. G. & KOBILKA, B. K. 2009. The structure and function of G-protein-coupled receptors. *Nature,* 459**,** 356-63.
ROTHMEIER, A. S. & RUF, W. 2012. Protease-activated receptor 2 signaling in inflammation. *Semin Immunopathol,* 34**,** 133-49.
ROY, S. S., SAIFEDDINE, M., LOUTZENHISER, R., TRIGGLE, C. R. & HOLLENBERG, M. D. 1998. Dual endothelium-dependent vascular activities of proteinase-activated receptor-2-activating peptides: evidence for receptor heterogeneity. *Br J Pharmacol,* 123**,** 1434-40.
RUSSELL, F. A., VELDHOEN, V. E., TCHITCHKAN, D. & MCDOUGALL, J. J. 2010. Proteinase-activated receptor-4 (PAR4) activation leads to sensitization of rat joint primary afferents via a bradykinin B2 receptor-dependent mechanism. *J Neurophysiol,* 103**,** 155-63.
RUSSELL, F. A., ZHAN, S., DUMAS, A., LAGARDE, S., POULIOT, M. & MCDOUGALL, J. J. 2011. The pronociceptive effect of proteinase-activated receptor-4 stimulation in rat knee joints is dependent on mast cell activation. *Pain,* 152**,** 354-60.
SALTER, M. W. & WOOLF, C. J. 2005. Cellular and molecular mechanisms of central sensitization. *In:* HUNT, S. & KOLTZENBURG, M. (eds.) *The Neurobiology of Pain: (Molecular and Cellular Neurobiology).* Oxford: Oxford University Press.
SANTULLI, R. J., DERIAN, C. K., DARROW, A. L., TOMKO, K. A., ECKARDT, A. J., SEIBERG, M., SCARBOROUGH, R. M. & ANDRADE-GORDON, P. 1995. Evidence for the presence of a protease-activated receptor distinct from the thrombin receptor in human keratinocytes. *Proc Natl Acad Sci U S A,* 92**,** 9151-5.
SCARBOROUGH, R. M., NAUGHTON, M. A., TENG, W., HUNG, D. T., ROSE, J., VU, T. K., WHEATON, V. I., TURCK, C. W. & COUGHLIN, S. R. 1992. Tethered ligand agonist peptides. Structural requirements for thrombin receptor activation reveal mechanism of proteolytic unmasking of agonist function. *J Biol Chem,* 267**,** 13146-9.
SCHEFF, N. N., WALL, I. M., NICHOLSON, S., WILLIAMS, H., CHEN, E., TU, N. H., DOLAN, J. C., LIU, C. Z., JANAL, M. N., BUNNETT, N. W. & SCHMIDT, B. L. 2022. Oral cancer induced TRPV1 sensitization is mediated by PAR2 signaling in

primary afferent neurons innervating the cancer microenvironment. *Scientific Reports,* 12**,** 4121.
SCHIFF, H. V., RIVAS, C. M., PEDERSON, W. P., SANDOVAL, E., GILLMAN, S., PRISCO, J., KUME, M., DUSSOR, G., VAGNER, J., LEDFORD, J. G., PRICE, T. J., DEFEA, K. A. & BOITANO, S. 2023. β-Arrestin-biased proteinase-activated receptor-2 antagonist C781 limits allergen-induced airway hyperresponsiveness and inflammation. *Br J Pharmacol,* 180**,** 667-680.
SCHMIDT, V. A., NIERMAN, W. C., FELDBLYUM, T. V., MAGLOTT, D. R. & BAHOU, W. F. 1997. The human thrombin receptor and proteinase activated receptor-2 genes are tightly linked on chromosome 5q13. *British journal of haematology,* 97**,** 523-529.
SCHOENFELD, A. J., GEIGER, J., PRINCIC, N., MOYNIHAN, M., VARKER, H., WANG, Z., SHI, L., STIEGLER, M. & MENZIE, A. M. 2024. EE359 Economic Burden of Managing Acute and Chronic Pain in the United States: National Estimates from 2022 Data. *Value in Health,* 27**,** S123-S124.
SCOTT, A., KHAN, K. M., COOK, J. L. & DURONIO, V. 2004. What is "inflammation"? Are we ready to move beyond Celsus? *Br J Sports Med,* 38**,** 248-9.
SCOTT, G., DENG, A., RODRIGUEZ-BURFORD, C., SEIBERG, M., HAN, R., BABIARZ, L., GRIZZLE, W., BELL, W. & PENTLAND, A. 2001. Protease-activated receptor 2, a receptor involved in melanosome transfer, is upregulated in human skin by ultraviolet irradiation. *J Invest Dermatol,* 117**,** 1412-20.
SEHNAL, D., ROSE, A., KOCA, J., BURLEY, S. & VELANKAR, S. Mol*: Towards a Common Library and Tools for Web Molecular Graphics. Workshop on Molecular Graphics and Visual Analysis of Molecular Data, 2018. The Eurographics Association;, 29-33.
SEIBERG, M., PAINE, C., SHARLOW, E., ANDRADE-GORDON, P., COSTANZO, M., EISINGER, M. & SHAPIRO, S. S. 2000. The protease-activated receptor 2 regulates pigmentation via keratinocyte-melanocyte interactions. *Exp Cell Res,* 254**,** 25-32.
SEITZBERG, J. G., KNAPP, A. E., LUND, B. W., MANDRUP BERTOZZI, S., CURRIER, E. A., MA, J.-N., SHERBUKHIN, V., BURSTEIN, E. S. & OLSSON, R. 2008. Discovery of potent and selective small-molecule PAR-2 agonists. *Journal of medicinal chemistry,* 51**,** 5490-5493.
SEVIGNY, L. M., AUSTIN, K. M., ZHANG, P., KASUDA, S., KOUKOS, G., SHARIFI, S., COVIC, L. & KULIOPULOS, A. 2011. Protease-activated receptor-2 modulates protease-activated receptor-1-driven neointimal hyperplasia. *Arterioscler Thromb Vasc Biol,* 31**,** e100-6.
SHAH, M. K., DING, Y., WAN, J., JANYARO, H., TAHIR, A. H., VODYANOY, V. & DING, M.-X. 2020. Electroacupuncture intervention of visceral hypersensitivity is involved in PAR-2-activation and CGRP-release in the spinal cord. *Scientific Reports,* 10**,** 11188.
SHAH, R. B. & ZHOU, M. 2019. Anatomy and Normal Histology of the Prostate Pertinent to Biopsy Interpretation. *Prostate Biopsy Interpretation: An Illustrated Guide.* Cham: Springer International Publishing.
SHAPIRO, M. J. & COUGHLIN, S. R. 1998. Separate signals for agonist-independent and agonist-triggered trafficking of protease-activated receptor 1. *J Biol Chem,* 273**,** 29009-14.
SHAPIRO, M. J., WEISS, E. J., FARUQI, T. R. & COUGHLIN, S. R. 2000. Protease-activated receptors 1 and 4 are shut off with distinct kinetics after activation by thrombin. *J Biol Chem,* 275**,** 25216-21.
SHEA, B. S., PROBST, C. K., BRAZEE, P. L., ROTILE, N. J., BLASI, F., WEINREB, P. H., BLACK, K. E., SOSNOVIK, D. E., VAN COTT, E. M., VIOLETTE, S. M., CARAVAN, P. & TAGER, A. M. 2017. Uncoupling of the profibrotic and hemostatic effects of thrombin in lung fibrosis. *JCI Insight,* 2.

SHEARER, A. M., RANA, R., AUSTIN, K., BALEJA, J. D., NGUYEN, N., BOHM, A., COVIC, L. & KULIOPULOS, A. 2016. Targeting Liver Fibrosis with a Cell-penetrating Protease-activated Receptor-2 (PAR2) Pepducin. *J Biol Chem,* 291**,** 23188-23198.

SHI, X., GANGADHARAN, B., BRASS, L. F., RUF, W. & MUELLER, B. M. 2004. Protease-activated receptors (PAR1 and PAR2) contribute to tumor cell motility and metastasis. *Mol Cancer Res,* 2**,** 395-402.

SHPACOVITCH, V. M., VARGA, G., STREY, A., GUNZER, M., MOOREN, F., BUDDENKOTTE, J., VERGNOLLE, N., SOMMERHOFF, C. P., GRABBE, S., GERKE, V., HOMEY, B., HOLLENBERG, M., LUGER, T. A. & STEINHOFF, M. 2004. Agonists of proteinase-activated receptor-2 modulate human neutrophil cytokine secretion, expression of cell adhesion molecules, and migration within 3-D collagen lattices. *J Leukoc Biol,* 76**,** 388-98.

SILVA, I. S., ALMEIDA, A. D., LIMA FILHO, A. C. M., FERNANDES-BRAGA, W., BARRA, A., OLIVEIRA, H. M. C., CASSALI, G. D., CAPETTINI, L. S. A., MENEZES, G. B., ALVAREZ-LEITE, J. I., LEITE, M. F. & KLEIN, A. 2023. Platelet-activating factor and protease-activated receptor 2 cooperate to promote neutrophil recruitment and lung inflammation through nuclear factor-kappa B transactivation. *Scientific Reports,* 13**,** 21637.

SMITH, R., JENKINS, A., LOURBAKOS, A., THOMPSON, P., RAMAKRISHNAN, V., TOMLINSON, J., DESHPANDE, U., JOHNSON, D. A., JONES, R. & MACKIE, E. J. 2000. Evidence for the activation of PAR-2 by the sperm protease, acrosin: expression of the receptor on oocytes. *FEBS letters,* 484**,** 285-290.

SMITH, T. H., CORONEL, L. J., LI, J. G., DORES, M. R., NIEMAN, M. T. & TREJO, J. 2016. Protease-activated Receptor-4 Signaling and Trafficking Is Regulated by the Clathrin Adaptor Protein Complex-2 Independent of beta-Arrestins. *J Biol Chem,* 291**,** 18453-64.

SOH, U. J., DORES, M. R., CHEN, B. & TREJO, J. 2010. Signal transduction by protease-activated receptors. *Br J Pharmacol,* 160**,** 191-203.

SOKOLOVA, E. & REISER, G. 2007. A novel therapeutic target in various lung diseases: airway proteases and protease-activated receptors. *Pharmacol Ther,* 115**,** 70-83.

STALHEIM, L., DING, Y., GULLAPALLI, A., PAING, M. M., WOLFE, B. L., MORRIS, D. R. & TREJO, J. 2005. Multiple independent functions of arrestins in the regulation of protease-activated receptor-2 signaling and trafficking. *Mol Pharmacol,* 67**,** 78-87.

STEINHOFF, M., BUDDENKOTTE, J., SHPACOVITCH, V., RATTENHOLL, A., MOORMANN, C., VERGNOLLE, N., LUGER, T. A. & HOLLENBERG, M. D. 2005. Proteinase-activated receptors: transducers of proteinase-mediated signaling in inflammation and immune response. *Endocr Rev,* 26**,** 1-43.

STEINHOFF, M., CORVERA, C. U., THOMA, M. S., KONG, W., MCALPINE, B. E., CAUGHEY, G. H., ANSEL, J. C. & BUNNETT, N. W. 1999. Proteinase-activated receptor-2 in human skin: tissue distribution and activation of keratinocytes by mast cell tryptase. *Exp Dermatol,* 8**,** 282-94.

STEINHOFF, M., VERGNOLLE, N., YOUNG, S., TOGNETTO, M., AMADESI, S., ENNES, H., TREVISANI, M., HOLLENBERG, M., WALLACE, J. & CAUGHEY, G. 2000a. Agonists of proteinase-activated receptor 2 induce inflammation by a neurogenic mechanism. *Nature medicine,* 6**,** 151.

STEINHOFF, M., VERGNOLLE, N., YOUNG, S. H., TOGNETTO, M., AMADESI, S., ENNES, H. S., TREVISANI, M., HOLLENBERG, M. D., WALLACE, J. L., CAUGHEY, G. H., MITCHELL, S. E., WILLIAMS, L. M., GEPPETTI, P., MAYER, E. A. & BUNNETT, N. W. 2000b. Agonists of proteinase-activated receptor 2 induce inflammation by a neurogenic mechanism. *Nat Med,* 6**,** 151-8.

STRIGGOW, F., RIEK, M., BREDER, J., HENRICH-NOACK, P., REYMANN, K. G. & REISER, G. 2000. The protease thrombin is an endogenous mediator of hippocampal neuroprotection against ischemia at low concentrations but causes degeneration at high concentrations. *Proc Natl Acad Sci U S A,* 97**,** 2264-9.

SUEN, J. Y., BARRY, G. D., LOHMAN, R. J., HALILI, M. A., COTTERELL, A. J., LE, G. T. & FAIRLIE, D. P. 2012. Modulating human proteinase activated receptor 2 with a novel antagonist (GB88) and agonist (GB110). *Br J Pharmacol,* 165**,** 1413-23.

SUN, G., STACEY, M. A., SCHMIDT, M., MORI, L. & MATTOLI, S. 2001. Interaction of mite allergens Der p3 and Der p9 with protease-activated receptor-2 expressed by lung epithelial cells. *The Journal of Immunology,* 167**,** 1014-1021.

SUN, L., GAI, J., SHI, S., ZHAO, J., BAI, X., LIU, B. & LI, X. 2021. Protease-Activated Receptor 2 (PAR-2) Antagonist AZ3451 Mitigates Oxidized Low-Density Lipoprotein (Ox-LDL)-Induced Damage and Endothelial Inflammation. *Chem Res Toxicol,* 34**,** 2202-2208.

SUN, Q., WANG, Y., ZHANG, J. & LU, J. 2017. ENMD-1068 inhibits liver fibrosis through attenuation of TGF-beta1/Smad2/3 signaling in mice. *Sci Rep,* 7**,** 5498.

SUNG, T. S., LU, H., SUNG, J., YEOM, J. H., PERRINO, B. A. & KOH, S. D. 2018. The functional role of protease-activated receptors on contractile responses by activation of Ca(2+) sensitization pathways in simian colonic muscles. *Am J Physiol Gastrointest Liver Physiol,* 315**,** G921-g931.

SUZUKI, N., HAJICEK, N. & KOZASA, T. 2009. Regulation and physiological functions of G12/13-mediated signaling pathways. *Neurosignals,* 17**,** 55-70.

SWEENEY, A. M., FLEMING, K. E., MCCAULEY, J. P., RODRIGUEZ, M. F., MARTIN, E. T., SOUSA, A. A., LEAPMAN, R. D. & SCIMEMI, A. 2017. PAR1 activation induces rapid changes in glutamate uptake and astrocyte morphology. *Sci Rep,* 7**,** 43606.

TAKEUCHI, T., HARRIS, J. L., HUANG, W., YAN, K. W., COUGHLIN, S. R. & CRAIK, C. S. 2000. Cellular localization of membrane-type serine protease 1 and identification of protease-activated receptor-2 and single-chain urokinase-type plasminogen activator as substrates. *Journal of Biological Chemistry,* 275**,** 26333-26342.

TANAKA, Y., SEKIGUCHI, F., HONG, H. & KAWABATA, A. 2008. PAR2 triggers IL-8 release via MEK/ERK and PI3-kinase/Akt pathways in GI epithelial cells. *Biochem Biophys Res Commun,* 377**,** 622-626.

TANGUAY-SABOURIN, C., FILLINGIM, M., GUGLIETTI, G. V., ZARE, A., PARISIEN, M., NORMAN, J., SWEATMAN, H., DA-ANO, R., HEIKKALA, E., BREITNER, J. C. S., MENES, J., POIRIER, J., TREMBLAY-MERCIER, J., PEREZ, J., KARPPINEN, J., VILLENEUVE, S., THOMPSON, S. J., MARTEL, M. O., ROY, M., DIATCHENKO, L., VACHON-PRESSEAU, E. & GROUP, P.-A. R. 2023. A prognostic risk score for development and spread of chronic pain. *Nature Medicine,* 29**,** 1821-1831.

TAY-UYBOCO, J., POON, M. C., AHMAD, S. & HOLLENBERG, M. D. 1995. Contractile actions of thrombin receptor-derived polypeptides in human umbilical and placental vasculature: evidence for distinct receptor systems. *Br J Pharmacol,* 115**,** 569-78.

TENG, S., LATORRE, R., BHANSALI, D., LEWIS, P. K., POLLARD, R. E., PEACH, C. J., SOKRAT, B., THANIGAI, G. S., CHIU, T., JENSEN, D. D., JIMENEZ-VARGAS, N. N., MOCHERNIAK, A., PARREIRAS-E-SILVA, L. T., BOUVIER, M., BOGYO, M., GASPARI, M. M., VANNER, S. J., PINKERTON, N. M., LEONG, K., SCHMIDT, B. L. & BUNNETT, N. W. 2024. Nanomedicines Targeting Signaling of Protease-activated Receptor 2 in Organelles Provide Sustained Analgesia. *bioRxiv***,** 2024.09.10.612022.

THIBEAULT, P. E., LESARGE, J. C., ARENDS, D., FERNANDES, M., CHIDIAC, P., STATHOPULOS, P. B., LUYT, L. G. & RAMACHANDRAN, R. 2020. Molecular

basis for activation and biased signaling at the thrombin-activated GPCR proteinase activated receptor-4 (PAR4). *J Biol Chem,* 295**,** 2520-2540.
THIBEAULT, P. E. & RAMACHANDRAN, R. 2020. Role of the Helix-8 and C-Terminal Tail in Regulating Proteinase Activated Receptor 2 Signaling. *ACS Pharmacol Transl Sci,* 3**,** 868-882.
THIYAGARAJAN, M., FERNÁNDEZ, J. A., LANE, S. M., GRIFFIN, J. H. & ZLOKOVIC, B. V. 2008. Activated protein C promotes neovascularization and neurogenesis in postischemic brain via protease-activated receptor 1. *J Neurosci,* 28**,** 12788-97.
THOMAS, J. R., SUN, J., DE LA ROSA VAZQUEZ, J. & LEE, A. 2025. Complex regulation of Cav2.2 N-type Ca2+ channels by Ca2+ and G-proteins. *PLoS One,* 20**,** e0314839.
THOMSEN, A. R. B., HAHN, H. & BUNNETT, N. W. 2022. Chapter 2 - Arrestin-mediated trafficking and compartmentalized biology of GPCRs. *In:* GUREVICH, V. V. (ed.) *Arrestins.* Academic Press.
THOMSON, A. & FOWLER, E. 1981. Carrageenan: a review of its effects on the immune system. *Agents and Actions,* 11**,** 265-273.
TILLU, D. V., HASSLER, S. N., BURGOS-VEGA, C. C., QUINN, T. L., SORGE, R. E., DUSSOR, G., BOITANO, S., VAGNER, J. & PRICE, T. J. 2015. Protease-activated receptor 2 activation is sufficient to induce the transition to a chronic pain state. *Pain,* 156**,** 859-67.
TIRUPPATHI, C., YAN, W., SANDOVAL, R., NAQVI, T., PRONIN, A. N., BENOVIC, J. L. & MALIK, A. B. 2000. G protein-coupled receptor kinase-5 regulates thrombin-activated signaling in endothelial cells. *Proceedings of the National Academy of Sciences,* 97**,** 7440-7445.
TODD, K. H., DUCHARME, J., CHOINIERE, M., CRANDALL, C. S., FOSNOCHT, D. E., HOMEL, P. & TANABE, P. 2007. Pain in the emergency department: results of the pain and emergency medicine initiative (PEMI) multicenter study. *J Pain,* 8**,** 460-6.
TRAYNELIS, S. F. & TREJO, J. 2007. Protease-activated receptor signaling: new roles and regulatory mechanisms. *Curr Opin Hematol,* 14**,** 230-5.
TREEDE, R.-D., RIEF, W., BARKE, A., AZIZ, Q., BENNETT, M. I., BENOLIEL, R., COHEN, M., EVERS, S., FINNERUP, N. B. & FIRST, M. B. 2019. Chronic pain as a symptom or a disease: the IASP Classification of Chronic Pain for the International Classification of Diseases (ICD-11). *pain,* 160**,** 19-27.
TREEDE, R. D., JENSEN, T. S., CAMPBELL, J. N., CRUCCU, G., DOSTROVSKY, J. O., GRIFFIN, J. W., HANSSON, P., HUGHES, R., NURMIKKO, T. & SERRA, J. 2008. Neuropathic pain: redefinition and a grading system for clinical and research purposes. *Neurology,* 70**,** 1630-5.
TREJO, J. 2003. Protease-Activated Receptors: New Concepts in Regulation of G Protein-Coupled Receptor Signaling and Trafficking. *Journal of Pharmacology and Experimental Therapeutics,* 307**,** 437-442.
TSUBOTA, M., OZAKI, T., HAYASHI, Y., OKAWA, Y., FUJIMURA, A., SEKIGUCHI, F., NISHIKAWA, H. & KAWABATA, A. 2018. Prostanoid-dependent bladder pain caused by proteinase-activated receptor-2 activation in mice: Involvement of TRPV1 and T-type Ca(2+) channels. *J Pharmacol Sci,* 136**,** 46-49.
TSUJII, K., ANDOH, T., LEE, J. B. & KURAISHI, Y. 2008. Activation of proteinase-activated receptors induces itch-associated response through histamine-dependent and -independent pathways in mice. *J Pharmacol Sci,* 108**,** 385-8.
TURNER, C. T., ZEGLINSKI, M. R., RICHARDSON, K. C., ZHAO, H., SHEN, Y., PAPP, A., BIRD, P. I. & GRANVILLE, D. J. 2019. Granzyme K Expressed by Classically Activated Macrophages Contributes to Inflammation and Impaired Remodeling. *J Invest Dermatol,* 139**,** 930-939.

UEHARA, A., MURAMOTO, K., IMAMURA, T., NAKAYAMA, K., POTEMPA, J., TRAVIS, J., SUGAWARA, S. & TAKADA, H. 2005. Arginine-specific gingipains from Porphyromonas gingivalis stimulate production of hepatocyte growth factor (scatter factor) through protease-activated receptors in human gingival fibroblasts in culture. *The Journal of Immunology,* 175**,** 6076-6084.

UNIYAL, A., TIWARI, V., TSUKAMOTO, T., DONG, X., GUAN, Y. & RAJA, S. N. 2023. Targeting sensory neuron GPCRs for peripheral neuropathic pain. *Trends Pharmacol Sci,* 44**,** 1009-1027.

URBAN, J. D., CLARKE, W. P., VON ZASTROW, M., NICHOLS, D. E., KOBILKA, B., WEINSTEIN, H., JAVITCH, J. A., ROTH, B. L., CHRISTOPOULOS, A., SEXTON, P. M., MILLER, K. J., SPEDDING, M. & MAILMAN, R. B. 2007. Functional selectivity and classical concepts of quantitative pharmacology. *J Pharmacol Exp Ther,* 320**,** 1-13.

VARDEH, D. & NARANJO, J. F. 2017. Peripheral and Central Sensitization. *In:* YONG, R. J., NGUYEN, M., NELSON, E. & URMAN, R. D. (eds.) *Pain Medicine: An Essential Review.* Cham: Springer International Publishing.

VERGNOLLE, N. 1999. Proteinase-activated receptor-2-activating peptides induce leukocyte rolling, adhesion, and extravasation in vivo. *The Journal of Immunology,* 163**,** 5064-5069.

VERGNOLLE, N. 2009. Protease-activated receptors as drug targets in inflammation and pain. *Pharmacol Ther,* 123**,** 292-309.

VERGNOLLE, N., BUNNETT, N. W., SHARKEY, K. A., BRUSSEE, V., COMPTON, S. J., GRADY, E. F., CIRINO, G., GERARD, N., BASBAUM, A. I., ANDRADE-GORDON, P., HOLLENBERG, M. D. & WALLACE, J. L. 2001a. Proteinase-activated receptor-2 and hyperalgesia: A novel pain pathway. *Nature Medicine,* 7**,** 821-826.

VERGNOLLE, N., DERIAN, C. K., D'ANDREA, M. R., STEINHOFF, M. & ANDRADE-GORDON, P. 2002. Characterization of thrombin-induced leukocyte rolling and adherence: a potential proinflammatory role for proteinase-activated receptor-4. *The Journal of Immunology,* 169**,** 1467-1473.

VERGNOLLE, N., HOLLENBERG, M. D., SHARKEY, K. A. & WALLACE, J. L. 1999. Characterization of the inflammatory response to proteinase-activated receptor-2 (PAR2)-activating peptides in the rat paw. *British journal of pharmacology,* 127**,** 1083-1090.

VERGNOLLE, N., WALLACE, J. L., BUNNETT, N. W. & HOLLENBERG, M. D. 2001b. Protease-activated receptors in inflammation, neuronal signaling and pain. *Trends Pharmacol Sci,* 22**,** 146-52.

VESEY, D. A., HOOPER, J. D., GOBE, G. C. & JOHNSON, D. W. 2007. Potential physiological and pathophysiological roles for protease-activated receptor-2 in the kidney (Review Article). *Nephrology,* 12**,** 36-43.

VESEY, D. A., SUEN, J. Y., SEOW, V., LOHMAN, R. J., LIU, L., GOBE, G. C., JOHNSON, D. W. & FAIRLIE, D. P. 2013. PAR2-induced inflammatory responses in human kidney tubular epithelial cells. *Am J Physiol Renal Physiol,* 304**,** F737-50.

VU, T. K., HUNG, D. T., WHEATON, V. I. & COUGHLIN, S. R. 1991. Molecular cloning of a functional thrombin receptor reveals a novel proteolytic mechanism of receptor activation. *Cell,* 64**,** 1057-68.

VYKHOVANETS, E. V., RESNICK, M. I., MACLENNAN, G. T. & GUPTA, S. 2007. Experimental rodent models of prostatitis: limitations and potential. *Prostate Cancer and Prostatic Diseases,* 10**,** 15-29.

WAGENLEHNER, F. M., VAN TILL, J. W., MAGRI, V., PERLETTI, G., HOUBIERS, J. G., WEIDNER, W. & NICKEL, J. C. 2013. National Institutes of Health Chronic Prostatitis Symptom Index (NIH-CPSI) symptom evaluation in multinational cohorts

of patients with chronic prostatitis/chronic pelvic pain syndrome. *Eur Urol,* 63**,** 953-9.
WALSH, P. N. & AHMAD, S. S. 2002. Proteases in blood clotting. *Essays Biochem,* 38**,** 95-111.
WANG, H., ZHENG, Y. & HE, S. 2006. Induction of release and up-regulated gene expression of interleukin (IL)-8 in A549 cells by serine proteinases. *BMC Cell Biol,* 7**,** 22.
WANG, P., CHEN, F. X., DU, C., LI, C. Q., YU, Y. B., ZUO, X. L. & LI, Y. Q. 2015. Increased production of BDNF in colonic epithelial cells induced by fecal supernatants from diarrheic IBS patients. *Sci Rep,* 5**,** 10121.
WANG, P. & DEFEA, K. A. 2006. Protease-activated receptor-2 simultaneously directs beta-arrestin-1-dependent inhibition and Galphaq-dependent activation of phosphatidylinositol 3-kinase. *Biochemistry,* 45**,** 9374-85.
WANG, S., DAI, Y., KOBAYASHI, K., ZHU, W., KOGURE, Y., YAMANAKA, H., WAN, Y., ZHANG, W. & NOGUCHI, K. 2012. Potentiation of the P2X3 ATP receptor by PAR-2 in rat dorsal root ganglia neurons, through protein kinase-dependent mechanisms, contributes to inflammatory pain. *Eur J Neurosci,* 36**,** 2293-301.
WANG, W., NAVEED, M., BAIG, M., ABBAS, M. & XIAOHUI, Z. 2018. Experimental rodent models of chronic prostatitis and evaluation criteria. *Biomed Pharmacother,* 108**,** 1894-1901.
WANG, Y. J., YU, S. J., TSAI, J. J., YU, C. H. & LIAO, E. C. 2021. Antagonism of Protease Activated Receptor-2 by GB88 Reduces Inflammation Triggered by Protease Allergen Tyr-p3. *Front Immunol,* 12**,** 557433.
WEI, H., WEI, Y., TIAN, F., NIU, T. & YI, G. 2016. Blocking proteinase-activated receptor 2 alleviated neuropathic pain evoked by spinal cord injury. *Physiol Res,* 65**,** 145-53.
WETTSCHURECK, N. & OFFERMANNS, S. 2005. Mammalian G proteins and their cell type specific functions. *Physiol Rev,* 85**,** 1159-204.
WILSON, B. J., HARADA, R., LEDUY, L., HOLLENBERG, M. D. & NEPVEU, A. 2009. CUX1 transcription factor is a downstream effector of the proteinase-activated receptor 2 (PAR2). *J Biol Chem,* 284**,** 36-45.
WILSON, S., GREER, B., HOOPER, J., ZIJLSTRA, A., WALKER, B., QUIGLEY, J. & HAWTHORNE, S. 2005. The membrane-anchored serine protease, TMPRSS2, activates PAR-2 in prostate cancer cells. *Biochemical Journal,* 388**,** 967-972.
WINTER, M. C., SHASBY, S. S., RIES, D. R. & SHASBY, D. M. 2006. PAR2 activation interrupts E-cadherin adhesion and compromises the airway epithelial barrier: protective effect of β-agonists. *American Journal of Physiology-Lung Cellular and Molecular Physiology,* 291**,** L628-L635.
WOLFE, B. L., MARCHESE, A. & TREJO, J. 2007. Ubiquitination differentially regulates clathrin-dependent internalization of protease-activated receptor-1. *J Cell Biol,* 177**,** 905-16.
WONG, B. 2011. Points of view: Color blindness. *Nature Methods,* 8**,** 441-441.
WOOLF, C. J. & MA, Q. 2007. Nociceptors--noxious stimulus detectors. *Neuron,* 55**,** 353-64.
WU, J., LIU, T. T., ZHOU, Y. M., QIU, C. Y., REN, P., JIAO, M. & HU, W. P. 2017. Sensitization of ASIC3 by proteinase-activated receptor 2 signaling contributes to acidosis-induced nociception. *J Neuroinflammation,* 14**,** 150.
WU, L., OSHIMA, T., SHAN, J., SEI, H., TOMITA, T., OHDA, Y., FUKUI, H., WATARI, J. & MIWA, H. 2015. PAR-2 activation enhances weak acid-induced ATP release through TRPV1 and ASIC sensitization in human esophageal epithelial cells. *Am J Physiol Gastrointest Liver Physiol,* 309**,** G695-702.
WU, Z. S., WANG, H. J., LEE, W. C., LUO, H. L., LIN, T. K. & CHUANG, Y. C. 2023. Low-Energy Shock Wave Suppresses Prostatic Pain and Inflammation by

Modulating Mitochondrial Dynamics Regulators on a Carrageenan-Induced Prostatitis Model in Rats. *Int J Mol Sci,* 24.
XING, J. & LI, J. 2017. Proteinase-Activated Receptor-2 Sensitivity of Amplified TRPA1 Activity in Skeletal Muscle Afferent Nerves and Exercise Pressor Reflex in Rats with Femoral Artery Occlusion. *Cell Physiol Biochem,* 44**,** 163-171.
XU, K., WANG, L., LIN, M. & HE, G. 2024. Update on protease-activated receptor 2 in inflammatory and autoimmune dermatological diseases. *Front Immunol,* 15**,** 1449126.
XU, W. F., ANDERSEN, H., WHITMORE, T. E., PRESNELL, S. R., YEE, D. P., CHING, A., GILBERT, T., DAVIE, E. W. & FOSTER, D. C. 1998. Cloning and characterization of human protease-activated receptor 4. *Proc Natl Acad Sci U S A,* 95**,** 6642-6.
XUE, M., CAMPBELL, D., SAMBROOK, P. N., FUKUDOME, K. & JACKSON, C. J. 2005. Endothelial protein C receptor and protease-activated receptor-1 mediate induction of a wound-healing phenotype in human keratinocytes by activated protein C. *J Invest Dermatol,* 125**,** 1279-85.
XUE, M., CHAN, Y. K., SHEN, K., DERVISH, S., MARCH, L., SAMBROOK, P. N. & JACKSON, C. J. 2012. Protease-activated receptor 2, rather than protease-activated receptor 1, contributes to the aggressive properties of synovial fibroblasts in rheumatoid arthritis. *Arthritis Rheum,* 64**,** 88-98.
YAGI, Y., OTANI, H., ANDO, S., OSHIRO, A., KAWAI, K., NISHIKAWA, H., ARAKI, H., FUKUHARA, S. & INAGAKI, C. 2006. Involvement of Rho signaling in PAR2-mediated regulation of neutrophil adhesion to lung epithelial cells. *European journal of pharmacology,* 536**,** 19-27.
YANG, L. 2018. Neuronal cAMP/PKA Signaling and Energy Homeostasis. *Adv Exp Med Biol,* 1090**,** 31-48.
YELLEPEDDI, V. K., RADHAKRISHNAN, J. & RADHAKRISHNAN, R. 2018. Penetration and pharmacokinetics of non-steroidal anti-inflammatory drugs in rat prostate tissue. *Prostate,* 78**,** 80-85.
YOSHIDA, N., KATADA, K., HANDA, O., TAKAGI, T., KOKURA, S., NAITO, Y., MUKAIDA, N., SOMA, T., SHIMADA, Y., YOSHIKAWA, T. & OKANOUE, T. 2007. Interleukin-8 production via protease-activated receptor 2 in human esophageal epithelial cells. *Int J Mol Med,* 19**,** 335-40.
YUDIN, Y. & ROHACS, T. 2018. Inhibitory Gi/O-coupled receptors in somatosensory neurons: potential therapeutic targets for novel analgesics. *Molecular pain,* 14**,** 1744806918763646.
ZENG, F., CHEN, H., YANG, J., WANG, L., CUI, Y., GUAN, X., WANG, Z., NIU, J., ZU, X., QI, L., ZHANG, X., TANG, Z. & LIU, L. 2014. Development and validation of an animal model of prostate inflammation-induced chronic pelvic pain: evaluating from inflammation of the prostate to pain behavioral modifications. *PLoS One,* 9**,** e96824.
ZHANG, J., LIANG, C., SHANG, X. & LI, H. 2020a. Chronic prostatitis/chronic pelvic pain syndrome: a disease or symptom? Current perspectives on diagnosis, treatment, and prognosis. *American journal of men's health,* 14**,** 1557988320903200.
ZHANG, J., ZHANG, X., CAI, Z., LI, N. & LI, H. 2019. The Lifetime Risk and Prognosis of Chronic Prostatitis/Chronic Pelvic Pain Syndrome in the Middle-Aged Chinese Males. *Am J Mens Health,* 13**,** 1557988319865380.
ZHANG, L. G., YU, Z. Q., YANG, C., CHEN, J., ZHAN, C. S., CHEN, X. G., ZHANG, L., HAO, Z. Y. & LIANG, C. Z. 2020b. Effect of Eriocalyxin B on prostatic inflammation and pelvic pain in a mouse model of experimental autoimmune prostatitis. *Prostate,* 80**,** 1394-1404.

ZHANG, M., GAO, C. X., WANG, Y. P., MA, K. T., LI, L., YIN, J. W., DAI, Z. G., WANG, S. & SI, J. Q. 2018. The association between the expression of PAR2 and TMEM16A and neuropathic pain. *Mol Med Rep,* 17**,** 3744-3750.

ZHANG, P., LEGER, A. J., BALEJA, J. D., RANA, R., CORLIN, T., NGUYEN, N., KOUKOS, G., BOHM, A., COVIC, L. & KULIOPULOS, A. 2015. Allosteric Activation of a G Protein-coupled Receptor with Cell-penetrating Receptor Mimetics. *J Biol Chem,* 290**,** 15785-98.

ZHANG, X., LEE, M. D., BUCKLEY, C., HOLLENBERG, M. D., WILSON, C. & MCCARRON, J. G. 2023. Endothelial PAR2 activation evokes resistance artery relaxation. *J Cell Physiol,* 238**,** 776-789.

ZHANG, Z., MELIA, T. J., HE, F., YUAN, C., MCGOUGH, A., SCHMID, M. F. & WENSEL, T. G. 2004. How a G protein binds a membrane. *J Biol Chem,* 279**,** 33937-45.

ZHAO, P., LIEU, T., BARLOW, N., SOSTEGNI, S., HAERTEIS, S., KORBMACHER, C., LIEDTKE, W., JIMENEZ-VARGAS, N. N., VANNER, S. J. & BUNNETT, N. W. 2015. Neutrophil Elastase Activates Protease-activated Receptor-2 (PAR2) and Transient Receptor Potential Vanilloid 4 (TRPV4) to Cause Inflammation and Pain. *J Biol Chem,* 290**,** 13875-87.

ZHENG, H., LOH, H. H. & LAW, P. Y. 2010. Agonist-selective signaling of G protein-coupled receptor: Mechanisms and implications. *IUBMB life,* 62**,** 112-119.

ZHU, J., MIAO, X. R., TAO, K. M., ZHU, H., LIU, Z. Y., YU, D. W., CHEN, Q. B., QIU, H. B. & LU, Z. J. 2017. Trypsin-protease activated receptor-2 signaling contributes to pancreatic cancer pain. *Oncotarget,* 8**,** 61810-61823.

ZHU, W.-J., YAMANAKA, H., OBATA, K., DAI, Y., KOBAYASHI, K., KOZAI, T., TOKUNAGA, A. & NOGUCHI, K. 2005. Expression of mRNA for four subtypes of the proteinase-activated receptor in rat dorsal root ganglia. *Brain Research,* 1041**,** 205-211.

ZHUO, X., WU, Y., FU, X., LIANG, X., XIANG, Y., LI, J., MAO, C. & JIANG, Y. 2022. The Yin-Yang roles of protease-activated receptors in inflammatory signalling and diseases. *The FEBS Journal,* 289**,** 4000-4020.

ZOUDILOVA, M., KUMAR, P., GE, L., WANG, P., BOKOCH, G. M. & DEFEA, K. A. 2007. Beta-arrestin-dependent regulation of the cofilin pathway downstream of protease-activated receptor-2. *J Biol Chem,* 282**,** 20634-46.